

# Exploring refinement of the early touch-response circuit in zebrafish neurodevelopment

Kendra Eileen Liu

Goodyear, Arizona

M.Phil. in Life Science, Hong Kong University of Science and Technology, Sai Kung, Hong Kong, 2019

B.S. in Neuroscience & Cognitive Science, University of Arizona, Tucson, Arizona, 2016

B.S. in Molecular & Cellular Biology, University of Arizona, Tucson, Arizona, 2016

A Dissertation presented to the Graduate Faculty of the University of Virginia  
in Partial Fulfillment of the Requirements for the  
Degree of Doctor of Philosophy

Department of Biology  
Neuroscience Graduate Program  
University of Virginia  
December, 2024

## ABSTRACT

---

During early development, the central and peripheral nervous systems are characterized by exuberant cells, projections, and synapses that are later pruned away to homeostatic levels. This pruning allows for tissue morphogenesis, regulation of cell populations, error correction, and optimization of neural connectivity. For neural circuits, this facilitates the establishment of rudimentary circuits which necessitate early organism survival and allow for later refinement. However, little is known about how these fundamental, developmental mechanisms lead to a nervous system precisely tuned for efficient behaviors, survival, and learning. In this dissertation, I first review these developmental concepts in relation to the importance of cell clearance. Then, I present my investigation into circuit refinement in the context of an early-formed touch-response circuit in zebrafish. I demonstrate surprising and strong evidence that contradicts previous studies: an essential component of the touch-response circuit, Rohon-Beard neurons, does not succumb to developmental programmed cell death. This work unveils new questions on the function of these surviving Rohon-Beard neurons and their effects on the dynamics and physiology of somatosensory processing.

# ACKNOWLEDGEMENTS

---

.It is incredibly difficult to explain what it means to complete a PhD until you're at the end, but then it feels almost impossible to put into words. As a kid who loved science and asking questions, I managed to stumble onto this path. I am incredibly fortunate and privileged to have so many mentors, friends, and family at many different stages of my life supporting me and my endeavors. This dissertation would not be possible without them. Further, this dissertation only exists because I received training and conducted studies on the past, present, and future land of the Sobaipuri, O'odham Jewed, Tohono O'odham, Hohokam, and Monacan peoples and Nations, the ancestral inhabitants of the lands currently occupied by the University of Arizona and University of Virginia.

Firstly, I would like to thank Prof. Sarah Kucenas for her support, passion, and excitement for science. I have learned so much from you and I am forever grateful for your mentorship. Thank you to the members of my committee, who have been with me since my qualification exam: Prof. Bettina Winckler, Prof. Tajie Harris, Prof. Hui Zong, and Prof. Ukpong Eyo. Your support and guidance over all these years has been invaluable and during many times where I thought I couldn't continue – your encouragement helped me persist. I also want to thank Profs. Janet Cross, Adrian Halme, David Auble, Mark Beenhakker, John Campbell, Barry Condron, and Yuh-Hwa Wang. You are all incredible people, mentors, and scientists. The past two years have been extraordinarily trying, and I greatly appreciate and thank you all for your kindness, mentorship, and advice.

Thank you to the past and present members of the Kucenas lab, who have been incredible sources of support, encouragement, and fun. I want to especially thank Lori Tocke for her hard work and dedication, none of this work would be possible without you! A large portion of my zebrafish training has come from Prof. Laura Fontenas and Dr. Drew Latimer, thank you for your critical minds and sharing your scientific wisdom. To Charles, Sarah Hunter-Chang, and Veronica – you all have seen me at my best, my worst, and my weirdest. Thank you all for your patience, grace, and friendship. I believe so strongly in all of you and I can't wait to attend your defenses!

I also would not be where I am today without truly fantastic mentors from earlier in my training. During my MPhil, I was lucky to learn from one of the most passionate and tenacious Alzheimer's disease critics – Prof. Karl Herrup. Thank you, Prof. Herrup for helping me sharpen my scientifically critical mind and for your invaluable understanding and support. To Profs. Lynne Oland and Leslie Tolbert, I would not have developed the confidence to pursue science without your fierce encouragement and support. I feel so incredibly fortunate to have started my scientific training with you both, and to stand upon your shoulders is of great honor.

To Kim Knotts, you are an absolutely incredible person and NGP is lucky to have you. Thank you, for your fierce support of students, quirky hilarity, steadfast leadership and girlboss attitude. You have done so much for NGP and you mean so much to me.

To all students of NGP – you all are awesome. Thank you for your patience when I interrupt with really off the wall questions and thank you for being an amazing community. I want to especially thank Josh Milstein and Dr. Joe Uweru for their encouragement and support, especially during my early years in the program. To my NGP cohort (Ryan Brown, Katriel Cho, Nick Conley, Jenny Fu, Daria Skwarzynska, Matt Ritger, David Tyus, and Kristine Zengeler), you all mean the world to me. It has been a long journey, and I am so incredibly proud of all of you. You have made Taco Tuesday a special place in my heart.

To my Biology friends Audrey Brown, Phoebe Cook, Luke Dillard, Adam Lenhart, Connor Murray, Daniel Nondorf, Phil Tubergen, and Chris Robinson. Thank you all for so many laughs, coffee breaks, dinners, and adventures. You have helped make Charlottesville a home.

I am also incredibly thankful to Kim Arena, Kendall Branham, Shaylyn Clancy, and Taylor Nystrom. You four are the four most incredible women scientists and the best of friends. I would not have survived my PhD without you, and I love you all dearly.

Lastly, to my family – Korri, Steve, Lisa, Cheryl, Twinkle, Bean, and Mila - I love you. This is for you.

# TABLE OF CONTENTS

---

<b>ABSTRACT</b> .....	<b>II</b>
<b>ACKNOWLEDGEMENTS</b> .....	<b>III</b>
<b>LIST OF ABBREVIATIONS</b> .....	<b>VIII</b>
<b>LIST OF FIGURES &amp; TABLES</b> .....	<b>X</b>
<b>CHAPTER 1: CLEARING YOUR MIND: MECHANISMS OF DEBRIS CLEARANCE AFTER CELL DEATH DURING NEURODEVELOPMENT</b> .....	<b>1</b>
1.0 PREFACE.....	1
1.1 ABSTRACT .....	2
1.2 NEURODEVELOPMENT .....	2
1.2.1 <i>Neurodevelopmental Timing and Trajectories</i> .....	4
1.2.2 <i>Cell Death in Neurodevelopment</i> .....	5
1.2.2.1 How is cell survival or death determined, and what triggers programmed cell death? .....	5
1.2.2.2 Why are some cell populations generated only to die? .....	6
1.2.3 <i>Synaptic Refinement and Elimination</i> .....	7
1.3 MAJOR PHAGOCYTES DURING NERVOUS SYSTEM DEVELOPMENT .....	8
1.3.1 <i>Microglia</i> .....	8
1.3.2 <i>Macrophages</i> .....	11
1.3.3 <i>Astrocytes</i> .....	11
1.3.4 <i>Retinal Pigment Epithelial Cells</i> .....	12
1.3.5 <i>Oligodendrocyte Progenitor Cells</i> .....	12
1.3.6 <i>Schwann Cells</i> .....	13
1.3.7 <i>Satellite Glial Cell Precursors</i> .....	13
1.3.7 <i>Neural Precursor Cells</i> .....	14
1.3.8 <i>Neural Crest Cells</i> .....	14
1.4 PATHWAYS OF CELL CLEARANCE .....	14
1.4.1 <i>“Find Me” Signals within the Central Nervous System</i> .....	15
1.4.1.1 ATP and Pannexin-1 .....	15
1.4.1.2 Fractalkine.....	15
1.4.2 <i>“Eat Me” Signaling within the Central Nervous System</i> .....	16
1.4.2.1 Phosphatidylserine .....	16
1.4.2.2 Calreticulin.....	17
1.4.2.3 Complement .....	17
1.5 PROCESSING OF CLEARED CARGO BY CENTRAL NERVOUS SYSTEM PHAGOCYTES.....	17
1.6 CELL AND DEBRIS CLEARANCE IN DISEASE .....	18
1.6.1 <i>Neurodevelopmental and Neuropsychiatric Disorders</i> .....	19
1.6.2 <i>Neurodegenerative Disorders</i> .....	20

1.7	WHERE DO WE GO FROM HERE? CHALLENGES AND OPPORTUNITIES .....	20
1.7.1	<i>Neurodevelopment: Immunologically Silent or Not?</i> .....	20
1.7.2	<i>Phagocyte State versus Fate</i> .....	21
1.7.3	<i>Visualizing Cell Death and Phagocytosis In Vivo</i> .....	22
1.8	SUPPLEMENTAL INFORMATION.....	24
1.10	ACKNOWLEDGEMENTS .....	25
<b>CHAPTER 2</b>	<b>MATERIALS &amp; METHODS .....</b>	<b>26</b>
2.1	FISH HUSBANDRY .....	26
2.2	ZEBRAFISH TRANSGENIC LINES .....	26
2.3	GENERATION OF TRANSGENIC LINES .....	27
2.4	<i>CSF1RA<sup>-/-</sup></i> IDENTIFICATION .....	29
2.5	<i>BLB<sup>-/-</sup></i> IDENTIFICATION .....	29
2.6	MOSAIC LABELING BY MICROINJECTION .....	29
2.7	<i>IN VIVO</i> CONFOCAL IMAGING .....	30
2.8	LASER INJURY AND ABLATION .....	31
2.9	D-TUBOCURARINE .....	31
2.10	CRYOSECTIONING .....	32
2.11	ACRIDINE ORANGE STAINING .....	32
2.12	TUNEL STAINING .....	32
2.13	QUANTIFICATIONS AND STATISTICAL ANALYSES.....	33
2.13.1	<i>Identifying RBs</i> .....	33
2.13.2	<i>Identifying other ngn1<sup>+</sup> cells</i> .....	34
2.13.3	<i>Acridine Orange Puncta Number</i> .....	34
2.13.4	<i>Annexin V Quantification</i> .....	35
2.13.5	<i>mpeg1<sup>+</sup> Professional Phagocyte Number</i> .....	35
2.13.6	<i>RB and other ngn1<sup>+</sup> cell Number Quantification</i> .....	36
2.13.7	<i>RB Soma Volume</i> .....	36
2.13.8	<i>Phagosome Number and Volume</i> .....	37
2.13.9	<i>Percent Survival Quantification</i> .....	38
2.13.10	<i>TUNEL Quantification</i> .....	39
2.13.11	<i>Statistical Analyses</i> .....	39
2.14	SCHEMATICS AND ILLUSTRATIONS.....	39
<b>CHAPTER 3:</b>	<b>ROHON-BEARD NEURONS DO NOT SUCCUMB TO PROGRAMMED CELL DEATH DURING ZEBRAFISH</b>	
	<b>DEVELOPMENT 40</b>	
3.1	ABSTRACT .....	40
3.2	INTRODUCTION .....	41
3.3	RESULTS .....	43
3.3.1	<i>RB neurons survive through early zebrafish development</i> .....	43
3.3.2	<i>The vast majority of RB neurons do not express canonical markers of cell death</i> .....	48

3.3.3	<i>RBs persist until 15 dpf</i> .....	54
3.4	DISCUSSION .....	57
3.5	SUPPLEMENTARY DATA .....	61
3.6	ACKNOWLEDGEMENTS .....	63
<b>CHAPTER 4:</b>	<b>DISCUSSION &amp; FUTURE DIRECTIONS</b> .....	<b>64</b>
4.1	SUMMARY .....	64
4.2	A LESSON IN CAREFUL, CRITICAL SCIENCE .....	64
4.3	THE LIVING DEAD: SURVIVING ROHON-BEARD NEURONS .....	66
4.3.1	<i>How long do Rohon-Beard neurons survive?</i> .....	66
4.3.2	<i>Do Rohon-Beard neurons undergo axon or synaptic remodeling?</i> .....	68
4.4	POTENTIAL FOR ROHON-BEARD NEURON SUBTYPES .....	70
4.5	FINAL REMARKS .....	71
<b>APPENDICES</b>	<b>INVESTIGATING NEURAL CREST CELLS AS NOVEL PHAGOCYTES IN EARLY DEVELOPMENT</b> .....	<b>72</b>
A.0	PREFACE .....	72
A.1	PHAGOCYtic NEURAL CREST CELLS IN EARLY ZEBRAFISH DEVELOPMENT .....	72
	.....	75
A.2	EXAMINING PHAGOCYtic CRANIAL NCCS IN NEURODEVELOPMENT .....	76
A.2.1	<i>Visualizing cranial NCCs in early zebrafish development</i> .....	76
A.2.2	<i>Cranial NCCs can respond to optic tectum injury</i> .....	82
A.3	STUDYING THE ROLE OF PHAGOCYtic NCCS IN NEURODEVELOPMENTAL TRAJECTORIES .....	84
A.4	CHARACTERIZING NCC PHAGOCYtic ACTIVITY IN THE ZEBRAFISH <i>CSF1RA</i> <sup>-/-</sup> MUTANT .....	85
A.4.1	<i>csf1ra</i> <sup>-/-</sup> mutants exhibit a loss of microglia in the optic tectum at 3 dpf .....	86
A.4.2	<i>csf1ra</i> <sup>-/-</sup> mutants display no difference in number of mpeg1 <sup>+</sup> professional phagocytes in the trunk between 36 and 48 hpf .....	90
A.4.3	<i>Increased cell death at 55 hpf in csf1ra</i> <sup>-/-</sup> embryos by acridine orange .....	93
A.4.3	<i>Discussion</i> .....	96
A.5	EXAMINING NCCs IN THE ZEBRAFISH <i>BLB (SLC37A2)</i> <sup>-/-</sup> MUTANT .....	98
A.5.1	<i>blb</i> embryos have increased numbers of dying cells in early development .....	99
A.5.2	<i>NCCs have altered phagosome morphology in blb embryos</i> .....	104
A.6	EXPLORING PHAGOCYtic NCCs BY scRNAseq .....	110
<b>REFERENCES</b>	.....	<b>112</b>

## LIST OF ABBREVIATIONS

---

4-OHT	(Z)-4-hydroxytamoxifen	MS	multiple sclerosis
AD	Alzheimer's disease	MΦ	macrophage(s)
ANOVA	analysis of variance	NCC	neural crest cell
AO	acridine orange	<i>ngn1</i>	<i>neurogenin1</i>
ASD	Autism spectrum disorder	NPC	neural precursor cell
BDNF	brain-derived neurotrophic factor	NTPOC	nuclei of the tract of the postoptic commissure
<i>blb</i>	<i>bubblebrain</i>	OPC	oligodendrocyte progenitor cell
bp	base pair	P	postnatal day
CNS	central nervous system	PBS	phosphate-buffered saline
CoLo	commissural local interneuron	PCD	programmed cell death
CoPA	commissural primary ascending interneuron	PD	Parkinson's disease
CreER <sup>T2</sup>	Cre recombinase – estrogen receptor T2	PFC	prefrontal cortex
CRT	calreticulin	PI(3)P	phosphatidylinositol 3-phosphate
CSF1R	colony-stimulating factor 1 receptor	PNS	peripheral nervous system
DAPI	4',6-diamidino-2-phenylindole	POM	periocular mesenchyme
DLF	dorsal longitudinal fasciculus	POS	photoreceptor outer segment
DNA	deoxyribonucleic acid	PtdSer	phosphatidylserine
DoLA	dorsal longitudinal ascending interneuron	PTU	1-phenyl-2-thiourea
dpf	days post fertilization	RB	Rohon-Beard
DRG	dorsal root ganglion	RFP	red fluorescent protein
E	embryonic day	RNA	ribonucleic acid
EGFP	enhanced green fluorescent protein	ROI	region of interest
Fgf	fibroblast growth factor	RPE	retinal pigmented epithelial cell
GFP	green fluorescent protein	RT	room temperature
hpf	hours post fertilization	S	stage
hpi	hours post-injury	SC	spinal cord
IFN-1	type 1 interferon	scRNAseq	single-cell RNA sequencing
IL	interleukin	SD	standard deviation
M	month	SEM	standard error of the mean
		SL	standard length

## LIST OF ABBREVIATIONS

---

SVZ	subventricular zone
TdT	terminal deoxynucleotidyl transferase
TUNEL	terminal deoxynucleotidyl transferase -mediated dUTP nick end labeling
Ucp2	uncoupling protein 2
W	gestational week
Y	year
YFP	yellow fluorescent protein

# LIST OF FIGURES & TABLES

---

Figure 1-1. Key developmental trajectories across species.....	3
Figure 1-2. The central nervous system (CNS) food network.....	10
Table 2-1. Descriptions and abbreviations of zebrafish lines.....	26
Table 2-2. Constructs and vector used.....	28
Table 2-3. <i>secA5</i> <sup>+</sup> puncta Imaris surface algorithm parameters.....	35
Table 2-4. RB soma Imaris surface algorithm parameters.....	37
Table 2-5. FYVE <sup>+</sup> phagosomes (weak GFP signal) Imaris surface rendering parameters.....	38
Table 2-6. FYVE <sup>+</sup> phagosomes (strong GFP signal) Imaris surface rendering parameters.....	38
Figure 3-1. RB neurons survive through early zebrafish development.....	45
Figure 3-2. RBs do not express canonical markers of cell death.....	49
Figure 3-3. RB survival is not due to decreased neural activity from tricaine administration.....	52
Figure 3-4. RBs persist until 15 dpf.....	55
Supplemental Table 1-1. <i>Drosophila</i> PtdSer Receptors.....	24
Supplemental Table 1-2. Mouse PtdSer Receptors.....	24
Supplemental Table 1-3: Human PtdSer Receptors.....	25
Supplemental Figure 3-1: Other <i>ngn1</i> <sup>+</sup> cells have similar trends to <i>ngn1</i> <sup>+</sup> RBs.....	61
Supplemental Figure 3-2: Other <i>ngn1</i> <sup>+</sup> cells have similar trends to <i>ngn1</i> <sup>+</sup> RBs in transverse slices.....	63
<u>Appendices</u>	
Figure A-1. Neural crest cells are novel phagocytes in zebrafish development.....	74
Figure A-2. Neural crest cells are novel phagocytes and express multiple phagocytic genes in an early window of zebrafish development.....	75
Figure A-3. Visualizing cranial NCCs by timelapse confocal imaging.....	79
Figure A-4: Cranial NCCs border the developing brain parenchyma.....	81
Figure A-5: Cranial NCCs respond to laser-induced injury of the optic tectum parenchyma.....	83
Figure A-6: <i>csf1ra</i> <sup>-/-</sup> mutants exhibit a loss of microglia in the optic tectum at 3 dpf.....	88

Figure A-7: *csf1ra* mutants display no difference in number of professional phagocytes in the periphery and spinal cord between 36 and 48 hpf.....92

Figure A-8: Increased cell death at 55 hpf in *csf1ra* embryos by acridine orange.....95

Figure A-9: *blb* mutants exhibit increased numbers of dying cells at 36 and 72 hpf by acridine orange.....101

Figure A-10: A subset of NCCs exhibit enlarged phagosomes in *blb* mutants.....105

Table A-1: Adjusted p values for multiple comparisons for Figure A-10C.....106

Figure A-11: NCC FYVE<sup>+</sup> phagosome volume data plotted as distributions.....109

Figure A-12: NCC sub-clusters in early development with *slc37a2* expression.....111

# CHAPTER 1: CLEARING YOUR MIND: MECHANISMS OF DEBRIS CLEARANCE AFTER CELL DEATH DURING NEURODEVELOPMENT

---

Kendra E. Liu<sup>\*,1,2</sup>, Michael H. Raymond<sup>\*,1,3</sup>, Kodi S. Ravichandran<sup>1,3,4,5</sup>, and Sarah Kucenas<sup>1,2,6</sup>

<sup>1</sup>Neuroscience Graduate Program, University of Virginia, Charlottesville, Virginia, USA

<sup>2</sup>Program in Fundamental Neuroscience, University of Virginia, Charlottesville, Virginia, USA

<sup>3</sup>Center for Cell Clearance, University of Virginia, Charlottesville, Virginia, USA

<sup>4</sup>Department of Microbiology, Immunology, and Cancer Biology, University of Virginia, Charlottesville, Virginia, USA

<sup>5</sup>VIB-UGent Center for Inflammation Research and the Department of Biomedical Molecular Biology, Ghent University, Ghent, Belgium

<sup>6</sup>Department of Biology, University of Virginia, Charlottesville, Virginia, USA

\*These authors contributed equally to this article.

2022 Annual Review of Neuroscience, 45:177-98, <https://doi.org/10.1146/annurev-neuro-110920-022431>

## 1.0 PREFACE

The contents of this chapter are largely from a published 2022 review in Annual Review of Neuroscience titled “Clearing Your Mind: Mechanisms of Debris Clearance After Cell Death During Neurodevelopment”<sup>1</sup>. The publication is co-first authored by Michael H. Raymond and I. The sections I contributed to are based on my area paper from 2021. I have updated the contents of this chapter to include relevant scientific findings published after the final submission of the article in December 2021 and added sections that were originally removed due to space.

## **1.1 ABSTRACT**

Neurodevelopment and efferocytosis have fascinated scientists for decades. How an organism builds a nervous system that is precisely tuned for efficient behaviors and survival and how it simultaneously manages constant somatic cell turnover are complex questions that have resulted in distinct fields of study. Although neurodevelopment requires the overproduction of cells that are subsequently pruned back, very few studies marry these fields to elucidate the cellular and molecular mechanisms that drive nervous system development through the lens of cell clearance. In this review, we discuss these fields to highlight exciting areas of future synergy. We first review neurodevelopment from the perspective of overproduction and subsequent refinement and then discuss who clears this developmental debris and the mechanisms that control these events. We then end with how a more deliberate merger of neurodevelopment and efferocytosis could reframe our understanding of homeostasis and disease and discuss areas of future study.

## **1.2 NEURODEVELOPMENT**

Efficient nervous system development involves intricately controlled cell-cell signaling, proliferation, cell death, and circuit pruning, all of which support organismal survival and reproduction. Timely debris clearance and the pruning and sculpting of cells and their connections are also integral parts of neurodevelopment. While neurodevelopment has been studied for decades, our knowledge on cell clearance during early neurogenesis is still limited. Recognition and clearance of apoptotic cells has largely been studied by immunologists, while neuroscientists have explored cell clearance in specific contexts (e.g., synaptic pruning). Thus, an effort to decipher debris and apoptotic cell clearance in the context of nervous system development is required. In this review, we introduce fundamental neurodevelopmental events shared among species and then explore the role of phagocytosis in shaping this development.

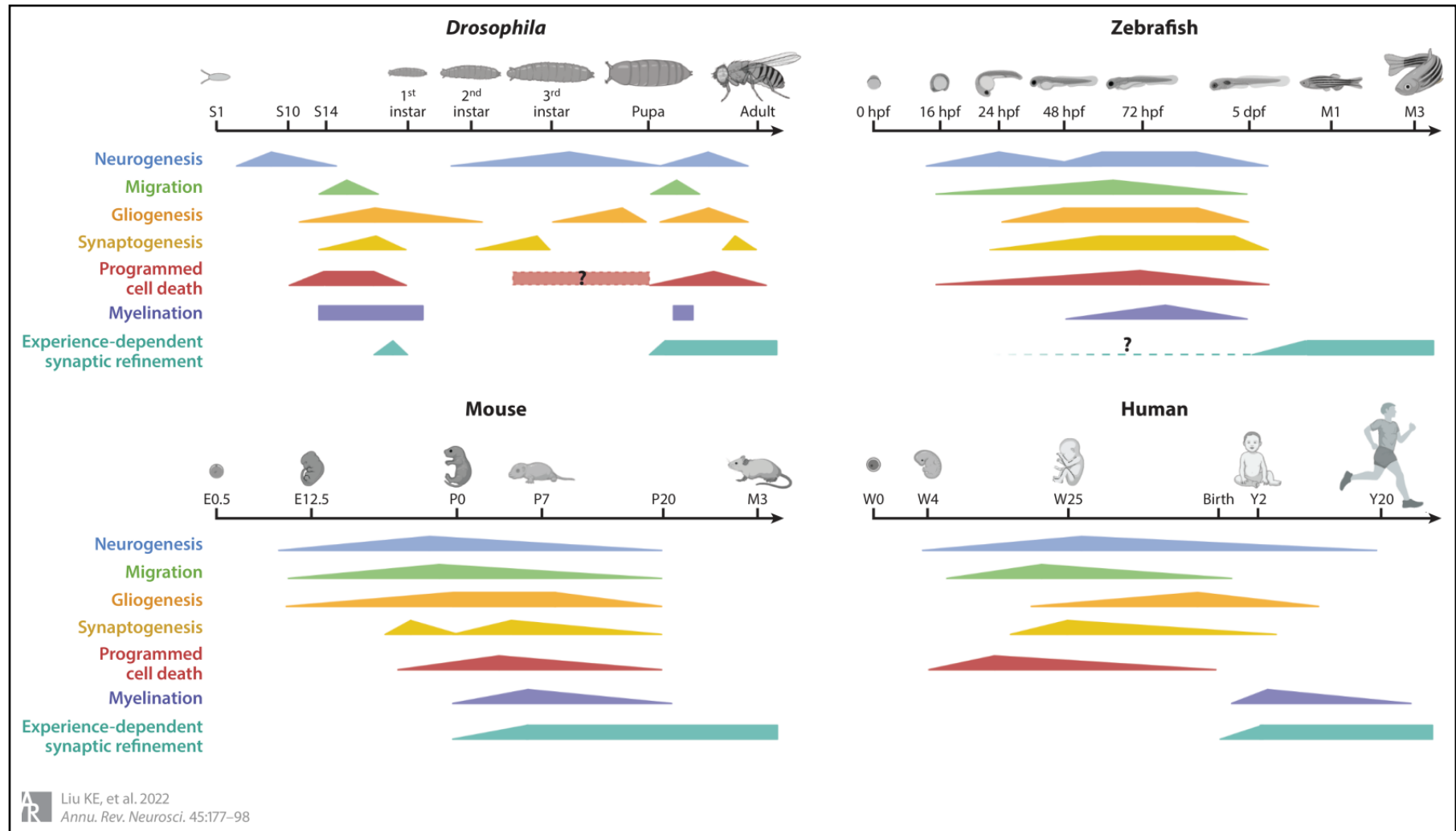


**Figure 1-1: Key developmental trajectories across species.** Developmental trajectories of *Drosophila*, zebrafish, mouse, and human are shown, with approximate timing and relative intensity reflected. Axonal myelination (vertebrates) and ensheathment (*Drosophila*) perform similar functions by creating a microenvironment capable of propagating action potentials along axons. Here (for simplicity) this process is referred to as myelination. Organisms are not to scale. Abbreviations: dpf, days post fertilization; E, embryonic day; hpf, hours post fertilization; M, month; P, postnatal day; S, stage; W, gestational week; Y, year. Figure adapted from image created with BioRender.com. Based on data from: Bai & Suzuki (2020), Baines & Bate (1998), Bin & Lyons (2016), Blauth et al. (2010), Boulanger-Weill & Sumbre (2019), Cantera et al. (2014), Chen et al. (2016), J. Chen et al. (2020), Cole & Ross (2001), Harris & Whittington (2001), Jacobson et al. (2018), Kim et al. (2008), Miyares & Lee (2019), Muthukumar et al. (2014), Pereanu et al. (2005), Pinto-Teixeira et al. (2016), Pop et al. (2020), Pressler & Auvin (2013), Rocha et al. (2020), Schepanski et al. (2018), Schmidt et al. (2013), Silbereis et al., 2016, Singh & Singh 1999, Tebbenkamp 2014, Xie 2019

### 1.2.1 Neurodevelopmental Timing and Trajectories

The developmental over-proliferation of neural cells and synaptic connections (called neural exuberance) was first described in the visual cortex, where exuberant projections into the corpus callosum were identified in kittens but not in adult cats<sup>2</sup>. Neural exuberance occurs at extraneous or transient axons (macroscopic) and at temporary branches or synapses within a confined cortical territory (microscopic). In multiple vertebrate species, both macro- and micro-exuberance are seen throughout the brain<sup>2</sup>. After neurogenesis begins, neurons quickly start making synaptic connections<sup>3</sup> (Figure 1-1). In teleost fishes, synaptic density increases sharply after hatching and correlates with early behavior (e.g., hatching, free swimming, acquiring visual acuity)<sup>4</sup>. In primates, synaptogenesis and synaptic density vary depending on brain region and age, suggesting that developmental trajectories are region specific<sup>5,6</sup>.

Recent studies highlight the importance of glia in synapse formation, pruning, and elimination. In *Drosophila melanogaster*, astrocyte-like glial infiltration of the neuropil is pro-synaptogenic<sup>7</sup>; in *Caenorhabditis elegans*, glia promote synapse formation between interneurons and control synaptogenesis during post-developmental growth<sup>8,9</sup>. Microglial contact induces pyramidal neuron dendrites to form filopodia and subsequently synapses<sup>10</sup>, and learning-dependent synapse formation is promoted through microglial brain-derived neurotrophic factor (BDNF)<sup>11</sup>, with a critical relationship between glia and synapse formation<sup>12,13</sup>.

The neural and synaptic exuberance observed in early development is regulated, as the number of cells and synapses decreases until reaching a homeostasis that is maintained throughout adulthood<sup>2</sup> (Figure 1-1). Death of exuberant cells can arise from both availability and competition for neurotrophic factors, growth factors, and neural activity<sup>14</sup>. This elimination occurs throughout the central and peripheral nervous systems (CNS and PNS) and is vital for neurodevelopment and circuit maturation and refinement<sup>15</sup>. In mouse models lacking key proapoptotic genes, pups were infertile or died perinatally<sup>16</sup> whereas a cell-specific knockout of pro-apoptotic factor *Bax* in Cajal-Retzius cells resulted in increases in dendrite complexity, spine density, memory deficits, and seizure susceptibility<sup>17-19</sup>. In contrast, other studies indicate that the survival of exuberant cells results in grossly normal development<sup>16</sup>. Some of these inconsistencies likely arise from species- and strain-specific differences<sup>20</sup>

and/or a threshold for tolerance and plasticity. In fact, many neural diseases (e.g., lissencephaly, Nasu-Hakola disease) and psychiatric disorders (e.g., autism spectrum disorder [ASD], schizophrenia) are linked to imbalances in key neurodevelopmental trajectories (e.g., neurogenesis, migration, myelination, synaptogenesis and pruning), yet many patients survive<sup>21-23</sup>. These observations demonstrate the importance of regulated early developmental trajectories during neurodevelopment.

## **1.2.2 Cell Death in Neurodevelopment**

Neurodevelopmental exuberance is corrected through the conserved process of programmed cell death (PCD)<sup>24</sup>. The most common form of PCD is caspase-dependent apoptosis, which is immunologically silent compared to other forms of cell death that are proinflammatory such as pyroptosis<sup>25</sup>. PCD has been detailed in multiple model organisms, with important studies in *Drosophila* and *C. elegans*. However, many questions remain.

### **1.2.2.1 How is cell survival or death determined, and what triggers programmed cell death?**

In most models, PCD within neural populations starts during embryogenesis<sup>16,26,27</sup> (Figure 1-1). Developmental apoptosis is a mechanism for regulating population size, removing cells for transient developmental functions, correcting errors, optimizing synaptic connections, and facilitating morphogenesis and is triggered by intrinsic or extrinsic signals (e.g., DNA damage, endoplasmic reticulum stress, decrease in survival factors or death ligands and receptors)<sup>28</sup>. During neurodevelopment, regressive events are facilitated in part by long-distance signaling through death receptors<sup>29</sup>. Phagocytosis itself can also trigger neurite degeneration and neuronal apoptosis<sup>30,31</sup>. Huge waves of apoptosis occur in cell populations to facilitate morphogenesis and tissue and organ sculpting, and in *Drosophila* apoptosis can induce nonautonomous apoptosis that relies on the TNF pathway<sup>32</sup>. Thus, continual, efficient clearance of apoptotic cells and debris is needed to avoid inflammation, autoimmunity, and uncontrolled spreading of apoptosis<sup>33,34</sup>.

### 1.2.2.2 Why are some cell populations generated only to die?

Interestingly, studies suggest an internal clock, where cells that were scheduled to die during development still died when grown *in vitro* or transplanted elsewhere in the brain<sup>35,36</sup>. To address whether the survival of cells destined to die affects development in *C. elegans*, loss-of-function mutants for proapoptotic genes *ced-3*, *ced-4*, and *egl-1* were generated, but there were no apparent defects. However, loss of *ced-9* (murine BCL2) resulted in embryonic lethality due to widespread ectopic cell death<sup>16</sup>. In *Drosophila* and mice, blocking proapoptotic genes during neurodevelopment produces variable results ranging from no observable phenotypes to multisystem defects and lethality<sup>20,37</sup>. While PCD is highly conserved, there are populations of cells that undergo PCD in one model but not another; spinal interneurons and retinal photoreceptors undergo PCD in mammals but not in birds<sup>16</sup>. Remarkably, the importance of PCD in neural tube closure varies between species, as PCD is required in chick embryos<sup>38</sup> but dispensable in mice<sup>39</sup>. Even within one species (mice), global knockouts of proapoptotic genes show strain-specific results ranging from no observable effects to perinatal lethality<sup>20</sup>. Although region-specific temporal patterns of PCD are observed, there is no consensus on whether PCD is necessary for neurodevelopment.

Several recent studies have addressed this question by examining the atypical survival of specific cell populations known to undergo PCD. In *C. elegans*, persisting RIM sister neurons structurally and functionally synapse onto wild-type circuits, resulting in changes in locomotor behavior<sup>40</sup>. In *Drosophila*, “undead” olfactory sensory neurons electrically respond to odorants and integrate into upstream glomerular organizing centers. Differences in the PCD of olfactory sensory neurons may explain the evolutionary variations observed in carbon dioxide-sensing<sup>41</sup>. One of the more convincing lines of evidence that PCD of specific cell populations is required for normal development stems from studies on Cajal-Retzius cells. In mammals, Cajal-Retzius cells are amongst the earliest born cortical neurons (appearing as early as embryonic day [E] 10.5 in mice<sup>42,43</sup>) and undergo extensive activity-dependent PCD during the second postnatal week<sup>17</sup>. Inhibiting PCD in Cajal-Retzius neurons results in the atypical survival of electrophysiologically immature Cajal-Retzius neurons up to postnatal day 24<sup>17</sup>. These surviving Cajal-Retzius neurons result in cellular (increased dendrite complexity, spine density, and interneuron number), functional (imbalanced excitation/inhibition, attenuated theta oscillations, and enhanced

gamma activity), and behavioral changes (impaired hippocampus-dependent memory and increased susceptibility to seizures in adulthood). Although some changes were only transiently observed during the establishment of juvenile circuitry (e.g. interneuron number returned to control levels in adulthood), the abnormal persistence of Cajal-Retzius neurons leads to functional and behavioral consequences observed in adulthood.<sup>18,19</sup> These recent findings make a convincing argument that PCD of certain cell populations is required for normal neurodevelopment, but other studies are needed to further explore the necessity and importance of PCD. Altogether, there is limited consensus on whether PCD (at a regional or cellular level) is required for normal neurodevelopment.

This is in part due to the difficulty of observing debris clearance, as apoptotic cells are efficiently cleared by phagocytes<sup>34</sup>. Additionally, disruptions in proapoptotic genes are classically studied in the context of whole-organism mutations, even though PCD is tightly regulated both spatially and temporally<sup>44</sup>. Improvements in genetic tools using cell population specific markers have been integral in furthering our understanding of PCD in development. Advances in imaging techniques have enabled visualization of apoptosis and engulfment, but these examinations are not frequently studied in the context of early neurodevelopment. Finally, there are different types of cell death (ferroptosis, necroptosis, pyroptosis) distinct from PCD<sup>45</sup>, and neurodevelopmental refinement may involve additional types of cell death<sup>46</sup>.

### **1.2.3 Synaptic Refinement and Elimination**

In addition to neurodevelopmental PCD, synapses undergo a process of elimination and pruning, which was first observed in geniculocortical visual afferents<sup>47</sup>. Synaptic pruning is not restricted to development and is a crucial process for learning, memory, and circuit refinement throughout life<sup>23,48</sup> (Figure 1-1). Key receptors for glial engulfment of debris (draper and CED-3) are necessary for pruning in *Drosophila*<sup>49</sup> and *C. elegans*<sup>50</sup>. In mice, signaling through microglial CX3CR1 contributes to postnatal thalamocortical synapse development<sup>51</sup>, experience-dependent refinement in visual cortices<sup>52</sup>, and hippocampal synapse development<sup>48</sup>. In the dorsal lateral geniculate nucleus, microglia exhibit activity- and complement-dependent engulfment of synapses<sup>53</sup> and can alter retinogeniculate connectivity<sup>54</sup>. Type 1 interferon (IFN-1)-responsive microglia engulf neurons in the

developing somatosensory cortex and can affect excitatory/inhibitory balance and tactile sensitivity<sup>55</sup>. The astrocyte phagocytic receptors MEGF10 and MERTK are also linked to synapse elimination of retinal ganglion cell synapses<sup>56</sup>.

### **1.3 MAJOR PHAGOCYTES DURING NERVOUS SYSTEM DEVELOPMENT**

We are beginning to appreciate the variety of phagocytes that clear cellular debris or whole cells during the development of neuronal circuitry and maintenance of homeostasis within the CNS and PNS. While phagocytes share properties, they are also unique in their location and function. Phagocytes come in three broad flavors: professional, which clear cells and debris routinely and voraciously (macrophages, microglia); nonprofessional, which can engulf but are limited in their capacity and efficiency (fibroblasts and mesenchymal cells)<sup>57,58</sup>; and specialized, which perform unique types of phagocytosis (retinal pigmented epithelial cells [RPEs]).

#### **1.3.1 Microglia**

Microglia, which arise from yolk sac progenitors and colonize the CNS beginning at E9.5–10.5 in mice and approximately 35 hours postfertilization (hpf) in zebrafish<sup>59,60</sup>, are the tissue-resident phagocytes who sense, respond to, and influence neurodevelopment<sup>61,62</sup>. These professional phagocytes arrive within the developing CNS before the onset of rapid neurogenesis within the cortex and adopt a high degree of heterogeneity<sup>63,64</sup>. Microglia are critical for clearing neuronal cells during development and postnatal neurogenesis<sup>65–68</sup>. In zebrafish, colonization of the CNS coincides with waves of neural precursor apoptosis<sup>69</sup>, and removal of microglia results in aberrant neuronal connectivity<sup>70,71</sup>. During development, microglia also prune non-neuronal cells, including oligodendrocyte progenitor cells<sup>72</sup> and astrocytes<sup>73</sup> (Figure 1-2). Axon-tract-associated microglia accumulate at cortical boundaries, are highly phagocytic, and maintain structural integrity during brain morphogenesis<sup>74</sup>. Thus, microglia act as both sentinels and sculptors of the CNS.

To facilitate efferocytosis, microglia express a variety of receptors and downstream signaling cascades. Transcriptional analysis of the cerebellum and developing white matter identified subsets of phagocytic microglia

that exist in a primed state to respond to high levels of cell turnover<sup>75</sup>. Microglia use phosphatidylserine (PtdSer) receptors to bind to and internalize apoptotic cells<sup>76</sup> (Supplemental Tables 1-1–1-3). In particular, TAM family members (Tyro3, Axl, MerTK) are implicated in microglia-mediated clearance of apoptotic cells<sup>77</sup>. A recent study also implicates Jedi-1/MEGF12 in microglial phagocytosis in the mouse ventricular-subventricular zone<sup>67</sup>. Additionally, microglia can also promote cell death and clearance, both initiating death and clearing the dead<sup>78</sup>. How microglia use different PtdSer receptors for efferocytosis or trogocytosis, a type of partial engulfment<sup>79</sup>, is unknown. Lastly, microglia can also alter synapses and neural connectivity through non-phagocytic mechanisms<sup>54,80</sup>.

Microglia also shape neuronal development beyond the physical removal of cells. Interestingly, secreted factors from microglia modulate the rate of neurogenesis and neuron survival<sup>81,82</sup>. These studies suggest that microglia serve as an important relay between the removal and maintenance of neurons. When this process is disturbed by the elimination of Slc37a2, microglia display enlarged phagosomes and reduced corpse resolution<sup>83</sup>. In conclusion, microglia function as primary phagocytes within the CNS and shape neurodevelopment.

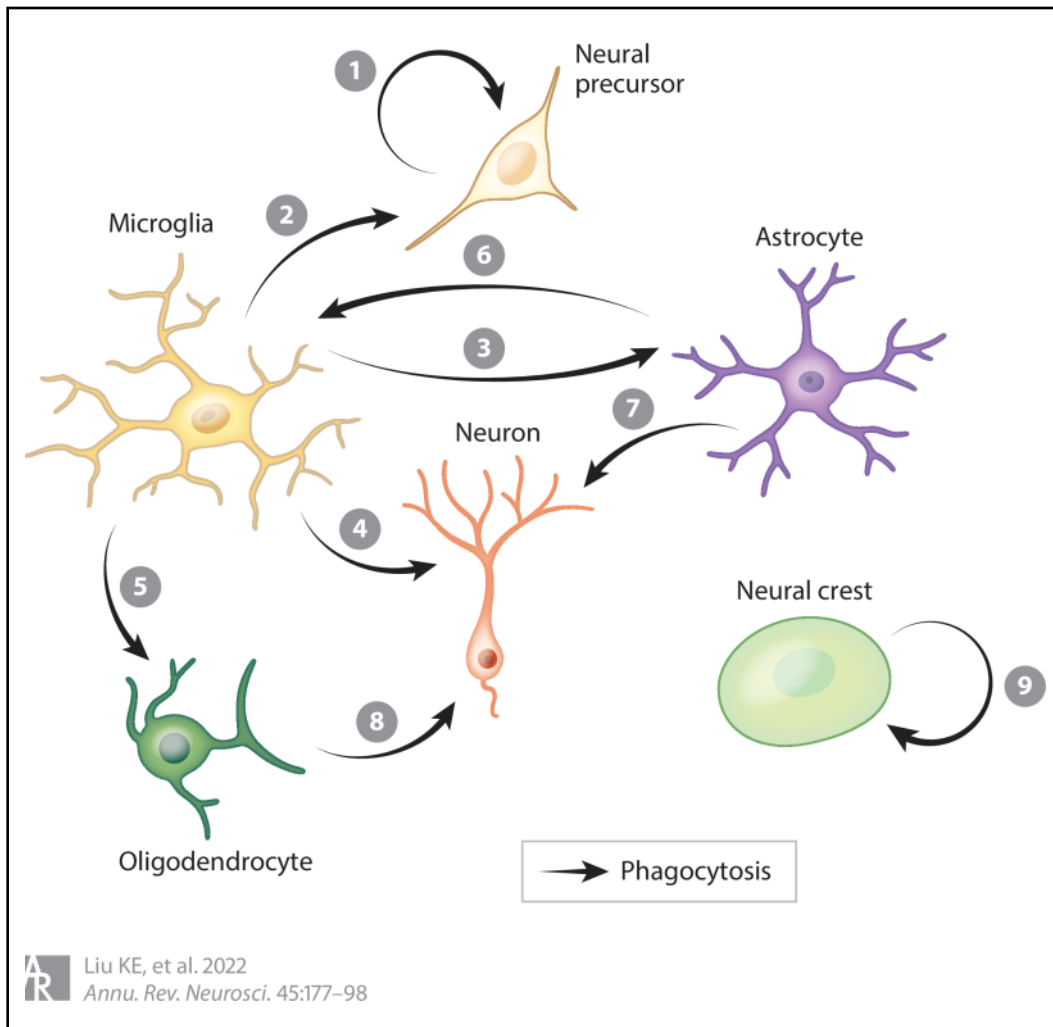


**Figure 1-2:** The central nervous system (CNS) food network. The CNS is host to a diverse network of cells, many of which regulate the form and function of the CNS through cell clearance. To date, several phagocyte and target cell relationships have been identified in vivo. Beginning with neural precursor cells, they have been identified to phagocytose their neighbors (1) (Lu et al. 2011), in addition to serving as a target for microglia (2) (Sierra et al. 2010). Microglia can regulate the abundance of astrocytes (3) (VanRyzin et al. 2019). Astrocytes have been demonstrated to remove microglia (6) (Konishi et al. 2020) and sculpt neurons (4) (Cunningham et al. 2013), and oligodendrocytes (5) (Hagemeyer et al. 2017, Nemes-Baran (8) (Buchanan et al. 2021). Neural crest cells (NCCs) have been demonstrated to remove other NCCs (9) neurons (7) (Chung et al. 2013, Lee et al. 2021). Oligodendrocytes have been found to internalize neurons (Zhu et al. 2019). These examples underscore the breadth of the phagocytic network within the CNS and draw attention to the unknown, missing links between phagocyte nodes. Figure adapted from image created with BioRender.com.

### 1.3.2 Macrophages

The function and ontogeny of CNS macrophages, which comprise a small fraction of total cells, is an area of intense investigation. CNS macrophages consist of meningeal, choroid plexus, perivascular, and border-associated macrophages<sup>84</sup>. Reservoirs of monocyte-derived precursors can supply the CNS during experimental conditions and certain periods of development, adding layers of spatial and functional heterogeneity to the CNS macrophage compartment<sup>85,86</sup>. The meninges are also an active site of monocyte development with well-defined roles in disease, furthering the breadth of monocyte involvement in the CNS<sup>87</sup>, albeit development is relatively less explored.

During *Drosophila* embryonic development, macrophages serve to remove developmentally generated apoptotic cells within the CNS<sup>88</sup>. This is important for proper organismal homeostasis and for mounting immune responses<sup>89,90</sup>. These macrophages use multiple phagocytic mechanisms to efficiently clear dying cells in the CNS<sup>91</sup>. Harnessing the genetic tractability of *Drosophila* to explore the efferocytic role of macrophages during embryonic CNS development could provide crucial new insights.

### 1.3.3 Astrocytes

Astrocytes are well known for their roles in development and disease, and immunological roles for them in the CNS are emerging. In mice, regional disruption of astrocytes alters the number of excitatory synapses, suggesting a link to the maintenance of circuitry<sup>92</sup>. Interestingly, when compared to microglia, astrocytes can surpass microglia during later stages of lateral geniculate nucleus developmental clearance and require MEGF10 and MerTK<sup>56</sup> (Supplemental Tables 1.1–1.3). MEGF10 is also important for the clearance of apoptotic neurons within the developing cerebellum<sup>93</sup>. Astrocyte phagocytosis of synapses by MEGF10 is implicated in ocular dominance plasticity during development<sup>94</sup>. Astrocytes also shape adult hippocampal circuitry, with MEGF10 deficiency resulting in altered hippocampal memory formation<sup>95</sup>. *Drosophila* astrocytes also exhibit a high rate of efferocytosis in the developing CNS. In the pupal neuropil, the astrocytes transition into phagocytes and engulf neural debris and synaptic material<sup>31</sup>. This engulfment requires the receptor Draper and downstream proteins

Mbc and dCed-12 (mammalian Dock1 and Elmo, respectively). The extent to which astrocytes can survey and sculpt both neuronal circuitry and apoptotic cells as key phagocytes remains to be clarified.

### 1.3.4 Retinal Pigment Epithelial Cells

Lining the rear of the retina is a specialized phagocyte, the RPE, which is responsible for engulfing photoreceptor outer segments (POSs) daily<sup>96</sup>. This clearance rhythm is necessary for retinal health, and defects in the PtdSer receptor MerTK result in a progressive form of blindness<sup>97</sup>. RPEs engage POSs akin to phagocyte and apoptotic cell interactions<sup>98</sup> and use several distinct receptors, including MerTK, integrins, and scavenger receptors<sup>99,100</sup>. Furthermore, POSs display PtdSer in a diurnal pattern, signaling the RPEs to engulf them in an orderly fashion<sup>98</sup>. In addition, RPEs are postmitotic and are not replaced through the life of an organism; thus, mechanisms by which RPEs handle the significant metabolic burden and repeat this exercise throughout life are fascinating and relevant for retinal diseases.

### 1.3.5 Oligodendrocyte Progenitor Cells

Oligodendrocyte progenitor cells (OPCs) are a glial population arising from the neuroepithelium and populating the developing CNS from E12.5 to E15 in mice and 36 to 55 hpf in zebrafish<sup>101,102</sup>. OPCs have been recently recognized as non-professional phagocytes. OPCs express genes associated with phagocytosis<sup>103,104</sup> (e.g. LRP1, *Mertk*, *Ptprj*, *Rap1gap*, *Xrkr4/6*) and OPCs within the visual cortex harbor neuronal material<sup>104,105</sup> and synapses<sup>103</sup>, demonstrating their engulfment ability *in vivo*. Sophisticated imaging and focal-ablation techniques in both zebrafish and mice have also revealed that OPCs regulate axon remodeling<sup>105</sup> and polarize toward the site of neuronal apoptosis and extend processes into the spatial void<sup>106</sup>. This presents an intriguing hypothesis that OPCs can sense and respond to cell death, and their role in homeostatic clearance and synaptic engulfment remains to be evaluated.

### 1.3.6 Schwann Cells

In the PNS, the role of myelinating glia in debris clearance contrasts starkly with what is known in the CNS. During development, perisynaptic Schwann cells (PSCs) engulf axosome debris and eliminate exuberant synapses at the neuromuscular junction (NMJ)<sup>107–110</sup>. Deletion of Schwann cells causes a decrease in NMJ synapses and motor neuron death<sup>111</sup> while ablation of PSCs specifically results in reduced NMJ growth<sup>112</sup>. While phagocytic PSCs play a critical role in NMJ development, studies have also explored the role of Schwann cells in peripheral nerve injury and Wallerian degeneration. Upon peripheral axon injury, Schwann cells are observed to break down and engulf myelin<sup>113</sup>. Schwann cells are joined by MΦ in the later stages of Wallerian degeneration which aid in myelin phagocytosis<sup>114,115</sup>. We now know that Schwann cells clear myelin by TAM receptor-mediated phagocytosis and selective autophagy<sup>116–118</sup>. After injury, responding Schwann cells upregulate phagocytic receptors Axl and Mertk, which are also used by phagocytes in other tissues (e.g. astrocytes in the brain<sup>56</sup> and retinal pigment epithelial cells in the retina<sup>119</sup>). Another type of glia to respond in peripheral nerve injury are perineurial glia, which are recruited to sites of injury by Schwann cells to phagocytose myelin and form bridges across the damaged axon to stimulate regrowth<sup>120</sup>. Although the full impact of phagocytic Schwann cells on the PNS is not yet understood, studies have established the importance of Schwann cell phagocytosis in peripheral nerve growth, maintenance, and injury.

### 1.3.7 Satellite Glial Cell Precursors

Satellite glial cells (SGC) are neural crest-derived glia that enwrap neuronal cell bodies in peripheral ganglia<sup>121</sup>. SGC precursors are the primary responding phagocyte for apoptotic cell clearance in the developing murine dorsal root ganglia<sup>122</sup> and human trigeminal ganglia<sup>123</sup>. These precursors phagocytose dying DRG neurons by engulfment receptors Jedi-1 and MEGF10 (mammalian homologues to *C. elegans* CED-1)<sup>122</sup>. SGC precursors utilize internal mechanisms similar to professional phagocytes; apoptotic cells and debris accumulated in LAMP-1<sup>+</sup> lysosomes<sup>122</sup>. Jedi-1 null mice exhibit aberrant neuronal DRG activity<sup>124</sup>, suggesting that phagocytic activity through Jedi-1 is necessary for appropriate neural function.

### 1.3.7 Neural Precursor Cells

Neural precursor cells (NPCs) give rise to both neurons and glia during development. Additionally, they execute efferocytosis during mouse development within neurogenic niches. Their phagocytic activity depends on the engulfment protein ELMO1 and disrupted phagocytosis of NPCs in Elmo1 null mice resulted in impaired hippocampal neurogenesis<sup>125</sup>. As this population of cells resides within neurogenic niches, their proximity to developmentally generated apoptotic cells positions them for rapid response. Whether NPCs exist as a unique population compared to their neighbors is currently unexplored.

### 1.3.8 Neural Crest Cells

Neural crest cells (NCCs) play a central role during development, giving rise to functionally distinct cell types. Remarkably, NCCs are phagocytic during early stages of zebrafish development (~24–36 hpf, before the presence of macrophages or microglia), exhibiting high levels of clearance and surveillance within the CNS and PNS<sup>126</sup>. Defining the targets of NCC phagocytosis, the response of NCCs during efferocytosis, and how phagocytic NCCs interact with incoming macrophages and microglia will be important to pursue. In considering the roles of these different phagocytes, with constantly improving *in vivo* approaches, our characterization of CNS phagocytes and their functional interplay will undoubtedly advance (Figure 1-2).

## 1.4 PATHWAYS OF CELL CLEARANCE

Recent works from multiple laboratories, in the context of mice, *Drosophila*, zebrafish, *C. elegans*, and humans, have given us a better appreciation for the phagocyte in its ability to balance numerous concurrent steps during the process of efferocytosis. Efferocytosis can be divided into three distinguishable steps that occur as a continuum. First, the phagocyte must identify and migrate toward the dying cell via sensing of soluble factors or “find me” signals released from dying cells<sup>127</sup>. Second, via surface receptors, the phagocyte engages apoptotic cells to initiate the clearance process<sup>34</sup>. Third, digestion occurs when the ingested corpse transitions through a series of intracellular phagosomal steps to degrade<sup>128</sup>. The digestion phase also includes the production and

release of anti-inflammatory mediators from the phagocytes that are important for making efferocytosis immunologically quiet.

### **1.4.1 “Find Me” Signals within the Central Nervous System**

During development and homeostasis, there is a high degree of cell turnover in tissues, yet apoptotic cells are rarely detectable experimentally. This is due to the rapid and efficient engulfment by phagocytes, which locate dying cells through “find me” signals. These signals are released during early stages of cell death (when the apoptotic cells are still intact) and facilitate the rapid and efficient recruitment of phagocytes. Only two “find me” signals are discussed here, but they have been reviewed extensively<sup>127</sup>.

#### **1.4.1.1 ATP and Pannexin-1**

During apoptosis, dying cells alert the environment via secreted and surface-displayed molecules. Of these, the release of ATP through the Pannexin-1 channel occurs in a regulated, caspase-dependent fashion<sup>129,130</sup>. Signals released from apoptotic cells are important for microglial colonization within the developing CNS<sup>69</sup>. Within active neurogenic niches and the subventricular (SVZ) and subgranular zones, Pannexin-1 also plays an important role in maintenance of the NPC pool, as removing Pannexin-1 from the NPC pool within the SVZ decreases the number of NPCs<sup>131</sup>. In zebrafish, NCCs are recruited to areas of cell death via IL-1 $\beta$  signaling<sup>126</sup>. Whether this is mediated by Pannexin-1 remains to be determined. Finally, recent work shows that a large collection of metabolites is secreted from apoptotic cells in a Pannexin-1-dependent manner<sup>132</sup>. Since metabolites have pleiotropic effects on surrounding cells, the role of these apoptotic metabolites during neurodevelopmental clearance could broaden the scope of find-me signaling in the CNS.

#### **1.4.1.2 Fractalkine**

Apoptotic cells can also undergo fragmentation and produce small extracellular vesicles and apoptopodia<sup>133</sup>. Within these vesicles is fractalkine, which is processed during apoptosis and helps to recruit macrophages via CX3CR1<sup>134</sup>. Fractalkine can also modulate microglial phenotype, including upregulation of machinery for PtdSer

recognition and microglial phagocytosis<sup>135</sup>. This signaling module could provide a local neuron to microglia axis to ensure efficient microglial removal of dying neurons.

## 1.4.2 “Eat Me” Signaling within the Central Nervous System

After responding phagocytes locate a dying cell, a different set of cues (“eat me” signals) help mediate the engagement between the phagocyte and apoptotic cell surfaces to begin engulfment. These signals begin to be exposed on the cell membrane of apoptotic cells and can either directly bind to receptors on phagocytes or bind bridging molecules that then engage receptors on phagocytes. A few of the “eat me” signals and their recognition are discussed below.

### 1.4.2.1 Phosphatidylserine

A canonical apoptotic cell ligand is PtdSer<sup>136</sup>. Typically found asymmetrically on the inner leaflet of the plasma membrane in healthy cells, PtdSer is flipped to the outer leaflet during apoptosis in a caspase-activated manner through the inactivation of flippases<sup>137,138</sup>. Once exposed, PtdSer recognition receptors on phagocytes bind to PtdSer either directly or via bridging molecules<sup>139</sup> (Supplemental Tables 1.1–1.3). PtdSer plays an important role in initiating efferocytosis in the CNS during development<sup>140,141</sup>.

The TAM family of phagocytic receptors (composed of the members Tyro3, Axl, and MerTK) uses bridging molecules Gas6 and Protein S to engage the apoptotic cell<sup>119</sup>. Mice lacking Axl and MerTK in microglia show elevated levels of apoptotic cells within the SVZ, implicating their importance<sup>77</sup>. Additional PtdSer receptors BAI1 and TIM4 play important roles for engulfment *in vivo* through their regulation of phagosome formation and stability, respectively<sup>76</sup>. Additionally, astrocytes use MEGF10 to bind C1q, a PtdSer binding molecule, to remove apoptotic neurons<sup>93</sup>. The context and consequences of PtdSer exposure will be important to decipher, as viable neurons aberrantly expose PtdSer upon accumulation of pathological proteins<sup>142</sup>.

#### 1.4.2.2 Calreticulin

Calreticulin (CRT) is an additional cell surface molecule, which is sensed by the phagocyte to initiate engulfment. Typically found in the endoplasmic reticulum, CRT translocates to the membrane during instances of cellular stress or death<sup>143</sup>. Phagocytes identify CRT through LRP1, which licenses engulfment signaling. However, CRT requires attenuation of “don’t eat me” signal CD47 at the cell surface<sup>144</sup>. Induced pluripotent stem cells carrying an autism-linked mutation had higher levels of CRT and inhibitory CD47, leading to excessive neuronal growth<sup>145</sup>.

#### 1.4.2.3 Complement

Often associated with immunological responses to pathogen- and damage- associated molecular patterns, the complement system assists in the removal of dendrites, synapses, and entire cells<sup>53,146,147</sup>. After deposition of complement onto the surface of a neuron, complement receptors engage with the cell for engulfment. Inhibition of complement deposition or blocking complement activity *in vivo* results in decreased neuronal pruning<sup>148–150</sup>. This plays a role in memory formation, as disruption of the complement system through CD55 resulted in preservation of memory and engram cells<sup>151</sup>. Thus, complement is a prime candidate for initiating neuronal sculpting during development and disease.

### 1.5 PROCESSING OF CLEARED CARGO BY CENTRAL NERVOUS SYSTEM PHAGOCYTES

Once a phagocyte has engaged an apoptotic cell through surface receptors, downstream signaling pathways are initiated, which ensure ingestion and digestion of the corpse. There are several pathways that converge on the activation of the GTPase Rac1, facilitating cytoskeletal rearrangement around the corpse<sup>89,152</sup>. A well-studied pathway is through the ELMO-Dock-Rac complex, which upon upstream activation leads to Rac activation and corpse internalization<sup>153,154</sup>. Upon sequestration of the apoptotic cell, the phagosome must be sealed through Dynamin-2<sup>128</sup>.

Following successful internalization, the corpse must be processed through a series of orchestrated steps to ensure corpse degradation<sup>128</sup>. The digestion process is thought to involve several sequential steps that include maturation of the phagosome and fusion with the lysosome. One pathway is via LC3 conjugation to the phagosome through Rubicon, PtdIns(3)P deposition, and NOX2 recruitment<sup>155</sup>. The LC3 digestive process results in macrophage skewing toward an M2-like state and suppression of interferon signaling<sup>156</sup>. To facilitate continual digestion, mitochondrial function plays an important role, with uncoupling protein 2 (Ucp2) being required in phagocytes for continual uptake as well as mitochondrial fission<sup>157,158</sup>. Furthermore, signals derived from the digested apoptotic cells promote increased uptake and lipid homeostasis, and are important for maintenance of an anti-inflammatory state<sup>159</sup>. Insight into these pathways during microglial efferocytosis implicated Annexin A1 in controlling PPAR $\gamma$  activation during neuronal engulfment<sup>160</sup>. In addition, signals derived from apoptotic cells are important for efficient phagocyte polarization, engulfment capacity, and digestion of cargo<sup>161,162</sup>. This final step of corpse resolution has been elegantly demonstrated *in vivo* where the solute carrier transporter Slc37a2 was identified as a key regulator of microglial phagosome function<sup>83</sup>. Mutations within these conserved pathways are implicated in CNS development and disease, adding to our understanding of this critical downstream process. Perturbations to any step within the orchestrated clearance process result in functional deficiencies, highlighting the multifaceted nature of efferocytosis.

## **1.6 CELL AND DEBRIS CLEARANCE IN DISEASE**

As discussed above, it is clear that cell death and cell clearance in the CNS are important during neurodevelopment. Further work has pointed to the assembly and refinement of neural circuitry in neurodevelopment as pivotal in the development of later-presenting neurodevelopmental and neuropsychiatric disorders. Also, many of the cellular processes key for neurodevelopment are found to be altered in neurodegenerative disorders. This section details a few of these disease contexts.

### 1.6.1 Neurodevelopmental and Neuropsychiatric Disorders

The linkage of phagocytosis in neurodevelopment to many disorders comes from mutations in genes associated with phagocytosis or genes integral to phagocyte function. Dendritic abnormalities, synaptic pruning, increased cellular debris, and neural excitatory/inhibitory imbalances are linked to multiple neural disorders<sup>23,163</sup>. While the implications of homeostatic phagocytic activity on the nervous system are just emerging, there are multiple disorders where abnormal phagocytosis is observed<sup>164</sup>.

ASD is a behavioral disorder characterized by varying severity of deficits in social behavior and linguistic abilities<sup>165</sup>. Multiple studies implicate abnormal microglial regulation of neuronal activity in ASD<sup>54,71</sup>, and postmortem ASD brains contain increased dendritic spine densities and increased microglial density and reactivity<sup>166,167</sup>. These microstructural differences result in aberrant callosal fiber length and cortex connectivity<sup>168,169</sup>. Mice lacking ATG7 (an enzyme critical for autophagy and vacuolar transport) recapitulate many of the micro- and macroscopic impairments observed in human ASD patients<sup>170,171</sup>. Loss of microglial MCT4 affects degradation of internalized cargo, resulting in defects in synaptic pruning, increased neuronal excitation, and anxiety-like behavior in mice<sup>172</sup>. Altogether, these experiments point to the dysregulation of synaptic pruning and neural connectivity refinement as a significant contributor to ASD severity. This is akin to patients with schizophrenia, a psychiatric disorder that commonly presents in patients 15–23 years old, when drastic changes in synaptic connectivity are occurring within the prefrontal cortex (PFC)<sup>173</sup>. Schizophrenia is thought to partly arise from developmental defects in synapse density and pruning, with postmortem studies revealing a decrease in PFC dendritic spine density<sup>174,175</sup>. Patients display decreased PFC gray matter volume, weakened connectivity across the brain, and abnormal protein expression levels associated with the Rac1 phagocytic pathway, suggesting exaggerated pruning in schizophrenia<sup>173,176</sup>. Thus, current hypotheses highlight the importance of synaptic pruning in maintaining the balance of excitatory and inhibitory neural connections, where aberrations can lead to disorders such as ASD or schizophrenia.

## 1.6.2 Neurodegenerative Disorders

Significant knowledge has been gained on debris clearance and phagocytosis in neurodegenerative disorders, particularly proteinopathies. Microglia in both Alzheimer's disease (AD) and Parkinson's disease (PD) associate with and engulf amyloid beta and Lewy bodies, respectively<sup>177,178</sup>. In genome-wide association studies, variants in genes associated with phagocyte function and migration, phagocytic receptors and adaptor proteins, and digestion of internalized debris are associated with increased risk of disease<sup>179</sup>. An early-onset progressive dementia called Nasu-Hakola arises from mutations in DAP12 (also called TYROBP) or TREM2<sup>180</sup>, which are linked to impaired microglial phagocytosis and accumulation of apoptotic neurons<sup>181</sup>. Coincidentally, dysfunctional DAP12 or TREM2 are also implicated in early AD and PD<sup>182</sup>.

Multiple sclerosis (MS), a CNS autoimmune and neurodegenerative disease, is characterized by an autoimmune attack on myelin sheaths, leading to myelin degeneration and eventual nerve damage. While the removal of myelin debris by microglia and macrophages is integral to promote repair<sup>183</sup>, these phagocytes also contribute to MS progression by presenting CNS-derived autoantigens and adopting an inflammatory phenotype<sup>184,185</sup>. *In vitro* studies suggest that MerTK is an essential receptor in myelin phagocytosis, and MS patient monocyte-derived macrophages express significantly lower levels of MerTK<sup>186</sup>. Thus, microglia and macrophages can act as double-edged swords: On the one hand, inhibiting their activities could potentially reduce presentation of autoantigens and the secretion of inflammatory mediators, yet on the other hand, enhancing their phagocytic activity to remove toxic debris could facilitate myelin repair<sup>182</sup>. This again highlights the importance of finely balanced phagocytosis in disease progression and that phagocyte functions are not unidimensional or static.

## 1.7 WHERE DO WE GO FROM HERE? CHALLENGES AND OPPORTUNITIES

### 1.7.1 Neurodevelopment: Immunologically Silent or Not?

The structural and cellular abundance during early development sets the stage for an intricate interplay between corpse and phagocyte, one which must be executed efficiently to ensure homeostasis. Overwhelming

evidence from a variety of non-CNS contexts suggests that developmental cell death and subsequent efferocytosis are largely anti-inflammatory. Yet, recent evidence suggests the presence of classical immunostimulatory cell death during CNS development<sup>46</sup>, adding yet another layer of complexity. Additionally, NCC recruitment to apoptotic cells is dependent on IL-1 $\beta$ <sup>126</sup>, a traditionally proinflammatory molecule. Evidence for induction of an inflammatory state within phagocytes is well-characterized, raising the question as to whether this inflammation-associated identity is a typical trajectory for all CNS phagocytes<sup>187,188</sup>. Considering these lines of evidence, a detailed analysis of phagocyte states during CNS development would further our understanding of how inflammatory cues might shape organismal growth and patterning. Furthermore, important future directions include the identity of the phagocytes that respond to these cues, whether their absence results in developmental deficits, and whether these mechanisms are region specific.

### **1.7.2 Phagocyte State versus Fate**

Phagocytosis has been long defined by immunologists and often studied via *in vitro* assays, with recent tools allowing for the visualization and quantification of phagocytosis *in vivo*. While our knowledge of phagocytes in the periphery informs our understanding of their function in the brain, the CNS is unique. The brain has been classically defined as an immune-privileged site; however, several discoveries such as meningeal lymphatic vessels<sup>189,190</sup> have revolutionized our understanding of the interface between the immune and nervous systems. Even more recently, data show that the meninges harbor a lymphopoietic niche capable of producing meningeal B cells, which could be important for maintaining tolerance against CNS-derived antigens<sup>191,192</sup>. With growing evidence that the brain and immune systems are linked, it would be interesting to think about how these systems may affect phagocytes in both the brain and periphery. Do phagocytes that are active in peripheral tissues act similarly in the brain? How does signaling from the immune system change the environment of the brain, and how does that affect brain-resident phagocytes? It is also unclear how different types of phagocytes respond to and process internalized debris, and there may be differing consequences. Emerging data point to phagocytosis as an active modulator of cell function rather than a passive process, as the secretome of phagocytic microglia was found to limit neurogenesis by driving neural progenitor cells toward a different fate compared to naïve

microglia *in vitro*<sup>82,193</sup>. Thus, phagocyte state and fate particularly may change and, in turn, affect responses within the CNS neighborhood.

### 1.7.3 Visualizing Cell Death and Phagocytosis *In Vivo*

Many of the biological processes discussed in this review occur at the cellular level and over timescales that would benefit from *in vivo* imaging paradigms. Central to *in vivo* imaging are fluorescent probes, both chemigenetic and fluorescent protein based, which permit cell- and tissue- specific labeling. Advancement of genetic tools to track caspase activity<sup>194</sup>, Annexin V<sup>195</sup>, calcium<sup>196</sup>, and acidification<sup>197</sup> has been instrumental in imaging cell death, removal, and tissue sculpting. Recently developed fluorescent reporters CharON and CharOFF allow for simultaneous visualization of both caspase activity and acidification<sup>198,199</sup>. An exciting development is the creation of chimeric phagocytic receptors which allow for unprecedented manipulation of phagocytic activity *in vitro* and *in vivo*<sup>200</sup>. Using these advanced genetic tools in combination with *in vivo* imaging will help answer questions related to cell death, removal, and tissue sculpting within the CNS during development and disease.

Zebrafish and *Drosophila* offer advantages to imaging, and these organisms would be good first choices for *in vivo* study of cell clearance before tackling more complex systems. Foundational work in these organisms will help build understanding of developmental cell clearance, providing insights on outstanding questions such as quantification of CNS cell death and clearance, identity of phagocytes during development, location of phagocytes during cell clearance, and mechanisms of cell clearance<sup>198</sup>. Previous work in zebrafish has identified locations of cell death machinery, periods of high cell turnover within the developing CNS, and the role of microglia and monocytes in clearing neuronal corpses during development<sup>69,201,202</sup>. In addition, several studies have employed live imaging to address phagocyte behavior during development, as well as identification of novel phagocyte populations<sup>76,126</sup>.

Mice are essential for understanding mammalian developmental cell clearance in homeostasis and disease. Imaging in mice has improved, and we highlight two techniques that permit long duration, live imaging. First,

advances in light-sheet imaging and computational analysis can be used to study *in toto* mouse gastrulation and early organogenesis<sup>203</sup>. Second, mouse embryonic development can be imaged from E9.5 to birth while tracking neural crest cell division by using sophisticated surgical and *in vivo* uterine window imaging techniques<sup>204</sup>. These exciting advances push the boundaries on what can be studied during mouse development and could provide a platform for the evaluation of cell death and cell clearance during mammalian neurodevelopment.

In conclusion, intimate and surprising links between the immune system and CNS development have emerged<sup>205</sup>. As maintenance of homeostasis is the most ancient and well-conserved role of the immune system, we must consider both regulated and coordinated cell death and efferocytosis as key contributors for developmental homeostasis of the CNS. Cell death and clearance is not a simple turnover process, as dying cells communicate with the surrounding microenvironment. The phagocytes that eat the dying cells then engage neighboring phagocytes and other cells in the environment, and finally, these shape the developing tissue as well as its subsequent homeostatic steady state. Emerging studies defining the key molecular players and pathways that control cell numbers within the CNS, maintain an anti-inflammatory state, and provide the right type of environment during development and disease are truly exciting. It is safe to say the research into these areas will provide plenty of food for thought.

## 1.8 SUPPLEMENTAL INFORMATION

**Supplemental Table 1-1:** *Drosophila* PtdSer Receptors. \*UMI count data reported by Davie et al., 2018<sup>206</sup>.

Gene Name	Cell Type	
	Hemocytes*	Ensheathing Glia*
Crq, Croquemort (CD36)	2.9	0.5
SIMU, Six-Microns-Under (Stab2)	12	0
Draper (Megf10)	1.6	1.08

**Supplemental Table 1-2:** Mouse PtdSer Receptors. \*FPKM data reported by Zhang et al., 2014<sup>207</sup>.

Gene Name	Cell Type				
	Microglia*	Astrocyte*	Endothelium*	OPC*	Oligodendrocyte*
MerTK	24.2	33.8	3.9	9.6	0.6
Tyro3	1.7	9.2	3	14.9	90.3
Axl	5.5	37.3	4.2	11.2	1.3
Bai1	3.4	43.9	0.2	61.4	13
Tim4	1.2	0.1	0.1	0.1	0.1
Stablin1	131.6	0.4	34.5	4.3	0.5
CD300b	1.9	0.1	0.1	0.1	0.1
$\alpha$ v	10	37	5.9	81	6
CD36	4	0.1	0.1	0.8	0.1
MEGF10	0.1	25.2	0.1	2.4	2.2
CD11b	371.6	0.2	0.1	29.4	4.5

**Supplemental Table 1-3:** Human PtdSer Receptors. \*FPKM data reported by Zhang et al., 2016<sup>208</sup>.

Gene Name	Cell Type			
	Microglia*	Astrocyte*	Endothelium*	Oligodendrocyte*
MerTK	35.9	32.8	4.7	3.1
Tyro3	0.1	2.8	0.7	3
Axl	30	25.5	3.1	3.4
Bai1	0.1	0.8	0.1	0.1
Tim4	0.9	0.1	0.1	0.1
Stablin1	1.5	0.1	0.1	0.1
CD300b	2	0.1	0.1	0.2
$\alpha v$	11.5	30	2.7	9.7
CD36	39.6	1.7	0.4	6.9
MEGF10	0.1	13.1	0.2	5.5
CD11b	19.4	0.3	0.1	1.4

## 1.10 ACKNOWLEDGEMENTS

In our attempt to write a concise, clear review on two overlapping scientific fields, we were not able to cite many studies that were integral to our knowledge today. Many of the reviews cited here include citations to foundational papers, and we encourage our readers to explore the cited reviews. The authors acknowledge the following funding sources: K.E.L. was supported by the Jefferson Scholars Foundation Fellowship (University of Virginia); S.K. was supported by grants from the National Institute of Neurological Disorders and Stroke (R01NS107525 and R21NS124164); and K.S.R. was supported by grants from the National Institute of General Medical Sciences (R35GM122542), the National Heart, Lung, and Blood Institute (P01HL120840), the National Institute of Allergy and Infectious Diseases (1R01AI159551), Chan Zuckerberg Initiative, FWO (Odysseus grant G0F5716N, EOS DECODE 30837538), and the European Research Council (835243).

## Chapter 2 MATERIALS & METHODS

---

### 2.1 FISH HUSBANDRY

All animal studies were approved by the University of Virginia Institutional Animal Care and Use Committee. Adult zebrafish were housed in tanks of 8–10 fish/L in 28.5°C system water. Pairwise mating of adult zebrafish generated zebrafish embryos for all experiments. The embryos were raised in egg water (0.3 g instant ocean sea salt per 1L of reverse osmosis water) in 100 mm Petri dishes (Fisher, cat. 08-757- 100B) and incubated between 28.5 and 30°C. Embryos used for experiments were staged by hours or days post fertilization (hpf or dpf, respectively) and by morphological features<sup>209</sup>. To minimize visual obstruction by pigmentation, egg water was replaced with 0.004% 1-phenyl-2-thiourea (PTU; Sigma cat. P7629) in egg water at 24 hpf for all imaging experiments. Tricaine-S (also called MS-222; The Pond Outlet MPN 15650) was utilized as an anesthetic for embryos and larvae used in live imaging and euthanasia. For all experiments, embryo and larvae sex were undetermined because sex cannot be defined until sexual maturity<sup>210</sup>.

### 2.2 ZEBRAFISH TRANSGENIC LINES

All details on the zebrafish strains and transgenic lines used in this study are summarized in Table 2-1. All transgenic lines described are stable and incorporated into the germline.

**Table 2-1: Descriptions and abbreviations of zebrafish lines used**

Full name	Abbreviation	Purpose	Reference Number
AB*	AB*	Wild-type background	ZIRC
<i>csf1ra</i> <sup>j4e1</sup>	<i>csf1ra</i> <sup>-/-</sup>	Mutant displaying loss of embryonic microglia	Parichy et al., 2000
<i>slc37a2</i> <sup>t30301</sup>	<i>blb</i> <sup>-/-</sup>	Mutant displaying impaired phagocytosis and digestion by microglia	Villani et al., 2019

<i>Et(e1b:GAL4-VP16)<sup>s1101</sup></i>	<i>Et(e1b:GAL4)</i>	Ubiquitous neuronal driver	Szobota et al., 2007
<i>gSAIzGFFD37A</i>	<i>Et(erbb3b:GAL4) Tg(UAS:EGFP)</i>	NCC marker	Brown et al., 2022
<i>Tg(GFAP:NTR-mCherry)<sup>scz129</sup></i>	<i>Tg(GFAP:NTR-mCherry)</i>	CNS parenchymal marker	Johnson et al., 2016
<i>Tg(mpeg1:EGFP)<sup>gl22</sup></i>	<i>Tg(mpeg1:EGFP)</i>	Macrophage & microglia marker	Ellett et al., 2011
<i>Tg(mpeg1:TagRFP)<sup>uva68</sup></i>	<i>Tg(mpeg1:TagRFP)</i>	Macrophage & microglia marker	Created here
<i>Tg(neuroD1:GAL4; cmlc2:EGFP)<sup>uva22</sup></i>	<i>Tg(neuroD:GAL4)</i>	Neuronal marker	Fontenas et al., 2019
<i>Tg(-3.1neurog1:GFP)<sup>sb2</sup></i>	<i>Tg(ngn1:GFP)</i>	Rohon-Beard marker	Blader et al., 2003
<i>Tg(-3.1neurog1:TagRFP)<sup>uva69</sup></i>	<i>Tg(ngn1:TagRFP)</i>	Rohon-Beard marker	Brown et al., 2024
<i>Tg(olig2:dsRed2)<sup>vu19</sup></i>	<i>Tg(olig2:dsRed)</i>	Oligodendrocyte marker	Kucenas et al., 2008 Nat Neuro
<i>Tg(sox10:eos)<sup>w9</sup></i>	<i>Tg(sox10:eos)</i>	NCC marker	Prendergast et al., 2012
<i>Tg(sox10:GAL4-VP16)<sup>sq9</sup></i>	<i>Tg(sox10:GAL4)</i>	NCC driver	Lee et al., 2013
<i>Tg(-4.9-sox10:TagRFP)<sup>uva5</sup></i>	<i>Tg(sox10:TagRFP)</i>	NCC marker	Zhu et al., 2019
<i>Tg(4xUAS:EGFP-FYVE)<sup>la214</sup></i>	<i>Tg(UAS:GFP-FYVE)</i>	PI(3)P lipid marker, enriched on endosomes and phagosomes	Rasmussen et al., 2015
<i>Tg(UAS:SEC-Hsa.ANXA5-YFP, myl7:RFP)<sup>f12</sup></i>	<i>Tg(UAS:secA5-YFP)</i>	Reporter for phosphatidylserine-expressing cells	Van Ham et al., 2010

## 2.3 GENERATION OF TRANSGENIC LINES

All constructs were created using the Tol2kit Gateway-based cloning system<sup>211</sup>. The following constructs were created through LR reactions (**Table 2-2**): *Tg(elavI3:CharON; cmlc2:EGFP)*, *Tg(mpeg1:CharON)*, *Tg(mpeg1:EGFP-CAAX; cmlc2:EGFP)*, *Tg(mpeg1:GAL4; cmlc2:EGFP)*, and *Tg(mpeg1:TagRFP-CAAX)*. The *Tg(mpeg1:TagRFP)* construct was previously created by Yunlu Zhu. Some of the resulting constructs were

amplified and validated by Sanger sequencing to confirm correct insertion. All Sanger sequencing described in this dissertation was conducted through GENEWIZ (Azenta Life Sciences; <https://www.genewiz.com/en>). To generate stable transgenic lines, constructs were microinjected at 20 ng/μL in combination with 100 ng/μL *Tol2* transposase mRNA into AB\* embryos at the one-cell stage. The injected embryos were then screened for founders<sup>212</sup>.

For creating the *Tg(mpeg1:TagRFP)* line, the F1 generation was crossed to *Tg(mpeg1:EGFP)*<sup>213</sup> (an already established line) and the resulting F2 embryos were mounted for confocal imaging. These F2 embryos displayed EGFP<sup>+</sup>, TagRFP<sup>+</sup>, and EGFP<sup>+</sup>/TagRFP<sup>+</sup> microglia and macrophages. The F1 tank chosen to continue creating a stable line had F2 embryos where there was near 100% EGFP<sup>+</sup>/TagRFP<sup>+</sup> microglia and macrophages with no ectopic expression.

**Table 2-2: Constructs and vectors used**

Construct	pDest	p5E	pME	p3E	Injected?	Stable Line?
<i>Tg(elavl3:CharON; cmlc2:EGFP)</i>	pDestTol2CG2 <sup>211</sup>	p5E-elavl3 <sup>214</sup>	pME-CharON <sup>198</sup>	p3E-polyA <sup>211</sup>	<input checked="" type="checkbox"/>	<input checked="" type="checkbox"/>
<i>Tg(mpeg1:CharON)</i>	pDestTol2CG2 <sup>211</sup>	p5E-mpeg1.1 <sup>213</sup>	pME-CharON <sup>198</sup>	p3E-polyA <sup>211</sup>	<input checked="" type="checkbox"/>	<input type="checkbox"/>
<i>Tg(mpeg1:EGFP-CAAX; cmlc2:EGFP)</i>	pDestTol2CG2 <sup>211</sup>	p5E-mpeg1.1 <sup>213</sup>	pME-EGFP-CAAX <sup>211</sup>	p3E-polyA <sup>211</sup>	<input type="checkbox"/>	<input type="checkbox"/>
<i>Tg(mpeg1:GAL4; cmlc2:EGFP)</i>	pDestTol2CG2 <sup>211</sup>	p5E-mpeg1.1 <sup>213</sup>	pME-EGFP-CAAX <sup>211</sup>	p3E-polyA <sup>211</sup>	<input checked="" type="checkbox"/>	<input checked="" type="checkbox"/>
<i>Tg(mpeg1:TagRFP)</i>	pDestTol2pA <sup>211</sup>	p5E-mpeg1.1 <sup>213</sup>	pME-TagRFP <sup>214</sup>	p3E-polyA <sup>211</sup>	<input checked="" type="checkbox"/>	<input checked="" type="checkbox"/>
<i>Tg(mpeg1:TagRFP-CAAX; cmlc2:EGFP)</i>	pDestTol2CG2 <sup>211</sup>	p5E-mpeg1.1 <sup>213</sup>	pME-TagRFP-CAAX <sup>215</sup>	p3E-polyA <sup>211</sup>	<input checked="" type="checkbox"/>	<input type="checkbox"/>

## 2.4 *csf1ra*<sup>-/-</sup> IDENTIFICATION

Crosses containing *csf1ra*<sup>+/+</sup>, *csf1ra*<sup>+/-</sup>, and *csf1ra*<sup>-/-</sup> embryos were genotyped to identify *csf1ra*<sup>-/-</sup> embryos after imaging. Embryos were carefully removed from mounting agarose and digested using HotSHOT DNA preparation<sup>216</sup> to isolate genomic DNA. Genomic DNA was used in PCR to synthesize a 203 base pair (bp) amplicon using a forward primer 5'-GTAGGGAAGACTCTTGGTGCTGG-3' and a reverse primer 5'-GCAAACCTTG CAGAGCTGTG-3' targeted to *csf1ra* genomic sequence ( $T_a = 56^\circ\text{C}$ ). A restriction digest was run on the 203 bp amplicon using the BssSI-V2 enzyme (NEB, cat. R0680S). The restriction digest was incubated for 75 to 90 minutes at 37°C before running on a 2% agarose (Sigma-Aldrich, cat. A9539) gel at 100 volts. *csf1ra*<sup>+/+</sup> and *csf1ra*<sup>+/-</sup> embryos retain the BssSI cut site and after successful digestion the 203 bp amplicon is cut into 83 and 120 bp segments. *csf1ra*<sup>-/-</sup> embryos lose the BssSI cut site due to a V614M substitution<sup>217</sup> and maintain the 203 bp amplicon.

## 2.5 *blb*<sup>-/-</sup> IDENTIFICATION

Starting at 4 dpf, *blb*<sup>-/-</sup> embryos are identifiable by “bubble” microglia in the brain<sup>83</sup> and visible by eye with white light through a Zeiss Stemi 2000 stereomicroscope with a transmitted light mirror base. Embryos where bubble microglia were not easily identified were not identified as *blb*<sup>-/-</sup>. In the studies reported here, WT and *blb*<sup>+/-</sup> embryos were combined as there is no reported and observed heterozygous phenotype. In some experiments (not shown here), WT and *blb*<sup>+/-</sup> embryos were distinguished by sequencing.

## 2.6 MOSAIC LABELING BY MICROINJECTION

Expression vector *ngn1:TagRFP* was microinjected (20 ng/μL) with *Tol2* transposase mRNA (20 ng/μL; mRNA synthesis described in 'Generation of synthetic mRNA') at the one-cell stage<sup>212</sup>. Red dye was also added to aid in injection visualization. Injected embryos were screened for RFP expression in the dorsal spinal cord at 24 hpf.

## 2.7 *IN VIVO* CONFOCAL IMAGING

All embryos imaged between 24 hpf and 5 dpf were immersed in 0.004% PTU in egg water starting at 24 hpf to mitigate pigmentation. Prior to mounting, embryos/larvae were anesthetized with Tricaine-S, immersed in 0.8% low-melting point agarose (Sigma, cat. A9414) and mounted in glass-bottomed 35 mm dishes (Greiner Bio-One, cat. 627871). After mounting, the dish was filled with egg water containing PTU and Tricaine to continually suppress pigment production and keep the embryos/larvae anesthetized during imaging. Immediately after imaging, embryos/larvae were carefully removed from the low-melting point agarose and revived in egg water.

For larvae imaged after 5 dpf, embryos were sterilized by 0.125% povidone-iodine (also called ovidine; Syndel) in egg water at 24 hpf for 2 minutes and washed three times with egg water<sup>218</sup>. Embryos were also kept in egg water without PTU. At 5 dpf, larvae were entered into our quarantine facility and allowed to grow until needed for imaging. For sequential imaging, larvae were removed from the system and mounted for imaging as described above, using similar glass-bottomed dishes (WillCo-Dish, cat. GWST-3512). After imaging, larvae were carefully removed from the low-melting point agarose and revived by gently flushing system water over their gills. For larvae older than 8 dpf, larvae were gently guided through system water with a dissection needle to simulate movement in addition to gently flushing system water over their gills. Depending on the age of the larva and the duration the larva was anesthetized, revival could take up to 30 minutes. To limit the amount of time a larva was anesthetized, larvae were mounted, imaged, and revived one at a time. Larvae were re-entered into the quarantine facility and allowed to grow until the next imaging timepoint.

Images of embryos/larvae younger than 8 dpf were acquired with a 40X water immersion objective (NA = 1.1) or 63X water immersion objective (NA = 1.2) mounted on a motorized Zeiss AxioObserver Z1 microscope equipped with a Quorum WaveFX-XI (Quorum Technologies) or Andor CSU-W1 (Andor Oxford Instruments) spinning disc confocal system. For larvae older than 9 dpf, images were acquired with a 20X objective (NA = 0.75) or a 40X oil immersion objective (NA = 1.3) mounted on a Leica Stellaris 5 laser scanning confocal system. Images and videos were processed with either Metamorph (Molecular Devices), IQ3 (Oxford Instruments), or

LAS X (Leica Microsystems) software. FIJI v1.54f (ImageJ) and Imaris v10.1 (Oxford Instruments) were used for post-hoc viewing, processing (cropping, adjusting brightness/contrast), and quantification.

## 2.8 LASER INJURY AND ABLATION

All injury and ablation experiments were performed using a galvo-controlled nitrogen-dye (435 nm) pulsed MicroPoint laser (Andor Technology) connected to a spinning disk confocal system (Quorum Technologies). Injuries and/or ablation experiments were conducted using either a 40X water (NA = 1.1) or 63X (NA = 0.8) objective. Ablation power ranged from 40 to 60 depending on what was targeted for injury and/or ablation, the age of the embryos, the mounting of the embryos, and the age of the nitrogen dye. The laser was pulsed within the designated region of interest (ROI) until injury and/or ablation was complete. Successful injuries and/or ablations were confirmed by the presence of cellular debris, the lack of fluorescence, and the lack of fluorescence resurgence for 10 minutes post-injury (a distinguishing feature compared to photobleaching)<sup>120</sup>.

For injury experiments of the brain parenchyma visualized by *Tg(GFAP:NTR-mCherry)*, a circular ROI between 15 – 20  $\mu\text{m}$  in diameter was drawn in the dorsomedial neuropil of the optic tectum. The ROI was positioned ~40 – 50  $\mu\text{m}$  away from NCCs (visualized by *Gt(erb3b:GAL4) Tg(UAS:EGFP)*).

## 2.9 D-TUBOCURARINE

For experiments using d-tubocurarine (Sigma, cat. 93750), embryos were manually de-chorionated using fine-tip forceps. 24 hpf embryos were immersed in either 10 mM d-tubocurarine in PTU egg water or PTU egg water with tricaine and incubated for 1 hour at room temperature (RT). Embryos were then mounted for *in vivo* confocal imaging as described above and the drugs were refreshed. Mounted embryos treated with 10 mM d-tubocurarine were immersed in 5 mM d-tubocurarine in PTU egg water for the duration of the timelapse imaging.

## 2.10 CRYOSECTIONING

Fixed larvae (24 hpf to 3 dpf) were mounted in sectioning agar (1.5% agar [Sigma, cat. A9539] 5% sucrose [Sigma, cat. S5016] in DEPC-treated [Sigma, cat. D5758] water). Blocks were trimmed with a razor blade to remove excess sectioning agar and cryopreserved in 30% sucrose in PBS overnight at 4°C. Agar blocks were frozen by placing them in a small weigh boat floating in 2-methylbutane (Sigma, cat. MX0760), the container of which was submerged in a bath of liquid nitrogen. Frozen agar blocks were sectioned at 20 µm with a cryostat microtome and mounted on microscope slides (VWR, cat. 48311). Slides were stored at -20°C in the dark until processed for immunofluorescence or imaged directly. Slides were coverslipped with DAPI Fluoromount-G (SouthernBiotech, cat. 010020) and stored at 4°C in the dark until imaging. Images were stitched together via the Stitching v.3.1.9 plugin<sup>219</sup> with FIJI v1.54f (ImageJ).

## 2.11 ACRIDINE ORANGE STAINING

The vital dye acridine orange (Santa Cruz Biotechnology, cat. sc-214488) was used to stain apoptotic cells as described previously<sup>220</sup>. Embryos were treated with 5 µM acridine orange in egg water or PTU egg water if younger or older than 24 hpf, respectively. Embryos were incubated for 20 minutes in the dark before being washed three times with egg water or PTU egg water. Embryos were immediately mounted in a dark room for imaging.

## 2.12 TUNEL STAINING

A modified protocol was used with the ApopTag Red *In Situ* Apoptosis Detection Kit (Sigma, cat. S7165). After embryos/larvae were fixed and processed for cryosectioning (see “2.10 Cryosectioning” for detailed methods), slides were re-fixed with 1% paraformaldehyde for 10 minutes at RT and then washed twice with PBS for 5 minutes each. Slides were then incubated in a 2:1 ratio of ethanol:acetic acid for 5 minutes at -20°C. Slides were washed twice with PBS for 5 minutes each before incubating in equilibration buffer covered with a coverslip for 10 to 60 minutes at RT. Excess equilibration buffer was removed before incubating in terminal deoxynucleotidyl transferase (TdT) enzyme mix for 60 minutes at 37°C in a humidified chamber. The reaction

was stopped by incubating slides in STOP/WASH buffer for 10 minutes at RT. Slides were rapidly washed three times with PBS. Slides were then incubated in anti-DIG antibody and solution overnight at 4°C in the dark. The next day, slides were washed with PBS and coverslipped with DAPI Fluoromount-G (SouthernBiotech, cat. 010020). Slides were stored at 4°C in the dark until imaging.

## 2.13 QUANTIFICATIONS AND STATISTICAL ANALYSES

### 2.13.1 Identifying RBs

For Figure 3-1, we defined RBs by their earliest morphological characterization, detailed in Chapter 3.2. In brief, RBs are identifiable by their stereotyped morphology starting at the 5 to 9 somite stage (~11.5 hours post-fertilization). This stereotyped morphology includes a large soma positioned in the dorsal spinal cord<sup>221,222</sup>, a rostrally projecting axon, a caudally projecting axon, and a peripheral axon that exits the spinal cord to innervate the skin<sup>223</sup>. Since *neurogenin1* (*ngn1*) expression is required for RB specification, we utilize *Tg(ngn1:GFP)* as a tool to fluorescently visualize RBs. At 24 hpf RBs are easily visible and identifiable by their stereotyped RB morphology in GFP<sup>+</sup> embryos. To aid in identification of RBs post-24 hpf, we also injected *ngn1:TagRFP*<sup>224</sup> into *Tg(ngn1:GFP)* embryos (see Chapter 2.6 *Mosaic labeling by microinjection* for details). At 24 hpf, we screened for GFP<sup>+</sup>/RFP<sup>+</sup> embryos before imaging, carefully selecting embryos where RFP<sup>+</sup> cells were RBs.

In post-hoc analyses, RBs were first marked and identified in all images from 24 hpf embryo. For identifying RBs post-24 hpf, images from all days of imaging were viewed simultaneously for a single embryo. We first identified the same RFP<sup>+</sup> RBs in all images over time to act as landmarks. This allowed us to more easily identify and track groups of GFP<sup>+</sup> RBs in between RFP<sup>+</sup> landmarks. RBs were identified by soma shape and location relative to RFP<sup>+</sup> landmarks and other RBs identified at 24 hpf. We also identified RBs by their laterally extending process, noting which side of the spinal cord the process exited and the branch morphology. If a *ngn1*<sup>+</sup> cell did not meet any of the above criteria at any timepoint it was not identified or counted as an RB.

### 2.13.2 Identifying other *ngn1*<sup>+</sup> cells

The *Tg(ngn1:GFP)* transgenic line used in this paper to visualize RBs also labels other spinal neurons<sup>225,226</sup>. Among these are dorsal longitudinal ascending interneurons (DoLAs) and ascending commissural neurons. While these cell types can be distinguished by their soma size and morphology, their close association with the DLF makes identification difficult without cell type specific markers or mosaic labeling. Here, we refer to these cell types as “other *ngn1*<sup>+</sup> cells”. Other *ngn1*<sup>+</sup> cells were identified by their lower GFP<sup>+</sup> fluorescence and more ventral soma location compared to RBs. Cell counts of other *ngn1*<sup>+</sup> cells were limited to the dorsal spinal cord with the ventral boundary defined by the DLF. If a *ngn1*<sup>+</sup> cell did not meet any of the above criteria at any timepoint it was not quantified. Other *ngn1*<sup>+</sup> cells were manually quantified using the FIJI v1.54f Cell Counter plug-in (<https://imagej.net/ij/plugins/cell-counter.html>).

### 2.13.3 Acridine Orange Puncta Number

Before quantifying acridine orange (AO) puncta, images underwent pre-processing via a custom FIJI macro. For each imaging position z-stack images were concatenated to create a maximum projection image. Since FIJI sometimes automatically optimizes brightness-contrast values, the brightness-contrast values were reset for each maximum projection image. Maximum projection images for an entire experiment were further concatenated to form a master stack. This master stack was subjected to thresholding according to the approximate mean brightness of particles. A size exclusion filter of 3  $\mu\text{m}$  was used to reduce the amount of AO<sup>+</sup> cellular debris that was included in the quantification<sup>227,228</sup>. Particles were counted using the analyze particles feature in FIJI v1.54f with the following settings: size (cm<sup>2</sup>): 15-Infinity, Circularity: 0.30-1.00, Exclude on edges: TRUE, Show: Outlines. For 36 hpf embryos, 6 embryos were imaged with 5 slightly overlapping positions set per fish spanning somites  $\sim 1 - x$ . Imaging and quantification were blinded as embryos were genotyped or phenotyped post-hoc and not matched to images until after quantification was complete.

For the number of AO<sup>+</sup> puncta in *csf1ra*<sup>-/-</sup> embryos versus wild-type/*csf1ra*<sup>+/-</sup> embryos at 34 hpf, an unpaired t-test with Welch’s correction was performed. For the 55 hpf time point, an unpaired t-test with Welch’s correction was performed on log-transformed data.

### 2.13.4 Annexin V Quantification

The number of Annexin V<sup>+</sup> (*secA5*<sup>+</sup>) puncta was quantified by creating a surface rendering using the Surfaces tool in Imaris. In brief, the surface rendering was created with the parameters detailed in Table 2-3. Surfaces were filtered by volume (> 25  $\mu\text{m}^3$ ) based on previously published methods<sup>229</sup>. *SecA5*<sup>+</sup> surfaces were not included in quantifications if they were located within the yolk sac or yolk sac projection. For all embryos, *secA5*<sup>+</sup> surfaces were generated from all imaging regions (somites 1-12).

**Table 2-3: *secA5*<sup>+</sup> puncta Imaris surface algorithm parameters**

Parameter	Setting
Smoothing	True
Surface Grain Size	0.30 $\mu\text{m}$
Eliminate Background	Enabled
Diameter of Largest Sphere	10.0 $\mu\text{m}$
Region Growing Estimated Diameter	3.00 $\mu\text{m}$
Region Growing Morphological Split	True
Filter Surfaces	"Volume" > 25

### 2.13.5 *mpeg1*<sup>+</sup> Professional Phagocyte Number

To quantify microglia in the brain, four individual z-stack images of the optic tectum of *csf1ra*<sup>+/+</sup>; *Tg(mpeg1:EGFP)*, *csf1ra*<sup>+/-</sup>; *Tg(mpeg1:EGFP)*, and *csf1ra*<sup>-/-</sup>; *Tg(mpeg1:EGFP)* embryos were analyzed. To quantify professional phagocytes in the spinal cord and periphery, embryos of the same genotype were imaged from somites 8 to 15. The number of *mpeg1*<sup>+</sup> cells were counted at 4-hour time intervals (36, 40, 44, and 48 hpf) in individual z-stack images. To ensure that *mpeg1*<sup>+</sup> cells were microglia, cells were checked to be within the spinal cord or brain parenchyma by referencing bright field images. For quantifications of the spinal cord, the number of *mpeg1*<sup>+</sup> phagocytes per somite was summed for each fish and divided by the number of somites

imaged. All data was tested for normality prior to further analyses. For the number of *mpeg1*<sup>+</sup> phagocytes in the optic tectum at 3 dpf, an unpaired t-test with Welch’s correction was performed. For the number of *mpeg1*<sup>+</sup> phagocytes in the spinal cord and periphery from 32 to 48 hpf, a two-way repeated measures ANOVA test was performed.

### 2.13.6 RB and other *ngn1*<sup>+</sup> cell Number Quantification

For early imaging (24 to 36 hpf) and daily imaging (1 to 5 dpf), RBs and other *ngn1*<sup>+</sup> cells were identified in somites 4 to 8 by several factors detailed in the “*Identifying RBs*” and “*Identifying other ngn1*<sup>+</sup> cells” sections, respectively. For the tricaine and d-tubocurarine experiments in Figure 3-3, RBs were identified over a distance of 460 μm (somites 3 to 8), starting with the anterior-most RB. RBs were counted using manual curation with the Spots tool in Imaris. Other *ngn1*<sup>+</sup> cells were manually quantified using the FIJI v1.54f Cell Counter plug-in. For quantifications normalized by distance or within a set distance, the Measurement Points tool in Imaris was used. The distance (in microns) was measured of the DLF, starting and ending at the same anterior-posterior position as the anterior-most and posterior-most RB being quantified, respectively.

### 2.13.7 RB Soma Volume

RB soma volume was quantified by creating a surface rendering using the Surfaces tool in Imaris. The surface rendering was created with the parameters detailed in Table 2-4.

**Table 2-4: RB soma Imaris surface algorithm parameters**

Parameter	Setting
Smoothing	True
Surface Grain Size	0.350 μm
Eliminate Background	Enabled
Diameter of Largest Sphere	10.0 μm

Region Growing Estimated Diameter	3.00 $\mu\text{m}$
Region Growing Morphological Split	True

### 2.13.8 Phagosome Number and Volume

Phagosomes visualized with *Tg(UAS:GFP-FYVE)* were quantified by creating surface renderings using the Surfaces tool in Imaris. In experiments using *Tg(sox10:GAL4;UAS:GFP-FYVE)* in combination, the GFP signal was observed to be relatively weak, except in a few observed *sox10*<sup>+</sup> cells. Two different surface algorithms were used to accurately render surfaces for both weak and strong GFP signals. These surface renderings were created with the parameters detailed in **Tables 2-5** and **2-6**, respectively. Rendered surfaces were compared to GFP signal in single z planes to ensure algorithm parameters did not artificially deflate or inflate surfaces compared to GFP signal. Phagosomes smaller than  $\mu\text{m}$  were excluded from surface renderings and further quantifications.

**Table 2-5: FYVE<sup>+</sup> phagosomes (weak GFP signal) Imaris surface rendering parameters**

Parameter	Setting
Smoothing	True
Surface Grain Size	0.25 $\mu\text{m}$
Eliminate Background	Enabled
Diameter of Largest Sphere	2 $\mu\text{m}$
Region Growing Estimated Diameter	2 $\mu\text{m}$
Region Growing Morphological Split	True

**Table 2-6: FYVE<sup>+</sup> phagosomes (strong GFP signal) Imaris surface rendering parameters**

Parameter	Setting
Smoothing	True
Surface Grain Size	0.25 $\mu\text{m}$
Eliminate Background	Enabled
Diameter of Largest Sphere	8 $\mu\text{m}$
Region Growing Estimated Diameter	2 $\mu\text{m}$
Region Growing Morphological Split	True
Threshold	>1,120

### 2.13.9 Percent Survival Quantification

For Figure 3-1H and Supplemental Figure 3-1D, RBs and other *ngn1*<sup>+</sup> cells were identified in 1 dpf images as detailed in the “*Identifying RBs*” and “*Identifying other ngn1<sup>+</sup> cells*” sections, respectively. For Figure 3-4, RBs were identified in 5 dpf images by their *ngn1* expression and soma location in the dorsomedial spinal cord and quantified between somites 6 to 12. For timepoints after 5 dpf, we looked for the same group of RBs identified

at 5 dpf. These RBs were identified by their *ngn1* expression, soma location, and their relative position compared to other identified RBs and RFP<sup>+</sup> cells and/or landmarks. Percent survival was calculated by normalizing the number of cells counted in later timepoints to the earliest timepoint quantified. Then this value was converted to a percentage.

#### 2.13.10 TUNEL Quantification

Five groups of cells were quantified from TUNEL staining of transverse sections: RBs (*ngn1*<sup>+</sup>/TUNEL<sup>-</sup>/DAPI<sup>+</sup>), dying RBs (*ngn1*<sup>+</sup>/TUNEL<sup>+</sup>/DAPI<sup>+</sup>), other *ngn1*<sup>+</sup> cells (*ngn1*<sup>+</sup>/TUNEL<sup>-</sup>/DAPI<sup>+</sup>), other dying *ngn1*<sup>+</sup> cells (*ngn1*<sup>+</sup>/TUNEL<sup>+</sup>/DAPI<sup>+</sup>), and *ngn1*<sup>-</sup> dying cells (*ngn1*<sup>-</sup>/TUNEL<sup>+</sup>/DAPI<sup>+</sup>). Please refer to the “*Identifying RBs*” and “*Identifying other ngn1<sup>+</sup> cells*” methods sections for details on distinguishing RBs and other *ngn1*<sup>+</sup> cells. For sections from 24 and 50 hpf embryos, only *ngn1*<sup>+</sup> cells in the upper half of the dorsal cord were quantified. For sections from 3 dpf embryos, only *ngn1*<sup>+</sup> cells in the upper third of the dorsal cord were quantified. The five groups of cells were identified and manually counted on single transverse sections for the entire image stack. Manual counting was completed with the FIJI v1.54f Cell Counter plug-in (<https://imagej.net/ij/plugins/cell-counter.html>).

#### 2.13.11 Statistical Analyses

All data was plotted, graphed, and underwent statistical analyses in Prism v10.2.3 (GraphPad). Plots are presented as means ± standard error of the mean (SEM), when applicable. For some embryos or fish that were imaged multiple times, quantifications could not be completed due to insufficient imaging (e.g. the spinal cord could not be imaged as deep in older fish). In these cases, data was omitted for that timepoint, was not plotted, and did not undergo statistical analyses.

### 2.14 SCHEMATICS AND ILLUSTRATIONS

All schematics and illustrations were created by Kendra Liu using Inkscape v1.3.1.

# CHAPTER 3: ROHON-BEARD NEURONS DO NOT SUCCUMB TO PROGRAMMED CELL DEATH DURING ZEBRAFISH DEVELOPMENT

---

Kendra E. Liu<sup>1,3</sup>, Sarah Kucenas<sup>1,2,3</sup>

<sup>1</sup>Neuroscience Graduate Program, University of Virginia, Charlottesville, Virginia, USA

<sup>2</sup>Department of Biology, University of Virginia, Charlottesville, VA, USA

<sup>3</sup>Program in Fundamental Neuroscience, University of Virginia, Charlottesville, VA, USA

2024 *Developmental Biology*, 515:186-198, <https://doi.org/10.1016/j.ydbio.2024.06.020>. Epub 2024 Jun 27.

## 3.1 ABSTRACT

During neural development, sculpting of early formed circuits by cell death and synaptic pruning is necessary to generate a functional and efficient nervous system. This allows for the establishment of rudimentary circuits which necessitate early organism survival to later undergo subsequent refinement. These changes facilitate additional specificity to stimuli which can lead to increased behavioral complexity. In multiple species, Rohon-Beard neurons (RBs) are the earliest mechanosensory neurons specified and are critical in establishing a rudimentary motor response circuit. Sensory input from RBs gradually becomes redundant as dorsal root ganglion (DRG) neurons develop and integrate into motor circuits. Previous studies demonstrate that RBs undergo a dramatic wave of cell death concurrent with development of the DRG. However, contrary to these studies, we show that *neurogenin1*<sup>+</sup> (*ngn1*) RBs do not undergo a widespread wave of programmed cell death during early zebrafish development and instead persist until at least 15 days post fertilization (dpf). Starting at 2 dpf, we also observed a dramatic medialization and shrinkage of *ngn1*<sup>+</sup> RB somas along with a gradual downregulation of *ngn1* in RBs. This alters a fundamental premise of early zebrafish neural development and opens new avenues to explore mechanisms of RB function, persistence, and circuit refinement.

## 3.2 INTRODUCTION

Vertebrate neural development is characterized by an over-proliferation of cells and connections that are successively pruned to produce a functional and efficient nervous system, allowing for organismal survival<sup>16,28,230,231</sup>. The two major processes that occur during this period of refinement include cell death and the removal of synaptic connections. Many neural structures that undergo refinement are conserved across vertebrate species and include trigeminal ganglionic neurons<sup>232–234</sup>, retinal ganglion cells<sup>235–239</sup>, and spinal motor neurons<sup>240–242</sup> (reviewed by Buss et al., 2006<sup>16</sup>). Additionally, there are entire neural populations and structures that are eliminated during development, including Cajal-Retzius neurons in the mouse cortex which undergo extensive activity-dependent cell death in the second postnatal week<sup>18</sup>. These neurons are mostly absent in adults, but their developmental death is necessary for establishment of excitatory/inhibitory balance and wiring of cortical circuits<sup>18,19</sup>.

Another example of a conserved, developmentally transient population of cells are Rohon-Beard neurons (RBs)<sup>243,244</sup>. RBs are early mechanosensory neurons that exist widely in the animal kingdom with pioneering studies exploring their development and physiology in anamniotes (including amphibians<sup>245–247</sup>, lampreys<sup>248,249</sup>, teleosts<sup>223</sup>). Other groups have identified RB ancestors in amphioxus<sup>250,251</sup> and ascidians<sup>252</sup>, and older studies also describe a morphologically similar population in human fetuses (named intramedullary neurons)<sup>253–255</sup>. In mice, it is unknown whether RB orthologues exist during early neural development. However, recent work demonstrates that loss of *Six1* and *Six4* leads to intramedullary sensory neuron-like cells and perturbed development of the secondary somatosensory system (consisting of dorsal root ganglion (DRG) neurons)<sup>256</sup>. More thorough investigations of RBs in mammals have stalled due to limitations of accessing tissues at such early developmental timepoints.

In experimentally tractable models, studies demonstrate RBs are necessary to establish an initial touch-response circuit<sup>221,257,258</sup>. Shortly after this rudimentary motor circuit is established, the entire RB neuron population is thought to undergo apoptosis and is replaced by DRG neurons as the sensory component of this circuit<sup>27,247,259–261</sup>. Previous work hypothesizes that this redundancy initially allows for organism survival and later

rearrangement of the circuit facilitates higher stimuli discrimination and processing, as well as more complicated motor movements.

RBs are primarily defined by their stereotyped morphology, which includes a large soma (~10 to 12  $\mu\text{m}$ )<sup>221,222</sup> positioned in the dorsal spinal cord, an axon that projects rostrally to the hindbrain, an axon that projects caudally, and a peripheral axon that exits the spinal cord and innervates the skin<sup>223</sup>. Previous studies examining RB death during development have largely relied on these morphological characteristics coupled with non-specific antibody labeling to separate dying RBs from other cells in the developing nervous system. In zebrafish, advancements in transgenesis now allow for *in vivo* visualization of RBs, although many of the currently available transgenic lines are still not specific to RBs. With these *in vivo* studies, characterization of RB death has expanded to include loss of fluorescence emitted by these lines. However, these measures do not directly assay RBs and their death. Additionally, using these criteria to identify RB neurons and characterize their death may have inadvertently led to conclusions about RB survival that were limited by the tools available. In fact, recent work demonstrates that some RBs may escape developmental death and persist<sup>222,262</sup>. However, these studies do not provide a definitive stance on how long RBs survive. RB survival presents intriguing questions in the context of the touch-response circuit, as sensory stimuli is thought to be processed through the later developed DRG.

To address these inconsistencies and investigate whether RBs (as a population) are eliminated during zebrafish development, we used serial *in vivo*, time-lapse imaging coupled with cell death assays. We find that the entirety of the RB neuron population survives through early zebrafish development (defined here from 24 to 72 hours post fertilization (hpf)) and does not express canonical markers of cell death. 92.6% of RBs identified at 24 hpf persist until 5 days post fertilization (dpf) while 87.92% of RBs identified at 5 dpf persist until 15 dpf. Our findings provide a more direct characterization of RBs during development and resolve previously published differences in RB survival. This allows for interesting, new future directions regarding the function of RB neurons and how their survival may affect the developing touch-response circuit.

### 3.3 RESULTS

#### 3.3.1 RB neurons survive through early zebrafish development

The touch-response circuit is one of the first established functional circuits in developing zebrafish embryos and is critical for generating early motor responses<sup>209,263,264</sup>. This circuit is comprised of RB neurons in the dorsal spinal cord that receive sensory information via their peripheral arbors in the skin (Figure 3-1A)<sup>223</sup>. RB neurons synapse onto ipsilateral primary ascending commissural (CoPA) interneurons, which project contralaterally through the ventral spinal cord to synapse on motor neurons<sup>258,265</sup>. This facilitates a tail recoil in response to sensory stimulation as early as 24 hours post-fertilization (hpf)<sup>263,264,266</sup>. Previous studies describe the refinement of this rudimentary circuit and demonstrate that over a span of 24 hours (24 to 48 hpf), RBs quickly die and are replaced by DRG neurons in the circuit<sup>27,261,267,268</sup>. These cellular and synaptic changes are hypothesized to lead to alterations in the touch-response circuit, allowing for more complicated and precise motor behavior in response to sensory stimuli.

Recently however, multiple studies provide evidence that a subset of RB neurons survive<sup>222,262</sup>. To investigate whether the entire RB population dies during early development, we conducted *in vivo*, time-lapse imaging utilizing *Tg(ngn1:GFP)* embryos where *neurogenin1* (*ngn1*) promoter sequences drive expression of cytoplasmic GFP<sup>225</sup>. *Ngn1* expression is required for RB specification<sup>269,270</sup>, is a ubiquitous early marker of RBs<sup>225,271</sup>, and GFP expression from *Tg(ngn1:GFP)* marks RBs as early as mid-somitogenesis<sup>225</sup>. Using *in vivo*, time-lapse imaging in *Tg(ngn1:GFP)* embryos between 24 to 36 hpf, we could easily identify *ngn1*<sup>+</sup> RBs by their large somas in the dorsal spinal cord and their characteristic laterally extending peripheral process (Figure 3-1B). We also observed other spinal neurons also labeled by *Tg(ngn1:GFP)* (as described previously<sup>225,226</sup>), but they were clearly distinguished from RBs due to their ventral positioning, smaller somas, lower GFP expression, and close association with the dorsal longitudinal fasciculus (DLF) (Figures 3-1B & C). In our time-lapse movies from 24 to 36 hpf, we were surprised to see that the number of *ngn1*<sup>+</sup> RBs was remarkably stable (Figure 3-1C, Video 3-1). In fact, we could track single RBs over the entirety of each time-lapse in every embryo we imaged. Additionally, we did not observe any cell fragmentation, a phenomenon commonly observed with cell death (Figure 3-1C)<sup>195,261,272</sup>. Therefore, we sought to quantify the number of *ngn1*<sup>+</sup> RBs per 100  $\mu\text{m}$  over time and found a

significant decrease between 24 and 36 hpf (Figure 3-1D). This contrasted with our observations from our time-lapse imaging where *ngn1*<sup>+</sup> RBs did not disappear (Video 3-1). This significant difference was negated when quantifying the absolute number of *ngn1*<sup>+</sup> RBs over time (Figure 3-1E). We also quantified other *ngn1*<sup>+</sup> cells, which have smaller somas, lower GFP fluorescence, and a more ventral position compared to *ngn1*<sup>+</sup> RBs. These other *ngn1*<sup>+</sup> cell somas were also tightly associated with the DLF. Similar to our quantifications for *ngn1*<sup>+</sup> RBs, we found the number of other *ngn1*<sup>+</sup> cells decreased significantly between all timepoints (Supplemental Figure 3-1A) when normalized by distance but no significant difference between the absolute number of other *ngn1*<sup>+</sup> cells between 24 and 36 hpf (Supplemental Figure 3-1B). We attribute this difference in quantification significance in both *ngn1*<sup>+</sup> RBs and other *ngn1*<sup>+</sup> cells to the large change in body axis and trunk size that occurs as the embryo grows between 24 and 36 hpf. These early time-lapses led us to ask whether the number of *ngn1*<sup>+</sup> RBs changed after 36 hpf.

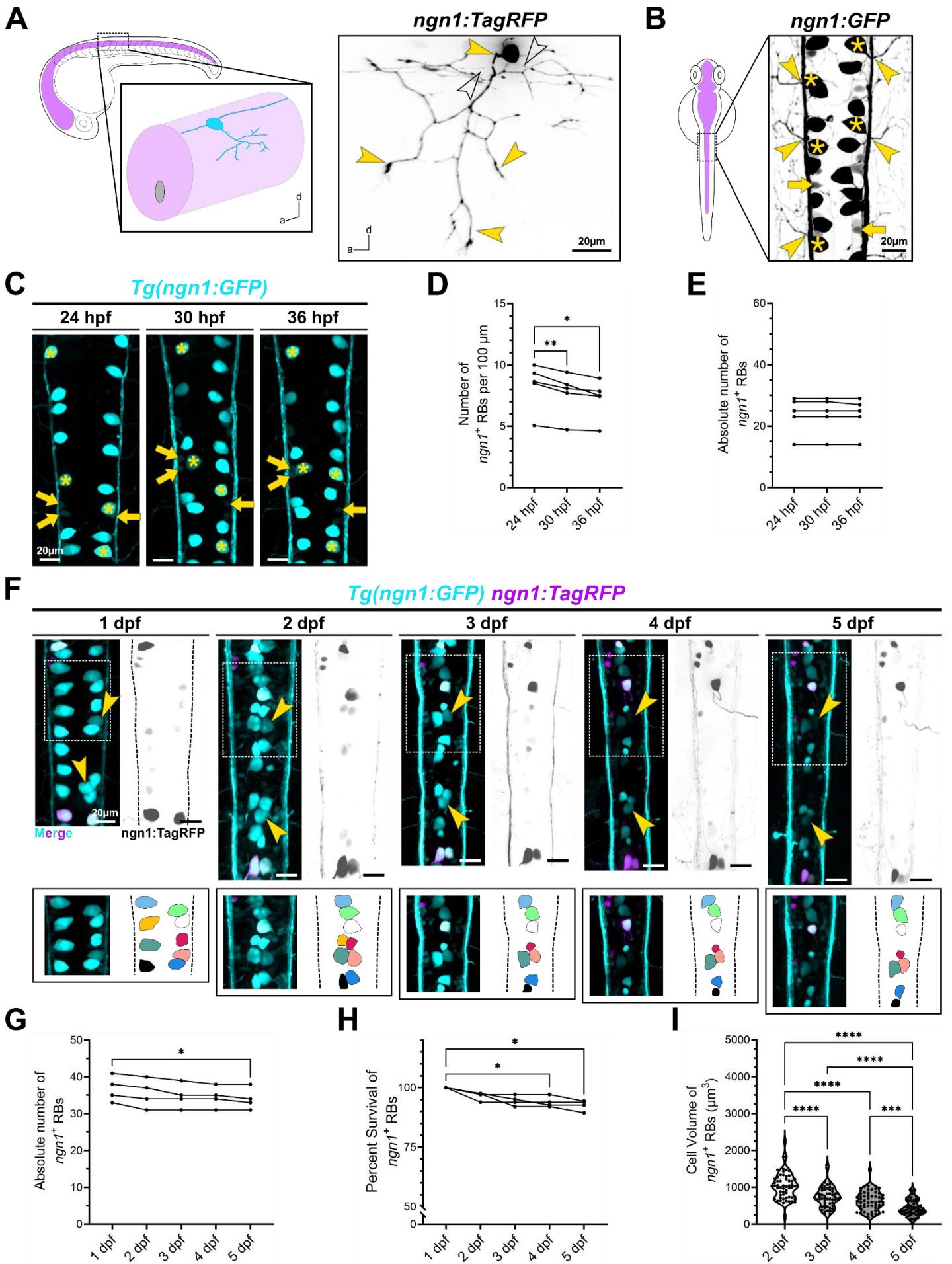


**Figure 3-1: RB neurons survive through early zebrafish development.** (**A, left**) Schematic of a 24 hpf zebrafish embryo viewed laterally with the central nervous system (CNS) in magenta. Inset shows a portion of the spinal cord with a RB neuron schematized in cyan. (**A, right**) Individual RB neuron imaged laterally labeled by *ngn1:TagRFP*. The lateral extending processes of the RB is marked by black arrowheads while the peripheral processes are marked by yellow arrowheads. (**B**) Schematic of a 24 hpf zebrafish embryo viewed dorsally with the CNS in magenta. Inset is a representative maximum projection confocal image of the dorsal spinal cord of a 24 hpf *Tg(ngn1:GFP)* embryo. Yellow asterisks mark examples of RB cell bodies and yellow arrowheads mark their respective peripheral processes. Yellow arrows denote other smaller *ngn1*<sup>+</sup> cells. (**C**) Representative maximum projection images at 24, 30, and 36 hpf of a *Tg(ngn1:GFP)* embryo. Example RB somas present in all three timepoints are marked with yellow asterisks. Examples of other *ngn1*<sup>+</sup> cells are marked by yellow arrows. (**D**) Quantification of the number of *ngn1*<sup>+</sup> RBs per 100  $\mu$ m at 24, 30, and 36 hpf of *Tg(ngn1:GFP)* embryos (n = 5 embryos). Repeated measures one-way ANOVA p value = 0.0092. Adjusted p values for multiple comparisons: 24 vs. 30 hpf p = 0.0076, 24 vs. 36 hpf p = 0.0231, 30 vs. 36 hpf p = 0.0943. Mean  $\pm$  standard error of the mean (SEM) values: 24 hpf:  $8.301 \pm 0.8553$ , 30 hpf:  $7.662 \pm 0.7903$ , 36 hpf:  $7.263 \pm 0.7136$ . (**E**) Quantification of the absolute number of *ngn1*<sup>+</sup> RBs of the same embryos in **D**. Repeated measures one-way ANOVA p value = 0.3739. Adjusted p values for 24 vs. 36 hpf and 30 vs. 36 hpf: p = 0.6152. Mean  $\pm$  SEM values: 24 hpf:  $23.80 \pm 2.672$ , 30 hpf:  $23.80 \pm 2.672$ , 36 hpf:  $23.60 \pm 2.600$ . All data in **D & E** was compared with the repeated measures one-way ANOVA with Geisser-Greenhouse correction and Tukey's multiple comparisons tests and each dot represents one embryo. (**F**) Images at 1, 2, 3, 4, and 5 dpf of the same *Tg(ngn1:GFP)* embryo injected with *ngn1:TagRFP* at the one-cell stage. Images were cropped so that the same group of RB neurons were visible in all images. The white-dashed boxes represent the inset depicted below each timepoint. Insets contain a cropped view of RBs (left) with each RB individually colored on a map (right). Yellow arrowheads denote examples of GFP<sup>+</sup> RBs where the fluorescence dims over time. Dashed black lines mark the dorsal longitudinal fasciculus (DLF). (**G**) Quantification of the absolute number of *ngn1*<sup>+</sup> RBs 1 thru 5 dpf of the same embryos in **F** (n = 4 embryos). Repeated measures one-way ANOVA p value = 0.0152. Adjusted p values for multiple comparisons: 1 vs. 2 dpf p = 0.0585, 1 vs. 3 dpf p = 0.0617, 1 vs. 4 dpf p = 0.0688, 1 vs. 5 dpf p = 0.0403, 2 vs. 3 dpf p = 0.5939, 2 vs. 4 dpf p = 0.5261, 2 vs. 5 dpf p = 0.3344, 3 vs. 4 dpf p = 0.8427, 3 vs. 5 dpf p = 0.2019, 4 vs. 5 dpf p = 0.5261. Mean  $\pm$  SEM values: 1 dpf:  $36.75 \pm 1.750$ , 2 dpf:  $35.50 \pm 1.936$ , 3 dpf:  $34.75 \pm 1.652$ , 4 dpf:  $34.50 \pm 1.443$ , 5 dpf:  $34.00 \pm 1.472$ . (**H**) Quantification of the percent surviving GFP<sup>+</sup> or GFP<sup>+</sup>/RFP<sup>+</sup> *ngn1*<sup>+</sup> RBs of the same embryos in **F** over time. Repeated measures one-way ANOVA p value = 0.0087. Adjusted p values for multiple comparisons: 1 vs. 2 dpf p = 0.0991, 1 vs. 3 dpf p = 0.0546, 1 vs. 4 dpf p = 0.486, 1 vs. 5 dpf p = 0.0258, 2 vs. 3 dpf p = 0.6063, 2 vs. 4 dpf p = 0.5271, 2 vs. 5 dpf p = 0.3280, 3 vs. 4 dpf p = 0.8427, 3 vs. 5 dpf p = 0.2055, 4 vs. 5 dpf p = 0.5273. Mean  $\pm$  SEM values: 1 dpf:  $100 \pm 0$ , 2 dpf:  $96.50 \pm 0.8588$ , 3 dpf:  $94.58 \pm 1.057$ , 4 dpf:  $93.97 \pm 1.126$ , 5 dpf:  $92.60 \pm 1.096$ . All data in **G & H** was compared with the repeated measures one-way ANOVA with Geisser-Greenhouse correction and Tukey's multiple comparisons tests and each dot represents one fish. (**I**) Quantification of the volume of GFP<sup>+</sup> or GFP<sup>+</sup>/RFP<sup>+</sup> *ngn1*<sup>+</sup> RB somas at 2, 3, 4, and 5 dpf in microns cubed (n = 58 cells from 2 embryos). Brown-Forsythe and Welch's ANOVAs p values: p < 0.0001. Adjusted p values for multiple comparisons: 2 vs. 3 dpf, 2 vs. 4 dpf, 2 vs. 5 dpf, and 3 vs. 5 dpf p < 0.0001, 3 vs. 4 dpf p = 0.2149, 4 vs. 5 dpf p = 0.0003. Mean  $\pm$  SEM values: 2 dpf:  $1038 \pm 46.98$ , 3 dpf:  $743.3 \pm 37.71$ , 4 dpf:  $643.3 \pm 34.85$ , 5 dpf:  $452.3 \pm 28.64$ . Data in **I** was compared with the Brown-Forsythe and Welch's ANOVAs with Games-Howell's multiple comparisons tests and one dot equals one cell. All images in **Figure 3-1** are representative, maximum projection confocal images.

To address this question, we injected one-cell *Tg(ngn1:GFP)* embryos with *ngn1:TagRFP* and conducted sequential imaging of individual embryos/larvae every day until 5 dpf. This allowed us to unambiguously determine the location and survival of individual GFP<sup>+</sup> or GFP<sup>+</sup>/RFP<sup>+</sup> RBs between 1 and 5 dpf. Similar to our earlier time-lapse imaging, we identified individual GFP<sup>+</sup> or GFP<sup>+</sup>/RFP<sup>+</sup> RBs and tracked them over time (Figure 3-1F). We found that the absolute number of *ngn1*<sup>+</sup> RBs differed significantly between 1 and 5 dpf (Figure 3-1G). When converting the data to percent survival, we found that there was a significant difference between 1 and 4 dpf as well as 1 and 5 dpf (Figure 3-1H). We also observed that the absolute number of other *ngn1*<sup>+</sup> cells differed significantly between 1 and 5 dpf and this was reflected in the percent survival for this population (Supplemental Figure 3-2C & D). Importantly, in our imaging, we noted a dimming of fluorescence in a subset of RBs labeled with the *Tg(ngn1:GFP)* line (Figure 3-1F) starting at 3 dpf. This decrease in *ngn1* fluorescence likely contributed to previous mischaracterization of RB cell death and made identification of RBs post-3 dpf difficult. Importantly, we never observed any fragmentation of *ngn1*<sup>+</sup> RBs and the decreases in *ngn1*<sup>+</sup> RB survival were all a result of gradual dimming (over days) of fluorescence until a RB was no longer visible. We hypothesize that because *ngn1* is required for RB specification<sup>269,270</sup>, *ngn1* may be downregulated after RBs mature, which would explain the observed decrease in fluorescent intensity. We believe this contributed to the decrease in absolute number and percent survival of *ngn1*<sup>+</sup> RBs at 4 and 5 dpf (Figures 3-1G & 3-1H). Additionally, we observed a dramatic relocation of *ngn1*<sup>+</sup> RB somas, with cell bodies converging medially between 1 and 2 dpf (Figure 3-1F). This aligned with elongation of the growing embryonic trunk and tail. We also observed a decrease in the size of RB cell bodies over time (Figure 3-1I), which aligns with recently published work<sup>222</sup>.

Altogether, our studies demonstrate that the absolute number of *ngn1*<sup>+</sup> RBs is consistent throughout early development (1 to 5 dpf), and we observed no morphological evidence of cell death. We also observed that *ngn1*<sup>+</sup> RBs exhibited significant changes in lateral-medial location and soma size, which may explain why previous studies concluded they die. Our data supports the hypothesis that RBs are longer-lived, which inspired us to look at this population more extensively throughout development.

### 3.3.2 The vast majority of RB neurons do not express canonical markers of cell death

To build on our imaging studies and examine RB cell death more directly, we conducted TUNEL labeling on *Tg(ngn1:GFP)* embryos and larvae, a canonical assay used to mark dying cells<sup>27,195,273</sup>. We labeled embryos and larvae at 24, 50, and 72 hpf, which spans the previously described period of RB cell death<sup>27</sup>. We identified RBs in transverse sections of embryos and larvae by their size, location, and *ngn1*<sup>+</sup>/DAPI<sup>+</sup> positivity. Other spinal neurons also labeled by *Tg(ngn1:GFP)* were distinguishable from RBs by their more ventral positioning and lower *ngn1* expression (Figure 3-2A). From these studies we found that the number of *ngn1*<sup>+</sup>/DAPI<sup>+</sup> RBs per transverse section significantly decreased between 24 and 72 hpf (Figure 3-2B), aligning with our previous findings (Figure 3-1D). However, in our previous imaging studies, we observed bilateral rows of RBs that centralized into a single medial row by 48 hpf (Figure 3-1F). We also observed this in our transverse sections (Figure 3-2A) where we saw multiple *ngn1*<sup>+</sup>/DAPI<sup>+</sup> RBs in transverse sections of 24 hpf embryos and later, single, medially localized *ngn1*<sup>+</sup>/DAPI<sup>+</sup> RBs in sections of 50 and 72 hpf larvae. Importantly, we observed no *ngn1*<sup>+</sup>/TUNEL<sup>+</sup>/DAPI<sup>+</sup> RBs (n = 30 transverse slices from 5 fish, per timepoint) in any of the transverse sections from any of the timepoints we examined. We were, however, able to identify TUNEL<sup>+</sup>/DAPI<sup>+</sup> cells in the spinal cord at 24 hpf and this number decreased significantly by 72 hpf (Figure 3-2C). This aligns with previous work characterizing spinal cord cell death during early development<sup>274</sup>. We also quantified the number of other *ngn1*<sup>+</sup> cells and found a significant decrease between 24 and 72 hpf as well as 50 and 72 hpf (Supplemental Figure 3-2A). We also observed very few other *ngn1*<sup>+</sup> cells that were also TUNEL<sup>+</sup> at 24, 50, and 72 hpf (Supplemental Figure 3-2B).

Previously, we found that the absolute number of RBs does not change over time, although the elongation of the trunk contributes to a perceived decrease in their number when normalizing over distance (Figure 3-1C – E). This is also observed in our transverse slices, as the medialization of RBs results in a decrease in the average number of *ngn1*<sup>+</sup>/DAPI<sup>+</sup> RBs per transverse section. We posit that this also explains the significant decrease in *ngn1*<sup>+</sup>/DAPI<sup>+</sup> RBs between 24 and 72 hpf we observe (Figure 3-2B). Overall, we directly investigated whether dying RBs could be identified in early development, and we have found no instances of dying RBs (*ngn1*<sup>+</sup>/TUNEL<sup>+</sup>/DAPI<sup>+</sup> RBs) at 24, 50 or 72 hpf.

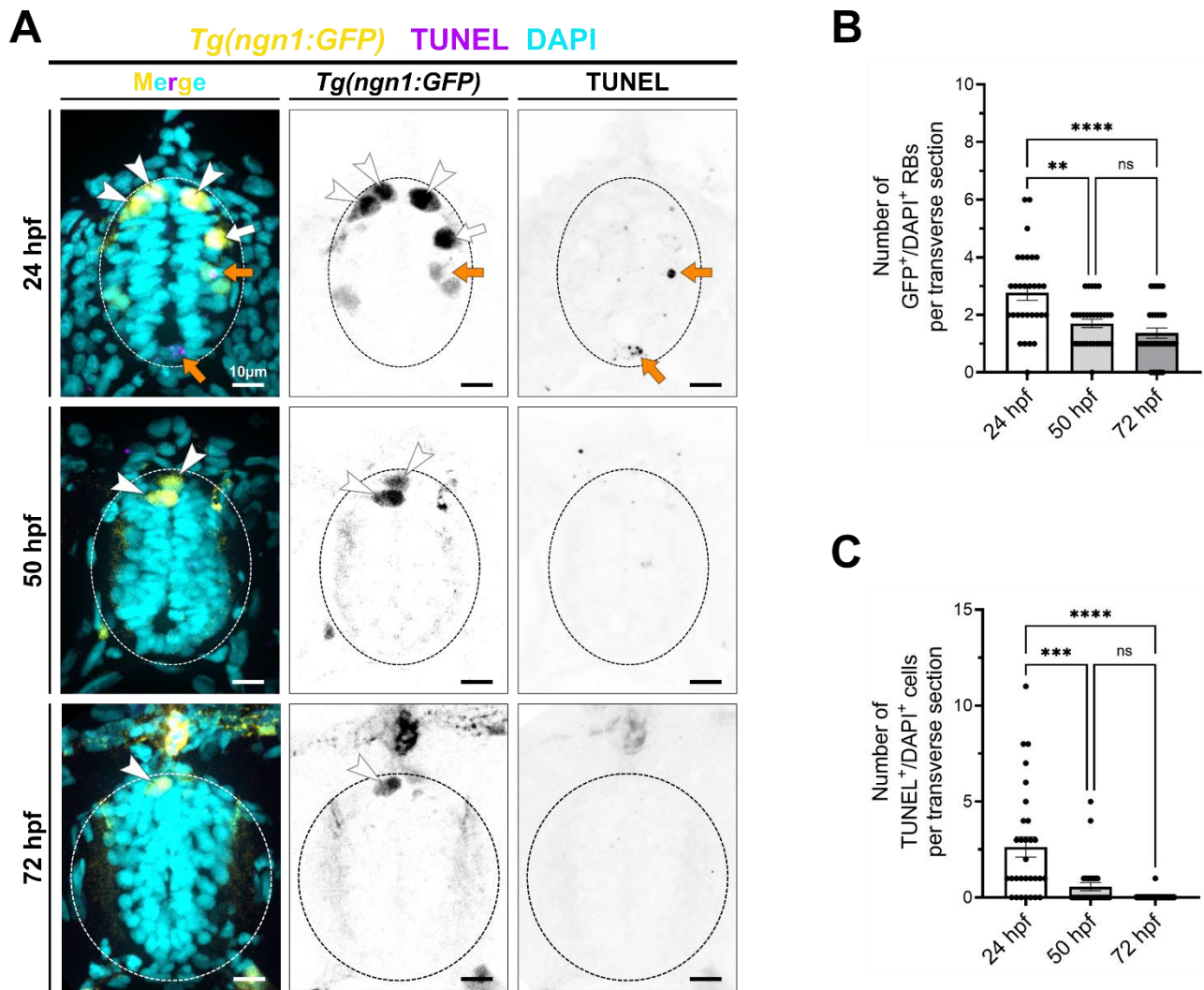


**Figure 3-2: RBs do not express canonical markers of cell death.** (A) TUNEL staining of transverse sections from 24, 50, and 72 hpf *Tg(ngn1:GFP)* embryos. White arrowheads denote *ngn1*<sup>+</sup>/DAPI<sup>+</sup> RBs. Other *ngn1*<sup>+</sup>/DAPI<sup>+</sup> cells (marked by white arrows) were also visible and distinguished from RBs by their relative ventral positioning. *ngn1*<sup>+</sup>/TUNEL<sup>+</sup>/DAPI<sup>+</sup> cells are marked by orange arrows. The edge of the spinal cord is denoted with a dashed white circle (in fluorescent merged images) or a dashed black circle (in single channel images). (B) Quantification of the number of *ngn1*<sup>+</sup> RBs (defined as GFP<sup>+</sup>/DAPI<sup>+</sup> cells located in the dorsal spinal cord) per transverse section for each timepoint. Brown-Forsythe and Welch's ANOVAs p values:  $p < 0.0001$  and  $p = 0.0002$ , respectively. Adjusted p values for multiple comparisons: 24 vs. 50 hpf  $p = 0.0026$ , 24 vs. 72 hpf  $p = 0.0001$ , 50 vs. 72 hpf  $p = 0.3811$ . Mean  $\pm$  SEM values: 24 hpf:  $2.767 \pm 0.2612$ , 50 hpf:  $1.700 \pm 0.1450$ , 72 hpf:  $1.367 \pm 0.1761$ . (C) Quantification of the number of dying cells (defined as TUNEL<sup>+</sup>/DAPI<sup>+</sup> cells) per transverse section for each timepoint. Brown-Forsythe and Welch's ANOVAs p values:  $p < 0.0001$ . Adjusted p values for multiple comparisons: 24 vs. 50 hpf  $p = 0.0024$ , 24 vs. 72 hpf  $p < 0.0001$ , 50 vs. 72 hpf  $p = 0.0554$ . Mean  $\pm$  SEM values: 24 hpf:  $2.633 \pm 0.5263$ , 50 hpf:  $0.5667 \pm 0.2127$ , 72 hpf:  $0.03333 \pm 0.03333$ . Data in B and C was compared with the Brown-Forsythe and Welch's ANOVAs with Dunnett's T3 multiple comparisons tests and one dot equals one transverse slice.  $n = 30$  transverse slices per timepoint, coming from 5 different embryos. All images in Figure 3-2 are representative, maximum projection confocal images.

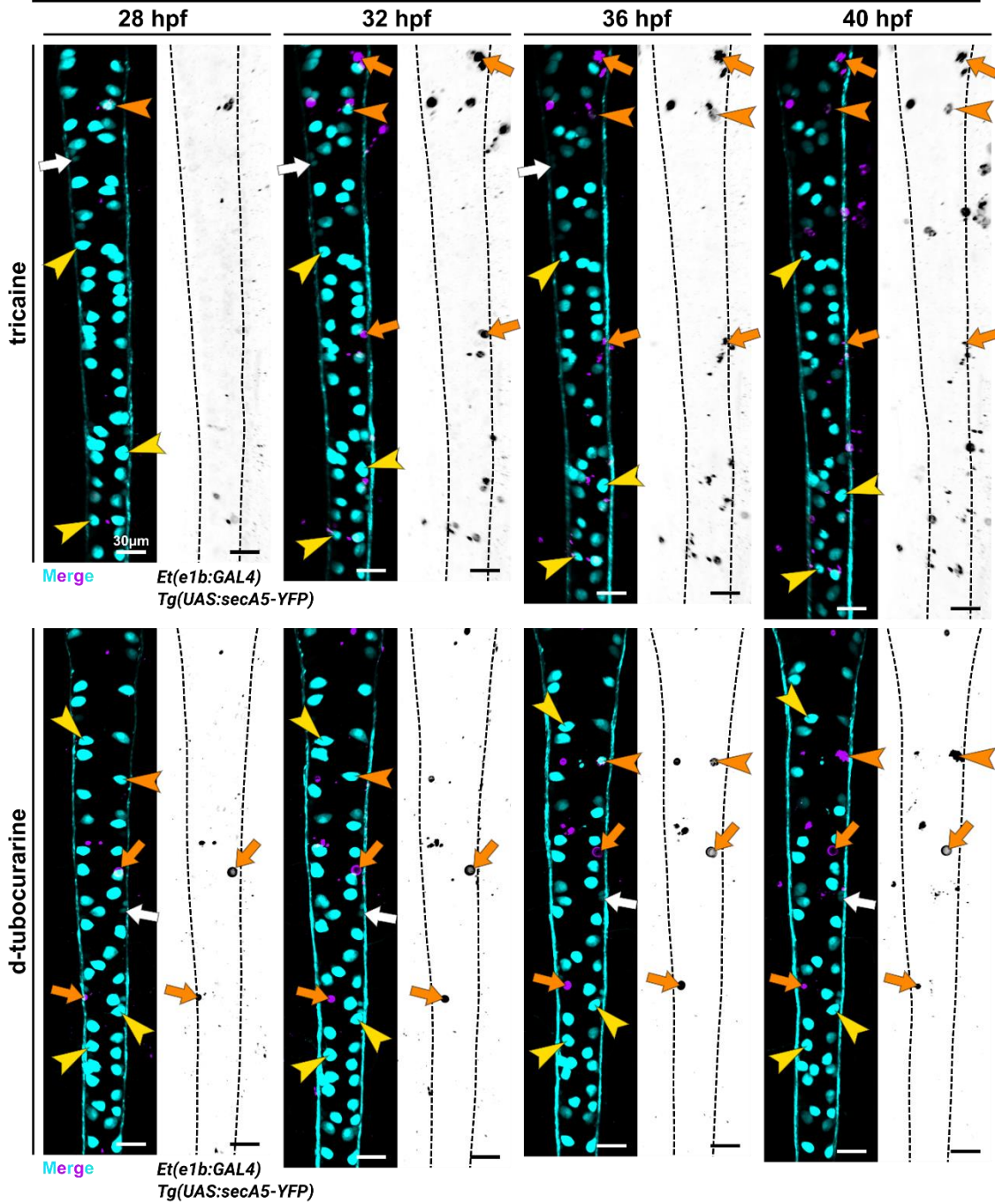
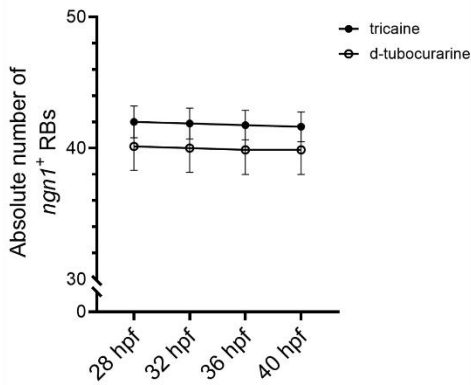
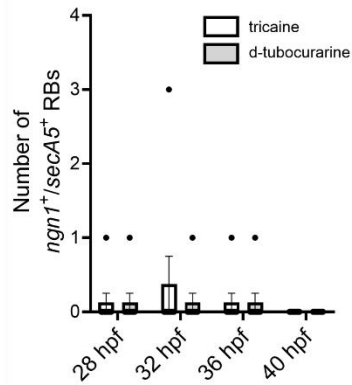
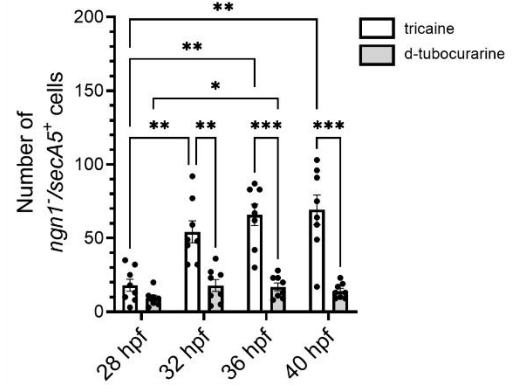
Developmental cell death is often influenced by neural activity<sup>16,230,231</sup> and previous work found that chronic dampening of neural activity impaired RB cell death<sup>268</sup>. We sought to investigate whether our observations from our previous time-lapse experiments were affected by the anesthetic used during imaging (tricaine, see **Materials & Methods: *In vivo* confocal imaging** for details). Tricaine inhibits neural voltage-gated sodium channels, leading to a reduction in neural activity<sup>275</sup>. To determine if blockade of neural activity could have affected our results, we opted to use d-tubocurarine, an antagonist for nicotinic acetylcholine receptors and a commonly used drug to immobilize zebrafish for electrophysiological or neuronal-activity dependent imaging<sup>276,277</sup>.

Simultaneously, we also sought to independently confirm that RBs were not dying by turning to an alternative method to visualize dying cells by imaging *Et(e1b:GAL4)<sup>278</sup>;Tg(UAS:secA5-YFP)<sup>195</sup>* embryos. *Tg(UAS:secA5-YFP)* expresses a YFP-tagged Annexin V protein, which binds with high affinity to phosphatidylserine, a lipid that is exposed on the membrane of dying cells<sup>279</sup>. *Et(e1b:GAL4);Tg(UAS:secA5-YFP)* in combination facilitates the visualization of almost all neurons in the zebrafish CNS<sup>280</sup>. Coupled with *Tg(ngn1:TagRFP)*, these lines allowed us to visualize dying neurons in a background that also labels RBs.

Starting at 24 hpf, we incubated *Et(e1b:GAL4);Tg(ngn1:TagRFP;UAS:secA5-YFP)* embryos in either tricaine or 10 mM d-tubocurarine and conducted *in vivo*, time-lapse imaging from 25 to 40 hpf. In these studies, we observed no gross differences between *Et(e1b:GAL4);Tg(ngn1:TagRFP;UAS:secA5-YFP)* embryos treated with tricaine or d-tubocurarine (Figure 3-3A). We found that the absolute number of *ngn1<sup>+</sup>* RBs did not differ significantly between drug treatments at 28, 32, 36, or 40 hpf (Figure 3-3B) and we observed very few instances of *ngn1<sup>+</sup>/secA5<sup>+</sup>* RB cells (Figures 3-3A & C). In one example, starting at 35 hpf, a *ngn1<sup>+</sup>* RB soma deformed and became *secA5<sup>+</sup>*. Within 10 minutes, the same *ngn1<sup>+</sup>/secA5<sup>+</sup>* RB cell adopted a rounded morphology and GFP fluorescence quickly fragmented. This *secA5<sup>+</sup>* RB corpse contained GFP<sup>+</sup> puncta and existed until the end of the time lapse, at 40 hpf (Figure 3-3A). These observations of a *ngn1<sup>+</sup>/secA5<sup>+</sup>* RB cell were incredibly rare, with only 8 *ngn1<sup>+</sup>/secA5<sup>+</sup>* RB cells identified over both treatment conditions (Figure 3-3C) (n = 8 embryos per

treatment; 4 embryos [one from tricaine group, 3 from d-tubocurarine group] observed to have one *ngn1*<sup>+</sup>/*secA5*<sup>+</sup> RB cell and one embryo from the tricaine group was observed to have 4 *ngn1*<sup>+</sup>/*secA5*<sup>+</sup> RB cells). We also quantified the total number of *secA5*<sup>+</sup> puncta and did however find statistically significant differences between timepoints and between treatment conditions (Figure 3-3D). From these data we conclude that death of other cell populations is affected by neural activity, as embryos treated with tricaine had increased numbers of *ngn1*<sup>+</sup>/*secA5*<sup>+</sup> puncta compared to embryos treated with d-tubocurarine. However, the absolute number of *ngn1*<sup>+</sup> RBs is not affected (Figure 3-3B) and the early survival of RBs we have observed in our imaging (Figures 3-1 & 3-2) was not due to decreased neural activity from the use of tricaine.

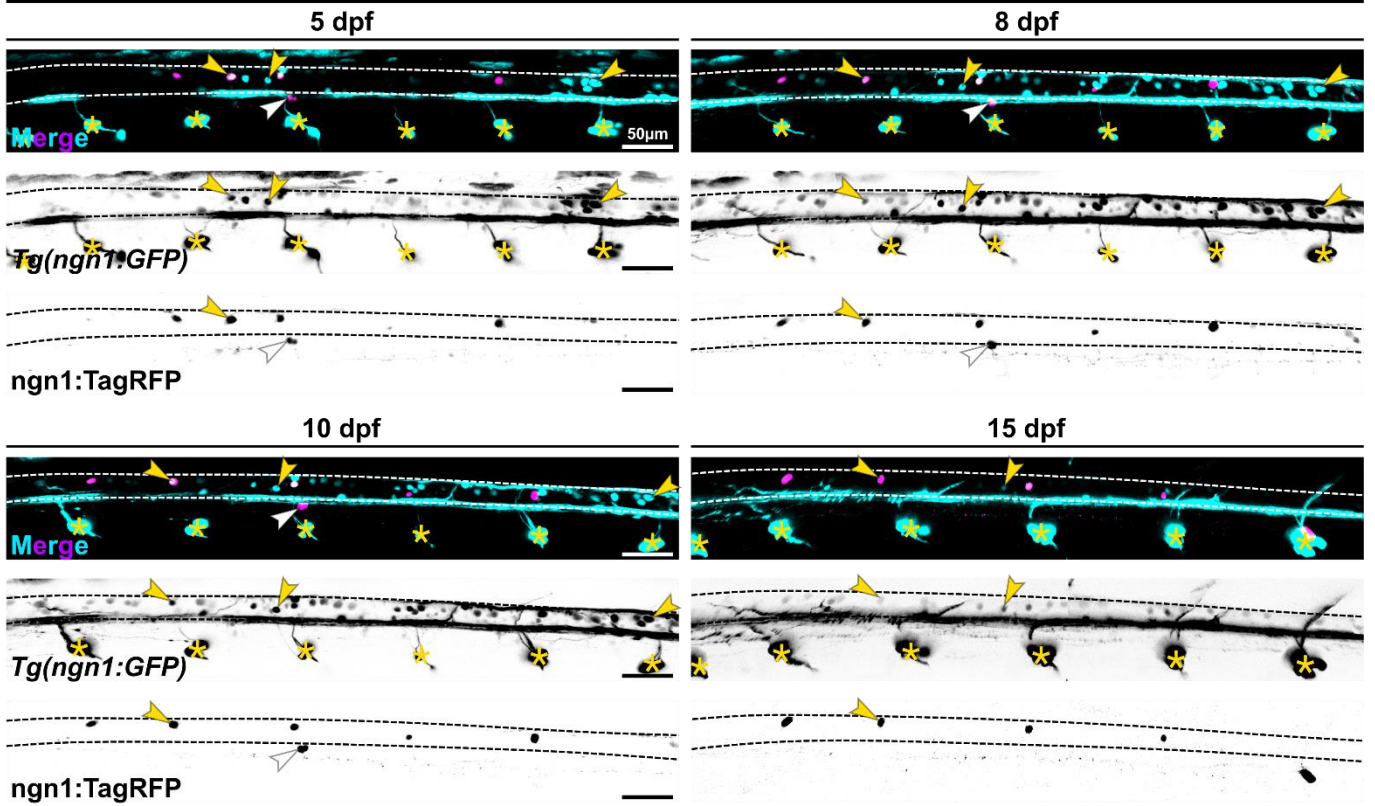
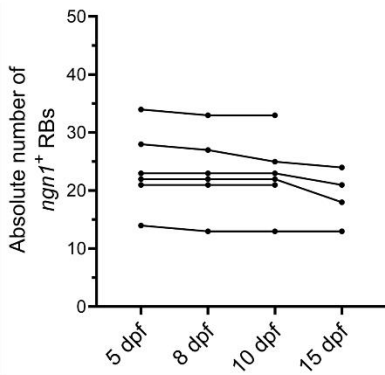
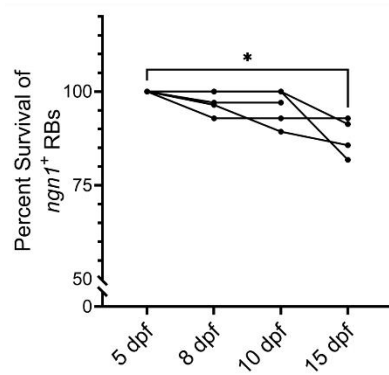
In these experiments, we sought to disambiguate whether the RB population succumbs to a developmental wave of cell death as previously described. In our studies, we identified zero dying RBs by TUNEL staining and only eight single dying RBs (out of 657 RBs) by live imaging. These instances of RB death are extremely rare and taken together with our previous findings, we conclude that the vast majority of *ngn1*<sup>+</sup> RBs are a stable population up to 5 dpf and do not die.

**A***Et(e1b:GAL4) Tg(ngn1:TagRFP;UAS:secA5-YFP)***B****C****D**

**Figure 3-3: RB survival is not due to decreased neural activity from tricaine administration. (A)** Images from a time-lapse movie of *Et(e1b:GAL4);Tg(ngn1:TagRFP;UAS:secA5-YFP)* embryos, one treated with tricaine (top) and one treated with d-tubocurarine (bottom). Images shown are in 4-hour increments from 28 to 40 hpf. Examples of *ngn1*<sup>+</sup> RBs tracked through the entirety of the time-lapse are marked with yellow arrowheads. An orange arrowhead points to a single *ngn1*<sup>+</sup>/*secA5*<sup>+</sup> RB in each embryo. White arrows denote other *ngn1*<sup>+</sup> cells and orange arrows denote *ngn1*<sup>+</sup>/*secA5*<sup>+</sup> cells. Dashed black lines in single channel images represent the DLF. **(B)** Quantification of the absolute number of *ngn1*<sup>+</sup> RBs at 28, 32, 36, and 40 hpf in *Et(e1b:GAL4);Tg(ngn1:TagRFP;UAS:secA5-YFP)* embryos treated with either tricaine (filled circles) or d-tubocurarine (empty circles, n = 8 embryos per treatment group). Repeated measures two-way ANOVA p values: Time x Drug p = 0.8958, Time p = 0.0298, Drug p = 0.4134, Embryo p < 0.0001. Adjusted p values for multiple comparisons: 28 hpf tricaine vs. d-tubocurarine p = 0.4070, 32 hpf tricaine vs. d-tubocurarine p = 0.4074, 36 hpf tricaine vs. d-tubocurarine p = 0.4110, 40 hpf tricaine vs. d-tubocurarine p = 0.4423, tricaine 28 vs. 32 hpf, tricaine 32 vs. 36 hpf, and tricaine 36 vs. 40 hpf p = 0.7545, tricaine 28 vs. 36 hpf and tricaine 32 vs. 40 hpf p = 0.4714, tricaine 28 vs. 40 hpf p = 0.2570, d-tubocurarine 28 vs. 32 hpf, d-tubocurarine 32 vs. 36 hpf, and d-tubocurarine 32 vs. 40 hpf p = 0.7545, d-tubocurarine 28 vs. 36 hpf and d-tubocurarine 28 vs. 40 hpf p = 0.4714. Mean ± SEM values for tricaine-treated embryos: 28 hpf: 42.000 ± 1.210, 32 hpf: 41.875 ± 1.172, 36 hpf: 41.750 ± 1.130, 40 hpf: 41.625 ± 1.133. Mean ± SEM values for d-tubocurarine-treated embryos: 28 hpf: 40.125 ± 1.817, 32 hpf: 40.000 ± 1.842, 36 and 40 hpf: 39.875 ± 1.884. **(C)** Quantification of the number of *ngn1*<sup>+</sup>/*secA5*<sup>+</sup> RBs of the same embryos in **B**. Data from embryos treated with tricaine are represented as white bars and data from embryos treated with d-tubocurarine are represented as grey bars. Repeated measures two-way ANOVA p values: Time x Drug p = 0.8139, Time p = 0.4164, Drug p = 0.6446, Embryo p = 0.1861. Adjusted p values for multiple comparisons: 28 hpf tricaine vs. d-tubocurarine and 36 hpf tricaine vs. d-tubocurarine p > 0.9999, 32 hpf tricaine vs. d-tubocurarine p = 0.5437, tricaine 28 vs. 32 hpf, tricaine 28 vs. 40 hpf, tricaine 32 vs. 40 hpf, and tricaine 36 vs. 40 hpf p = 0.7545, tricaine 28 vs. 36 hpf p > 0.9999, tricaine 32 vs. 36 hpf p = 0.9267, d-tubocurarine 28 vs. 32 hpf, d-tubocurarine 28 vs. 36 hpf, and d-tubocurarine 32 vs. 36 hpf p > 0.9999, d-tubocurarine 28 vs. 40 hpf, d-tubocurarine 32 vs. 40 hpf, and d-tubocurarine 36 vs. 40 hpf p = 0.7545. Mean ± SEM values: tricaine 28 hpf: 0.125 ± 0.125, tricaine 32 hpf: 0.375 ± 0.375, tricaine 36 hpf: 0.125 ± 0.125, tricaine 40 hpf, 0.000 ± 0.000, d-tubocurarine 28 hpf, d-tubocurarine 32 hpf, and d-tubocurarine 36 hpf: 0.125 ± 0.125, d-tubocurarine 40 hpf: 0.000 ± 0.000. One dot equals one embryo. All data in **B** & **C** was compared with repeated measures two-way ANOVA with Geisser-Greenhouse correction and Tukey's multiple comparisons tests. **(D)** Quantification of the number of *ngn1*<sup>+</sup>/*secA5*<sup>+</sup> puncta at 28, 32, 36, and 40 hpf of the same embryos in **B**. Data from embryos treated with tricaine are represented as white bars and data from embryos treated with d-tubocurarine are represented as grey bars. Mixed effects model p values: Time, Drug, and Time x Drug p < 0.0001. Adjusted p values for multiple comparisons: 28 hpf tricaine vs. d-tubocurarine p = 0.0835, 32 hpf tricaine vs. d-tubocurarine p = 0.0013, 36 hpf tricaine vs. d-tubocurarine p = 0.0001, 40 hpf tricaine vs. d-tubocurarine p = 0.0008, tricaine 28 vs. 32 hpf p = 0.0070, tricaine 28 vs. 36 hpf p = 0.0024, tricaine 28 vs. 40 hpf p = 0.0059, tricaine 32 vs. 36 hpf p = 0.4193, tricaine 32 vs. 40 hpf p = 0.6023, tricaine 36 vs. 40 hpf p = 0.9174, d-tubocurarine 28 vs. 32 hpf p = 0.1829, d-tubocurarine 28 vs. 36 hpf p = 0.0341, d-tubocurarine 28 vs. 40 hpf p = 0.2522, d-tubocurarine 32 vs. 36 hpf p = 0.9531, d-tubocurarine 32 vs. 40 hpf p = 0.6299, d-tubocurarine 36 vs. 40 hpf p = 0.4543. Mean ± SEM values: tricaine 28 hpf: 18.000 ± 4.114, tricaine 32 hpf: 54.250 ± 7.449, tricaine 36 hpf: 65.750 ± 7.250, tricaine 40 hpf, 69.250 ± 10.030, d-tubocurarine 28 hpf: 9.143 ± 2.109, d-tubocurarine 32 hpf: 17.875 ± 4.073, d-tubocurarine 36 hpf: 16.875 ± 2.669, d-tubocurarine 40 hpf: 14.125 ± 1.807. All data in **D** was compared with a mixed effects model with Geisser-Greenhouse correction and Tukey's multiple comparisons tests and one dot equals one embryo. All images in **Figure 3-3** are representative, maximum projection confocal images.

### 3.3.3 RBs persist until 15 dpf

Our characterization of RB survival up to 5 dpf led us to investigate how long RBs persist in the developing zebrafish. To do this, we extended our imaging of the same *Tg(ngn1:GFP)* embryos/larvae over several days that were injected at the one-cell stage with *ngn1:TagRFP*. We took advantage of cellular expression “landmarks” from the mosaic labeling by *ngn1:TagRFP* which allowed us to identify individual RBs and track them over several days. In these injected larvae we observed *ngn1*<sup>+</sup> RBs in the dorsal spinal cord as late as 15 dpf (Figure 3-4A). Starting at 10 dpf, fluorescence of several *ngn1*<sup>+</sup> RBs became so low that reliable identification was not possible. Due to the dimming of fluorescence in *ngn1*<sup>+</sup> RBs over time, we were unable to investigate *ngn1*<sup>+</sup> RB survival past 15 dpf. Still, the absolute number of *ngn1*<sup>+</sup> RBs did not differ significantly over time (Figure 3-4B). From our studies, we observed an average of 87.92% *ngn1*<sup>+</sup> RBs survived until 15 dpf. When calculating percent survival for these cells, there was a statistically significant decrease in *ngn1*<sup>+</sup> RB survival between 5 and 15 dpf (Figure 3-4C). From these studies, we conclude that RBs persist until at least 15 dpf in zebrafish.

**A***Tg(ngn1:GFP)* *ngn1:TagRFP***B****C**

**Figure 3-4: RBs persist until 15 dpf.** (A) Images of the same *Tg(ngn1:GFP)* larva that was injected with *ngn1:TagRFP* at the one-cell stage at 5, 8, 10, and 15 dpf. Representative examples of GFP<sup>+</sup> or GFP<sup>+</sup>/RFP<sup>+</sup> *ngn1*<sup>+</sup> RBs that persist until 15 dpf are marked by yellow arrowheads. *Ngn1*<sup>+</sup> DRGs are designated with yellow asterisks. Dashed white lines in fluorescent images and dashed black lines in single channel images mark the DLF. (B) Quantification of the absolute number of *ngn1*<sup>+</sup> RBs at 5, 8, 10, and 15 dpf of the same embryos in A (n = 6 embryos). Mixed effects model p value = 0.0344. Adjusted p values for multiple comparisons: 5 vs. 8 dpf p = 0.2327, 5 vs. 10 dpf p = 0.3924, 5 vs. 15 dpf p = 0.0908, 8 vs. 10 dpf p = 0.7567, 8 vs. 15 dpf p = 0.1325, 10 vs. 15 dpf p = 0.1802. Mean ± SEM values: 5 dpf: 23.67 ± 2.765, 8 dpf: 23.17 ± 2.713, 10 dpf: 22.83 ± 2.638, 15 dpf: 19.00 ± 2.345. (C) Quantification of the percent surviving GFP<sup>+</sup> or GFP<sup>+</sup>/RFP<sup>+</sup> *ngn1*<sup>+</sup> RBs of the same embryos in B over time. Mixed effects model p value = 0.0126. Adjusted p values for multiple comparisons: 5 vs. 8 dpf p = 0.3208, 5 vs. 10 dpf p = 0.3426, 5 vs. 15 dpf p = 0.0411, 8 vs. 10 dpf p = 0.7567, 8 vs. 15 dpf p = 0.1775, 10 vs. 15 dpf p = 0.2630. Mean ± SEM values: 5 dpf: 100.0 ± 0.000, 8 dpf: 97.72 ± 1.174, 10 dpf: 96.53 ± 1.847, 15 dpf: 87.92 ± 2.548. All data in B and C was compared with a mixed effects model with Geisser-Greenhouse correction and Tukey's multiple comparisons tests and one dot equals one fish. All images in **Figure 3-4** are representative, maximum projection confocal images.

### 3.4 DISCUSSION

Programmed cell death is a fundamental mechanism of neural development that facilitates error correction, pruning, and optimization of both cellular connections and neural circuits<sup>16,28,230,231</sup>. Work in multiple model systems have focused on Rohon-Beard neurons (RBs), as they are described to undergo global death during early development<sup>127,245–247,249,259–261</sup>. However, recent work demonstrates that a subset of zebrafish RBs survive into larval stages<sup>222,262</sup>. We set out to investigate this discrepancy and determine what proportion, if any, of the RB population persists. Our results demonstrate that *ngn1*<sup>+</sup> RBs do not die during early zebrafish development and survive until at least 16 dpf. We also observed several morphological changes, including a medial convergence of RBs and a decrease in RB soma size. We conclude that the vast majority of the RB population escapes developmental programmed cell death and persists.

Multiple studies characterize a disappearance of zebrafish RBs by a wave of cell death occurring between 1 and 3 dpf. However, these experiments lacked RB-specific markers and heavily relied on RB morphology and antibody labeling as primary methods to identify RBs. Additionally, antibody labeling alone (e.g. HNK-1/zn-12<sup>281,282</sup>, Isl1/2<sup>271,283–285</sup>, HuA<sup>268</sup>) is not RB-specific and labels other cells (including other spinal neurons). This makes identification of RBs difficult, especially at later stages of development given their medial convergence and somal shrinking (Figure 3-1). By repetitive imaging of individual fish coupled with mosaic *ngn1* expression, we overcome these obstacles to unambiguously identify and track individual RBs through development. Our work and others have described drastic changes in RB cell morphology<sup>222</sup>, which likely contributed to misidentification of RBs at later developmental stages. We find that with the growth of the developing embryo and elongation of the trunk, RBs undergo slight anterior-posterior displacement. Taking this into account, we find that the absolute number of RBs does not change. It is likely that previous quantifications of RB number standardized by distance or somite would have misled those to conclude that RB number decreases over development.

In our studies, we also observed a gradual dimming of fluorescence of *ngn1*<sup>+</sup> RBs (visualized via the *Tg(ngn1:GFP)*<sup>225</sup> transgene) starting at 3 dpf that spanned multiple days (Figure 3-1F). In some cases, the

gradual dimming continued until a previously fluorescent *ngn1*<sup>+</sup> RB was no longer visible. This contrasted with the sudden fragmentation and loss of fluorescence that occurred in a *ngn1*<sup>+</sup> RB that became *secA5*<sup>+</sup> 10 minutes later, an event we observed only eight times (Figure 3-3C). We argue that the gradual dimming of fluorescence of *ngn1*<sup>+</sup> RBs is not evidence of RB cell death, but rather downregulation of *ngn1*. However, we did not experimentally test this hypothesis. Further experiments utilizing *in situ* hybridization or RNAScope to assay *ngn1* expression in RBs would clarify whether the observed fluorescent dimming of *ngn1*<sup>+</sup> RBs is in fact due to loss of *ngn1* expression. The work presented here would be strengthened by completing the same experiments using an alternative transgenic tool to visualize RBs, ideally one that is continuously and strongly expressed in RBs throughout development.

Coincidentally and independent of our own investigations, we have discovered that work by Joaquín Navajas Acedo has completed these exact experiments and has separately come to the same conclusion: the RB population does not succumb to programmed cell death in early zebrafish development<sup>286</sup>. Using *Tg(isl2b:GFP)*<sup>zc7</sup> to label RBs, Navajas Acedo conducted serial imaging and found that the absolute number of *isl2b*<sup>+</sup> RBs is the same between 1 and 5 dpf<sup>286</sup>. Further, Navajas Acedo found that 97 to 100% of *isl2b*<sup>+</sup> RBs identified at 3 dpf survived until 15 dpf<sup>286</sup>. In alignment with our findings, Navajas Acedo found no dying RBs by either TUNEL staining or use of the *Tg(bAct:secA5-YFP)* transgenic tool<sup>286</sup>. While recent work described that a subset of RBs survive<sup>222,262</sup>, our work here and by Navajas Acedo provide strong evidence for survival of the near entirety of the RB population.

If RBs are not the dying cells in the dorsal spinal cord, what cells could they be? Many of the transgenic lines used to label RBs (*islet1[ssj]*<sup>262,287</sup>, *islet2b*<sup>288,289</sup>, *neurogenin1*<sup>225,226</sup>) also label various spinal interneurons, some which are in close proximity to RBs (e.g. dorsal longitudinal ascending interneurons, DoLAs). In our own imaging, we observed slightly smaller *ngn1*<sup>+</sup> cells just ventral to RB cell bodies, with their somas closely associated with the DLF (Figure 3-1B, C, F, 3-2A, & 3-3A).

We also observed much smaller *ngn1*<sup>+</sup> cells (~3 to 5 μm in diameter) with substantially lower fluorescence and ventral location. Due to the difficulty in distinguishing DoLA and ascending commissural neuron morphology, we did not separate these neuronal subsets here. In more caudal regions of the spinal cord, these potential *ngn1*<sup>+</sup> DoLAs are harder to distinguish from RBs and if undergoing cell death, could have been misinterpreted to be RBs. Also, earlier studies on RB death opted to image the spinal cord laterally rather than dorsally. Without markers of the dorsal boundary of the spinal cord, death of surrounding cells could be misidentified as dying RBs.

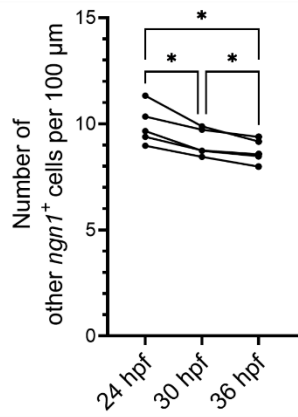
RBs and their death during development have been studied in multiple other species, including amphibians<sup>245–247</sup>, lampreys<sup>248,249</sup>, and other teleosts<sup>243,244</sup>. RB ancestors are also observed in phylogenetically earlier groups, such as amphioxus<sup>250,251</sup> and ascidians<sup>252</sup>. While some observations point to RB-like cells in human fetuses<sup>253–255</sup>, it is still unclear whether RBs definitively exist in other vertebrates. One hypothesis that explains the phylogenetic disappearance of RBs in amniotes is that somatosensory systems gradually evolved to rely on extramedullary sensory neurons (e.g. DRG neurons) rather than the more primitive intramedullary cells (e.g. RBs)<sup>256</sup>. A possible explanation for this is the survival of anamniote progeny may more heavily rely on early, functional sensorimotor circuitry due to their relative lack of protection from multiple predator species during development. This contrasts to amniotes whose progeny are laid within eggs or carried within an organism and may not have to rely on the same early circuitry to survive. Given our findings here and by Navajas Acedo, exciting new questions arise, including: Have RBs in other species also been misidentified and thought to be lost via cell death and therefore might also persist through development? And does this event of persisting RBs appear in species at a specific phylogenetic point?

RBs are a neuronal population known for their role in early somatosensory circuitry across multiple species. They have been described to undergo a drastic wave of developmental programmed cell death to make way for DRG neurons to integrate into neural circuitry. Recent studies have described a potential subset of RBs that survive past early development<sup>222,262</sup>. Building on this, we and Navajas Acedo assert that the vast majority of the RB population survives. With RBs surviving long past DRG formation and integration, this opens multiple

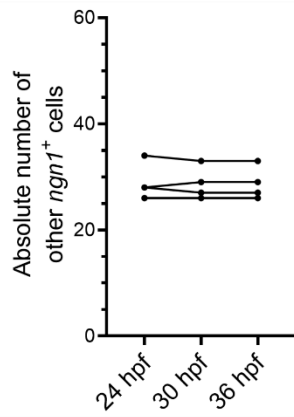
interesting avenues for future investigation. For example, how do surviving RBs affect the processing of sensory information and the physiology of somatosensory circuits? One possibility is that surviving RBs are repurposed for something else, but little is known about RB function aside from their role in early circuitry. Experiments dissecting the transcriptional state of RBs<sup>290</sup> and how RB gene signatures change over time may provide clues as to their function after development. Ultimately, the work here and that of Navajas Acedo opens many new avenues of exploration of RBs and somatosensory development.

### 3.5 SUPPLEMENTARY DATA

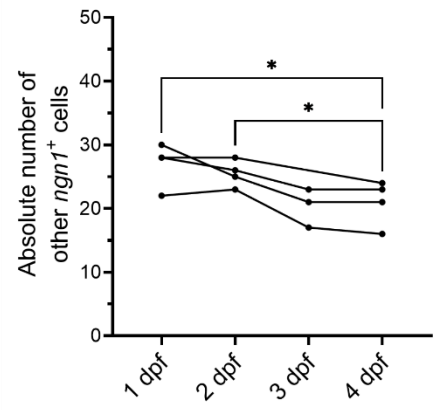
**A**



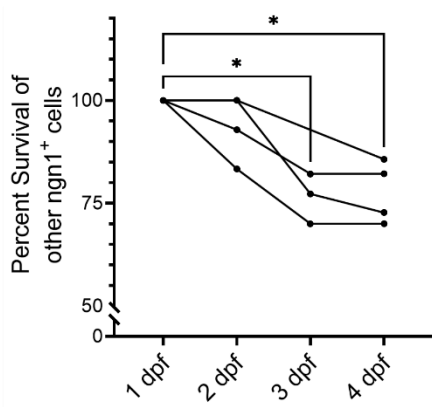
**B**



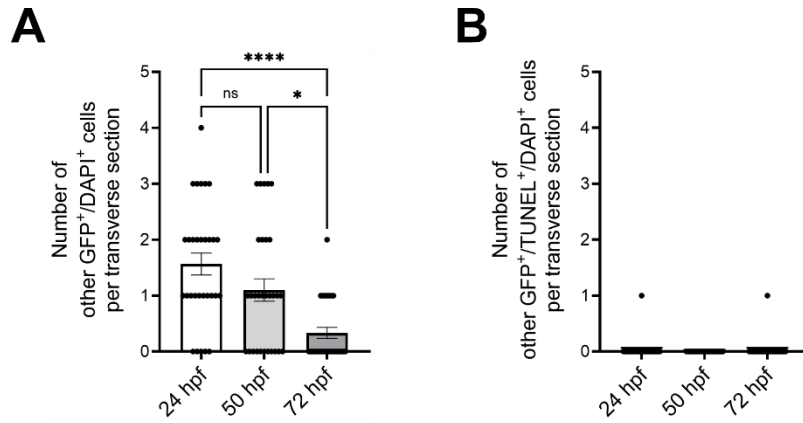
**C**



**D**



**Supplemental Figure 3-1: Other *ngn1*<sup>+</sup> cells have similar trends to *ngn1*<sup>+</sup> RBs.** **(A)** Quantification of the number of other *ngn1*<sup>+</sup> cells per 100  $\mu$ m at 24, 30, and 36 hpf of *Tg(ngn1:GFP)* embryos (n = 5 embryos), the same embryos reported in Figures 1D & 1E. Repeated measures one-way ANOVA p value = 0.0059. Adjusted p values for multiple comparisons: 24 vs. 30 hpf p = 0.0167, 24 vs. 36 hpf p = 0.0159, 30 vs. 36 hpf p = 0.0308. Mean  $\pm$  standard error of the mean (SEM) values: 24 hpf: 9.937  $\pm$  0.4141, 30 hpf: 9.105  $\pm$  0.2915, 36 hpf: 8.716  $\pm$  0.2511. **(B)** Quantification of the absolute number of other *ngn1*<sup>+</sup> cells of the same data in **A**. Repeated measures one-way ANOVA p value = 0.6213. Adjusted p values for multiple comparisons: 24 vs. 30 hpf and 24 vs. 36 hpf p = 0.8594. Mean  $\pm$  standard error of the mean (SEM) values: 24 hpf: 28.40  $\pm$  1.470, 30 and 36 hpf: 28.20  $\pm$  1.319. All data in **A** & **B** was compared with the repeated measures one-way ANOVA with Geisser-Greenhouse correction and Tukey's multiple comparisons tests and each dot represents one embryo. **(C)** Quantification of the absolute number of other GFP<sup>+</sup> *ngn1*<sup>+</sup> cells in *Tg(ngn1:GFP)* embryos injected with *ngn1:TagRFP* at the one-cell stage, the same embryos reported in Figures 3-1F – 3-1I. Mixed effects model p value = 0.0220. Adjusted p values for multiple comparisons: 1 vs. 2 dpf p = 0.6982, 1 vs. 3 dpf p = 0.0840, 1 vs. 4 dpf p = 0.0343, 2 vs. 3 dpf p = 0.0857, 2 vs. 4 dpf p = 0.0410, 3 vs. 4 dpf p = 0.8060. Mean  $\pm$  SEM values: 1 dpf: 27.00  $\pm$  1.732, 2 dpf: 25.50  $\pm$  1.041, 3 dpf: 20.33  $\pm$  1.764, 4 dpf: 21.00  $\pm$  1.780. **(D)** Quantification of the percent surviving GFP<sup>+</sup> other *ngn1*<sup>+</sup> cells of the same embryos in **C** over time. Mixed effects model p value = 0.0011. Adjusted p values for multiple comparisons: 1 vs. 2 dpf p = 0.5285, 1 vs. 3 dpf p = 0.0473, 1 vs. 4 dpf p = 0.0280, 2 vs. 3 dpf p = 0.0993, 2 vs. 4 dpf p = 0.0625, 3 vs. 4 dpf p = 0.9478. Mean  $\pm$  SEM values: 1 dpf: 100.0  $\pm$  0.000, 2 dpf: 94.05  $\pm$  3.948, 3 dpf: 76.47  $\pm$  3.528, 4 dpf: 77.65  $\pm$  3.741. All data in **C** & **D** was compared with a mixed effects model with Geisser-Greenhouse correction and Tukey's multiple comparisons tests and each dot represents one embryo.



**Supplemental Figure 3-2: Other *ngn1*<sup>+</sup> cells have similar trends to *ngn1*<sup>+</sup> RBs in transverse slices. (A)** Quantification of the number of other *ngn1*<sup>+</sup> cells per transverse section for each timepoint. Brown-Forsythe and Welch's ANOVAs p values < 0.0001. Adjusted p values for multiple comparisons: 24 vs. 50 hpf p = 0.2698, 24 vs. 72 hpf p < 0.0001, 50 vs. 72 hpf p = 0.0040. Mean ± SEM values: 24 hpf: 1.567 ± 0.1958, 50 hpf: 1.100 ± 0.1997, 72 hpf: 0.3333 ± 0.09981. **(B)** Quantification of the number of dying other *ngn1*<sup>+</sup> cells per transverse section for each timepoint. Brown-Forsythe ANOVA p value = 0.6091. Since the number of dying other *ngn1*<sup>+</sup> cells per transverse section at 50 hpf is zero for all slices counted, Welch's ANOVA and Dunnett's T3 multiple comparisons test could not be used and adjusted p values could not be calculated. Mean ± SEM values: 24 hpf and 72 hpf: 0.03333 ± 0.03333, 50 hpf: 0.000 ± 0.000. Data in **A** and **B** was compared with the Brown-Forsythe and Welch's ANOVAs with Dunnett's T3 multiple comparisons tests, one dot equals one transverse slice, and n = 30 transverse slices per timepoint coming from 5 different embryos.

### 3.6 ACKNOWLEDGEMENTS

We would like to first thank Lori Tocke for exceptional fish care, as none of our work is possible without her skills and dedication. We would also like to thank the members of the Kucenas Lab, past and present, for their incredibly valuable insight and discussions. We thank Prof. Alvaro Sagasti and Prof. Alex Nechiporuk who offered valuable guidance for this project. We also thank Dr. Oded Mayseless for connecting us with Prof. Alex Schier and Dr. Joaquín Navajas Acedo. We would like to thank Dr. Navajas Acedo for his enthusiasm, collaborative spirit, and suggestions. Lastly, we extend many thanks to ZFIN ([www.zfin.org](http://www.zfin.org)) for being an extensive, invaluable resource for this project and the entire zebrafish community.

# Chapter 4: DISCUSSION & FUTURE DIRECTIONS

---

## 4.1 SUMMARY

Altogether this dissertation examined programmed cell death and circuit refinement in zebrafish neurodevelopment. Surprisingly, I found that contrary to many previous studies Rohon-Beard (RB) neurons do not succumb to developmental programmed cell death. I found that RB neurons are not marked by TUNEL staining or by an *in vivo* reporter of cell death. My quantifications demonstrated that the absolute number of RB neurons do not change over early development, and the vast majority of RB neurons persist until at least 15 dpf. **Chapter 3** provides a discussion on these findings therefore the remainder of this chapter will discuss specific experimental future directions and broader implications of the survival of RBs on zebrafish neurodevelopment.

## 4.2 A LESSON IN CAREFUL, CRITICAL SCIENCE

In **Chapter 3.4**, I provide several reasons why previous studies may have mischaracterized early RB death. In brief, non-specific markers for RBs, lateral whole-mount imaging, and standardizing quantifications by distance or somite all likely contributed to the misidentification of dying RBs. Multiple studies interpreted a loss of fluorescence (by either transgene or antibody), somal shrinkage, and development of beaded peripheral processes as indications of cell death. However, equally plausible interpretations of this data are certain genes in RBs are downregulated over development, RB somas undergo remodeling, and artifacts from transgene expression or antibody staining led to the appearance of beads in peripheral processes. So why was one interpretation favored over the others? Some studies do report cell death markers in RB neurons (e.g. caspase-3<sup>222</sup>, TUNEL<sup>27,261,267,268,291</sup>, Annexin V<sup>195,222</sup>), but this was observed in very few RBs and not widespread within the RB population. Perhaps in light of these findings, similar observations from amphibians<sup>245–247</sup> and lampreys<sup>248,249</sup>, and a lack of evidence for RB soma and process remodeling, scientists opted for the most agreeable conclusion.

Recent evidence has unveiled non-apoptotic roles for caspases in development<sup>292</sup>. Of relevance here is cleaved caspase-3, an apoptosis effector caspase commonly measured in assays for apoptotic cells<sup>293–295</sup>.

Interestingly, cleaved caspase-3 localizes to synapses, axons, and dendrites that undergo remodeling in *Drosophila*<sup>296–298</sup>, *C. elegans*<sup>299</sup>, zebra finch<sup>300</sup>, zebrafish<sup>301</sup>, *ex vivo* rat hippocampal slices<sup>302</sup>, and mice<sup>298,303,304</sup>. Emerging work has also implicated cleaved caspase-3 in extracellular vesicle protein cleavage<sup>305</sup>, cell differentiation<sup>306,307</sup>, synaptogenesis<sup>308</sup>, and long-term depression<sup>309</sup>. Given these non-apoptotic roles of caspase-3, it is plausible that previous, sparsely positive cleaved caspase-3 RBs were undergoing remodeling. In conclusion, assaying cell death with cleaved caspase-3 staining should be validated with secondary measures (e.g. TUNEL staining, pharmacological manipulations of apoptosis, etc.) and awareness of the non-apoptotic roles of caspase-3 (and other caspases) should be at the forefront when interpreting data.

Detection of DNA fragmentation has long been considered the gold standard for assaying cell death<sup>295</sup>. One of the most common assays is TUNEL, which labels double-stranded DNA breaks<sup>273</sup>. One caveat of the TUNEL assay is it does not discriminate between cells dying through apoptosis, necrosis, pyroptosis, or autolytic forms of cell death<sup>310,311</sup>. While double-stranded DNA breaks occur during cell death, they also play roles in DNA repair<sup>312</sup>, gene transcription and expression<sup>313–316</sup>, and neuronal differentiation and maturation processes<sup>317–319</sup>. The quantity of double-stranded DNA breaks involved in these processes versus the quantity that results in apoptosis are generally unknown. Even so, TUNEL has been shown to mark cells undergoing active DNA repair<sup>320</sup>, gene transcription<sup>313</sup>, or proliferation<sup>321</sup>. There is also evidence that TUNEL<sup>+</sup> cells can recover and escape from the brink of cell death<sup>322–326</sup>.

Altogether, there are multiple reasons why previous researchers misidentified RB neurons as dying. Recent advancements in genetics and imaging have resolved some of these difficulties but have also highlighted others, namely the non-apoptotic roles of caspases and double-stranded DNA breaks. Thus, measures of cell death should be validated by a second, independent measure and accompanied by rigorous controls whenever possible<sup>295,327</sup>. It is likely that previously identified TUNEL<sup>+</sup> or cleaved caspase-3-positive RB neurons were undergoing changes in gene expression and/or structural remodeling rather than cell death. This aligns with my observations that laterally positioned RB somas converge medially, and this medialization is accompanied by significant somal shrinkage between 1 and 2 dpf. Overall, this critique is meant as a reminder that we should be

mindful of the caveats associated with our methods and measures in addition to considering and testing alternative interpretations of our data.

### 4.3 THE LIVING DEAD: SURVIVING ROHON-BEARD NEURONS

Originally, RBs were hypothesized to die off in early zebrafish development to allow dorsal root ganglion (DRG) neuron integration into the touch-response circuit<sup>27,223,261</sup> (see **Chapter 3**). Since Joaquín Navajas-Acedo and myself have established that almost all RBs survive past early development<sup>328,329</sup>, several important questions about RB survival and function arise. Additionally, the experiments presented in **Chapter 3** focused on RB cell bodies and were not able to determine whether RB peripheral axons also survive until 15 dpf. It seems unlikely that RBs and their axons would persist if they are not needed, as extraneous cells are pruned in early development in part by a hypothesized effort to conserve energy and resources<sup>16,28</sup>. Here, I propose several experimental directions to interrogate the survival and function of RBs in later zebrafish development.

#### 4.3.1 How long do Rohon-Beard neurons survive?

A critical unanswered question stemming from my work is whether RB neurons survive post-15 dpf. Experiments examining sensory innervation of the scales suggest that RB axon innervation is lost during late juvenile stages, around ~14 mm standard length (SL)<sup>330,331</sup>. Interestingly, this timing coincides with scale formation, which begins around 8 mm SL<sup>332</sup>, and one hypothesis is that scale development coordinates the transition from RB to DRG innervation<sup>331</sup>. Regarding RB survival, these experiments only directly visualized DRG axons and did not use an RB-specific marker to visualize RB somas or axons. And, as previously discussed, loss of RB axon innervation does not necessarily equate to cell death. Repeated imaging experiments (similar to those completed in **Figures 3-1 & 3-4**)

of fish extending post-15 dpf would determine the duration of RB survival. Given the dimming of fluorescence in RBs that I observed in *Tg(ngn1:GFP)* larvae (**Figure 3-4**), different transgenes should be used in these experiments. Both *Tg(isl2b:GFP)<sup>zc7</sup>* and *Et(prdm14:GAL4)<sup>277</sup> Tg(UAS:EGFP)* strongly label RBs<sup>289,290,328,A</sup> and

---

<sup>A</sup> Alex V. Nechiporuk (personal communication, November 16, 2023)

would be good starting places for visualizing RBs post-15 dpf. Lastly, great care should be taken in interpreting cell survival from fluorescent transgene expression and cell death should be rigorously evaluated as discussed previously.

In my experiments detailed in **Chapter 3**, I observe that RBs labeled by *Tg(ngn1:GFP)* decrease in fluorescence over time and I hypothesized that this may be due to loss of *ngn1* expression. Other studies examining RBs during early development have also likely misinterpreted a loss of fluorescent signal as evidence of cell death. Additionally, one published paper included images of *Tg(isl2b:GFP)* fish at 15, 20, and 26 dpf which demonstrated a progressive loss of RBs labeled by GFP<sup>289</sup>. These observations suggest that RB neurons may exhibit multiple changes in gene expression over zebrafish development. Thus, experiments should include methods to distinguish between the downregulation of *isl2b* (or any gene) and subsequent decrease of GFP fluorescence in RBs versus RB cell death. One avenue is to combine RB-specific transgenes with a more ubiquitous neuronal reporter (e.g. *elav3*<sup>333,334</sup>) that is not anticipated to be downregulated. This would allow for early identification of RBs and continued visualization of these identified RBs over time, even after downregulation of RB-specific transgenes. Given the large number of neurons in the spinal cord, this would only be feasible if *elav3*<sup>+</sup> RB somas could be distinguished from other *elav3*<sup>+</sup> neurons.

Another experimental approach would take advantage of the inducible *Cre/lox* system to facilitate labeling of RB neurons. The *Cre/lox* system has been widely used for inducible spatiotemporal control of gene expression and lineage tracing in multiple model systems. In zebrafish, inducible *Cre/lox* systems have been developed to include 4-OHT<sup>335,336</sup>, heat shock<sup>337,338</sup>, and photosensitive<sup>339</sup> modalities. To assay RB survival, an inducible *Cre* driven by an early-expressed RB-specific promoter (e.g. *isl2b*, *ngn1*, *prdm14*) in concert with a ubiquitous promoter driving a loxP-flanked fluorophore could be used. For example, 4-OHT treatment of *Tg(isl2b:CreER<sup>T2</sup>; ubi:loxp-EGFP-loxp-mCherry<sup>cz1701</sup>)*<sup>331,340</sup> embryos at 48 hpf would induce *CreER<sup>T2</sup>* expression in *isl2b*<sup>+</sup> cells (including RBs), resulting in EGFP excision and permanent mCherry expression. Thus, mCherry<sup>+</sup> RBs could be visualized and tracked over time regardless of *isl2b* downregulation. However, a common caveat of inducible *Cre/lox* systems is nonspecific or leaky expression of *CreER<sup>T2</sup>*<sup>335,337,341,342</sup>. Recent advancements in genetic

engineering have produced improved alternatives but these limitations should be kept in mind when interpreting experimental results. The experiments proposed here would greatly contribute to our knowledge of RBs and address a major question that arose from my work presented in **Chapter 3**.

### 4.3.2 Do Rohon-Beard neurons undergo axon or synaptic remodeling?

RBs were first characterized by their role in the touch-response circuit during early zebrafish development. RB neurons synapse on ipsilateral primary ascending commissural (CoPA) interneurons<sup>265,343</sup>, which synapse on contralateral descending interneurons that activate motor neurons<sup>258</sup>. Altogether, this connectivity results in a functional touch-response circuit by 24 hpf<sup>209,263,264</sup>. The predominant hypothesis for RB cell death was to allow for integration of DRG neurons into the touch-response circuit, which would facilitate more complicated and precise motor behavior in response to sensory stimuli. Now that I have established that the vast majority of RBs persist until at least 15 dpf, an interesting future direction is to ascertain whether RB peripheral axons and RB-CoPA synapses exist and are functional past early development. There is some evidence that RB peripheral axons exist until ~14 mm SL<sup>331</sup> but it is currently unknown whether these peripheral axons contribute to somatosensory processing. Interestingly, RBs were found to synapse on a subpopulation of V2a interneurons by 4 dpf<sup>344</sup>. V2a interneurons are a class of premotor excitatory interneurons that contribute to turning and controlling locomotion frequency<sup>266,344–346</sup>. When using the *isl2b* promoter to express Botulinum toxin to block synaptic release, tail-beat frequency and speed were markedly reduced<sup>344</sup>. *Isl2b* is not exclusive to RBs and is also expressed by DRG<sup>289,347</sup> and trigeminal neurons<sup>288</sup>. Thus, it is possible that these populations also contribute to locomotor frequency and speed. A separate study demonstrated that activation of caudal RBs elicited activity in commissural local (CoLo) interneurons in 42.4% of trials<sup>348</sup>. This variability in CoLo activation by RBs suggests a multi-synaptic connection where input from other sources (or multiple RBs) may contribute to CoLo firing. Altogether, these experiments suggest that RBs undergo synaptic remodeling after establishment of the early touch-response circuit. However, no studies have visualized the development of RB synapses and determined the precise timing where RB-V2a and RB-CoLo synapses are formed.

One way to determine whether RB axons undergo remodeling after early development is to conduct repeated *in vivo* imaging of individual *Tg(isl2b:GFP)* or *Et(prdm14:GAL4) Tg(UAS:EGFP)* fish to visualize RBs over development. These fish should also contain a transgene to visualize early born and mature DRG neurons<sup>349</sup> (e.g. *Tg(elavl3:mCherry)* or *Tg(sox10:Cre<sup>zf384</sup>; ubi:loxP-GFP-loxP-mCherry<sup>cz1701</sup>)*<sup>331,340,350</sup><sup>B</sup>). Around 54 hpf, RB neurons innervate within the skin layers<sup>351</sup> and the pectoral fin by 5 dpf<sup>352</sup> while DRG neurons begin extending towards developing scales at ~14 mm SL (~54 dpf)<sup>331</sup>. This suggests that even though DRG neurons differentiate at ~36 hpf<sup>349,353</sup>, sensory innervations from the spinal cord to the skin are predominantly from RB neurons until zebrafish are juveniles. Repeated imaging of RBs, DRG neurons, and their axons projecting to the skin or pectoral fin beginning at 5 dpf and extending until juvenile stages would elucidate whether RB peripheral axons undergo structural remodeling. Previous imaging studies demonstrate that RBs differ by anterior-posterior positioning<sup>354</sup>, arborization patterns<sup>262</sup>, gene expression<sup>262,355</sup>, and physiology<sup>356</sup> which suggest there are subtypes of RB neurons (see Chapter 4.4 Potential for Rohon-Beard neuron subtypes). Thus, it is possible that certain subtypes of RBs undergo remodeling while others do not. Depending on the degree of overlap between different RBs and their peripheral axons, injection of a differently colored transgene (e.g. *Tg(isl2b:TagBFP-CAAX)*) at the 1-cell stage to facilitate mosaic expression in RBs could help in visually differentiating between peripheral arbors. Alternatively, labeling via Zebrafish Brainbow (e.g. *Et(prdm14:GAL4) Tg(UAS:Zebrabow)*<sup>357</sup> coupled with injecting Cre protein at the blastula stage or 4-OHT treatment of *Tg(isl2b:CreER<sup>T2</sup>; ubi:Zebrabow)* embryos) would result in a combinatorial expression of RFP, YFP, and CFP resulting in a range of 3 to 30 colors<sup>357</sup>. This approach would allow for finer distinction between neighboring and/or overlapping RB somas and peripheral arbors.

Many studies have established that RB neurons are synaptically connected to CoPA<sup>258,265,343</sup>, V2a<sup>344</sup>, and CoLo<sup>348</sup> interneurons through electrophysiological studies. However, only one study has imaged RB synaptic connections<sup>358</sup> but limited their examination to 19 to 28 hpf. It is currently unknown whether RB-CoPA synapses exist past early development and the dynamics of RB-V2a and RB-CoLo synaptic formation. To address this question, I would conduct imaging of embryos with transgenes marking RBs (e.g. *Et(prdm14:GAL4)*

---

<sup>B</sup> Depending on which transgene is chosen to visualize DRG neurons, the fluorophore driven by GAL4-UAS system to visualize RBs should be a different color.

*Tg(UAS:mCherry)*), CoPAs (e.g. *Tg(tbx16:GFP)<sup>812C</sup>*<sup>359</sup>), and synapses (e.g. *Tg(UAS:sypb-EGFP)<sup>ion7d</sup>*<sup>360</sup> or *Tg(UAS:PSD95-GFP)*<sup>361,362</sup>) at different timepoints between 36 hpf and 4 dpf. These imaging data would provide answers as to whether there are changes in the number or distribution of RB-CoPA synapses over early development. It is also possible that RB-CoPA synapses undergo remodeling after 4 dpf, which is also when RB-V2a synapses become functional<sup>344</sup>. Similar imaging experiments can be done visualizing V2a (via *Tg(chx10:dsRed)<sup>nns3</sup>*<sup>363</sup>) or CoLo interneurons (via Tol-056)<sup>364</sup>. Currently, electrophysiological studies of RB synapses have been limited to 6 dpf (RB-CoLo experiments were completed on 4 to 6 dpf larvae<sup>348</sup>). Alternatively, synapses can be labeled by the pan-MAGUK antibody which labels postsynaptic density proteins PSD-95, PSD-93, and SAP102<sup>365</sup>.

If these experiments find evidence of synaptic remodeling in RBs (perhaps by a change in the number or distribution of RB synapses), many exciting avenues could be pursued. For example, investigating how synaptic function may change over time or remodeling by examining RB neural activity and subsequent interneuron responses by tools such as GCaMP6s<sup>366,367</sup> or iGluSnFR<sup>368,369</sup>. Additional functional experiments can include optogenetic, electrophysiological, and behavioral methods to further dissect RB functionality and interrogate changes in somatosensory circuitry after early development.

Altogether, the experiments proposed here would offer crucial, new insight into RBs and whether there are changes in RB axon and synapse structure and function after early development.

#### **4.4 POTENTIAL FOR ROHON-BEARD NEURON SUBTYPES**

Several studies have demonstrated that RBs differ by anterior-posterior positioning<sup>354</sup>, arborization patterns<sup>262</sup>, gene expression<sup>262,355</sup>, and physiology<sup>356</sup> which suggest there are subtypes within the RB population. Recent single-cell RNA sequencing (scRNAseq) datasets support these observations.

Multiple scRNAseq datasets have identified RBs in developing zebrafish ranging from 14 to 96 hpf<sup>290,370–373</sup>. Lencer et al., 2021 identified the RB population as expressing canonical genes (e.g. *isl1*<sup>271,284,287,374</sup>, *isl2a/b*<sup>285,375–</sup>

<sup>377</sup>, *prdm14*<sup>290,378</sup>) and others (e.g. *drgx*<sup>379</sup>, *p2rx3a*<sup>262,380</sup>, *scrt2*<sup>381</sup>). Unique to this RB population is the expression of *cxcr4b*, *fgf13a/b*, and *pou4f4* – all which have not been previously known to be expressed by RBs<sup>371</sup>. Lencer's findings were corroborated by comparison to a different scRNAseq dataset, which also had an annotated cluster of RBs<sup>370</sup>. Another separate scRNAseq dataset by Tuttle et al., 2024 enriched for spinal neurons found that RBs had increased expression of fibroblast growth factor (Fgf) targets and pharmacological or genetic inhibition of Fgf signaling resulted in loss of RB axons. This may be one molecular avenue for later degeneration of RB peripheral axons as discussed in **Chapter 4.3.2**. Interestingly, this dataset also identified three sub-clusters within the RB population<sup>290</sup>: *kitb*<sup>+</sup> RBs, *calca*<sup>+</sup> RBs, and *adcyap1*<sup>+</sup> RBs. By comparing these three RB sub-clusters to a single-nucleus RNA sequencing dataset of adult mouse trigeminal and DRG neurons, Tuttle et al., 2024 speculate that *calca*<sup>+</sup> RBs may function in mechanoreception and nociception. *Kitb*<sup>+</sup> RBs also highly express *trpa1*, which is implicated in irritant sensing and itch-like behavior in mammals<sup>382–384</sup> and adult zebrafish<sup>385</sup>. Interestingly, *adcyap1*<sup>+</sup> RB sub-cluster was not transcriptionally similar to any mammalian trigeminal or DRG neuron subtypes and is an avenue for future investigation. Altogether, these transcriptional data point to potential novel functions of RBs in nociception and itch sensation in larval and juvenile fish.

While these emerging studies have provided valuable insight into the RB transcriptome, these scRNAseq datasets are often marred by small amounts of isolated cells and an even smaller fraction that are identified as RBs. The Lencer dataset contained only 36 cells in the RB cluster while Tuttle examined 447 4 dpf RBs (from Kelly et al., 2023). Currently, there are no transcriptional datasets examining RBs post-7 dpf; thus, it is unknown whether the transcriptional profiles discussed previously also define RBs in later development.

## 4.5 FINAL REMARKS

Altogether, the data and hypotheses presented in this dissertation have unveiled a surprising finding of RB survival in face of many previous reports. These findings illuminate many potential avenues for future work on exploring RBs state and function in later development. This work also unveils interesting implications for mechanisms of somatosensory integration and function over development.

# Appendices INVESTIGATING NEURAL CREST CELLS AS NOVEL PHAGOCYTES IN EARLY DEVELOPMENT

---

## A.0 PREFACE

The contents of these appendices are organized into different research directions I pursued during my time in the Kucenas Lab. The data included in this section may have been included in poster presentations and informal talks but has not been currently published, as of October 30<sup>th</sup>, 2024, otherwise.

## A.1 PHAGOCYtic NEURAL CREST CELLS IN EARLY ZEBRAFISH DEVELOPMENT

With dying cells present as early as neural tube closure, phagocytes play a critical role in the rapid and efficient clearance of dying cells<sup>16,38,386</sup>. This clearance is crucial, as delayed engulfment of dying cells leads to inflammation and autoimmunity<sup>33,387</sup>. In the nervous system, phagocytes (microglia) also play a role in synapse engulfment (i.e. “pruning”), a process essential to both developmental circuit formation and learning-dependent circuit plasticity<sup>53,65,80,388</sup>. In **Chapter 1**, I review why sculpting of the central and peripheral nervous systems (CNS and PNS, respectively) during neurodevelopment is necessary to generate a functional and adaptable organism. In brief, this sculpting involves the over-proliferation of neurons and subsequent pruning of their projections and synapses to homeostatic levels. Thus phagocyte activity in development, homeostasis, and learning is vital, and aberrant debris clearance and pruning are heavily implicated in multiple neurodevelopmental (Nasu-Hakola disease, Rett syndrome)<sup>389</sup> and neurodegenerative (Parkinson’s disease, multiple sclerosis)<sup>390,391</sup> disorders. Emerging evidence also points to early dysregulation of synaptic and circuit pruning by phagocytes in the pathophysiology of neuropsychiatric disorders (schizophrenia, Autism spectrum disorder)<sup>48,392,393</sup>. Intriguingly, even though there are many dying cells present, there are no professional phagocytes (namely microglia or macrophages [MΦ]) present in early development to clear them. Thus, understanding the cellular mechanisms behind phagocytosis and the effects of phagocytic populations on neurodevelopment is crucial to understanding their aberrant behavior in disease, which can provide new avenues for effective therapeutics<sup>164,231,394–399</sup>.

In studies using zebrafish, the Kucenas lab recently identified neural crest cells (NCCs) as novel phagocytes that actively consume dying cells during an early developmental period (~24 to 40 hours post fertilization [hpf], **Figure A-1 & A-2**)<sup>126</sup>. Similar to professional phagocytes<sup>400,401</sup>, NCCs engulf debris through PI(3)P<sup>+</sup> and LAMP1<sup>+</sup> phagolysosomes and are recruited to apoptotic cells via IL-1 $\beta$ . Unlike other non-professional phagocytes, NCCs are surprisingly motile and respond to apoptotic cells and injury more than 100  $\mu$ m away<sup>126</sup>. These results frame NCCs as novel phagocytes and central players in debris and cell corpse clearance, synaptic pruning, and circuit formation in early development. Mechanisms behind how phagocytic NCCs recognize and clear debris, interact with other cells, and tune neural function are unknown. I sought to fill this void by answering questions related to the functional importance of NCC phagocytosis in neurodevelopment and how NCCs communicate with later-infiltrating professional phagocytes.

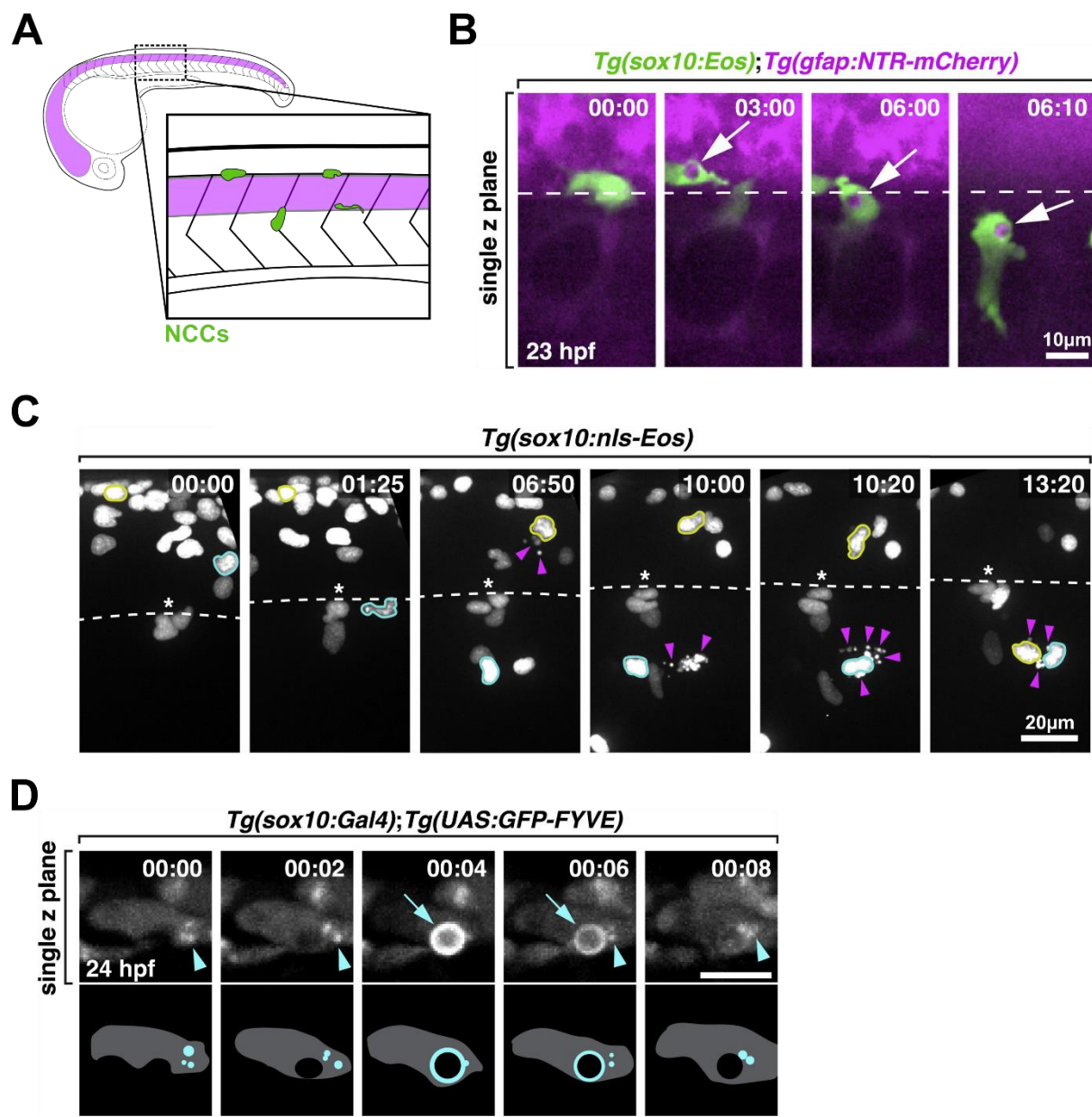


**Figure A-1: Neural crest cells are novel phagocytes in zebrafish development.** (A) Schematic of a laterally mounted zebrafish embryo at 24 hpf with the spinal cord highlighted in magenta. Inset shows a magnified view with NCCs illustrated in green. (B) Single z plane images from a time-lapse of a *Tg(sox10:eos; GFAP:NTR-mCherry)* embryo with *sox10*<sup>+</sup> NCCs pseudo-colored as green and *GFAP*<sup>+</sup> radial glia as magenta. Arrows denote NCC engulfment vesicle filled with *GFAP*<sup>+</sup> radial glia debris. (C) Images from a time-lapse of a *Tg(sox10:nls-eos)* embryo starting at 21 hpf. NCCs that migrated toward debris are outlined in yellow and cyan. Magenta arrowheads denote dead NCCs. Dashed line (B & C) marks the ventral edge of the spinal cord. (D) Images from a time-lapse of a *Tg(sox10:GAL4; UAS:GFP-FYVE)* embryo starting at 24 hpf. Over time, scattered PI(3)P signals (cyan arrowheads) fuse with an engulfment vesicle (cyan arrows). Schematic diagrams are shown below. Scale bar is 10 μm. **Figure A-1B – D** are from Zhu et al., 2019.

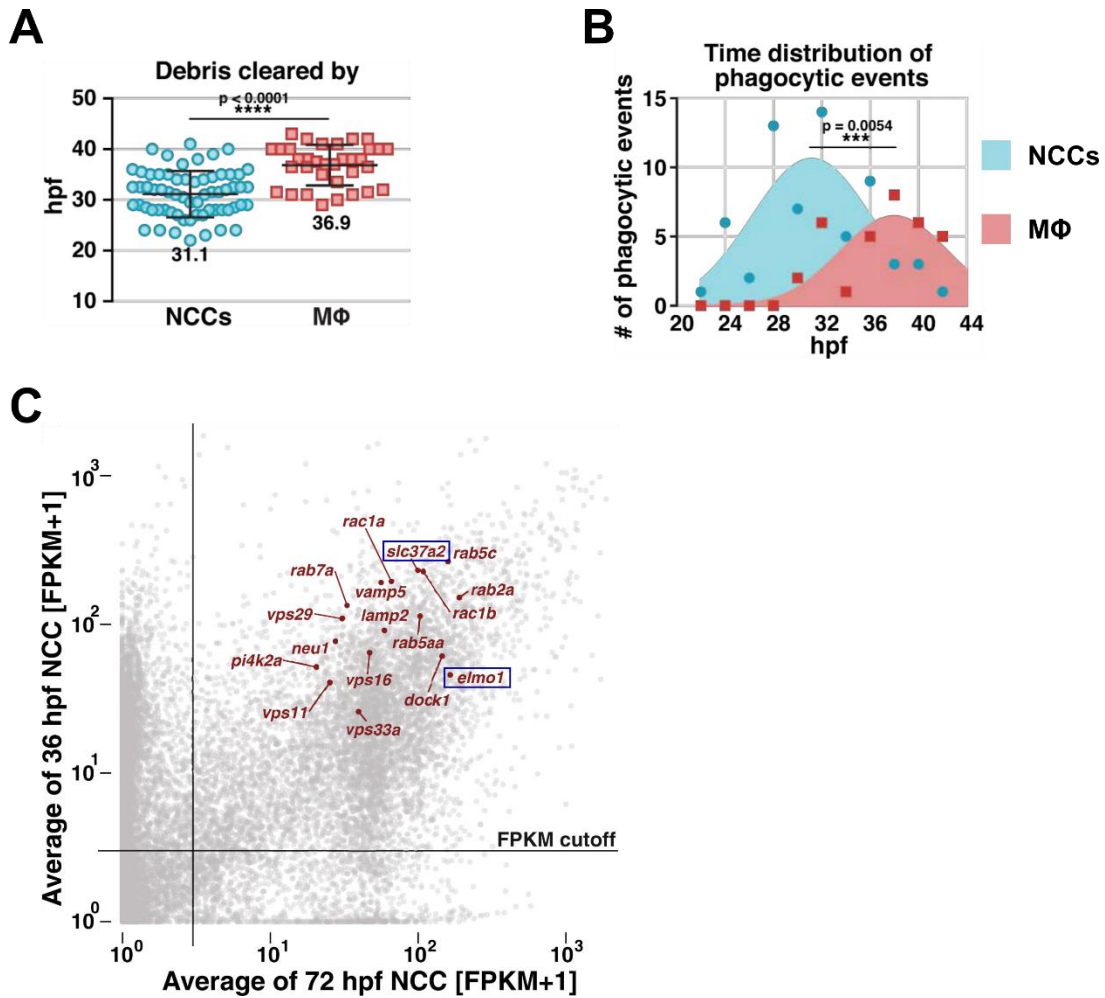


**Figure A-2: Neural crest cells are novel phagocytes and express multiple phagocytic genes in an early window of zebrafish development.** (A) Quantification of phagocytic events performed by NCCs and macrophages (MΦ) between 22 and 44 hpf (mean ± SD). (B) Histogram of data in A fitted with a Gaussian distribution ( $R^2 = 0.7573/0.6164$  for NCCs/ MΦ). (C) X-Y dot plot of NCC bulk RNA-seq dataset. Genes critical to phagocytosis are highlighted in red. Genes of interest in these studies are boxed in blue. **Figure A-2** is from Zhu et al., 2019.

## A.2 EXAMINING PHAGOCYTOTIC CRANIAL NCCS IN NEURODEVELOPMENT

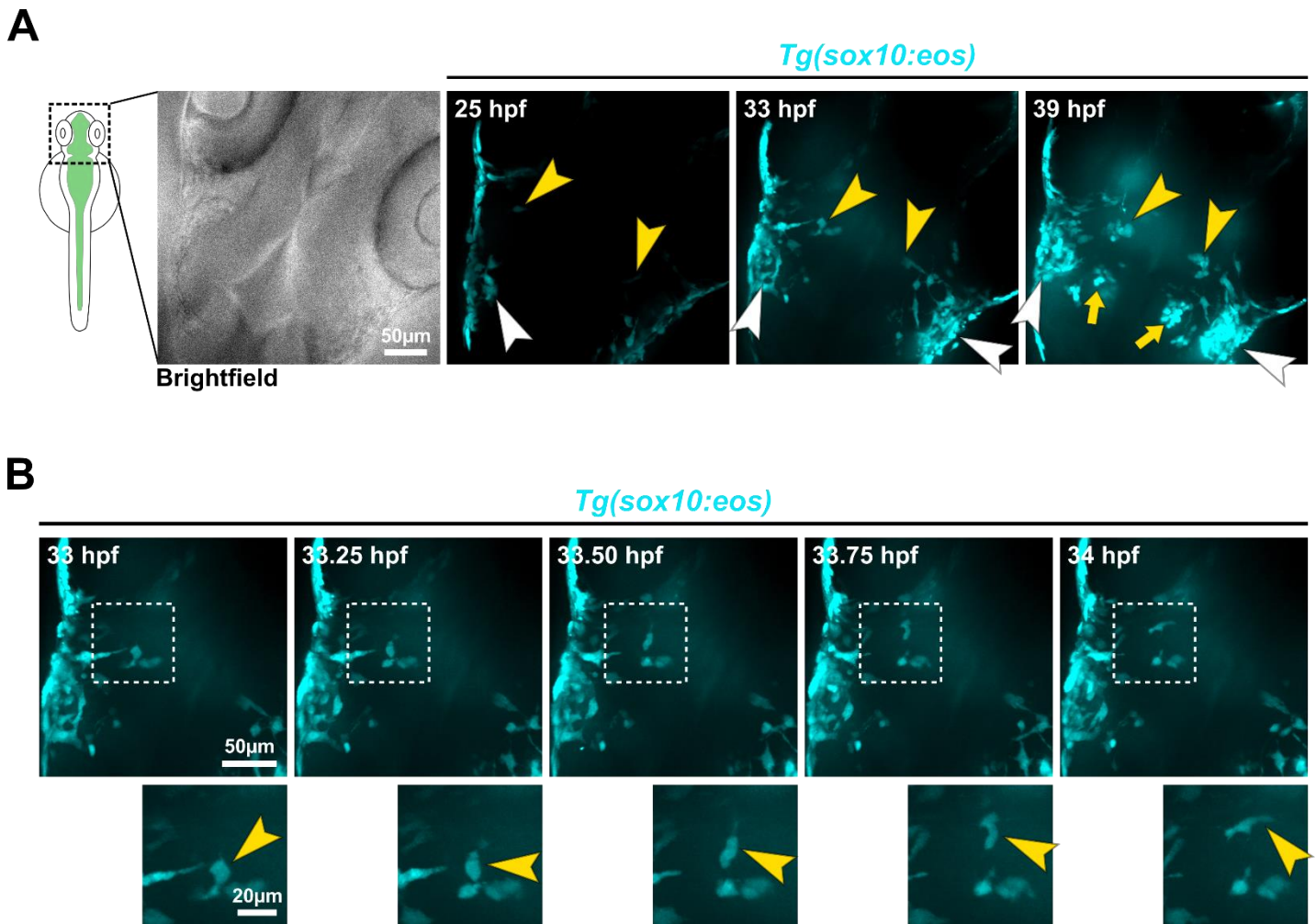
In the developing brain, the timing of neurogenesis, synaptogenesis, and programmed cell death (PCD) are region-dependent, with some areas undergoing higher levels of PCD and pruning before others<sup>5,6,27,32</sup> (also refer to **Chapter 1.2 Neurodevelopment**). Some of these events also occur before infiltration by microglia, which leaves areas of the brain without phagocytes to clear dying cells. The Kucenas lab's discovery of NCCs as novel phagocytes in early development alleviates this discrepancy as phagocytic NCCs clear debris and dying cells before infiltration by M $\Phi$  or microglia (**Figure A-1 & A-2**). The Kucenas lab focused primarily on NCCs in the developing zebrafish trunk and only reported one observation of a phagocytosing cranial NCC<sup>126</sup>. In zebrafish, the optic tectum undergoes a remarkable wave of PCD (~36 to 72 hpf) that precedes and is partially required for microglial infiltration (which occurs at ~48 hpf)<sup>27,69,402,403</sup>. But how does the developing optic tectum tolerate the accumulation of dying cells and escape consequences from delayed cell clearance prior to microglial infiltration? I hypothesized that a subset of cranial NCCs may infiltrate the optic tectum to phagocytose dying cells between 36 and 48 hpf, prior to brain infiltration by microglia. To investigate this hypothesis, I first conducted early experiments visualizing cranial NCCs and their movement from ~24 to 40 hpf. Secondly, I more closely examined the location of cranial NCCs in relation to the brain parenchyma and their interactions with apoptotic cells in the optic tectum. Lastly, I conducted injury experiments to determine whether cranial NCCs respond to parenchymal injury.

### A.2.1 Visualizing cranial NCCs in early zebrafish development

To begin my investigations into cranial NCCs, I started by experimenting with different mounting set-ups to best visualize cranial NCCs by confocal microscopy. The Kucenas lab has extensive imaging experience and standardly images laterally mounted fish, which is not ideal for visualizing the developing optic tectum. I found that mounting embryos in a "headstand" pose resulted in the best visualization of the optic tectum and cranial NCCs. In timelapse confocal imaging of *Tg(sox10:eos)* embryos from 25 to 40 hpf, I was able to visualize and identify many *sox10*<sup>+</sup> cells and structures, many appearing bilaterally (**Figure A-3**). I also observed the medial bilateral migration of single, pioneering *sox10*<sup>+</sup> cells (**Figure A-3A**, yellow arrowheads) which were quickly followed by migration of additional *sox10*<sup>+</sup> cells along the established tracts. Based on the location and timing,

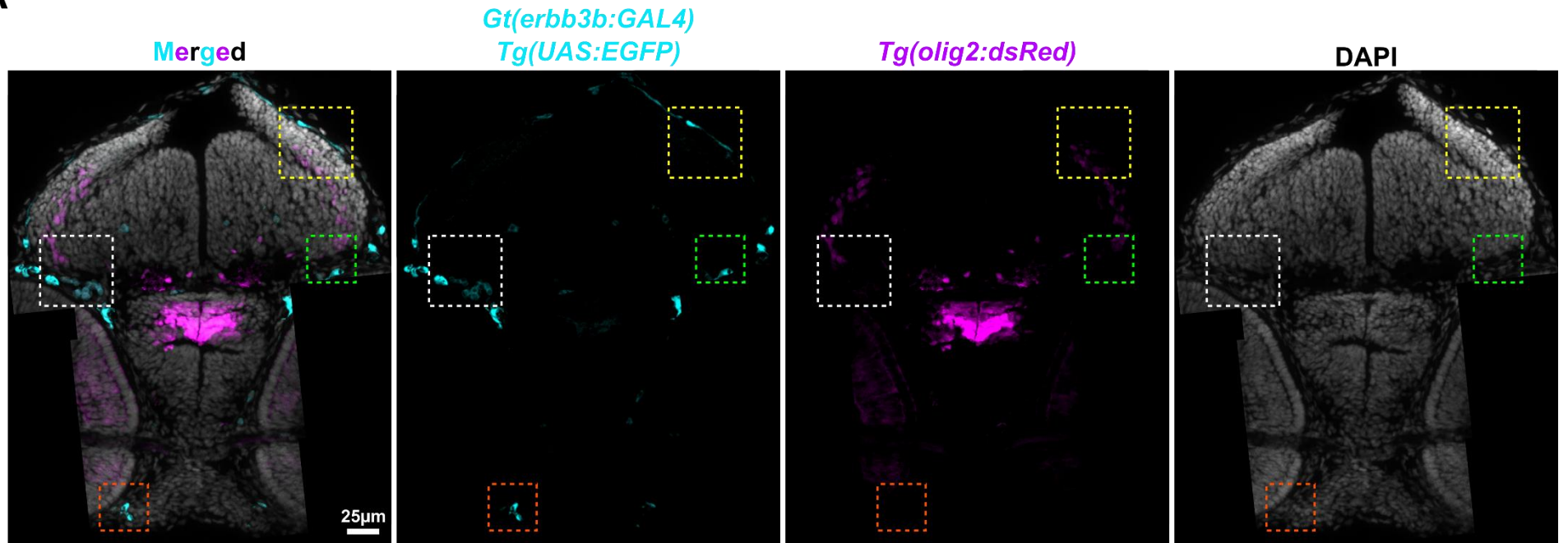
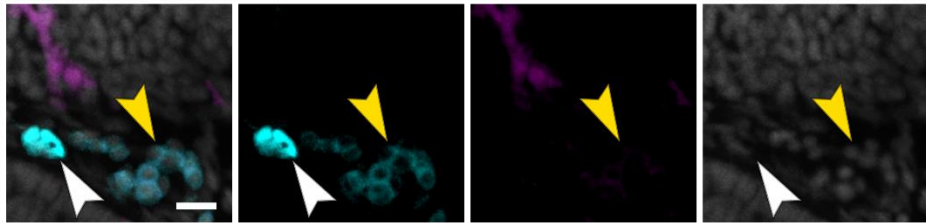
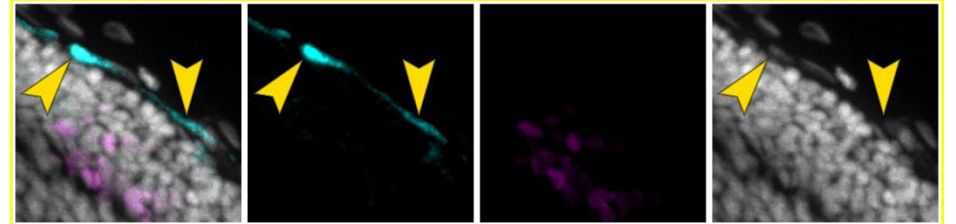
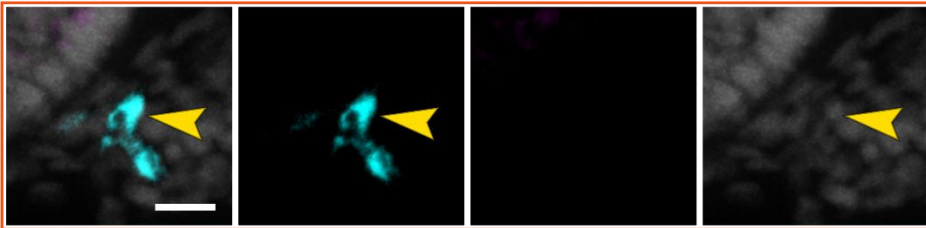
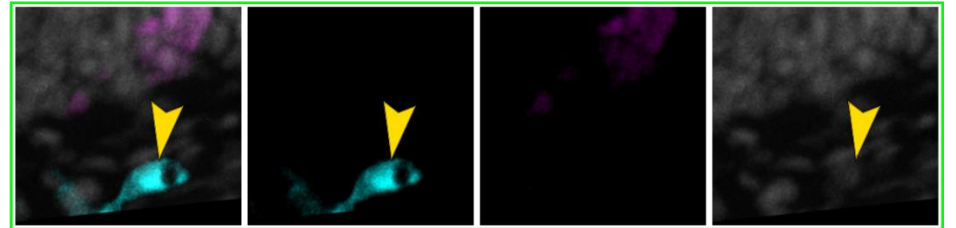
these *sox10*<sup>+</sup> cell clusters may be the nuclei of the postoptic commissure tract and the periorbital mesenchyme (POM). This aligns with work demonstrating that cranial NCCs migrate to the POM and contribute to the developing eye<sup>404</sup>. In general, neurons in the zebrafish brain do not express *sox10* albeit there is evidence that some sub-populations of neurons may have transient expression<sup>405</sup>. Importantly, *sox10* is not specific to cranial NCCs and is also expressed in oligodendrocyte precursor cells (OPCs)<sup>406,407</sup> and chondrocytes<sup>408,409</sup>. Thus, without using additional markers, the identification of these *sox10*<sup>+</sup> cell clusters remain tentative.

In timelapse confocal imaging of *Tg(sox10:eos)* embryos from 25 to 40 hpf, I observed several *sox10*<sup>+</sup> cells that were incredibly dynamic and migratory (**Figure A-3B**). These *sox10*<sup>+</sup> cells were usually located just caudal to the eye and migrated in both anterior-posterior and medial-lateral directions. At some point, these active *sox10*<sup>+</sup> cells migrated more ventrally and out of the imaging window. I was never able to track or conduct follow-up experiments on these cells, but I hypothesize they are likely to be either *sox10*<sup>+</sup> cranial NCCs migrating to the POM<sup>404,410</sup>, a subset of midbrain cranial NCCs that dive between the eyes to form the palatal shelves<sup>411</sup>, or *sox10*<sup>+</sup> OPCs.



**Figure A-3: Visualizing cranial NCCs by timelapse confocal imaging.** **(A)** 24 hpf zebrafish embryo schematized to far left with the CNS in green. Inset is a maximum projection brightfield confocal image of the dorsal optic tectum of a 24 hpf *Tg(sox10:eos)* embryo taken before the beginning of timelapse imaging. Images to the right are maximum projection confocal images at 25, 33, and 39 hpf taken from a 24 to 40 hpf timelapse. Bilateral *sox10*<sup>+</sup> structures are identifiable as early as 25 hpf (yellow arrowheads), based on the location and timing these may be the nuclei of the tract of the postoptic commissure (NTPOC). White arrowheads point to larger groups of *sox10*<sup>+</sup> cells of a placode. Yellow arrows also denote two, bilateral *sox10*<sup>+</sup> clusters of cells (likely neurons) that appear later. **(B)** A series of maximum projection confocal images every 15 minutes starting at 33 hpf of a *Tg(sox10:eos)* embryo. Insets highlight an incredibly dynamic and migratory *sox10*<sup>+</sup> cell (yellow arrowheads). The white dotted boxes represent the inset below each image. All images in Figure A-3 are representative, maximum projection confocal images.

From these imaging experiments, I became curious as to whether pre-migratory cranial NCCs were within the brain parenchyma or simply decorated the surface of the developing embryo. To distinguish between these possibilities and to more accurately differentiate between cell types, I cryosectioned and imaged *Gt(herbb3b:GAL4) Tg(UAS:EGFP, olig2:dsRed)* embryo heads at 30, 38, and 50 hpf (images from 30 and 50 hpf embryos not shown). *Erb3b* is essential for NCC development and function<sup>220,412</sup> and is expressed in pre-migratory and migratory NCCs as well as NCC derivatives<sup>413</sup> (e.g. satellite glia, Schwann cells). *Erb3b* is also expressed in a subset of OPCs and oligodendrocytes<sup>414,415</sup> while *olig2* is a marker for the oligodendrocyte lineage<sup>406,416,417</sup> and is not expressed by NCCs. When used in conjunction, *erbb3b*<sup>+</sup> cells can be identified as neural crest-derived or, if when co-expressed with *olig2*, belonging to the oligodendrocyte lineage. In coronal sections of a 38 hpf *Gt(herbb3b:GAL4) Tg(UAS:EGFP, olig2:dsRed)* embryo head, I identified several distinct types of *erbb3b*<sup>+</sup> cells (**Figure A-4**). Several *erbb3b*<sup>+</sup> *olig2*<sup>-</sup> cranial NCCs were within the putative POM (**Figure A-4B & E**). There were also *erbb3b*<sup>+</sup> *olig2*<sup>-</sup> cranial NCCs that bordered the brain parenchyma (**Figure A-4C**). Several *erbb3b*<sup>+</sup> *olig2*<sup>-</sup> cranial NCCs had EGFP<sup>-</sup> intracellular compartments that are characteristic of phagocytosing NCCs<sup>126</sup> (**Figure A-4D & E**). Importantly, I did not observe any *erbb3b*<sup>+</sup> *olig2*<sup>-</sup> cranial NCCs within the parenchyma of the developing diencephalon or mesencephalon. A few *erbb3b*<sup>+</sup> *olig2*<sup>-</sup> cells were observed in the parenchyma (**Figure A-4**) but were often located bilaterally and were auto-fluorescent, the latter being a characteristic of vasculature. Thus, these cells are likely not cranial NCCs. Multiple round *erbb3b*<sup>+</sup> *olig2*<sup>+</sup> cells near the developing eye (**Figure A-4B**) were also auto-fluorescent and were not able to be identified.

**A****B****C****D****E**

**Figure A-4: Cranial NCCs border the developing brain parenchyma.** (A) Images of a single coronal section of a *Gt(erb3b:GAL4) Tg(UAS:EGFP, olig2:dsRed)* embryo head at 38 hpf. Left-most image is a composite image including all channels. Images to the right are single channel images. White-, yellow-, green-, and orange-dashed boxes represent areas magnified in B – E, respectively. (B) Magnified region marked by the white-dashed box in A. Two distinct types of *erb3b*<sup>+</sup> cells are identifiable. The round cells (yellow arrowhead) are likely neurovascular. The *erb3b*<sup>+</sup> *olig2*<sup>-</sup> cranial NCC (white arrowhead) is located within the perocular mesenchyme (POM) and will likely give rise to POM derivatives. (C) Magnified region marked by the yellow-dashed box in A. Two *erb3b*<sup>+</sup> *olig2*<sup>-</sup> cranial NCCs (yellow arrowheads) border the brain parenchyma. (D) Magnified region marked by the orange-dashed box in A. An *erb3b*<sup>+</sup> *olig2*<sup>-</sup> cell (yellow arrowhead) located ventral to the developing eye with an intracellular EGFP<sup>-</sup> compartment characteristic of phagocytosing cells. (E) Magnified region marked by the green-dashed box in A. An *erb3b*<sup>+</sup> *olig2*<sup>-</sup> cranial NCC (yellow arrowhead) with an intracellular EGFP<sup>-</sup> compartment that may be located within the POM. Scale bars are 10µm in B and D and apply to C & E. All images in Figure A-4 are representative, maximum projection confocal images.

## A.2.2 Cranial NCCs can respond to optic tectum injury

Some non-professional phagocytes become capable of engulfing cells and debris during instances of injury, inflammation, or loss of professional phagocyte populations. Since cranial NCCs do not enter the optic tectum even with the presence of dying cells (data not shown), I was curious to know whether they would respond to injury similar to their counterparts in the trunk<sup>126</sup>. I used *Gt(erb3b:GAL4) Tg(GFAP:NTR-mCherry, UAS:EGFP)* embryos, which allows for visualization of both NCCs and the CNS parenchyma (by *Tg(GFAP:NTR-mCherry)*). In 28 hpf embryos, I generated an injury in the optic tectum parenchyma between 15 and 20µm in diameter using a nitrogen-pulsed laser and time-lapse imaged from 28 to 44 hpf (**Figure A-5**). At two hours post-injury (hpi), I found a neighboring *erb3b*<sup>+</sup> cranial NCC began to extend its process towards the site of injury, away from its original migration path. At 4 hpi, multiple *erb3b*<sup>+</sup> cranial NCCs with extended processes were in close proximity to the injury site. By 5 hpi, these same *erb3b*<sup>+</sup> cranial NCCs had extended their processes into the damaged parenchyma. These results suggest that cranial NCCs can migrate and respond to sites of parenchymal injury.

In other iterations of this experiment, there was large variability in whether *erb3b*<sup>+</sup> cranial NCCs would respond and migrate to sites of injury and in many cases *erb3b*<sup>+</sup> cranial NCCs did not respond. These variable results may arise from differences in embryo age. In my early experiments, I relied on morphological features to define embryo age, which is a common and established method for staging zebrafish embryos<sup>209</sup>. Regarding cranial NCCs, a difference of one to two hours in embryo age translates into cranial NCC specification versus the beginning of migration, for example. I switched to counting somites as a more specific measure of embryo age<sup>209</sup> later in my training and never returned to these experiments, which would benefit from more stringent control of embryo age.

*Gt(erbb3b:GAL4) Tg(GFAP:NTR-mCherry;UAS:EGFP)*

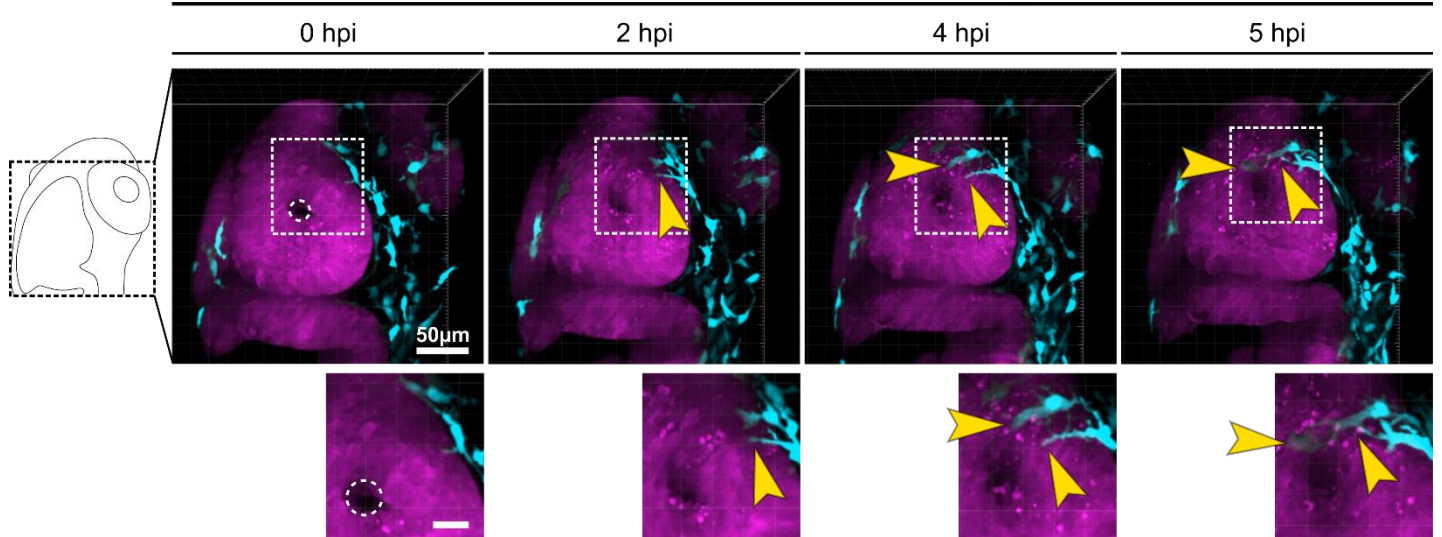


**Figure A-5: Cranial NCCs respond to laser-induced injury of the optic tectum parenchyma.** Schematic of 28 hpf embryo head, fluorescent images to right. Images are maximum projection confocal images at 28, 30, 32, and 33 hpf taken from a timelapse from 28 to 40 hpf of a *Gt(erbb3b:GAL4) Tg(GFAP:NTR-mCherry, UAS:EGFP)* embryo. The white dashed circle represents the injury site, which also lacks mCherry fluorescence from laser-induced injury. At 2 hours post injury (hpi), a cranial NCC is seen extending its process towards the site of injury (yellow arrowhead). At 4 hpi, multiple cranial NCCs are migrating to the injury (yellow arrowheads). At 5 hpi, multiple cranial NCC processes are within the injury site in the optic tectum parenchyma (yellow arrowheads). The white dashed boxes represent the inset below each image. Scale bar in inset is 20 μm. All images in Figure A-6 are representative, maximum projection confocal images.

### A.3 STUDYING THE ROLE OF PHAGOCYtic NCCS IN NEURODEVELOPMENTAL TRAJECTORIES

As discussed in **Chapter 1**, neurodevelopment is comprised of multiple, crucial cellular processes that are tightly controlled in timing and location and are conserved in multiple species (**Figure 1-1**). These developmental trajectories include neurogenesis, migration, gliogenesis, synaptogenesis, programmed cell death, myelination, and experience-dependent synaptic refinement. Clearance of debris and pruning of cells, connections, and circuits by phagocytes during these developmental trajectories are critical to creating a functional, adaptable organism. Multiple neurodevelopmental and psychiatric disorders have been suggested to arise from early aberrations in neurodevelopmental trajectories (see **Chapter 1.6.1**). The discovery of NCCs as novel phagocytes positions them as early, crucial mediators of efferocytosis and multiple neurodevelopmental processes.

Some of the earliest-formed circuits are involved in sensorimotor function and are critical for organism survival. In zebrafish, one of the earliest developed circuits is the touch-response circuit, which is established by 24 hpf. The touch-response circuit is comprised of primary sensory neurons (called Rohon-Beard [RB] neurons) in the zebrafish dorsal spinal cord, which connect to local interneurons and primary motor neurons<sup>258,261,267</sup>. Shortly after the touch-response circuit is established it undergoes drastic remodeling as RBs degenerated and were completely replaced by dorsal root ganglion neurons by 72 hpf<sup>27,261,267</sup>. I noticed that this remodeling occurs during the NCC phagocytic window. Thus, I hypothesized that phagocytic NCCs were responsible for cell and debris clearance associated with RB neuron death and that NCCs are critical for remodeling the touch-response circuit. In my subsequent experiments I was surprised to discover that RBs do not succumb to developmental programmed cell death and actually persist until at least 15 dpf<sup>329</sup>. This published story is detailed in **Chapter 3**. These experiments and those separately conducted by Joaquín Navajas Acedo<sup>328</sup> redefine our knowledge of RBs and the touch-response circuit.

## A.4 CHARACTERIZING NCC PHAGOCYtic ACTIVITY IN THE ZEBRAFISH *CSF1RA*<sup>-/-</sup> MUTANT

While current research is building on our knowledge of phagocytes (see **Chapter 1.3**) and the mechanisms behind cargo recognition, engulfment, and digestion (see **Chapter 1.4**), knowledge on inter-phagocyte communication, coordination, and distribution of phagocytic load is severely lacking. Communication between phagocytes likely occurs, as phagocytes in the brain respect separate phagocytic territories<sup>106,418</sup> and professional phagocytes modulate the phagocytic efficiency of non-professional phagocytes in close proximity<sup>419,420</sup>. A recent study showed that cargo transfer between Müller glia and microglia precedes cell clearance by microglia *in vivo*<sup>421</sup>. Aberrant phagocytes and phagocytosis have been implicated in multiple neurodevelopmental and neurodegenerative diseases and disorders<sup>422–424</sup>. Interrogating phagocyte interactions would provide valuable insight to mechanisms behind phagocytic communications and responses at homeostasis and in inflammation, injury, and disease.

Phagocytic NCCs have emerged as a new non-professional phagocyte and respond to dying cells and debris within an early window of zebrafish development. Interestingly, the number of phagocytic events by NCCs sharply decreases as MΦ and microglia infiltrate and take over cell and debris clearance<sup>126</sup> (**Figure A-2B**). I hypothesized that later-infiltrating MΦ and microglia interact with phagocytic NCCs to close the NCC phagocytic window. To address this hypothesis, I proposed manipulating the presence of MΦ and microglia using *csf1ra*<sup>-/-</sup> zebrafish mutants to examine changes in the NCC phagocytic window. MΦ and microglia are critically dependent on colony-stimulating factor 1 receptor (CSF1R) signaling for survival in mice<sup>425</sup> and zebrafish<sup>60,403,426</sup>. CSF1R and its ligands (CSF1 and IL-34) are critical for myeloid cell development and colonization<sup>60,62,403,427–432</sup>. In zebrafish, IL-34 and neuronal apoptosis are the primary drivers for the primitive macrophage migration and colonization of the brain<sup>403</sup>. Zebrafish possess two *csf1r* paralogues (*csf1ra* and *csf1rb*), which exhibit divergent expression during embryonic development and adulthood<sup>426,433,434</sup>. *csf1ra*<sup>-/-</sup> loss of function zebrafish mutants are completely devoid of embryonic brain microglia until 6 dpf<sup>403,434,435</sup>. Importantly, a subset of neural crest-derived cells express *csf1ra*<sup>217,433,436</sup> and *csf1ra*<sup>-/-</sup> adult mutants lack stripes, which arises from melanocyte death<sup>217</sup>.

This project was undertaken by Ginger Smith, an undergraduate student I worked with from Fall 2020 to Spring 2023. We worked together to create three experimental aims for Ginger to explore during her time in the lab: 1) validating the microglial phenotype in the optic tectum, 2) characterizing the infiltration of spinal cord (SC) microglia, and 3) assaying the NCC phagocytic window in *csf1ra*<sup>-/-</sup> mutants.

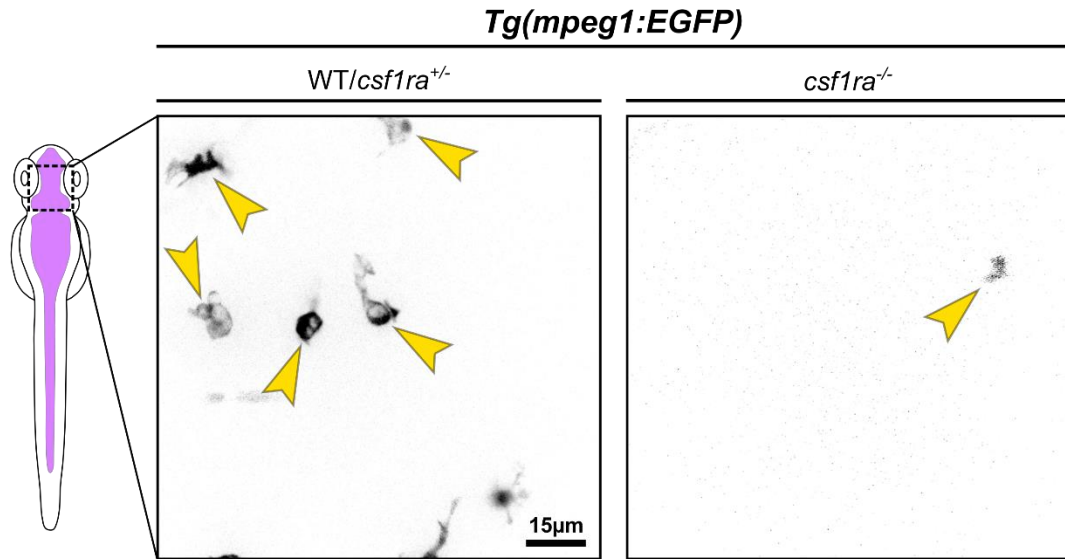
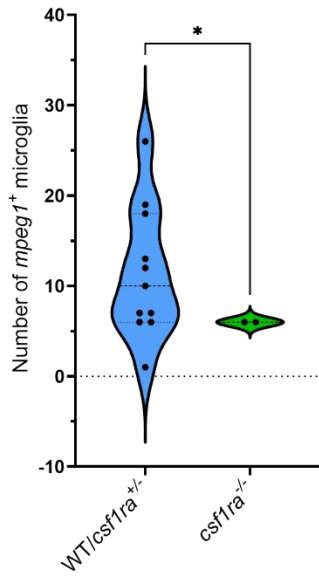
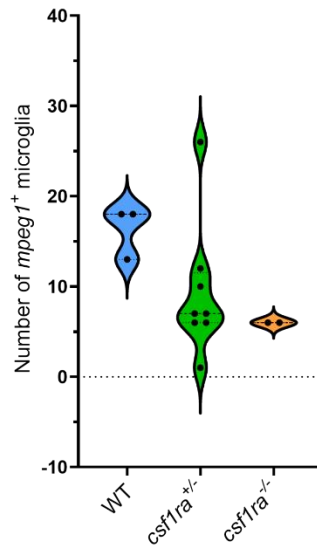
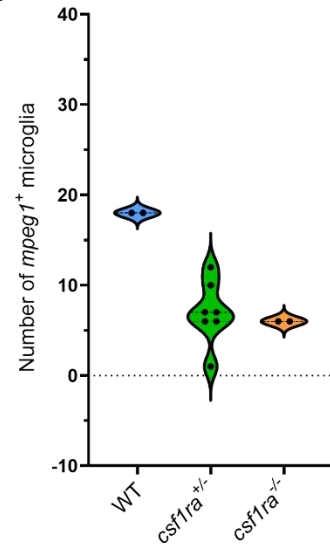
#### **A.4.1 *csf1ra*<sup>-/-</sup> mutants exhibit a loss of microglia in the optic tectum at 3 dpf**

We decided to quantify the number of *mpeg1*<sup>+</sup> microglia in the optic tectum to validate the *csf1ra* mutants, which exhibit a loss of brain microglia starting at 3 dpf. To do this, Ginger performed *in vivo* confocal imaging of the zebrafish optic tectum on 3 dpf embryos from an incross of *csf1ra*<sup>+/-</sup>; *Tg(mpeg1:EGFP)* transgenic fish. After imaging, she counted the number of EGFP<sup>+</sup> cells within the brain parenchyma. Ginger found a statistically significant decrease in the number of EGFP<sup>+</sup> cells in the optic tectum of *csf1ra*<sup>-/-</sup> versus WT/*csf1ra*<sup>+/-</sup> embryos (**Figure A-6A & B**), which aligns with the published phenotype of *csf1ra*<sup>-/-</sup> mutants. This experiment consisted of one experiment, which contained only two *csf1ra*<sup>-/-</sup> mutant embryos.

In further post-hoc analyses where I separated count data for WT and *csf1ra*<sup>+/-</sup> embryos, I discovered multiple important findings. Upon statistical testing of the separated count data, I found no statistically significant difference in the number of EGFP<sup>+</sup> cells in the optic tectum between genotypes (**Figure A-6C**). After noticing a potential outlier data point in the count data for *csf1ra*<sup>+/-</sup> embryos, I ran Grubbs' test which identified two outliers: one data point in the WT and one in the *csf1ra*<sup>+/-</sup> group. When excluding these data points and re-running statistical analyses, I found a statistically significant difference in the median number of EGFP<sup>+</sup> cells in the optic tectum between genotypes ( $p = 0.0424$ ), but no significant difference between any groups from the multiple comparisons test (**Figure A-6D**).

These data conflict with previous studies, which report a statistically significant decrease in the number of microglia in the optic tectum at 3 dpf in both *csf1ra*<sup>+/-</sup> and *csf1ra*<sup>-/-</sup> embryos compared to WT<sup>434,437</sup>. This discrepancy is very likely due to the study being underpowered. With count data from WT and *csf1ra*<sup>+/-</sup> embryos separated, n values were only two and three embryos, respectively. This experiment should be repeated for definitive results. *Csf1ra*<sup>-/-</sup> fish also lack posterior pigment stripes<sup>217</sup>, which we also observed for the *csf1ra*<sup>-/-</sup> adult

fish we had received as embryos. Lastly, we conducted genotyping by restriction digest to validate the *csf1ra*<sup>-/-</sup> adult fish (data not shown). Taking all these lines of evidence into consideration, we concluded that the *csf1ra*<sup>-/-</sup> adult fish we received mirrored the published phenotypes and we decided to move on to experiments for Ginger's second aim.

**A****B****C****D**

**Figure A-6: *csf1ra*<sup>-/-</sup> mutants exhibit a loss of microglia in the optic tectum at 3 dpf.** (A) 3 dpf zebrafish embryo schematized to far left with the CNS in magenta. Inset is a representative maximum projection confocal image of the dorsal optic tectum of 3 dpf embryos with microglia labeled by *Tg(mpeg1:EGFP)* in WT/*csf1ra*<sup>+/-</sup> (left image) and *csf1ra*<sup>-/-</sup> (right image) embryos. Yellow arrowheads point to example *mpeg1*<sup>+</sup> microglia. (B) Quantification of the number of EGFP<sup>+</sup> cells in the optic tectum at 3 dpf. Unpaired t-test with Welch's correction was performed and yielded  $p = 0.0339$ . Mean  $\pm$  SEM values: WT/*csf1ra*<sup>+/-</sup>:  $11.36 \pm 2.184$ , *csf1ra*<sup>-/-</sup>:  $6 \pm 0.000$ . (C) Quantification of the number of EGFP<sup>+</sup> cells in the zebrafish optic tectum at 3 dpf separated by genotype, from same data shown in B. Repeated measures one-way ANOVA  $p$  value = 0.0542. Adjusted  $p$  values for multiple comparisons: WT vs. *csf1ra*<sup>+/-</sup>  $p = 0.2234$ , WT vs. *csf1ra*<sup>-/-</sup>  $p = 0.0958$ , *csf1ra*<sup>+/-</sup> vs. *csf1ra*<sup>-/-</sup>  $p > 0.9999$ . Mean  $\pm$  SEM values: WT:  $16.33 \pm 1.667$ , *csf1ra*<sup>+/-</sup>:  $9.375 \pm 2.632$ , *csf1ra*<sup>-/-</sup>:  $6 \pm 0.000$ . (D) Quantification of the number of EGFP<sup>+</sup> cells in the zebrafish optic tectum at 3 dpf separated by genotype minus two outliers. Outliers were identified using Grubbs' test and removed for re-plotting and re-analysis. Repeated measures one-way ANOVA  $p$  value = 0.0424. Adjusted  $p$  values for multiple comparisons: WT vs. *csf1ra*<sup>+/-</sup>  $p = 0.1495$ , WT vs. *csf1ra*<sup>-/-</sup>  $p = 0.0899$ , *csf1ra*<sup>+/-</sup> vs. *csf1ra*<sup>-/-</sup>  $p > 0.9999$ . Mean  $\pm$  SEM values: WT:  $18.00 \pm 0.000$ , *csf1ra*<sup>+/-</sup>:  $7.000 \pm 1.309$ , *csf1ra*<sup>-/-</sup>:  $6 \pm 0.000$ . For B – D each dot represents one embryo. For B & C, WT  $n = 3$  embryos, *csf1ra*<sup>+/-</sup>  $n = 8$  embryos and *csf1ra*<sup>-/-</sup>  $n = 2$  embryos. For C & D, re-plotting and re-analysis were on same data plotted in B and underwent Kruskal-Wallis one-way ANOVA with Dunn's multiple comparisons test. **Figure A-8A & B** are adapted from Ginger Smith's 2023 Distinguished Majors Program Undergraduate Thesis.

#### A.4.2 *csf1ra*<sup>-/-</sup> mutants display no difference in number of *mpeg1*<sup>+</sup> professional phagocytes in the trunk between 36 and 48 hpf

While previous studies extensively describe brain microglia in *csf1ra*<sup>-/-</sup> embryos, it is unknown whether SC microglia are affected in the same mutants. Currently, there are few studies examining the differences between brain and SC microglia infiltration in development. In humans, amoeboid-like microglia-macrophages appear in the spinal cord one gestational week later than infiltration of the brain<sup>438</sup>. This aligns with work done in zebrafish, where primitive macrophages infiltrate the brain starting at 36 hpf<sup>60,403</sup> and SC microglia are observed later, around 72 hpf<sup>201,439,440</sup>. It is hypothesized that primitive macrophages colonize the brain before migrating posteriorly to reach the spinal cord<sup>60</sup>. Additional work in mice and zebrafish suggests that brain and SC microglia display differing expression levels and sensitivities to CSF1<sup>441,442</sup> and IL34<sup>403</sup>, both of which are implicated in microglia survival and infiltration<sup>425,443,444</sup>. Still, there is no direct evidence that SC microglia infiltrate by mechanisms different than brain microglia.

Based on the current literature, I hypothesized that SC microglia would also be depleted in *csf1ra*<sup>-/-</sup> embryos. If *csf1ra*<sup>-/-</sup> embryos do lack SC microglia, this would allow us to examine changes in the NCC phagocytic window when microglia fail to infiltrate the trunk. First, we had to characterize the number and infiltration dynamics of SC microglia in *csf1ra*<sup>-/-</sup> embryos. Ginger started by examining SC microglia and MΦ during the latter half of the NCC phagocytic window (**Figure A-7B**) by in-crossing *csf1ra*<sup>+/-</sup> *Tg(mpeg1:EGFP)* transgenic fish and conducting time-lapse imaging from 32 to 48 hpf. This experiment would answer two questions: 1) when exactly do microglia colonize the spinal cord in WT embryos? and 2) are SC microglia depleted in *csf1ra*<sup>-/-</sup> embryos?

At 36, 40, 44, and 46 to 48 hpf, Ginger counted the number of EGFP<sup>+</sup> microglia and MΦ in the spinal cord and periphery, respectively. We found that before 48 hpf, there are virtually no spinal cord EGFP<sup>+</sup> microglia in either WT/*csf1ra*<sup>+/-</sup> or *csf1ra*<sup>-/-</sup> embryos (**Figure A-7C**). This aligns with previous observations of SC microglia, which are not observed until 72 hpf<sup>201,439,440</sup>. In the periphery, we found no statistically significant difference in the number of EGFP<sup>+</sup> MΦ between WT/*csf1ra*<sup>+/-</sup> and *csf1ra*<sup>-/-</sup> embryos (**Figure A-7D**). Previous studies have also found no statistically significant difference in the number of primitive or peripheral MΦ between WT and *csf1ra*<sup>-/-</sup> embryos<sup>60,403,434</sup>. We also analyzed the aggregated number of EGFP<sup>+</sup> microglia and MΦ in the spinal cord and

periphery and found no statistically significant difference between WT/*csf1ra*<sup>+/-</sup> and *csf1ra*<sup>-/-</sup> embryos (**Figure A-7B**).

For these experiments, Ginger used brightfield images to determine whether an EGFP<sup>+</sup> microglial cell was within the boundaries of the spinal cord. In future studies, using *Tg(GFAP:NTR-mCherry)* to visualize the spinal cord parenchyma would aid in defining EGFP<sup>+</sup> microglia. In quantifying peripheral MΦ, Ginger counted the number of EGFP<sup>+</sup> cells that were within the imaging window but not within the boundaries of the spinal cord. Ginger's imaging windows did not include positions ventral to the notochord (e.g. over the rostral blood island, ventral wall of dorsal aorta, or the posterior blood island), where peripheral MΦ arise from and are concentrated<sup>445,446</sup>. A more accurate analysis of peripheral MΦ would include imaging of these areas. For all analyses WT and *csf1ra*<sup>+/-</sup> embryos should be separated, as *csf1ra*<sup>+/-</sup> embryos display an intermediate phenotype of decreased brain microglia<sup>437</sup>. I hypothesize that *csf1ra*<sup>+/-</sup> embryos likely have an intermediate phenotype for SC microglia, so count analyses of WT and *csf1ra*<sup>+/-</sup> embryos should not be binned together unless rigorously established that no intermediate phenotype exists. Lastly, additional experiments (particularly imaging between 48 and 72 hpf) and analyses are needed to 1) more finely characterize the spatiotemporal dynamics of microglia infiltration of the spinal cord and 2) to determine whether SC microglia are depleted in *csf1ra*<sup>-/-</sup> embryos.

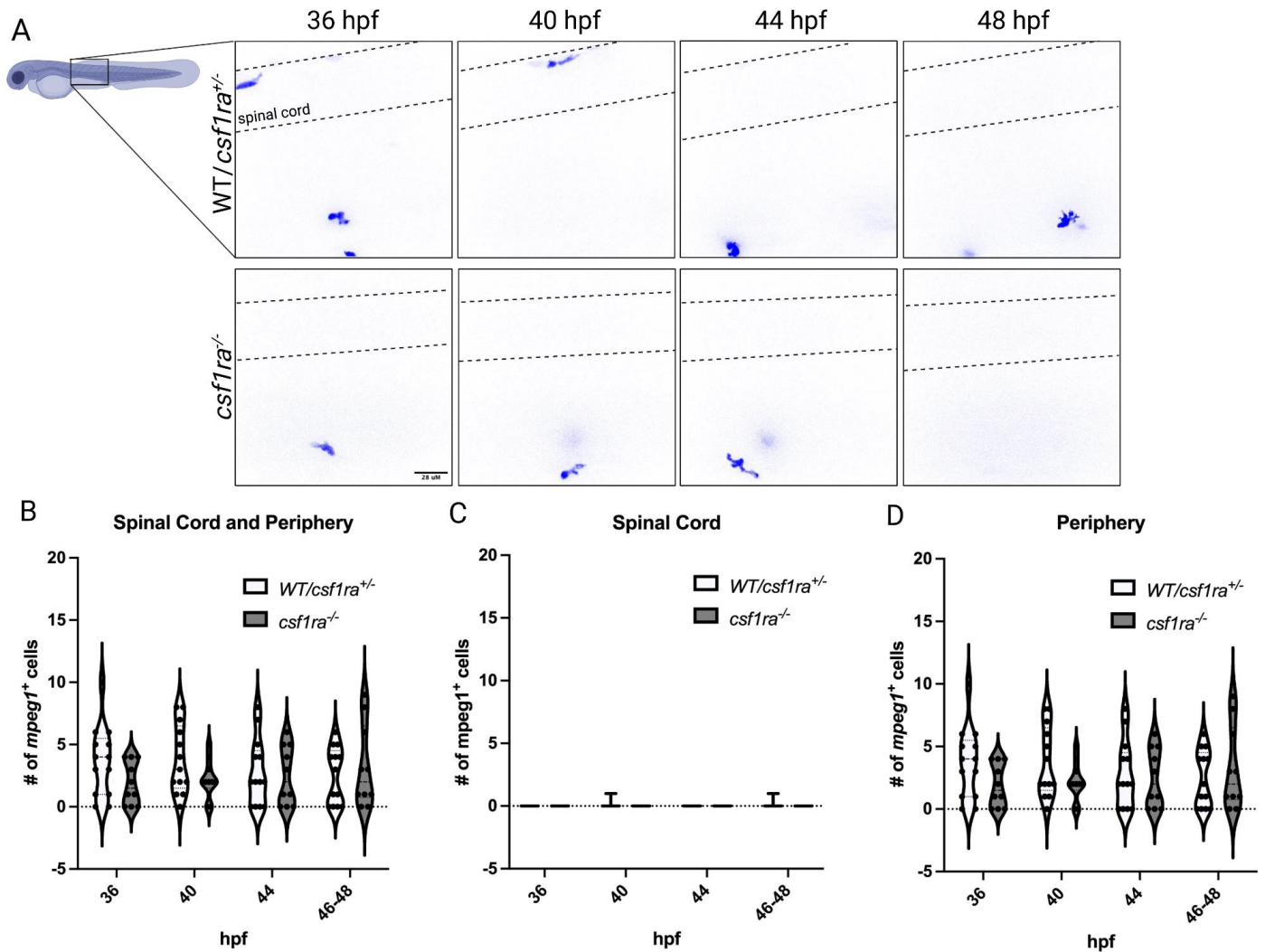


**Figure A-7: *csf1ra* mutants display no difference in number of professional phagocytes in the periphery and spinal cord between 36 and 48 hpf.** (A) Zebrafish embryo is schematized to far left, created with BioRender. Representative confocal images of macrophages and microglia labeled by *Tg(mpeg1:EGFP)* in the zebrafish trunk at 36, 40, 44, and 48 hpf in WT/*csf1ra*<sup>+/+</sup> (top row) and *csf1ra*<sup>-/-</sup> (bottom row) larvae. (B) Quantification of the number of *mpeg1*<sup>+</sup> professional phagocytes in the zebrafish spinal cord and periphery from 36 to 46/48 hpf. Two-way repeated measures ANOVA test was performed yielding no statistically significant result between the groups at any time point. For WT/*csf1ra*<sup>+/+</sup> n = 13 embryos and for *csf1ra*<sup>-/-</sup> n = 10 embryos. (C) Quantification of *mpeg1*<sup>+</sup> microglia in the spinal cord (same data as B). Two-way repeated measures ANOVA test was performed yielding no statistically significant result between the groups at any time point. (D) Quantification of the number of *mpeg1*<sup>+</sup> macrophages in the periphery (same data as B). Two-way repeated measures ANOVA test was performed yielding no statistically significant result between the groups at any time point. For B – D, one dot equals one embryo. Figure A-7 is from Ginger Smith’s 2023 Distinguished Majors Program Undergraduate Thesis.

### A.4.3 Increased cell death at 55 hpf in *csf1ra*<sup>-/-</sup> embryos by acridine orange

Previously, the Kucenas lab has shown that NCCs phagocytose dying cells and debris between 24 and 30 hpf. Starting at ~30 hpf, infiltrating MΦ take over cell and debris clearance (refer to **Figure A-2B**). I hypothesized that later-infiltrating MΦ and microglia interact with phagocytic NCCs to close the NCC phagocytic window, and aberrations in professional phagocyte infiltration would affect phagocytic NCCs. As an indirect way to ascertain changes in NCC efferocytosis, Ginger incrossed *csf1ra*<sup>+/-</sup> *Tg(mpeg1:TagRFP)* transgenic fish and stained the WT/*csf1ra*<sup>+/-</sup> and *csf1ra*<sup>-/-</sup> embryos with Acridine Orange (AO), which labels dying cells<sup>220,227</sup>. Ginger stained and imaged at two timepoints: 34 and 55 hpf. These two timepoints begin at the peak of the NCC phagocytic window and extend past the time when NCC phagocytosis ceases and professional phagocytes take over efferocytosis. 72 hpf also served as an internal positive control, as the optic tectum in WT embryos display elevated cell death in the optic tectum at the same timepoint<sup>60,402</sup>. Unfortunately, Ginger was not able to complete the 72 hpf timepoint.

From these experiments, Ginger found that at 34 hpf there was no statistically significant difference in the number of AO<sup>+</sup> puncta between WT/*csf1ra*<sup>+/-</sup> and *csf1ra*<sup>-/-</sup> embryos (**Figure A-8B**). At 55 hpf, we did find a statistically significant difference (**Figure A-8C**). There are multiple possible interpretations of these findings. One is that NCC efferocytosis is unaffected at 34 hpf in *csf1ra*<sup>-/-</sup> embryos. Or, NCC efferocytosis is significantly affected at 34 hpf but a different phagocyte population (e.g. neutrophils) is able to compensate, leading to no change in the number of AO<sup>+</sup> puncta. At 55 hpf, the statistically significant difference in the number of AO<sup>+</sup> puncta may represent a deficit in efferocytosis by microglia and/or peripheral MΦ. If peripheral MΦ do have functional deficits and/or SC microglia are depleted in *csf1ra*<sup>-/-</sup> embryos, this result could also indicate compensation from a less efficient phagocyte population (e.g. NCCs, neutrophils). Alternatively, there may be an increase in the number of dying cells in *csf1ra*<sup>-/-</sup> embryos independent of efferocytosis by NCCs, microglia, peripheral MΦ, or another phagocyte population. Since the number of AO<sup>+</sup> puncta were quantified for both the spinal cord and periphery, we also do not know whether the increase in AO<sup>+</sup> puncta at 55 hpf was regionally restricted. The location of the dying cells would provide clues as to which phagocyte population is potentially affected and/or involved.

Making conclusions from these results are difficult because the results can be interpreted in multiple different ways and there are several ways these experiments should be improved upon. Due to Ginger's schedule, we opted to complete the time points on different days from different crosses and clutches. This method is appropriate when enough experimental repetitions can be completed, otherwise there is a higher probability that differences in data may arise from a clutch effect. Currently, this experiment is vastly underpowered and more replicates or using a different approach is advised. A better approach for this type of experiment would be to stain different groups of embryos from the same clutch for each timepoint. Ideally, this would be repeated with two other clutches. Lastly, these experiments lacked the 72 hpf timepoint, which was critical as an internal positive control. Data from 72 hpf would aid in analyzing for statistical differences between clutches and crosses. While there are many ways to improve upon these experiments, the results shown here are intriguing and raise additional, interesting follow-up questions.

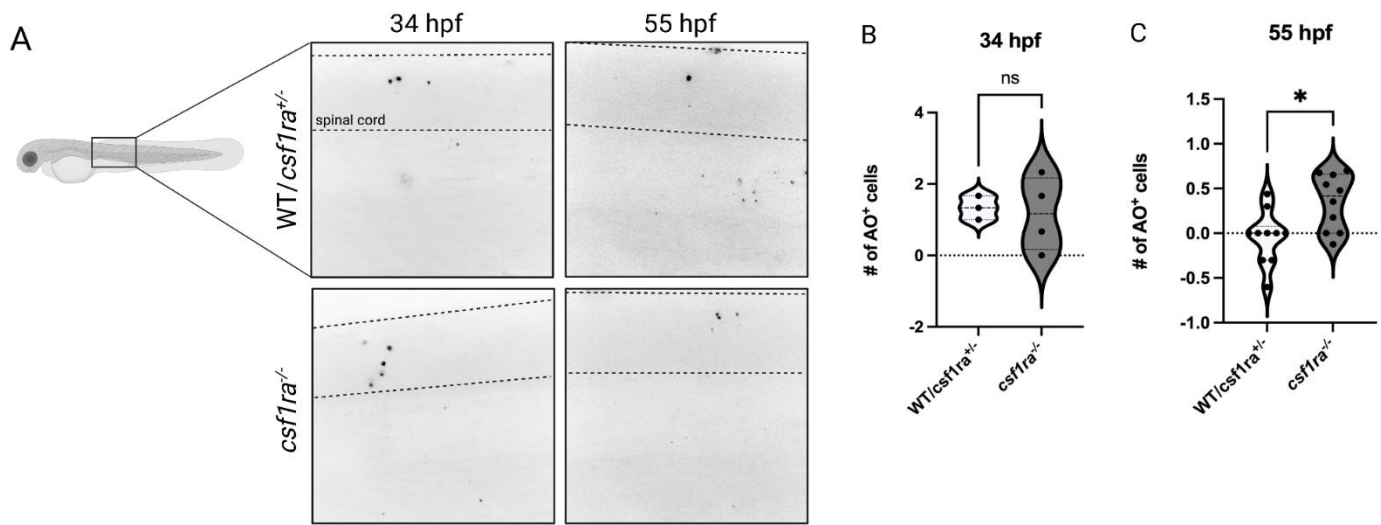


**Figure A-8: Increased cell death at 55 hpf in *csf1ra*<sup>-/-</sup> embryos by acridine orange (A)** Zebrafish embryo is schematized to far left, created with BioRender. Representative confocal maximum projection images of macrophages and microglia labeled by *Tg(mpeg1:EGFP)* in the zebrafish trunk at 36, 40, 44, and 48 hpf in WT/*csf1ra*<sup>+/-</sup> (top row) and *csf1ra*<sup>-/-</sup> (bottom row) embryos. Dashed line represents dorsoventral boundaries of the spinal cord. **(B)** Quantification of the number of AO<sup>+</sup> puncta in the spinal cord and periphery at 34 hpf between WT/*csf1ra*<sup>+/-</sup> and *csf1ra*<sup>-/-</sup> embryos. No statistical significance was found ( $p = 0.7790$ ). For WT/*csf1ra*<sup>+/-</sup>  $n = 3$  embryos and for *csf1ra*<sup>-/-</sup>  $n = 4$  embryos. **(C)** Quantification of the number of AO<sup>+</sup> puncta in the spinal cord and periphery at 55 hpf between WT/*csf1ra*<sup>+/-</sup> and *csf1ra*<sup>-/-</sup> embryos. Data underwent a log transformation before statistical analysis and plotting. T-test  $p = 0.0103$ . For WT/*csf1ra*<sup>+/-</sup>  $n = 10$  embryos and for *csf1ra*<sup>-/-</sup>  $n = 10$  embryos. For **B & C**, an unpaired t test with Welch's correction was performed and one dot equals one embryo. Figure **A-8** is from Ginger Smith's 2023 Distinguished Majors Program Undergraduate Thesis.

### A.4.3 Discussion

In these experiments Ginger and I wanted to investigate NCC phagocytosis in the absence of microglia. I previously hypothesized that SC microglia would also be depleted in *csf1ra*<sup>-/-</sup> embryos, which exhibit a loss of brain microglia<sup>403,434,435</sup>. To our surprise, little is known about the timing of microglial infiltration of the spinal cord and SC microglia have not been investigated in *csf1ra*<sup>-/-</sup> embryos (to my knowledge). Thus, Ginger also sought to describe the spatiotemporal dynamics of microglial infiltration of the spinal cord.

The results from Ginger's experiments of the spinal cord and periphery (**Figure A-7**) confirm that microglial infiltration happens after 48 hpf. This aligns with previous literature and my personal observations, where SC microglia are not present until 72 hpf<sup>201,439,440</sup>. It is thought that primitive MΦ colonize the brain, and a subset migrate posteriorly to colonize the spinal cord. Another possibility is that primitive MΦ arising from the rostral blood island migrate to directly colonize the anterior spinal cord. *In vivo* timelapse imaging experiments in embryos where MΦ and microglia are labeled (e.g. via fluorophores driven by *mpeg1* or *pu.1* promoter expression) would help discern between these two possibilities and provide important spatiotemporal information on microglial colonization of the spinal cord.

To investigate whether NCC efferocytosis is affected in *csf1ra*<sup>-/-</sup> embryos, Ginger stained dying cells to act as an indirect readout of efferocytosis. At 34 hpf, there is no statistically significant difference in the number of dying cells between WT/*csf1ra*<sup>+/-</sup> and *csf1ra*<sup>-/-</sup> embryos (**Figure A-8B**). However, there is a statistically significant difference at 55 hpf (**Figure A-8C**). These results suggest that there are changes in efferocytosis by phagocytes or the rate of dying cells. It is difficult to distinguish between these options without definitively knowing whether SC microglia are depleted in *csf1ra*<sup>-/-</sup> embryos. Thus, the experiments described above are critical to this project. If we assume *csf1ra*<sup>-/-</sup> embryos lack spinal cord microglia, then the next step is to quantify the number of dying cells at different time points encompassing the NCC and MΦ/microglia phagocytic window (e.g. 24, 32, 40, and 48 hpf) in embryos expressing fluorescent markers for these populations. Timelapse experiments with phagosomes fluorescently labeled (e.g. via *UAS:GFP-2xFYVE*<sup>447</sup>) and subsequent quantifications of number and volume of phagosomes over time would more directly assay efferocytosis of NCCs, MΦ, and microglia in *csf1ra*<sup>-/-</sup> embryos. A different option is to conduct injury response experiments, which are a common method to

assay migration and efferocytosis in phagocytes<sup>†83,448</sup>. Neutrophils are another phagocyte population to keep in mind, as they sometimes expand when MΦ and microglia are depleted or ablated<sup>436,449–451</sup>.

The aim of these experiments was to investigate why NCC phagocytosis decreases starting at ~32 hpf (**Figure A-2B**). Previous studies demonstrate that phagocyte inter-communication occurs and, in some instances, result in changes to phagocytic efficiency<sup>106,418–420</sup>. Stemming from this, one of my hypotheses is that later-infiltrating MΦ and microglia interact with phagocytic NCCs to close the NCC phagocytic window. Since phagocytic NCCs were described in the developing trunk, I opted to concentrate my studies there. If SC microglia are depleted in *csf1ra*<sup>-/-</sup> embryos, future experiments investigating cell replication and death dynamics, NCC phagosomes, and NCC phagocytic events (detailed previously) would elucidate whether the NCC phagocytic window is controlled by infiltrating SC microglia. If SC microglia are not depleted in *csf1ra*<sup>-/-</sup> embryos, there are alternatives to investigate phagocytic NCCs without infiltration by MΦ and microglia. These include the *irf8*<sup>-/-</sup> mutant (specifically *irf8*<sup>st95</sup>, which completely lack microglia and macrophages until 5 dpf<sup>449,452</sup>), the *csf1ra*<sup>-/-</sup> *csf1rb*<sup>-/-</sup> double mutant (specifically *csf1ra*<sup>4e1</sup>*csf1rb*<sup>re01</sup>, which lack brain microglia<sup>403,434,435</sup> and primitive macrophages have decreased expansion and migration as well as functional deficits<sup>403,453</sup>), and a MΦ/microglia promoter-driven inducible nitroreductase system that causes cell death<sup>454</sup>.

An alternative explanation for the closing of the NCC phagocytic window is that as migratory NCCs become specified and eventually differentiate, they lose the capacity to phagocytose. This aligns with studies demonstrating the phagocytic capability of other progenitor populations, which have since been characterized as non-professional phagocytes<sup>103,104,125</sup> (e.g. OPCs, NPCs) (see **Chapter 1.3**). Photoconversion experiments of phagocytic NCCs found that the vast majority (79.5%) migrated laterally and adopted morphologies similar to pigment cells. A smaller subset (16.3%) migrated medially to associate with motor nerves, indicating that phagocytic NCCs are not lineage-restricted<sup>126</sup>.

---

† I've had a lot of difficulty in establishing an injury assay for NCCs. Either NCCs would not respond to an injury or the number of responding NCCs were not statistically significant compared to uninjured embryos (data not shown). I hope someone else will have better luck!

An interesting avenue to explore is whether phagocytic NCCs are affected in *csf1ra*<sup>-/-</sup> mutants, since *csf1ra* is expressed in premigratory NCCs<sup>217,433,436</sup>. Initial studies observed that 3 dpf *csf1ra*<sup>-/-</sup> embryos lack yellow color compared to WT embryos. This points to defects in a subset of neural crest-derived precursor cells called xanthoblasts, which subsequently give rise to a class of yellow pigment cells called xanthophores<sup>455</sup>. Indeed, *csf1ra* is expressed by cells in the xanthophore lineage and promotes their migration from the neural crest<sup>217</sup>. In a study examining the *csf1ra* ligand, *csf1a*, *csf1ra*<sup>+</sup> neural crest-derived xanthophores fail to migrate past the horizontal myoseptum in 48 hpf *csf1a*<sup>-/-</sup> (e.g. *csf1a*<sup>hkz9</sup>) embryos<sup>403</sup>. A separate temperature-sensitive *csf1ra* mutant (e.g. *csf1ra*<sup>ut.r4e174A</sup>) exhibits a null phenotype when shifted to 33°C that matches previous studies when in trans with *csf1ra*<sup>ie1217,456</sup>. When shifting 24 hpf *csf1ra*<sup>ut.r4e174A</sup> *csf1ra*<sup>ie1</sup> embryos to 33°C for 2 to 3 hours, there is a dramatic increase in TUNEL<sup>+</sup> neural crest cells<sup>456</sup>. Interestingly, preliminary staining for *csf1ra* by *in situ* hybridization shows that the only *csf1ra*<sup>+</sup> NCCs are those migrating dorsolaterally, which eventually give rise to pigment cells<sup>457</sup>. Altogether, these studies demonstrate that a subset of NCCs depend on *csf1ra-csf1a* signaling for survival and migration. Future experiments investigating whether phagocytosis by *csf1ra*<sup>+</sup> NCCs is 1) dependent on *csf1ra* expression and 2) affected in *csf1ra*<sup>-/-</sup> mutants would give newfound insight into the mechanisms behind NCC phagocytosis in neurodevelopment.

## A.5 EXAMINING NCCs IN THE ZEBRAFISH *BLB (SLC37A2*<sup>-/-</sup>) MUTANT

Aberrant phagocytosis is implicated in several devastating neurodevelopmental (e.g. Nasu-Hakola disease<sup>181,182</sup>, Rett syndrome<sup>458</sup>) and neurodegenerative (e.g. Alzheimer's disease<sup>459-462</sup>, multiple sclerosis<sup>186,391</sup>) disorders. Emerging evidence also indicates that early impairments in phagocytosis, circuit formation, and circuit refinement play roles in multiple psychiatric disorders (e.g. schizophrenia<sup>463-466</sup>, Autism spectrum disorder<sup>170,171,467-469</sup>). This positions the early phagocytosis by NCCs as an important investigative avenue to understand the function and implications of cell and debris clearance on early neurodevelopment. Phagocytic NCCs are active during an early developmental time window (**Figure A-2B**) simultaneous to key neurodevelopmental trajectories (**Figure 1-1**) and the formation of critical neural circuits. Thus, I hypothesized that phagocytic NCCs are essential for neural development and that aberrant NCC phagocytosis would lead to abnormal circuit formation and developmental phenotypes.

Bulk RNA sequencing data from the Kucenas lab shows an upregulation of phagocytosis-related genes in NCCs at 36 hpf, including *slc37a2* (a solute carrier transporter)<sup>126</sup> (**Figure A-2C**). Slc37a2 is a putative glucose 6-phosphate transporter anchored to endoplasmic reticulum membranes<sup>470,471</sup> and is expressed by MΦ<sup>83,472,473</sup> and microglia<sup>83,207,474</sup>. Recently, Slc37a2 has been shown to localize to phagosomes in mammalian MΦ *in vitro* and microglia in the zebrafish optic tectum. The *bubblebrain* (*blb*, *slc37a2*<sup>-/-</sup>) zebrafish mutant results in phagocytosis-deficient microglia, where a statistically significant decrease in the rate of microglia engulfment results in statistically significant increase in the number of apoptotic neurons in the optic tectum starting at 3.5 dpf. These microglia also fail to migrate to sites of injury in *blb* embryos. At 4 dpf, microglia in *blb* mutants feature a large gasosome, which arises from impaired phagosomal shrinkage. Of note, the authors did not describe whether and/or how SC microglia are affected in *blb* mutants. Trunk MΦ do not develop a gasosome unless under conditions of increased apoptosis (e.g. camptothecin)<sup>83</sup>.

Since NCCs express *slc37a2* during their phagocytic window (**Figure A-2C**), we previously hypothesized that 1) NCC phagocytosis would be impaired in *blb* embryos and 2) we could use *blb* embryos to examine how impaired NCC phagocytosis alters development. In multiple time-lapse confocal imaging studies of *blb* embryos with NCCs fluorescently labeled (e.g. by *Tg(sox10:eos)*, *Tg(sox10:TagRFP)*, and later *Gt(erb3b3:GAL4) Tg(UAS:EGFP)*) from 24 to 40 hpf, there were no observable differences between NCCs in wild-type (WT) versus heterozygous (*blb*<sup>+/-</sup>) or *blb* mutant embryos. I also did not observe any gross phagosomal differences or development of a gasosome in NCCs labeled in *blb* embryos. (Data not shown.) Since there was no obvious NCC phenotype in *blb* embryos, my further studies aimed to determine whether NCCs in *blb* embryos displayed more subtle phenotypes.

### **A.5.1 *blb* embryos have increased numbers of dying cells in early development**

We have previously established that NCCs phagocytose dying cells and debris between 24 and 30 hpf. Starting at ~30 hpf, infiltrating MΦ take over cell and debris clearance (**Figure A-2B**). As an indirect way to ascertain changes in NCC efferocytosis, I stained WT, *blb*<sup>+/-</sup>, and *blb* mutant embryos at 36, 65, and 72 hpf with AO, which labels dying cells<sup>220,227</sup>. These three timepoints represent three distinct stages of efferocytosis in early zebrafish development. At 36 hpf, cell and debris clearance has just switched from NCCs to MΦ. I hypothesized

that if NCC efferocytosis was affected, this timepoint would reflect a maximal accumulation of uncleared apoptotic cells. At 72 hpf, microglia display a gastrosome<sup>83</sup> and are present in the spinal cord<sup>439,475</sup>. I hypothesized that this timepoint would serve as a positive control and I would expect to see an increase in AO<sup>+</sup> puncta, as microglial efferocytosis is diminished in *blb* mutants. I also included a middle timepoint, 65 hpf, which I hypothesized would be when SC microglia had normal efferocytic responses prior to the development of the gastrosome.

In this experiment I found that the number of AO<sup>+</sup> puncta was largely localized to the spinal cord for all embryos (**Figure A-9A, C, and E**). At both 36 and 72 hpf, there was a statistically significant increase in the number of AO<sup>+</sup> puncta in *blb* mutant embryos compared to WT/*blb*<sup>+/-</sup> embryos (**Figure A-9A & B**). At 65 hpf, there was no statistically significant difference. These data align with my aforementioned hypotheses and the statistically significant increase in the number of AO<sup>+</sup> puncta between *blb* mutant and WT/*blb*<sup>+/-</sup> embryos points to defects in early efferocytosis by NCCs.

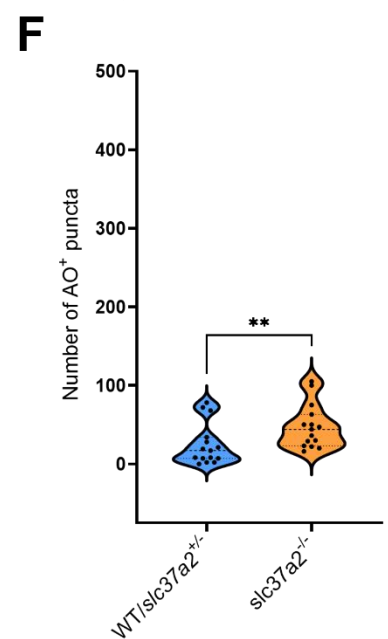
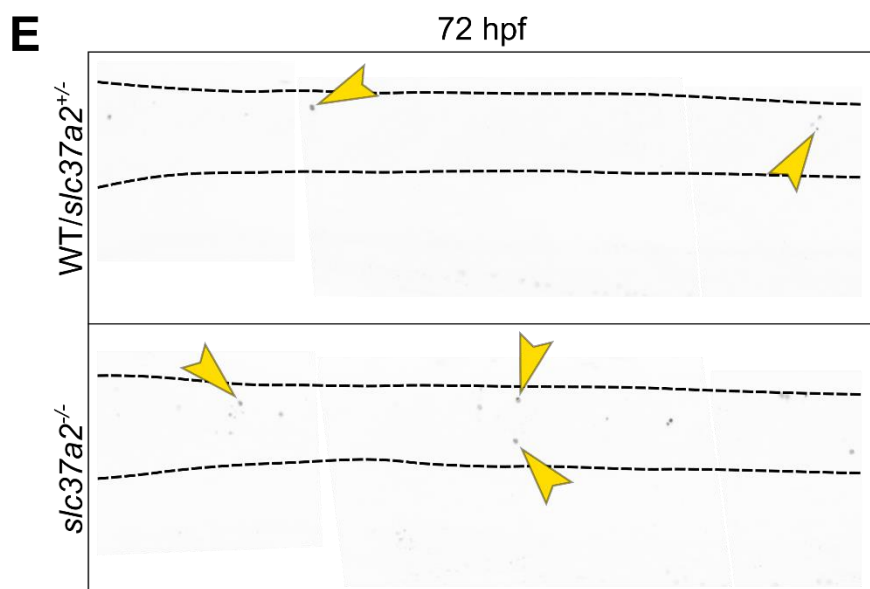
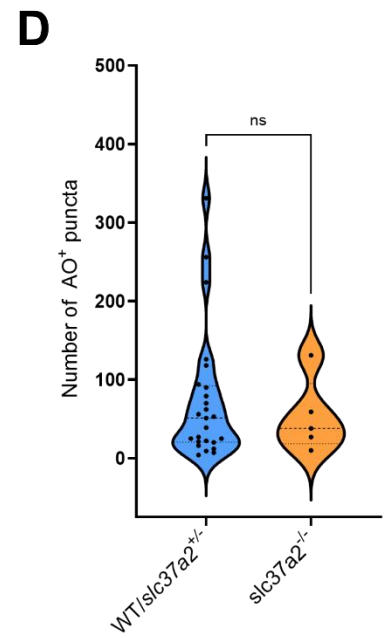
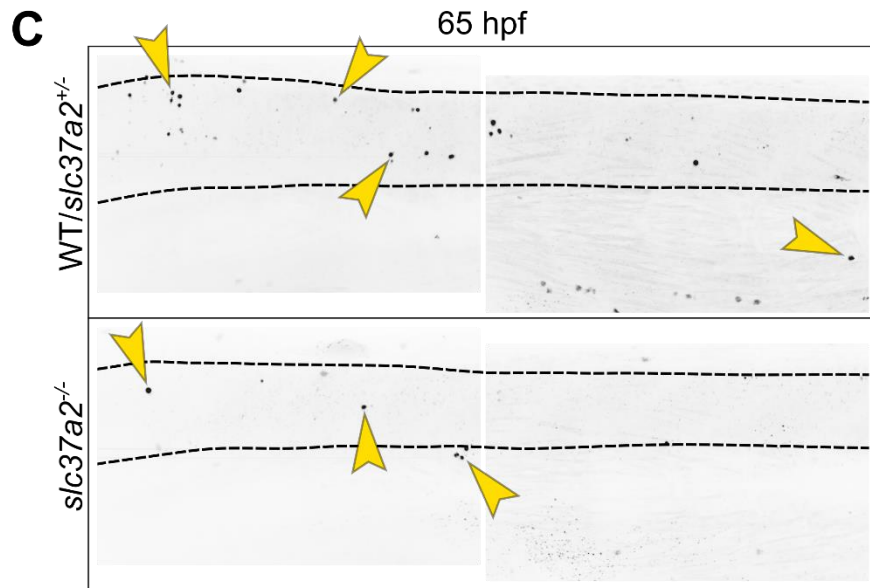
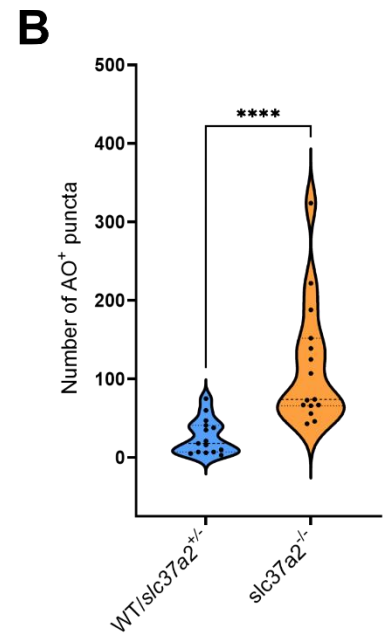
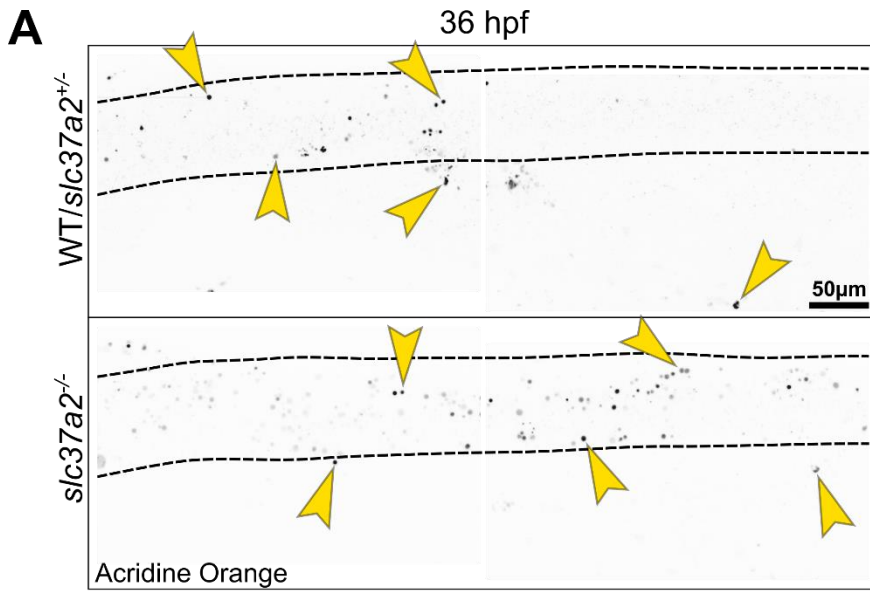


**Figure A-9: *blb* mutants exhibit increased numbers of dying cells at 36 and 72 hpf by acridine orange. (A, C, E) Lateral trunk of WT/*blb*<sup>+/-</sup> (top) or *blb* (bottom) embryos with dying cells labeled by acridine orange (AO) at 36, 65, and 72 hpf, respectively. Yellow arrowheads point to example AO<sup>+</sup> puncta. (B, D, F) Quantifications of the number of AO<sup>+</sup> puncta per embryo for WT/*blb*<sup>+/-</sup> (blue) or *blb* (orange). Mann-Whitney U-Tests p values: \*\*p = 0.0095, \*\*\*\* p < 0.0001. For B, mean ± SEM: WT/*blb*<sup>+/-</sup> = 25.93 ± 5.767, *blb* = 116.6 ± 20.28. For D, p value = 0.9665 and mean ± SEM: WT/*blb*<sup>+/-</sup> = 73.48 ± 16.63, *blb* = 53.00 ± 21.06. For F, mean ± SEM: WT/*blb*<sup>+/-</sup> = 24.73 ± 6.894, *blb* = 47.33 ± 7.192. For 36 hpf n = 3 fish each, for 65 hpf n = 5 (WT/*blb*<sup>+/-</sup>) and n = 1 (*blb*<sup>-/-</sup>), for 72 hpf n = 3 fish each. One dot equals one somite per fish, 5 somites sampled per fish. All images in Figure A-9 are representative, maximum projection confocal images.**

While promising, there are several caveats to this data. Firstly, AO intercalates within DNA and RNA<sup>476,477</sup> and is not a direct measure of cell death. As a DNA intercalator, it is possible that AO<sup>+</sup> puncta may also represent replicating cells<sup>478,479</sup>. There is some evidence that AO cannot intercalate DNA in a living cell<sup>480</sup> and in zebrafish it has been used as an assay for cell death assay<sup>60,220,402</sup>. While AO staining was chosen because of convenience and ease of use, this experiment would be improved upon by using a more direct and specific measure of cell death (e.g. TUNEL assay<sup>273</sup>). Secondly, this experiment is not a direct measure of NCC efferocytosis. Another interpretation of the data in **Figure A-9** is that *blb* embryos have increased rates of dying cells, independent of the rate of NCC efferocytosis. Targeted ablation experiments quantifying NCC phagocytic ability in *WT/blb<sup>+/-</sup>* versus *blb* embryos would provide a more direct examination of NCC efferocytosis. Lastly, this experiment lacks sufficient power and the data presented in **Figure A-9** comes from only one technical replicate. *WT* and *blb<sup>+/-</sup>* embryos were also combined into one group because there is no reported heterozygous phenotype. However, I should have confirmed there was no statistically significant difference between the number of AO<sup>+</sup> puncta in *WT* and *blb<sup>+/-</sup>* embryos before combining them. Even with these caveats, the results from this pilot study encouraged me to conduct further experiments that would more closely examine NCC efferocytosis in *blb* mutant embryos.

## A.5.2 NCCs have altered phagosome morphology in *blb* embryos

If NCC phagocytosis was impaired in ways similar to microglia and M $\Phi$  in *blb* embryos, we had hypothesized that NCCs would develop a large gastrosome. To directly observe NCC phagosomes I started by doing timelapse confocal imaging of WT, *blb*<sup>+/-</sup>, or *blb* *Tg(sox10:TagRFP; sox10:GAL4; UAS:GFP-2xFYVE)* embryos from 24 to 40 hpf. *Tg(UAS:GFP-2xFYVE)* is a fluorescent reporter of PI(3)P, a phospholipid enriched on endosomal and phagosomal membranes<sup>447,481</sup>. This combination of transgenes allows for *in vivo* visualization of *sox10*<sup>+</sup> NCCs and their phagosomes (**Figure A-10A**).

At later timepoints of the timelapse (post-32 hpf ish) I noticed that some NCCs were very strongly expressing GFP while others were relatively weaker (imaging data not shown). To accurately calculate phagosome volume, I optimized two different Imaris rendering parameters for FYVE<sup>+</sup> phagosomes (see **Chapter 2.13.8, Table 2-5, & Table 2-6**) to account for this difference in fluorescent intensity. In *blb* embryos, I noticed that a small subset of NCCs developed enlarged FYVE<sup>+</sup> phagosomes by the end of the timelapse (**Figure A-10B**). This was often accompanied by a rapid decrease in migration followed by extension of multiple processes. However, there was no statistically significant difference between the number of FYVE<sup>+</sup> phagosomes per NCC or average FYVE<sup>+</sup> phagosome volume per NCC in WT/*blb*<sup>+/-</sup> and *blb* embryos at 24, 28, 32, 36, or 40 hpf (**Figure A-10C**). I also opted to begin repeating my imaging using the 63X objective, which would facilitate the higher resolution needed for accurate measurements of phagosomes, starting with the 24 hpf timepoint.

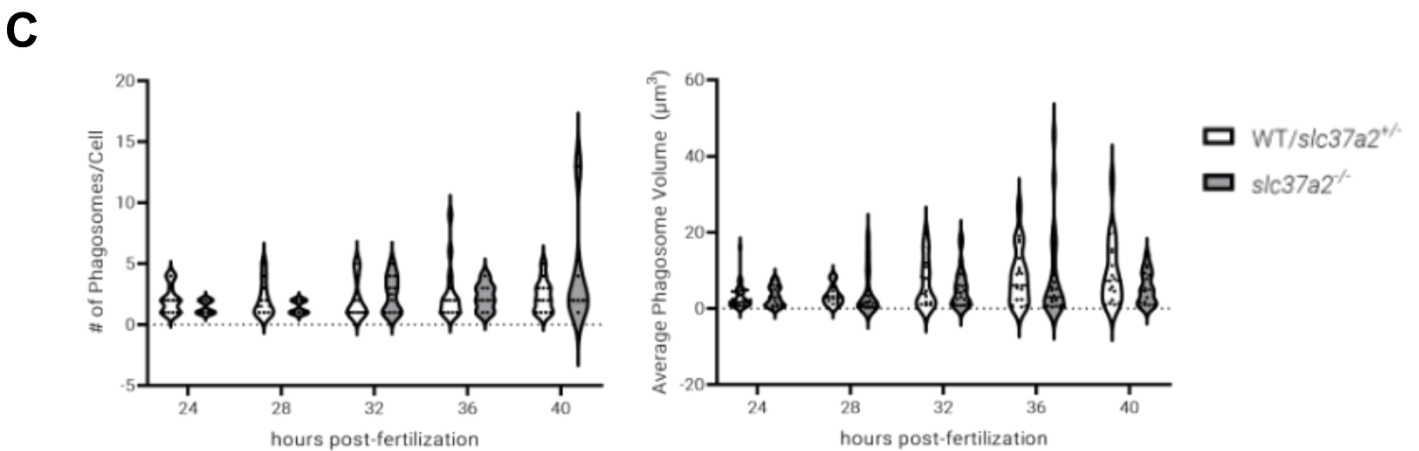
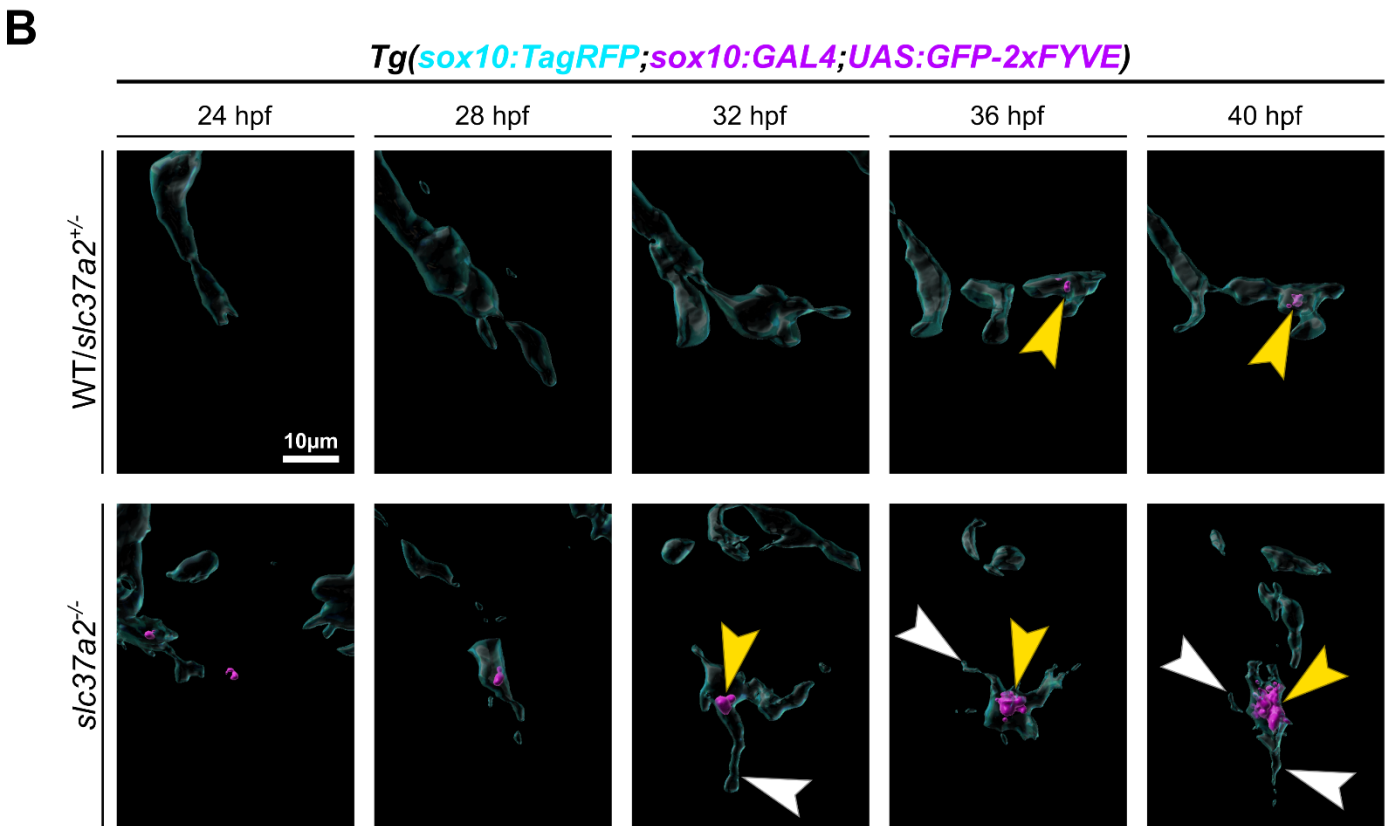
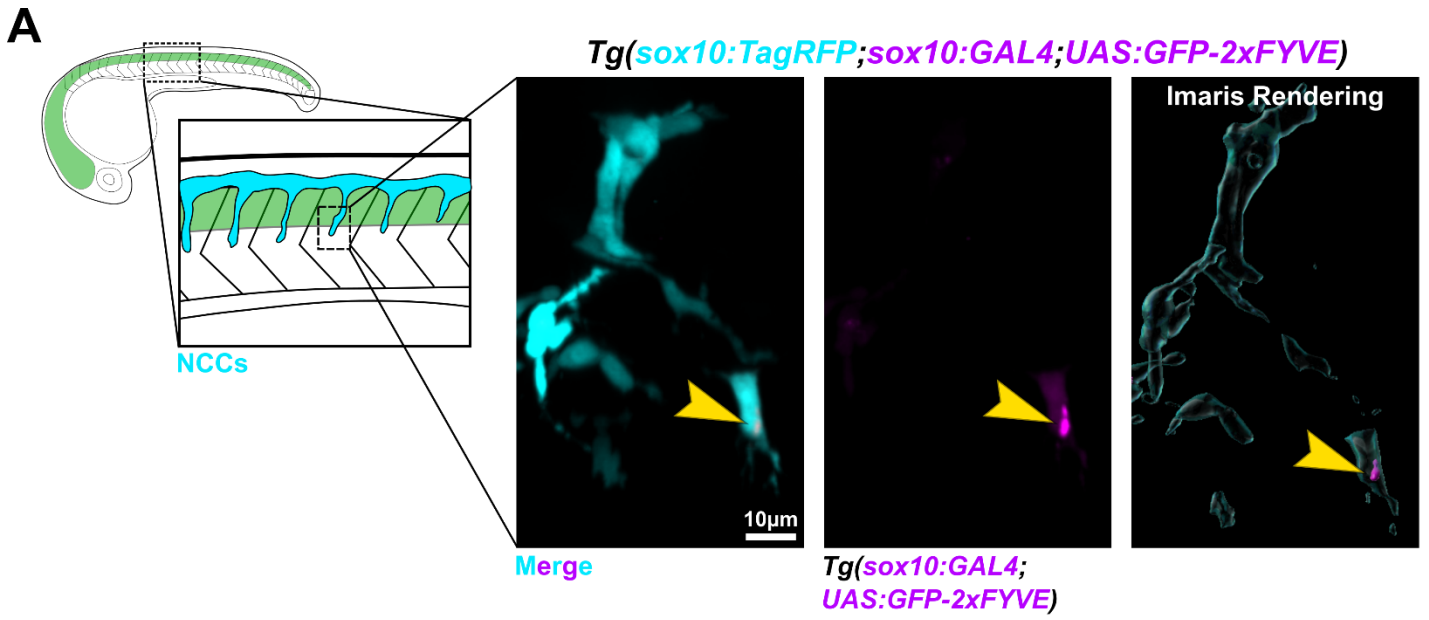


**Figure A-10: A subset of NCCs exhibit enlarged phagosomes in *blb* mutants.** (A) Zebrafish embryo is schematized to far left, with CNS in green and NCCs in blue. Inset shows representative confocal maximum projection images of NCCs and NCC phagosomes in 24 hpf *Tg(sox10:TagRFP; sox10:GAL4; UAS:GFP-2xFYVE)* embryos. Far right panel demonstrates Imaris surface renderings of confocal data. (B) Maximum projection confocal images at 24, 28, 32, 36, and 40 hpf of *Tg(sox10:TagRFP; sox10:GAL4; UAS:GFP-2xFYVE)* embryos. Top panels are images from a *WT/blb<sup>+/-</sup>* embryo while bottom row is from a *blb* mutant embryo. Yellow arrowheads point to a FYVE<sup>+</sup> phagosome. White arrowhead points to multiple projections that emerge after the NCC stops migrating. (C) Quantification of the number of phagosomes per cell (left plot) and average phagosome volume in  $\mu\text{m}^3$  (right plot) in *WT/blb<sup>+/-</sup>* embryos (white violin plots) and *blb* mutant embryos (grey violin plots) over time. All data in C was compared with a two-way ANOVA with Tukey's multiple comparisons test. Two-way ANOVA p value for interaction = 0.2714, p value for hpf = 0.1208, and p value for genotype = 0.7636. See **Table A-1** for adjusted p values for multiple comparisons.

**Table A-1: Adjusted p values for multiple comparisons for Figure A-10C**

Comparison	p value
24:WT/ <i>blb<sup>+/-</sup></i> vs. 24: <i>blb</i>	0.9985
24:WT/ <i>blb<sup>+/-</sup></i> vs. 28:WT/ <i>blb<sup>+/-</sup></i> 24:WT/ <i>blb<sup>+/-</sup></i> vs. 32:WT/ <i>blb<sup>+/-</sup></i> 24:WT/ <i>blb<sup>+/-</sup></i> vs. 36: <i>blb</i> 24:WT/ <i>blb<sup>+/-</sup></i> vs. 40:WT/ <i>blb<sup>+/-</sup></i> 24: <i>blb</i> vs. 28: <i>blb</i> 28:WT/ <i>blb<sup>+/-</sup></i> vs. 32:WT/ <i>blb<sup>+/-</sup></i> 28:WT/ <i>blb<sup>+/-</sup></i> vs. 32: <i>blb</i> 28:WT/ <i>blb<sup>+/-</sup></i> vs. 36: <i>blb</i> 28:WT/ <i>blb<sup>+/-</sup></i> vs. 40:WT/ <i>blb<sup>+/-</sup></i> 32:WT/ <i>blb<sup>+/-</sup></i> vs. 32: <i>blb</i> 32:WT/ <i>blb<sup>+/-</sup></i> vs. 36: <i>blb</i> 32:WT/ <i>blb<sup>+/-</sup></i> vs. 40:WT/ <i>blb<sup>+/-</sup></i> 32: <i>blb</i> vs. 36:WT/ <i>blb<sup>+/-</sup></i> 32: <i>blb</i> vs. 36: <i>blb</i> 32: <i>blb</i> vs. 40:WT/ <i>blb<sup>+/-</sup></i> 36: WT/ <i>blb<sup>+/-</sup></i> vs. 36: <i>blb</i> 36: WT vs. 40: WT/ <i>blb<sup>+/-</sup></i> 36: <i>blb</i> vs 40: WT/ <i>blb<sup>+/-</sup></i>	>0.9999
24:WT/ <i>blb<sup>+/-</sup></i> vs. 28: <i>blb</i>	0.9976
24:WT/ <i>blb<sup>+/-</sup></i> vs. 32: <i>blb</i> 28:WT/ <i>blb<sup>+/-</sup></i> vs. 36:WT/ <i>blb<sup>+/-</sup></i>	0.9998
24:WT/ <i>blb<sup>+/-</sup></i> vs. 36:WT/ <i>blb<sup>+/-</sup></i>	0.9991
24:WT/ <i>blb<sup>+/-</sup></i> vs. 40: <i>blb</i>	0.3987
24: <i>blb</i> vs. 28:WT/ <i>blb<sup>+/-</sup></i>	0.9988
24: <i>blb</i> vs. 32:WT/ <i>blb<sup>+/-</sup></i>	0.9987

24: <i>blb</i> vs. 32: <i>blb</i>	0.9645
24: <i>blb</i> vs. 36:WT/ <i>blb</i> <sup>+/-</sup>	0.9328
24: <i>blb</i> vs. 36: <i>blb</i>	0.9958
24: <i>blb</i> vs. 40:WT/ <i>blb</i> <sup>+/-</sup>	0.9854
24: <i>blb</i> vs. 40: <i>blb</i>	0.2202
28:WT/ <i>blb</i> <sup>+/-</sup> vs. 28: <i>blb</i>	0.9983
28:WT/ <i>blb</i> <sup>+/-</sup> vs. 40: <i>blb</i>	0.5384
28: <i>blb</i> vs. 32:WT/ <i>blb</i> <sup>+/-</sup>	0.998
28: <i>blb</i> vs. 32: <i>blb</i>	0.95
28: <i>blb</i> vs. 36:WT/ <i>blb</i> <sup>+/-</sup>	0.9013
28: <i>blb</i> vs. 36: <i>blb</i>	0.9943
28: <i>blb</i> vs. 40:WT/ <i>blb</i> <sup>+/-</sup>	0.9784
28: <i>blb</i> vs. 40: <i>blb</i>	0.1674
32:WT/ <i>blb</i> <sup>+/-</sup> vs. 36:WT/ <i>blb</i> <sup>+/-</sup>	0.9997
32:WT/ <i>blb</i> <sup>+/-</sup> vs. 40: <i>blb</i>	0.4785
36:WT/ <i>blb</i> <sup>+/-</sup> vs. 40: <i>blb</i>	0.7781
36: <i>blb</i> vs. 40: <i>blb</i>	0.7632
40:WT/ <i>blb</i> <sup>+/-</sup> vs. 40: <i>blb</i>	0.6727

Since there may be changes in FYVE<sup>+</sup> phagosomes in a small subset of NCCs, I began working with Dr. Marieke Jones to understand how to visualize and model my data. We opted to examine the distribution of the phagosome volume data (**Figure A-11**). The distribution data between *WT/blb<sup>+/-</sup>* and *blb* embryos appear grossly similar and some distributions appear to be bimodal. At 28 hpf, we did observe a difference in the mean density of FYVE<sup>+</sup> phagosome volumes between *WT/blb<sup>+/-</sup>* and *blb* embryos (**Figure A-11B**). In working with the 63X data at 24 hpf, we found that the distribution of phagosome volume was bimodal for both *WT/blb<sup>+/-</sup>* and *blb* embryos (**Figure A-11F**). This suggests that there the NCC population consists of two groups of NCCs, one characterized by smaller phagosomal volumes and another by large. This aligns with the Kucenas lab's previous observations that only a subset of NCCs are phagocytically active<sup>126</sup>. We realized that the next step is to interpret the FYVE<sup>+</sup> phagosome volume data in the context of NCC volume. Unfortunately, this analysis was halted due to other ongoing experimental directions.

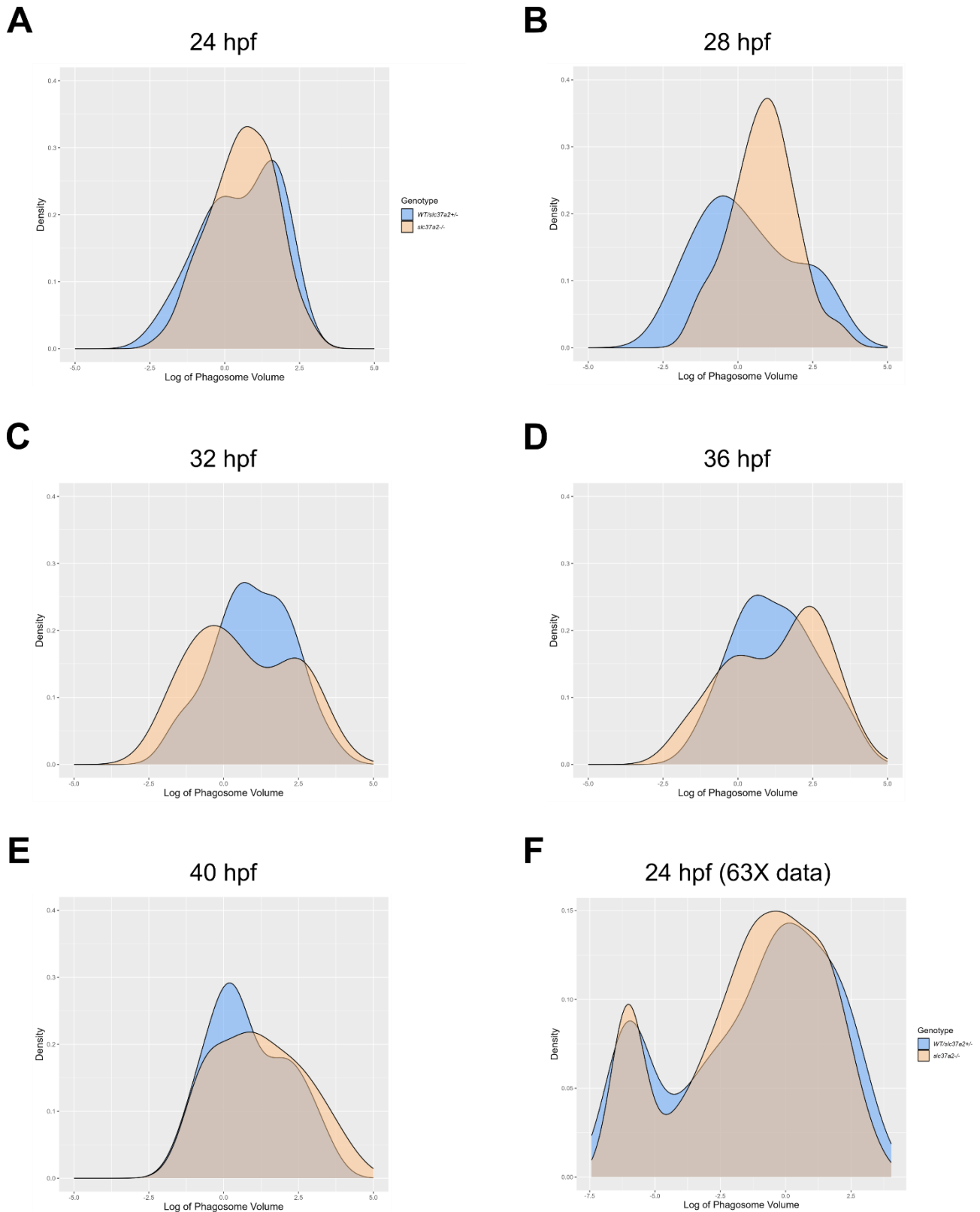


**Figure A-11: NCC FYVE<sup>+</sup> phagosome volume data plotted as distributions. (A - E)** NCC FYVE<sup>+</sup> phagosome volume data from Figure A-10C (left) plotted as a distribution from WT/*blb*<sup>+/-</sup> (in blue) and *blb* (in orange) embryos. **(F)** NCC FYVE<sup>+</sup> phagosome volume data from 63X imaging from WT/*blb*<sup>+/-</sup> (in blue) and *blb* (in orange) embryos. Created with R v4.4.1 and RStudio v3.6.0.

## A.6 EXPLORING PHAGOCYTOTIC NCCs BY scRNAseq

Before NCC specification, it has been assumed that the NCC population is homogenous, and it is not until NCC migration begins that developmental timing and interactions with signaling molecules and surrounding cells cause NCCs to differentiate. Intriguingly, only ~10% of NCCs were observed to phagocytose in the developing PNS<sup>126</sup>. This unveils an interesting debate: are phagocytotic NCCs responding because of minute differences in their sensitivity thresholds to efferocytotic signals? Or, are phagocytotic NCCs different from the rest of the NCC population? The photoconversion lineage tracing results of phagocytotic NCCs suggest the former, since phagocytotic NCCs are not lineage restricted<sup>126</sup>.

Recently, several publicly available scRNAseq datasets have provided the opportunity to investigate the NCC transcriptome<sup>482,483</sup>. By using NCC transcriptomic data I sought to see if I could determine whether phagocytotic NCCs are transcriptomically similar or if they are widespread throughout the NCC population. Working with Addison Webster, I have been able to do some rudimentary scRNAseq analysis. First, I selected for cells that were classified as neural crest cell clusters (clusters 37 and 44) and then filtered the data for specific timepoints spanning from 21 to 44 hpf. From there, I re-clustered the cells and found 3 sub-clusters (Figure A-12A). Then, I decided to examine *slc37a2* expression which was identified to be expressed in NCCs by the Kucenas lab bulk-RNAseq. *Slc37a2* was widely expressed throughout the sub-clusters with only a handful of cells demonstrating high expression (Figure A-12B). While these are ongoing analyses, this preliminary plot suggests that phagocytotic NCCs may not represent a subset of NCCs.

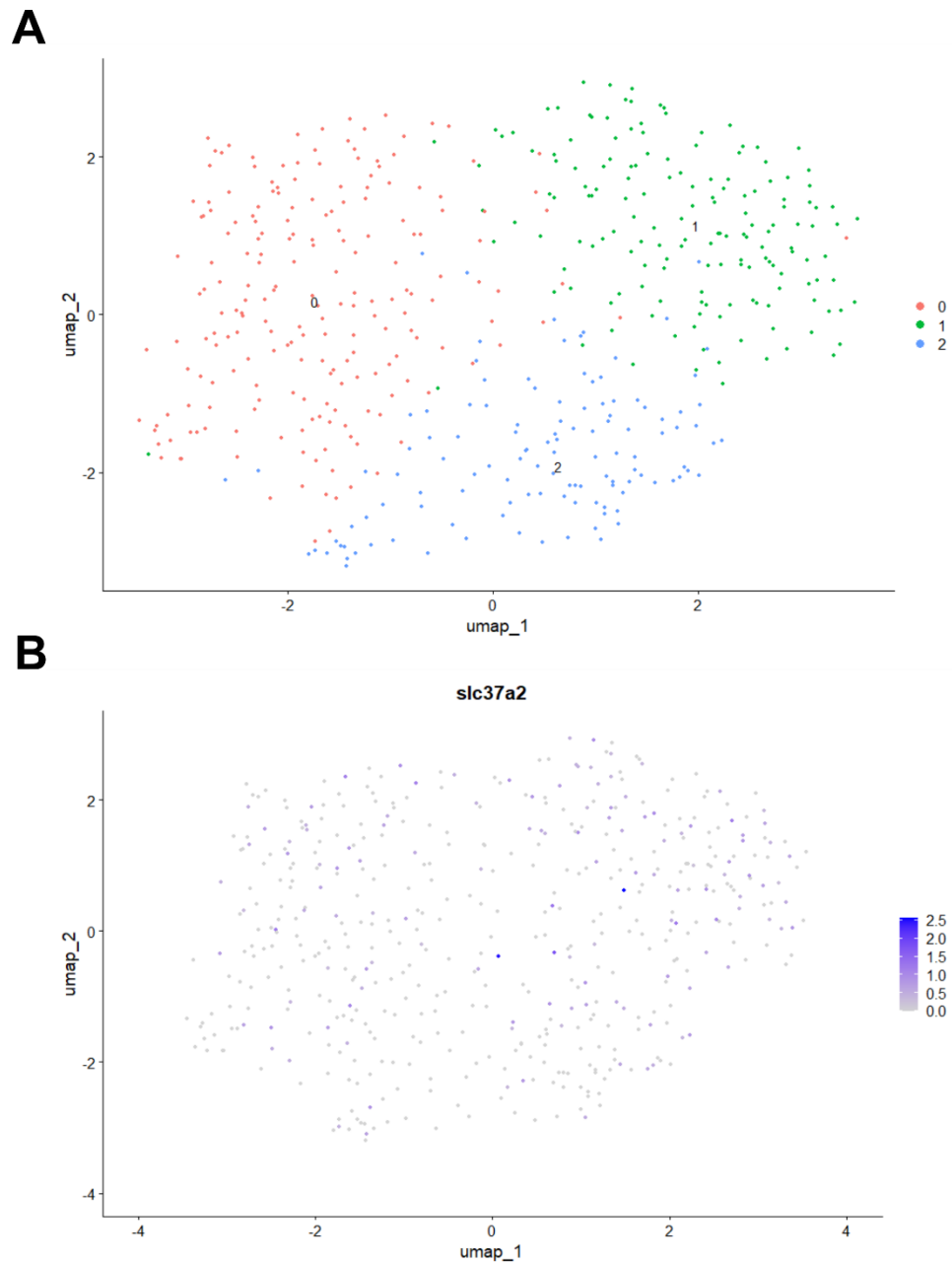


**Figure A-12: NCC sub-clusters in early development with *slc37a2* expression.** (A) UMAP of early NCCs (21 to 44 hpf) re-clustered from Danio cell<sup>482, 483</sup> showing 3 separate sub-clusters. (B) UMAP of early NCCs from A displaying expression of *slc37a2*.

## References

---

1. Liu, K. E., Raymond, M. H., Ravichandran, K. S., & Kucenas, S. (2022). Clearing Your Mind: Mechanisms of Debris Clearance After Cell Death During Neural Development. *Annual Review of Neuroscience*, *45*, 177–198. <https://doi.org/10.1146/annurev-neuro-110920-022431>
2. Innocenti, G. M., & Price, D. J. (2005). Exuberance in the development of cortical networks. *Nature Reviews Neuroscience*, *6*(12), 955–965. <https://doi.org/10.1038/nrn1790>
3. Waites, C. L., Craig, A. M., & Garner, C. C. (2005). Mechanisms of vertebrate synaptogenesis. *Annual Review of Neuroscience*, *28*, 251–274. <https://doi.org/10.1146/annurev.neuro.27.070203.144336>
4. Zeutzius, I., & Rahmann, H. (1980). Quantitative Ultrastructural Investigations on Synaptogenesis in the Cerebellum and the Optic Tectum of Light-Reared and Dark-Reared Rainbow Trout (*Salmo gairdneri* Rich.). *Differentiation*, *17*(1–3), 181–186. <https://doi.org/10.1111/j.1432-0436.1980.tb01094.x>
5. Bourgeois, J. P., & Rakic, P. (1993). Changes of synaptic density in the primary visual cortex of the macaque monkey from fetal to adult stage. *Journal of Neuroscience*, *13*(7), 2801–2820. <https://doi.org/10.1523/jneurosci.13-07-02801.1993>
6. Huttenlocher, P. R., & Dabholkar, A. S. (1997). Regional differences in synaptogenesis in human cerebral cortex. *Journal of Comparative Neurology*, *387*(2), 167–178. [https://doi.org/10.1002/\(SICI\)1096-9861\(19971020\)387:2<167::AID-CNE1>3.0.CO;2-Z](https://doi.org/10.1002/(SICI)1096-9861(19971020)387:2<167::AID-CNE1>3.0.CO;2-Z)
7. Muthukumar, A. K., Stork, T., & Freeman, M. R. (2014). Activity-dependent regulation of astrocyte GAT levels during synaptogenesis. *Nature Neuroscience*, *17*(10), 1340–1350. <https://doi.org/10.1038/nn.3791>
8. Colón-Ramos, D. A., Margeta, M. A., & Shen, K. (2007). Glia promote local synaptogenesis through UNC-6 (Netrin) signaling in *C. elegans*. *Science*, *318*(5847), 103–106. <https://doi.org/10.1126/science.1143762>
9. Shao, Z., Watanabe, S., Christensen, R., Jorgensen, E. M., & Colón-Ramos, D. A. (2013). Synapse location during growth depends on glia location. *Cell*, *154*(2), 337. <https://doi.org/10.1016/j.cell.2013.06.028>
10. Miyamoto, A., Wake, H., Ishikawa, A. W., Eto, K., Shibata, K., Murakoshi, H., Koizumi, S., Moorhouse, A. J., Yoshimura, Y., & Nabekura, J. (2016). Microglia contact induces synapse formation in developing somatosensory cortex. *Nature Communications*, *7*, 1–12. <https://doi.org/10.1038/ncomms12540>
11. Parkhurst, C. N., Yang, G., Ninan, I., Savas, J. N., Yates, J. R., Lafaille, J. J., Hempstead, B. L., Littman, D. R., & Gan, W. B. (2013). Microglia promote learning-dependent synapse formation through brain-derived neurotrophic factor. *Cell*, *155*(7), 1596–1609. <https://doi.org/10.1016/j.cell.2013.11.030>
12. Lee, E., & Chung, W. S. (2019). Glial control of synapse number in healthy and diseased brain. *Frontiers in Cellular Neuroscience*, *13*(February), 1–8. <https://doi.org/10.3389/fncel.2019.00042>
13. Wilton, D. K., Dissing-Olesen, L., & Stevens, B. (2019). Neuron-Glia Signaling in Synapse Elimination. *Annual Review of Neuroscience*, *42*(1), 107–127. <https://doi.org/10.1146/annurev-neuro-070918-050306>
14. de la Rosa, E. J., & de Pablo, F. (2000). Cell death in early neural development: beyond the neurotrophic theory. *Trends in Neurosciences*, *23*(10), 454–458.

15. Riccomagno, M. M., & Kolodkin, A. L. (2015). Sculpting Neural Circuits by Axon and Dendrite Pruning. *Annual Review of Cell and Developmental Biology*, 31(1), 779–805. <https://doi.org/10.1146/annurev-cellbio-100913-013038>
16. Buss, R. R., Sun, W., & Oppenheim, R. W. (2006). Adaptive roles of programmed cell death during nervous system development. *Annual Review of Neuroscience*, 29, 1–35. <https://doi.org/10.1146/annurev.neuro.29.051605.112800>
17. Ledonne, F., Orduz, D., Mercier, J., Angulo, M. C., Pierani, A., Coppola, E., Ledonne, F., Orduz, D., Mercier, J., Vigier, L., Grove, E. A., Tissir, F., & Angulo, M. C. (2016). Targeted Inactivation of Bax Reveals a Subtype-Specific Mechanism of Cajal-Retzius Neuron Death in the Postnatal Cerebral Cortex Report Targeted Inactivation of Bax Reveals a Subtype-Specific Mechanism of Cajal-Retzius Neuron Death in the Postnatal Cereb. *CellReports*, 17(12), 3133–3141. <https://doi.org/10.1016/j.celrep.2016.11.074>
18. Riva, M., Genescu, I., Habermacher, C., Orduz, D., Ledonne, F., Rijli, F. M., López-Bendito, G., Coppola, E., Garel, S., Angulo, M. C., & Pierani, A. (2019). Activity-dependent death of transient cajal-retzius neurons is required for functional cortical wiring. *ELife*, 8(i), 1–18. <https://doi.org/10.7554/eLife.50503>
19. Riva, M., Moriceau, S., Morabito, A., Dossi, E., Sanchez-Bellot, C., Azzam, P., Navas-Olive, A., Gal, B., Dori, F., Cid, E., Ledonne, F., David, S., Trovero, F., Bartolomucci, M., Coppola, E., Rebola, N., Depaulis, A., Rouach, N., de la Prida, L. M., ... Pierani, A. (2023). Aberrant survival of hippocampal Cajal-Retzius cells leads to memory deficits, gamma rhythmopathies and susceptibility to seizures in adult mice. *Nature Communications*, 14(1). <https://doi.org/10.1038/s41467-023-37249-7>
20. Leonard, J. R., Klocke, B. J., D'sa, C., Flavell, R. A., & Roth, K. A. (2002). Strain-dependent neurodevelopmental abnormalities in caspase-3-deficient mice. *Journal of Neuropathology and Experimental Neurology*, 61(8), 673–677. <https://doi.org/10.1093/jnen/61.8.673>
21. Duncan, I. D., & Radcliff, A. B. (2016). Inherited and acquired disorders of myelin: The underlying myelin pathology. *Experimental Neurology*, 283, 452–475. <https://doi.org/10.1016/j.expneurol.2016.04.002>
22. Buchsbaum, I. Y., & Cappello, S. (2019). Neuronal migration in the CNS during development and disease: Insights from in vivo and in vitro models. *Development (Cambridge)*, 146(1). <https://doi.org/10.1242/dev.163766>
23. Lago-Baldaia, I., Fernandes, V. M., & Ackerman, S. D. (2020). More Than Mortar: Glia as Architects of Nervous System Development and Disease. *Frontiers in Cell and Developmental Biology*, 8(December), 1–26. <https://doi.org/10.3389/fcell.2020.611269>
24. Hofmann, K. (2019). The evolutionary origins of programmed cell death signaling. *Cold Spring Harbor Perspectives in Biology*, 12(9), 1–16. <https://doi.org/10.1101/cshperspect.a036442>
25. Man, S. M., Karki, R., & Kanneganti, T.-D. (2017). Molecular mechanisms and functions of pyroptosis, inflammatory caspases and inflammasomes in infectious diseases. *Immunological Reviews*, 277(1), 61–75. <https://doi.org/10.1111/imr.12534>
26. Abrams, J. M., White, K., Fessler, L. I., & Steller, H. (1993). Programmed cell death during Drosophila embryogenesis. *Development*, 117(1), 29–43.

27. Cole, L. K., & Ross, L. S. (2001). Apoptosis in the developing zebrafish embryo. *Developmental Biology*, 240(1), 123–142. <https://doi.org/10.1006/dbio.2001.0432>
28. Yamaguchi, Y., & Miura, M. (2015). Programmed cell death in neurodevelopment. *Developmental Cell*, 32(4), 478–490. <https://doi.org/10.1016/j.devcel.2015.01.019>
29. Pathak, A., Clark, S., Bronfman, F. C., Deppmann, C. D., & Carter, B. D. (2020). Long-distance regressive signaling in neural development and disease. *Wiley Interdisciplinary Reviews: Developmental Biology*, April, 1–22. <https://doi.org/10.1002/wdev.382>
30. Reddien, P. W., Cameron, S., & Horvitz, R. H. (2001). Phagocytosis promotes programmed cell death in *C. elegans*. *Nature*, 412(6843), 198–202. <https://doi.org/10.1038/35084096>
31. Tasdemir-Yilmaz, O. E., & Freeman, M. R. (2013). Astrocytes engage unique molecular programs to engulf pruned neuronal debris from distinct subsets of neurons. *Genes and Development*, 28(1), 20–33. <https://doi.org/10.1101/gad.229518.113>
32. Pérez-Garijo, A., Fuchs, Y., & Steller, H. (2013). Apoptotic cells can induce non-autonomous apoptosis through the TNF pathway. *ELife*, 2013(2), 1–18. <https://doi.org/10.7554/eLife.01004>
33. Nagata, S., Hanayama, R., & Kawane, K. (2010). Autoimmunity and the Clearance of Dead Cells. *Cell*, 140(5), 619–630. <https://doi.org/10.1016/j.cell.2010.02.014>
34. Arandjelovic, S., & Ravichandran, K. S. (2015). Phagocytosis of apoptotic cells in homeostasis. *Nature Immunology*, 16(9), 907–917. <https://doi.org/10.1016/j.physbeh.2017.03.040>
35. Saunders, J. W. (1966). Death in embryonic systems. *Science*, 154(3749), 604–612. <https://doi.org/10.1126/science.154.3749.604>
36. Southwell, D. G., Paredes, M. F., Galvao, R. P., Jones, D. L., Froemke, R. C., Sebe, J. Y., Alfaro-Cervello, C., Tang, Y., Garcia-Verdugo, J. M., Rubenstein, J. L., Baraban, S. C., & Alvarez-Buylla, A. (2012). Intrinsically determined cell death of developing cortical interneurons. *Nature*, 491(7422), 109–113. <https://doi.org/10.1038/nature11523>
37. Pinto-Teixeira, F., Konstantinides, N., & Desplan, C. (2016). Programmed cell death acts at different stages of *Drosophila* neurodevelopment to shape the central nervous system. *FEBS Letters*, 590, 2435–2453. <https://doi.org/10.1002/1873-3468.12298>
38. Weil, M., Jacobson, M. D., & Raff, M. C. (1997). Is programmed cell death required for neural tube closure? *Current Biology*, 7(4), 281–284. [https://doi.org/10.1016/S0960-9822\(06\)00125-4](https://doi.org/10.1016/S0960-9822(06)00125-4)
39. Massa, V., Savery, D., Ybot-Gonzalez, P., Ferraro, E., Rongvaux, A., Cecconi, F., Flavell, R., Greene, N. D. E., & Copp, A. J. (2009). Apoptosis is not required for mammalian neural tube closure. *Proceedings of the National Academy of Sciences*, 106(20), 8233–8238. <https://doi.org/10.1073/pnas.0900333106>
40. Kochersberger, A., Torkashvand, M. M., Lee, D., Baskoylu, S., Sengupta, T., Koonce, N., Emerson, C. E., Patel, N. V., Colón-Ramos, D., Flavell, S., Horvitz, R. H., Venkatachalam, V., & Hammarlund, M. (2023). Programmed Cell Death Modifies Neural Circuits and Tunes Intrinsic Behavior. *BioRxiv*.
41. Prieto-Godino, L. L., Silbering, A. F., Khallaf, M. A., Cruchet, S., Bojkowska, K., Pradervand, S., Hansson, B. S., Knaden, M., & Benton, R. (2020). Functional integration of “undead” neurons in the olfactory system.

*Science Advances*, 6(11), 1–12.

42. Hevner, R. F., Neogi, T., Englund, C., Daza, R. A. M., & Fink, A. (2003). Cajal–Retzius cells in the mouse: transcription factors , neurotransmitters, and birthdays suggest a pallial origin. *Developmental Brain Research*, 141, 39–53.
43. Elorriaga, V., Pierani, A., & Causeret, F. (2023). Cajal-retzius cells: Recent advances in identity and function. *Current Opinion in Neurobiology*, 79, 102686. <https://doi.org/10.1016/j.conb.2023.102686>
44. McKay, S. E., & Oppenheim, R. W. (1991). Lack of evidence for cell death among avian spinal cord interneurons during normal development and following removal of targets and afferents. *Journal of Neurobiology*, 22(7), 721–733. <https://doi.org/10.1002/neu.480220707>
45. Galluzzi, L., Vitale, I., Aaronson, S. A., Abrams, J. M., Adam, D., Agostinis, P., Alnemri, E. S., Altucci, L., Amelio, I., Andrews, D. W., Annicchiarico-Petruzzelli, M., Antonov, A. V., Arama, E., Baehrecke, E. H., Barlev, N. A., Bazan, N. G., Bernassola, F., Bertrand, M. J. M., Bianchi, K., ... Kroemer, G. (2018). Molecular mechanisms of cell death: Recommendations of the Nomenclature Committee on Cell Death 2018. *Cell Death and Differentiation*, 25(3), 486–541. <https://doi.org/10.1038/s41418-017-0012-4>
46. Lammert, C. R., Frost, E. L., Bellinger, C. E., Bolte, A. C., McKee, C. A., Hurt, M. E., Paysour, M. J., Ennerfelt, H. E., & Lukens, J. R. (2020). AIM2 inflammasome surveillance of DNA damage shapes neurodevelopment. *Nature*, 580(7805), 647–652. <https://doi.org/10.1038/s41586-020-2174-3>
47. Hubel, D. H., Wiesel, T. N., & LeVay, S. (1977). Plasticity of ocular dominance columns in monkey striate cortex. *Philosophical Transactions of the Royal Society of London. Series B, Biological Sciences*, 278(961), 377–409. <https://doi.org/10.1098/rstb.1977.0050>
48. Paolicelli, R. C., & Ferretti, M. T. (2017). Function and dysfunction of microglia during brain development: Consequences for synapses and neural circuits. *Frontiers in Synaptic Neuroscience*, 9(MAY), 1–17. <https://doi.org/10.3389/fnsyn.2017.00009>
49. Awasaki, T., Tatsumi, R., Takahashi, K., Arai, K., Nakanishi, Y., Ueda, R., & Ito, K. (2006). Essential Role of the Apoptotic Cell Engulfment Genes draper and ced-6 in Programmed Axon Pruning during Drosophila Metamorphosis. *Neuron*, 50(6), 855–867. <https://doi.org/10.1016/j.neuron.2006.04.027>
50. Hoopfer, E. D., McLaughlin, T., Watts, R. J., Schuldiner, O., O’Leary, D. D. M., & Luo, L. (2006). Wlds Protection Distinguishes Axon Degeneration following Injury from Naturally Occurring Developmental Pruning. *Neuron*, 50(6), 883–895. <https://doi.org/10.1016/j.neuron.2006.05.013>
51. Hoshiko, M., Arnoux, I., Avignone, E., Yamamoto, N., & Audinat, E. (2012). Deficiency of the Microglial Receptor CX3CR1 Impairs Postnatal Functional Development of Thalamocortical Synapses in the Barrel Cortex. *Journal of Neuroscience*, 32(43), 15106–15111. <https://doi.org/10.1523/JNEUROSCI.1167-12.2012>
52. Tremblay, M.-È., Lowery, R. L., & Majewska, A. K. (2010). Microglial interactions with synapses are modulated by visual experience. *PLoS Biology*, 8(11). <https://doi.org/10.1371/journal.pbio.1000527>
53. Schafer, D. P., Lehrman, E. K., Kautzman, A. G., Koyama, R., Mardinly, A. R., Yamasaki, R., Ransohoff, R. M., Greenberg, M. E., Barres, B. A., & Stevens, B. (2012). Microglia Sculpt Postnatal Neural Circuits in an

- Activity and Complement-Dependent Manner. *Neuron*, 74(4), 691–705. <https://doi.org/10.1016/j.neuron.2012.03.026>
54. Cheadle, L., Rivera, S. A., Phelps, J. S., Ennis, K. A., Stevens, B., Burkly, L. C., Lee, W.-C. A., & Greenberg, M. E. (2020). Sensory Experience Engages Microglia to Shape Neural Connectivity through a Non-Phagocytic Mechanism. *Neuron*, 1–18. <https://doi.org/10.1016/j.neuron.2020.08.002>
55. Escoubas, C. C., Dorman, L. C., Nguyen, P. T., Lagares-Linares, C., Nakajo, H., Anderson, S. R., Barron, J. J., Wade, S. D., Cuevas, B., Vainchtein, I. D., Silva, N. J., Guajardo, R., Xiao, Y., Lidsky, P. V., Wang, E. Y., Rivera, B. M., Taloma, S. E., Kim, D. K., Kaminskaya, E., ... Molofsky, A. V. (2024). Type-I-interferon-responsive microglia shape cortical development and behavior. *Cell*, 187(8), 1936-1954.e24. <https://doi.org/10.1016/j.cell.2024.02.020>
56. Chung, W. S., Clarke, L. E., Wang, G. X., Stafford, B. K., Sher, A., Chakraborty, C., Joung, J., Foo, L. C., Thompson, A., Chen, C., Smith, S. J., & Barres, B. A. (2013). Astrocytes mediate synapse elimination through MEGF10 and MERTK pathways. *Nature*, 504(7480), 394–400. <https://doi.org/10.1038/nature12776>
57. Parnaik, R., Raff, M. C., & Scholes, J. (2000). Differences between the clearance of apoptotic cells by professional and non-professional phagocytes. *Current Biology*, 10(14), 857–860. [https://doi.org/10.1016/S0960-9822\(00\)00598-4](https://doi.org/10.1016/S0960-9822(00)00598-4)
58. Wood, W., Turmaine, M., Weber, R., Camp, V., Maki, R. A., McKercher, S. R., & Martin, P. (2000). Mesenchymal cells engulf and clear apoptotic footplate cells in macrophageless PU.1 null mouse embryos. *Development*, 127(24), 5245–5252.
59. Alliot, F., Lecain, E., Grima, B., & Pessac, B. (1991). Microglial progenitors with a high proliferative potential in the embryonic and adult mouse brain. *Proceedings of the National Academy of Sciences*, 88(4), 1541–1545. <https://doi.org/10.1073/pnas.88.4.1541>
60. Herbomel, P., Thisse, B., & Thisse, C. (2001). Zebrafish early macrophages colonize cephalic mesenchyme and developing brain, retina, and epidermis through a M-CSF receptor-dependent invasive process. *Developmental Biology*, 238(2), 274–288. <https://doi.org/10.1006/dbio.2001.0393>
61. Nimmerjahn, A., Kirchhoff, F., & Helmchen, F. (2005). Resting Microglial Cells Are Highly Dynamic Surveillants of Brain Parenchyma in Vivo. *Science*, 308(5726), 1314–1318. <https://doi.org/10.1126/science.1110647>
62. Ginhoux, F., Greter, M., Leboeuf, M., Nandi, S., See, P., Gokhan, S., Mehler, M. F., Conway, S. J., Ng, L. G., Stanley, E. R., Samokhvalov, I. M., & Merad, M. (2010). Fate Mapping Analysis Reveals That Adult Microglia Derive from Primitive Macrophages. *Science*, 701(November), 841–845. <https://doi.org/10.1126/science.1194637>
63. Miller, F. D., & Gauthier, A. S. (2007). Timing is everything: making neurons versus glia in the developing cortex. *Neuron*, 54(3), 357–369. <https://doi.org/10.1016/j.neuron.2007.04.019>
64. Masuda, T., Sankowski, R., Staszewski, O., Böttcher, C., Amann, L., Scheiwe, C., Nessler, S., Kunz, P., van Loo, G., Coenen, V., Reinacher, P., Michel, A., Sure, U., Gold, R., Priller, J., Stadelmann, C., & Prinz, M. (2019). Spatial and temporal heterogeneity of mouse and human microglia at single-cell resolution. *Nature*,

- 566(7744), 388–392. <https://doi.org/10.1038/s41586-019-0924-x>
65. Sierra, A., Encinas, J. M., Deudero, J. J. P., Chancey, J. H., Enikolopov, G., Overstreet-Wadiche, L. S., Tsirka, S. E., & Maletic-Savatic, M. (2010). Microglia shape adult hippocampal neurogenesis through apoptosis-coupled phagocytosis. *Cell Stem Cell*, 7(4), 483–495. <https://doi.org/10.1016/j.stem.2010.08.014>
66. Anderson, S. R., Zhang, J., Steele, M. R., Romero, C. O., Kautzman, A. G., Schafer, D. P., & Vetter, M. L. (2019). Complement targets newborn retinal ganglion cells for phagocytic elimination by microglia. *Journal of Neuroscience*, 39(11), 2025–2040. <https://doi.org/10.1523/JNEUROSCI.1854-18.2018>
67. Morrison, V., Houpert, M., Trapani, J., Bix, G., Ihrie, R., Carter, B., Morrison, V., Houpert, M., Trapani, J., Brockman, A., Kingsley, P., & Katdare, K. (2023). Jedi-1/MEGF12-mediated phagocytosis controls the pro-neurogenic properties of microglia in the ventricular-subventricular zone. *Cell Reports*, 42(11), 113423. <https://doi.org/10.1016/j.celrep.2023.113423>
68. Beiter, R. M., Sheehan, P. W., & Schafer, D. P. (2024). Microglia phagocytic mechanisms: Development informing disease. *Current Opinion in Neurobiology*, 86, 102877. <https://doi.org/10.1016/j.conb.2024.102877>
69. Casano, A. M., Albert, M., & Peri, F. (2016). Developmental Apoptosis Mediates Entry and Positioning of Microglia in the Zebrafish Brain. *Cell Reports*, 16(4), 897–906. <https://doi.org/10.1016/j.celrep.2016.06.033>
70. Cunningham, C. L., Martínez-Cerdeño, V., & Noctor, S. C. (2013). Microglia regulate the number of neural precursor cells in the developing cerebral cortex. *Journal of Neuroscience*, 33(10), 4216–4233. <https://doi.org/10.1523/JNEUROSCI.3441-12.2013>
71. Squarzoni, P., Oller, G., Hoeffel, G., Lorena, P.-L., Rostaing, P., Low, D., Bessis, A., Ginhoux, F., & Garel, S. (2014). *Microglia Modulate Wiring of the Embryonic Forebrain*. 8(5), 1271–1279. <https://doi.org/10.1016/j.celrep.2014.07.042>
72. Nemes-Baran, A. D., White, D. R., & DeSilva, T. M. (2020). Fractalkine-Dependent Microglial Pruning of Viable Oligodendrocyte Progenitor Cells Regulates Myelination. *Cell Reports*, 32(7), 108047. <https://doi.org/10.1016/j.celrep.2020.108047>
73. VanRyzin, J. W., Marquardt, A. E., Argue, K. J., Vecchiarelli, H. A., Ashton, S. E., Arambula, S. E., Hill, M. N., & McCarthy, M. M. (2019). Microglial Phagocytosis of Newborn Cells Is Induced by Endocannabinoids and Sculptures Sex Differences in Juvenile Rat Social Play. *Neuron*, 102(2), 435–449.e6. <https://doi.org/10.1016/j.neuron.2019.02.006>
74. Lawrence, A. R., Canzi, A., Bridlance, C., Olivíé, N., Lansonneur, C., Catale, C., Pizzamiglio, L., Kloeckner, B., Silvin, A., Munro, D. A. D., Fortoul, A., Boido, D., Zehani, F., Cartonnet, H., Viguié, S., Oller, G., Squarzoni, P., Candat, A., Helft, J., ... Garel, S. (2024). Microglia maintain structural integrity during fetal brain morphogenesis. *Cell*, 187(4), 962–980. <https://doi.org/10.1016/j.cell.2024.01.012>
75. Ayata, P., Badimon, A., Strasburger, H. J., Duff, M. K., Montgomery, S. E., Loh, Y.-H. E., Ebert, A., Pimenova, A. A., Ramirez, B. R., Chan, A. T., Sullivan, J. M., Purushothaman, I., Scarpa, J. R., Goate, A. M., Busslinger, M., Shen, L., Losic, B., & Schaefer, A. (2019). Epigenetic regulation of brain region-specific microglia clearance activity. *Nature Neuroscience*, 21(8), 1049–1060. <https://doi.org/10.1038/s41593-018->

76. Mazaheri, F., Breus, O., Durdu, S., Haas, P., Wittbrodt, J., Gilmour, D., & Peri, F. (2014). Distinct roles for BAI1 and TIM-4 in the engulfment of dying neurons by microglia. *Nature Communications*, 5(May), 1–11. <https://doi.org/10.1038/ncomms5046>
77. Furgeaud, L., Través, P. G., Tufail, Y., Leal-Bailey, H., Lew, E. D., Burrola, P. G., Callaway, P., Zagorska, A., Rothlin, C. V., Nimmerjahn, A., & Lemke, G. (2016). TAM receptors regulate multiple features of microglial physiology. *Nature*, 532(7598), 240–244. <https://doi.org/10.1038/nature17630>
78. Marín-Teva, J. L., Dusart, I., Colin, C., Gervais, A., Van Rooijen, N., & Mallat, M. (2004). Microglia Promote the Death of Developing Purkinje Cells. *Neuron*, 41(4), 535–547. [https://doi.org/10.1016/S0896-6273\(04\)00069-8](https://doi.org/10.1016/S0896-6273(04)00069-8)
79. Weinhard, L., Bartolomei, G., Bolasco, G., Machado, P., Schieber, N. L., Neniskyte, U., Exiga, M., Vadisiute, A., Raggioli, A., Schertel, A., Schwab, Y., & Gross, C. T. (2018). Microglia remodel synapses by presynaptic trogocytosis and spine head filopodia induction. *Nature Communications*, 9(1), 1228. <https://doi.org/10.1038/s41467-018-03566-5>
80. Favuzzi, E., Huang, S., Saldi, G. A., Binan, L., Ibrahim, L. A., Fernández-Otero, M., Cao, Y., Zeine, A., Sefah, A., Zheng, K., Xu, Q., Khlestova, E., Farhi, S. L., Bonneau, R., Datta, S., Stevens, B., & Fishell, G. (2021). GABA-receptive microglia selectively sculpt developing inhibitory circuits. *Cell*, 184(15), 4048-4063.e32. <https://doi.org/10.1016/j.cell.2021.06.018>
81. Ueno, M., Fujita, Y., Tanaka, T., Nakamura, Y., Kikuta, J., Ishii, M., & Yamashita, T. (2013). Layer V cortical neurons require microglial support for survival during postnatal development. *Nature Neuroscience*, 16(5), 543–551. <https://doi.org/10.1038/nn.3358>
82. Diaz-Aparicio, I., Paris, I., Sierra-Torre, V., Plaza-Zabala, A., Rodríguez-Iglesias, N., Márquez-Ropero, M., Beccari, S., Abiega, O., Alberdi, E., Matute, C., Bernales, I., Schulz, A., Otrokocsi, L., Sperlágh, B., Happonen, K. E., Lemke, G., Maletic-Savatic, M., Valero, J., & Sierra, A. (2020). Microglia actively remodels adult hippocampal neurogenesis through the phagocytosis secretome. *Journal of Neuroscience*, 40(7), 1453–1482. <https://doi.org/10.1101/583849>
83. Villani, A., Benjaminsen, J., Moritz, C., Henke, K., Hartmann, J., Norlin, N., Richter, K., Schieber, N. L., Franke, T., Schwab, Y., & Peri, F. (2019). Clearance by Microglia Depends on Packaging of Phagosomes into a Unique Cellular Compartment. *Developmental Cell*, 49(1), 77-88.e7. <https://doi.org/10.1016/j.devcel.2019.02.014>
84. Mrdjen, D., Pavlovic, A., Hartmann, F. J., Schreiner, B., Utz, S. G., Leung, B. P., Lelios, I., Heppner, F. L., Kipnis, J., Merkler, D., Greter, M., & Becher, B. (2018). High-Dimensional Single-Cell Mapping of Central Nervous System Immune Cells Reveals Distinct Myeloid Subsets in Health, Aging, and Disease. *Immunity*, 48(2), 380–395. <https://doi.org/10.1016/j.immuni.2018.01.011>
85. Cronk, J. C., Filiano, A. J., Louveau, A., Marin, I., Marsh, R., Ji, E., Goldman, D. H., Smirnov, I., Geraci, N., Acton, S., Overall, C. C., & Kipnis, J. (2018). Peripherally derived macrophages can engraft the brain independent of irradiation and maintain an identity distinct from microglia. *Journal of Experimental Medicine*,

86. Chen, H.-R., Sun, Y.-Y., Chen, C.-W., Kuo, Y.-M., Kuan, I. S., Li, Z.-R., Short-Miller, J. C., Smucker, M. R., & Kuan, C.-Y. (2020). Fate mapping via CCR2-CreER mice reveals monocyte-to-microglia transition in development and neonatal stroke. *Science Advances*, 6(35), eabb2119. <https://doi.org/10.1126/sciadv.abb2119>
87. Cugurra, A., Mamuladze, T., Rustenhoven, J., Dykstra, T., Beroshvili, G., Greenberg, Z. J., Baker, W., Papadopoulos, Z., Drieu, A., Blackburn, S., Kanamori, M., Brioschi, S., Herz, J., Schuettpelz, L. G., Colonna, M., Smirnov, I., & Kipnis, J. (2021). Skull and vertebral bone marrow are myeloid cell reservoirs for the meninges and CNS parenchyma. *Science*, 373(6553), eabf7844. <https://doi.org/10.1126/science.abf7844>
88. Wood, W., & Martin, P. (2017). Macrophage Functions in Tissue Patterning and Disease: New Insights from the Fly. *Developmental Cell*, 40(3), 221–233. <https://doi.org/10.1016/j.devcel.2017.01.001>
89. Evans, I. R., Ghai, P. A., Urbančič, V., Tan, K.-L., & Wood, W. (2013). SCAR/WAVE-mediated processing of engulfed apoptotic corpses is essential for effective macrophage migration in *Drosophila*. *Cell Death and Differentiation*, 20(5), 709–720. <https://doi.org/10.1038/cdd.2012.166>
90. Weavers, H., Evans, I. R., Martin, P., & Wood, W. (2016). Corpse Engulfment Generates a Molecular Memory that Primes the Macrophage Inflammatory Response. *Cell*, 165(7), 1658–1671. <https://doi.org/10.1016/j.cell.2016.04.049>
91. Davidson, A. J., & Wood, W. (2020). Macrophages Use Distinct Actin Regulators to Switch Engulfment Strategies and Ensure Phagocytic Plasticity In Vivo. *Cell Reports*, 31(8), 107692. <https://doi.org/10.1016/j.celrep.2020.107692>
92. Tsai, H.-H., Li, H., Fuentealba, L. C., Molofsky, A. V., Raquel, T.-M., Zhuang, H., Tenney, A., Murnen, A. T., Fancy, S. P. J., Merkle, F., Kessaris, N., Arturo, A.-B., Richardson, W. D., & Rowitch, D. H. (2012). Regional astrocyte allocation regulates CNS synaptogenesis and repair. *Science*, 337(6092), 358–362. <https://doi.org/10.1126/science.1222381>
93. Iram, T., Ramirez-Ortiz, Z., Byrne, M. H., Coleman, U. A., Kingery, N. D., Means, T. K., Frenkel, D., & El Khoury, J. (2016). Megf10 Is a receptor for C1Q that mediates clearance of apoptotic cells by astrocytes. *Journal of Neuroscience*, 36(19), 5185–5192. <https://doi.org/10.1523/JNEUROSCI.3850-15.2016>
94. Lee, J.-H., Kim, J., Kim, M., Shin, C.-H., & Chung, W.-S. (2022). Astrocytic synapse elimination controls ocular dominance plasticity. *BioRxiv*.
95. Lee, J.-H., Kim, J., Noh, S., Lee, H., Lee, S., Mun, J., Park, H., & Chung, W.-S. (2021). Astrocytes phagocytose adult hippocampal synapses for circuit homeostasis. *Nature*, 590(7847), 612–617. <https://doi.org/10.1038/s41586-020-03060-3>
96. Prasad, D., Rothlin, C., Burrola, P., Burstyn-Cohen, T., Lu, Q., Frutos, P., & Lemke, G. (2006). TAM receptor function in the retinal pigment epithelium. *Molecular and Cellular Neuroscience*, 33(1), 96–108.
97. Burstyn-Cohen, T., Lew, E. D., Través, P. G., Burrola, P. G., Hash, J. C., & Lemke, G. (2012). Genetic dissection of TAM receptor-ligand interaction in retinal pigment epithelial cell phagocytosis. *Neuron*, 76(6),

- 1123–1132. <https://doi.org/10.1016/j.neuron.2012.10.015>
98. Ruggiero, L., Connor, M. P., Chen, J., Langen, R., & Finnemann, S. C. (2012). Diurnal, localized exposure of phosphatidylserine by rod outer segment tips in wild-type but not *Itgb5*<sup>-/-</sup> or *Mfge8*<sup>-/-</sup> mouse retina. *Proceedings of the National Academy of Sciences*, *109*(21), 8145–8148. <https://doi.org/10.1073/pnas.1121101109>
99. Penberthy, K. K., Lysiak, J. J., & Ravichandran, K. S. (2018). Rethinking Phagocytes: Clues from the Retina and Testes. *Trends in Cell Biology*, *28*(4), 317–327. <https://doi.org/10.1016/j.tcb.2018.01.004>
100. Müller, C., & Finnemann, S. C. (2020). RPE Phagocytosis. In A. Klettner & S. Dithmar (Eds.), *Retinal Pigment Epithelium in Health and Disease*. [https://doi.org/10.1007/978-3-030-28384-1\\_3](https://doi.org/10.1007/978-3-030-28384-1_3)
101. Pringle, N. P., & Richardson, W. D. (1993). A singularity of PDGF alpha-receptor expression in the dorsoventral axis of the neural tube may define the origin of the oligodendrocyte lineage. *Development*, *117*(2), 525–533.
102. Ravanelli, A. M., & Appel, B. (2015). Motor neurons and oligodendrocytes arise from distinct cell lineages by progenitor recruitment. *Genes and Development*, *29*(23), 2504–2515. <https://doi.org/10.1101/gad.271312.115>
103. Auguste, Y. S. S., Ferro, A., Kahng, J. A., Xavier, A. M., Dixon, J. R., Vrudhula, U., Nichitiu, A.-S., Rosado, D., Wee, T.-L., Pedmale, U. V., & Cheadle, L. (2022). Oligodendrocyte precursor cells engulf synapses during circuit remodeling in mice. *Nature Neuroscience*, *25*(October). <https://doi.org/10.1038/s41593-022-01170-x>
104. Buchanan, J., Elabbady, L., Collman, F., Jorstad, N. L., Bakken, T. E., Ott, C., Glatzer, J., & Bleckert, A. A. (2022). Oligodendrocyte precursor cells ingest axons in the mouse neocortex. *Proceedings of the National Academy of Sciences*, *119*(48), 1–11. <https://doi.org/10.1073/pnas>.
105. Xiao, Y., Petrucco, L., Hoodless, L. J., Portugues, R., & Czopka, T. (2022). Oligodendrocyte precursor cells sculpt the visual system by regulating axonal remodeling. *Nature Neuroscience*, *25*(March). <https://doi.org/10.1038/s41593-022-01023-7>
106. Damisah, E. C., Hill, R. A., Rai, A., Chen, F., Rothlin, C. V., Ghosh, S., & Grutzendler, J. (2020). Astrocytes and microglia play orchestrated roles and respect phagocytic territories during neuronal corpse removal in vivo. *Science Advances*, *6*(26), 1–13. <https://doi.org/10.1126/sciadv.aba3239>
107. Bishop, D. L., Misgeld, T., Walsh, M. K., Gan, W. B., & Lichtman, J. W. (2004). Axon branch removal at developing synapses by axosome shedding. *Neuron*, *44*(4), 651–661. <https://doi.org/10.1016/j.neuron.2004.10.026>
108. Darabid, H., Arbour, D., & Robitaille, R. (2013). Glial cells decipher synaptic competition at the mammalian neuromuscular junction. *Journal of Neuroscience*, *33*(4), 1297–1313. <https://doi.org/10.1523/JNEUROSCI.2935-12.2013>
109. Smith, I. W., Mikesch, M., Lee, Y. II, & Thompson, W. J. (2013). Terminal Schwann cells participate in the competition underlying neuromuscular synapse elimination. *Journal of Neuroscience*, *33*(45), 17724–17736. <https://doi.org/10.1523/JNEUROSCI.3339-13.2013>

110. Lee, Y. I., Li, Y., Mikesch, M., Smith, I., Nave, K. A., Schwab, M. H., & Thompson, W. J. (2016). Neuregulin1 displayed on motor axons regulates terminal Schwann cell-mediated synapse elimination at developing neuromuscular junctions. *Proceedings of the National Academy of Sciences*, *113*(4), E479–E487. <https://doi.org/10.1073/pnas.1519156113>
111. Wolpowitz, D., Mason, T. B. A., Dietrich, P., Mendelsohn, M., Talmage, D. A., & Role, L. W. (2000). Cysteine-rich domain isoforms of the Neuregulin-1 gene are required for maintenance of peripheral synapses. *Neuron*, *25*(1), 79–91. [https://doi.org/10.1016/S0896-6273\(00\)80873-9](https://doi.org/10.1016/S0896-6273(00)80873-9)
112. Reddy, L. V., Koirala, S., Sugiura, Y., Herrera, A. A., & Ko, C. P. (2003). Glial cells maintain synaptic structure and function and promote development of the neuromuscular junction in vivo. *Neuron*, *40*(3), 563–580. [https://doi.org/10.1016/S0896-6273\(03\)00682-2](https://doi.org/10.1016/S0896-6273(03)00682-2)
113. Liu, H. M., Yang, L. H., & Yang, Y. J. (1995). Schwann cell properties: 3. C-fos expression, bFGF production, phagocytosis and proliferation during Wallerian degeneration. *Journal of Neuropathology and Experimental Neurology*, *54*(4), 487–496.
114. Perry, V. H., Tsao, J. W., Feam, S., & Brown, M. C. (1995). Radiation-induced Reductions in Macrophage Recruitment Have Only Slight Effects on Myelin Degeneration in Sectioned Peripheral Nerves of Mice. *European Journal of Neuroscience*, *7*(2), 271–280. <https://doi.org/10.1111/j.1460-9568.1995.tb01063.x>
115. Hirata, K., & Kawabuchi, M. (2002). Myelin phagocytosis by macrophages and nonmacrophages during Wallerian degeneration. *Microscopy Research and Technique*, *57*(6), 541–547. <https://doi.org/10.1002/jemt.10108>
116. Gomez-Sanchez, J. A., Carty, L., Iruarrizaga-Lejarreta, M., Palomo-Irigoyen, M., Varela-Rey, M., Griffith, M., Hantke, J., Macias-Camara, N., Azkargorta, M., Aurrekoetxea, I., De Juan, V. G., Jefferies, H. B. J., Aspichueta, P., Elortza, F., Aransay, A. M., Martínez-Chantar, M. L., Baas, F., Mato, J. M., Mirsky, R., ... Jessen, K. R. (2015). Schwann cell autophagy, myelinophagy, initiates myelin clearance from injured nerves. *Journal of Cell Biology*, *210*(1), 153–168. <https://doi.org/10.1083/jcb.201503019>
117. Jang, S. Y., Shin, Y. K., Park, S. Y., Park, J. Y., Lee, H. J., Yoo, Y. H., Kim, J. K., & Park, H. T. (2015). Autophagic myelin destruction by schwann cells during wallerian degeneration and segmental demyelination. *Glia*, *64*(5), 730–742. <https://doi.org/10.1002/glia.22957>
118. Lutz, A. B., Chung, W. S., Sloan, S. A., Carson, G. A., Zhou, L., Lovelett, E., Posada, S., Zuchero, J. B., & Barres, B. A. (2017). Schwann cells use TAM receptor-mediated phagocytosis in addition to autophagy to clear myelin in a mouse model of nerve injury. *Proceedings of the National Academy of Sciences*, *114*(38), E8072–E8080. <https://doi.org/10.1073/pnas.1710566114>
119. Lemke, G. (2013). Biology of the TAM receptors. *Cold Spring Harbor Perspectives in Biology*, *5*(11), 1–18. <https://doi.org/10.1101/cshperspect.a009076>
120. Lewis, G. M., & Kucenas, S. (2014). Perineurial glia are essential for motor axon regrowth following nerve injury. *Journal of Neuroscience*, *34*(38), 12762–12777. <https://doi.org/10.1523/JNEUROSCI.1906-14.2014>
121. Pannese, E. (2010). The structure of the perineuronal sheath of satellite glial cells (SGCs) in sensory ganglia. *Neuron Glia Biology*, *6*(1), 3–10. <https://doi.org/10.1017/S1740925X10000037>

122. Wu, H.-H., Bellmunt, E., Scheib, J. L., Venegas, V., Burkert, C., Reichardt, L. F., Zhou, Z., Farías, I., & Carter, B. D. (2009). Glial precursors clear sensory neuron corpses during development via Jedi-1, an engulfment receptor. *Nature Neuroscience*, *12*(12), 1534–1541. <https://doi.org/10.1038/nn.2446>
123. van Velzen, M., Laman, J., KleinJan, A., Poot, A., Osterhaus, A. D. M. E., & Verjans, G. M. G. M. (2009). Neuron-Interacting Satellite Glial Cells in Human Trigeminal Ganglia Have an APC Phenotype. *Journal of Immunology*, *183*(4), 2456–2461. <https://doi.org/10.4049/jimmunol.0900890>
124. Trevisan, A. J., Bauer, M. B., Brindley, R. L., Currie, K. P. M., & Carter, B. D. (2020). Jedi-1 deficiency increases sensory neuron excitability through a non-cell autonomous mechanism. *Scientific Reports*, *10*(1), 1–15. <https://doi.org/10.1038/s41598-020-57971-2>
125. Lu, Z., Elliott, M. R., Chen, Y., Walsh, J. T., Klibanov, A. L., Ravichandran, K. S., & Kipnis, J. (2011). Phagocytic activity of neuronal progenitors regulates adult neurogenesis. *Nature Cell Biology*, *13*(9), 1076–1084. <https://doi.org/10.1038/ncb2299>
126. Zhu, Y., Crowley, S. C., Latimer, A. J., Lewis, G. M., Nash, R., & Kucenas, S. (2019). Migratory Neural Crest Cells Phagocytose Dead Cells in the Developing Nervous System. *Cell*, *179*(1), 74-89.e10. <https://doi.org/10.1016/j.cell.2019.08.001>
127. Elliott, M. R., & Ravichandran, K. S. (2016). The dynamics of apoptotic cell clearance. *Developmental Cell*, *38*(2), 147–160. <https://doi.org/10.1016/j.physbeh.2017.03.040>
128. Kinchen, J. M., & Ravichandran, K. S. (2008). Phagosome maturation : going through the acid test. *Nature Reviews Molecular Cell Biology*, *9*, 781–795. <https://doi.org/10.1038/nrm2515>
129. Elliott, M. R., Chekeni, F. B., Trampont, P. C., Lazarowski, E. R., Kadl, A., Walk, S. F., Park, D., Woodson, R. I., Ostankovich, M., Sharma, P., Lysiak, J. J., Harden, T. K., Leitinger, N., & Ravichandran, K. S. (2009). Nucleotides released by apoptotic cells act as a find-me signal to promote phagocytic clearance. *Nature*, *461*(September), 2–7. <https://doi.org/10.1038/nature08296>
130. Chekeni, F. B., Elliott, M. R., Sandilos, J. K., Walk, S. F., Kinchen, J. M., Lazarowski, E. R., Armstrong, A. J., Penuela, S., Laird, D. W., Salvesen, G. S., Isakson, B. E., Bayliss, D. A., & Ravichandran, K. S. (2010). Pannexin 1 channels mediate ‘find-me’ signal release and membrane permeability during apoptosis. *Nature Letter*, *467*, 863–867. <https://doi.org/10.1038/nature09413>
131. Wicki-Stordeur, L. E., Sanchez-Arias, J. C., Dhaliwal, J., Carmona-Wagner, E. O., Shestopalov, V. I., Lagace, D. C., & Swayne, L. A. (2016). Pannexin 1 Differentially Affects Neural Precursor Cell Maintenance in the Ventricular Zone and Peri-Infarct Cortex. *Journal of Neuroscience*, *36*(4), 1203–1210. <https://doi.org/10.1523/jneurosci.0436-15.2016>
132. Medina, C. B., Mehrotra, P., Arandjelovic, S., Perry, J. S. A., Guo, Y., Morioka, S., Barron, B., Walk, S. F., Ghesquière, B., Krupnick, A. S., Lorenz, U., & Ravichandran, K. S. (2020). Metabolites released from apoptotic cells act as tissue messengers. *Nature*, *580*(April). <https://doi.org/10.1038/s41586-020-2121-3>
133. Poon, I. K. H., Chiu, Y.-H. H., Armstrong, A. J., Kinchen, J. M., Juncadella, I. J., Bayliss, D. A., & Ravichandran, K. S. (2014). Unexpected link between an antibiotic, pannexin channels and apoptosis. *Nature*, *507*(7492), 329–334. <https://doi.org/10.1038/nature13147>

134. Truman, L. A., Ford, C. A., Pasikowska, M., Pound, J. D., Wilkinson, S. J., Dumitriu, I. E., Melville, L., Melrose, L. A., Ogden, C. A., Nibbs, R., Graham, G., Combadiere, C., & Gregory, C. D. (2008). CX3CL1 / fractalkine is released from apoptotic lymphocytes to stimulate macrophage chemotaxis. *Blood*, *112*(13), 5026–5036. <https://doi.org/10.1182/blood-2008-06-162404>.The
135. Leonardi-Essmann, F., Emig, M., Kitamura, Y., Spanagel, R., & Gebicke-Haerter, P. J. (2005). Fractalkine-upregulated milk-fat globule EGF factor-8 protein in cultured rat microglia. *Journal of Neuroimmunology*, *160*(1–2), 92–101. <https://doi.org/10.1016/j.jneuroim.2004.11.012>
136. Fadok, V. A., Voelker, D. R., Campbell, P. A., Cohen, J. J., Bratton, D. L., & Henson, P. M. (1992). Exposure of phosphatidylserine on the surface of apoptotic lymphocytes triggers specific recognition and removal by macrophages. *Journal of Immunology*, *148*(7), 2207–2216.
137. Segawa, K., Kurata, S., Yanagihashi, Y., Brummelkamp, T. R., Matsuda, F., & Nagata, S. (2014). Caspase-mediated cleavage of phospholipid flippase for apoptotic phosphatidylserine exposure. *Science*, *344*(6188), 1164–1168. <https://doi.org/10.1126/science.1252809>
138. Neniskyte, U., Kuliesiute, U., Vadisiute, A., Jevdokimenko, K., Coletta, L., Deivasigamani, S., Pamedylyte, D., Daugelaviciene, N., Dabkeviciene, D., Perlas, E., Bali, A., Basilico, B., Gozzi, A., Ragozzino, D., & Gross, C. T. (2023). Phospholipid scramblase Xkr 8 is required for developmental axon pruning via phosphatidylserine exposure. *EMBO Journal*, *42*, 1–18. <https://doi.org/10.15252/emj.2022111790>
139. Doran, A. C., Yurdagul, A., & Tabas, I. (2020). Efferocytosis in health and disease. *Nature Reviews Immunology*, *20*(4), 254–267. <https://doi.org/10.1038/s41577-019-0240-6>
140. Sapar, M. L., Ji, H., Wang, B., Poe, A. R., Dubey, K., Ren, X., Ni, J.-Q., & Han, C. (2018). Phosphatidylserine Externalization Results from and Causes Neurite Degeneration in *Drosophila*. *Cell Reports*, *24*(9), 2273–2286. <https://doi.org/10.1016/j.celrep.2018.07.095>
141. Scott-Hewitt, N., Perrucci, F., Morini, R., Erreni, M., Mahoney, M., Witkowska, A., Carey, A., Faggiani, E., Schuetz, L. T., Mason, S., Tamborini, M., Bizzotto, M., Passoni, L., Filipello, F., Jahn, R., Stevens, B., & Matteoli, M. (2020). Local externalization of phosphatidylserine mediates developmental synaptic pruning by microglia. *EMBO Journal*, *39*(16), 1–20. <https://doi.org/10.15252/emj.2020105380>
142. Brelstaff, J., Tolkovsky, A. M., Ghetti, B., Goedert, M., & Spillantini, M. G. (2018). Living Neurons with Tau Filaments Aberrantly Expose Phosphatidylserine and Are Phagocytosed by Microglia. *Cell Reports*, *24*(8). <https://doi.org/10.1016/j.celrep.2018.07.072>
143. Panaretakis, T., Kepp, O., Brockmeier, U., Tesniere, A., Bjorklund, A., Chapman, D. C., Durchschlag, M., Joza, N., Pierron, G., van Endert, P., Yuan, J., Zitvogel, L., Madeo, F., Williams, D. B., & Kroemer, G. (2009). Mechanisms of pre-apoptotic calreticulin exposure in immunogenic cell death. *EMBO Journal*, *28*(5), 578–590. <https://doi.org/10.1038/emboj.2009.1>
144. Gardai, S. J., McPhillips, K. A., Frasch, C. S., Janssen, W. J., Starefeldt, A., Murphy-Ulrich, J. E., Bratton, D. L., Oldenbord, P.-A., Michalak, M., & Henson, P. M. (2005). Cell-surface calreticulin initiates clearance of viable or apoptotic cells through trans-activation of LRP on the phagocyte. *Cell*, *123*(2), 321–334. <https://doi.org/10.1016/j.cell.2005.08.032>

145. Li, J., Brickler, T., Banuelos, A., Marjon, K., Shcherbina, A., Banerjee, S., Bian, J., Narayanan, C., Weissman, I. L., & Chetty, S. (2021). Overexpression of CD47 is associated with brain overgrowth and 16p11.2 deletion syndrome. *Proceedings of the National Academy of Sciences*, *118*(15), e2005483118. <https://doi.org/10.1073/pnas.2005483118>
146. Stevens, B., Allen, N. J., Vazquez, L. E., Howell, G. R., Christopherson, K. S., Nouri, N., Micheva, K. D., Mehalow, A. K., Huberman, A. D., Stafford, B., Sher, A., Litke, A. M. M., Lambris, J. D., Smith, S. J., John, S. W. M., & Barres, B. A. (2007). The Classical Complement Cascade Mediates CNS Synapse Elimination. *Cell*, *131*(6), 1164–1178. <https://doi.org/10.1016/j.cell.2007.10.036>
147. Anderson, S. R., Zhang, J., Steele, M. R., Romero, C. O., Kautzman, A. G., Schafer, D. P., & Vetter, M. L. (2019). Complement Targets Newborn Retinal Ganglion Cells for Phagocytic Elimination by Microglia. *J Neurosci*, *39*(11), 2025–2040. <https://doi.org/10.1523/jneurosci.1854-18.2018>
148. Cong, Q., Soteros, B. M., Wollet, M., Kim, J. H., & Sia, G.-M. (2020). The endogenous neuronal complement inhibitor SRPX2 protects against complement-mediated synapse elimination during development. *Nature Neuroscience*, *23*(September), 1067–1078. <https://doi.org/10.1038/s41593-020-0672-0>
149. Werneburg, S., Jung, J., Kunjamma, R. B., Ha, S. K., Luciano, N. J., Willis, C. M., Gao, G., Biscola, N. P., Havton, L. A., Crocker, S. J., Popko, B., Reich, D. S., & Schafer, D. P. (2020). Targeted Complement Inhibition at Synapses Prevents Microglial Synaptic Engulfment and Synapse Loss in Demyelinating Disease. *Immunity*, *52*(1), 167-182.e7. <https://doi.org/10.1016/j.immuni.2019.12.004>
150. Baum, M. L., Wilton, D. K., Fox, R. G., Carey, A., Hsu, Y.-H. H., Fahey, J. B., Muthukumar, A. K., Salla, N., Hu, R., Jääntti, H. J., Crotty, W., Scott-Hewitt, N., Bien, E., Sabatini, D. A., Lanser, T. B., Frouin, A., Gergits, F., Håvik, B., Gialeli, C., ... Stevens, B. (2024). CSMD1 regulates brain complement activity and circuit development. *Brain, Behavior, and Immunity*, *119*(November 2023), 317–332. <https://doi.org/10.1016/j.bbi.2024.03.041>
151. Wang, C., Yue, H., Hu, Z., Shen, Y., Ma, J., Li, J., Wang, X. D., Wang, L., Sun, B., Shi, P., Wang, L., & Gu, Y. (2020). Microglia mediate forgetting via complement-dependent synaptic elimination. *Science*, *367*(6478), 688–694. <https://doi.org/10.1126/science.aaz2288>
152. Castellano, F., Montcourrier, P., & Chavrier, P. (2000). Membrane recruitment of Rac1 triggers phagocytosis. *Journal of Cell Science*, *113*(17), 2955–2961.
153. Brugnera, E., Haney, L., Grimsley, C., Lu, M., Walk, S. F., Annie-Carole, T.-T., Macara, I. G., Madhani, H., Fink, G. R., & Ravichandran, K. S. (2002). Unconventional Rac-GEF activity is mediated through the Dock180-ELMO complex. *Nature Cell Biology*, *4*(8), 574–582. <https://doi.org/10.1038/ncb824>
154. Park, D., Tosello-Trampont, A. C., Elliott, M. R., Lu, M., Haney, L. B., Ma, Z., Klibanov, A. L., Mandell, J. W., & Ravichandran, K. S. (2007). BAI1 is an engulfment receptor for apoptotic cells upstream of the ELMO/Dock180/Rac module. *Nature*, *450*(7168), 430–434. <https://doi.org/10.1038/nature06329>
155. Martinez, J., Malireddi, R. K. S., Lu, Q., Cunha, L., Pelletier, S., Gingras, S., Orchard, R., Guan, J.-L., Tan, H., Peng, J., Kanneganti, T.-D., Virgin, H. W., & Green, D. R. (2015). Molecular characterization of LC3-associated phagocytosis reveals distinct roles for Rubicon, NOX2 and autophagy proteins. *Nature Cell*

*Biology*, 17(7), 893–906. <https://doi.org/10.1038/ncb3192>

156. Cunha, L. D., Yang, M., Carter, R., Guy, C., Harris, L., Crawford, J. C., Quarato, G., Emilio, B.-R., Kalkavan, H., Johnson, M., Natarajan, S., Turnis, M. E., Finkelstein, D., Opferman, J. T., Gawad, C., & Green, D. R. (2018). LC3-Associated Phagocytosis in Myeloid Cells Promotes Tumor Immune Tolerance. *Cell*, 175(2), 429-441.e16. <https://doi.org/10.1016/j.cell.2018.08.061>
157. Park, D., Han, C. Z., Elliott, M. R., Kinchen, J. M., Trampont, P. C., Das, S., Collins, S., Lysiak, J. J., Hoehn, K. L., & Ravichandran, K. S. (2011). Continued clearance of apoptotic cells critically depends on the phagocyte Ucp2 protein. *Nature*, 477(7363), 220–224. <https://doi.org/10.1038/nature10340>
158. Wang, Y., Subramanian, M., Yurdagul Jr, A., Barbosa-Lorenzi, V. C., Cai, B., de Juan-Sanz, J., Ryan, T. A., Nomura, M., Maxfield, F. R., & Tabas, I. (2017). Mitochondrial Fission Promotes the Continued Clearance of Apoptotic Cells by Macrophages. *Cell*, 171(2), 331-345.e22. <https://doi.org/10.1016/j.cell.2017.08.041>
159. Noelia, A. G., Bensinger, S. J., Hong, C., Beceiro, S., Bradley, M. N., Zelcer, N., Deniz, J., Ramirez, C., Díaz, M., Gallardo, G., de Galarreta, C., Salazar, J., Lopez, F., Edwards, P., Parks, J., Andujar, M., Tontonoz, P., & Castrillo, A. (2009). Apoptotic cells promote their own clearance and immune tolerance through activation of the nuclear receptor LXR. *Immunity*, 31(2), 245–258. <https://doi.org/10.1016/j.immuni.2009.06.018>
160. Oliveira da Rocha, G. H., Loiola, R. A., Pantaleão, L. do N., Reutelingsperger, C., Solito, E., & Farsky, S. H. P. (2019). Control of expression and activity of peroxisome proliferated-activated receptor  $\gamma$  by Annexin A1 on microglia during efferocytosis. *Cell Biochemistry and Function*, 37(7), 560–568. <https://doi.org/10.1002/cbf.3433>
161. Shen, K., Sidik, H., & Talbot, W. S. (2016). The Rag-Ragulator Complex Regulates Lysosome Function and Phagocytic Flux in Microglia. *Cell Reports*, 14(3), 547–559. <https://doi.org/10.1016/j.celrep.2015.12.055>
162. Yurdagul Jr, A., Subramanian, M., Wang, X., Crown, S. B., Ilkayeva, O. R., Darville, L., Kolluru, G. K., Rymond, C. C., Gerlach, B. D., Zheng, Z., Kuriakose, G., Kevil, C. G., Koomen, J. M., Cleveland, J. L., Muoio, D. M., & Tabas, I. (2020). Macrophage Metabolism of Apoptotic Cell-Derived Arginine Promotes Continual Efferocytosis and Resolution of Injury. *Cell Metabolism*, 31(3), 518–533. <https://doi.org/10.1016/j.cmet.2020.01.001>
163. Nelson, S. B., & Valakh, V. (2015). Excitatory/Inhibitory Balance and Circuit Homeostasis in Autism Spectrum Disorders. *Neuron*, 87(4), 684–698. <https://doi.org/10.1016/j.neuron.2015.07.033>
164. Morioka, S., Maueröder, C., & Ravichandran, K. S. (2019). Living on the Edge: Efferocytosis at the Interface of Homeostasis and Pathology. *Immunity*, 50(5), 1149–1162. <https://doi.org/10.1016/j.immuni.2019.04.018>
165. Rapin, I. (1997). Autism. *New England Journal of Medicine*, 337(2), 97–104.
166. Hutsler, J. J., & Zhang, H. (2010). Increased dendritic spine densities on cortical projection neurons in autism spectrum disorders. *Brain Research*, 1309, 83–94. <https://doi.org/10.1016/j.brainres.2009.09.120>
167. Tetreault, N. A., Hakeem, A. Y., Jiang, S., Williams, B. A., Allman, E., Wold, B. J., & Allman, J. M. (2012). Microglia in the cerebral cortex in autism. *Journal of Autism and Developmental Disorders*, 42(12), 2569–

2584. <https://doi.org/10.1007/s10803-012-1513-0>
168. Lewis, J. D., Theilmann, R. J., Fonov, V., Bellec, P., Lincoln, A., Evans, A. C., & Townsend, J. (2013). Callosal fiber length and interhemispheric connectivity in adults with autism: Brain overgrowth and underconnectivity. *Human Brain Mapping, 34*(7), 1685–1695. <https://doi.org/10.1002/hbm.22018>
169. Lewis, J. D., Theilmann, R. J., Townsend, J., & Evans, A. C. (2013). Network efficiency in autism spectrum disorder and its relation to brain overgrowth. *Frontiers in Human Neuroscience, 7*(December), 1–12. <https://doi.org/10.3389/fnhum.2013.00845>
170. Tang, G., Gudsnuk, K., Kuo, S. H., Cotrina, M. L., Rosoklija, G., Sosunov, A., Sonders, M. S., Kanter, E., Castagna, C., Yamamoto, A., Yue, Z., Arancio, O., Peterson, B. S., Champagne, F., Dwork, A. J., Goldman, J., & Sulzer, D. (2014). Loss of mTOR-Dependent Macroautophagy Causes Autistic-like Synaptic Pruning Deficits. *Neuron, 83*(5), 1131–1143. <https://doi.org/10.1016/j.neuron.2014.07.040>
171. Kim, H. J., Cho, M. H., Shim, W. H., Kim, J. K., Jeon, E. Y., Kim, D. H., & Yoon, S. Y. (2017). Deficient autophagy in microglia impairs synaptic pruning and causes social behavioral defects. *Molecular Psychiatry, 22*(11), 1576–1584. <https://doi.org/10.1038/mp.2016.103>
172. Monsorno, K., Ginggen, K., Ivanov, A., Buckinx, A., Lalive, A. L., Tchenio, A., Benson, S., Vendrell, M., Alessandro, A. D., Beule, D., Pellerin, L., Marnett, M., & Paolicelli, R. C. (2023). Loss of microglial MCT4 leads to defective synaptic pruning and anxiety-like behavior in mice. *Nature Communications, 14*. <https://doi.org/10.1038/s41467-023-41502-4>
173. Selemon, L. D., & Zecevic, N. (2015). Schizophrenia: A tale of two critical periods for prefrontal cortical development. *Translational Psychiatry, 5*(8). <https://doi.org/10.1038/tp.2015.115>
174. Keshavan, M. S., Anderson, S., & Pettegrew, J. W. (1994). Is Schizophrenia due to excessive synaptic pruning in the prefrontal cortex? The Feinberg hypothesis revisited. *Journal of Psychiatric Research, 28*(3), 239–265. [https://doi.org/10.1016/0022-3956\(94\)90009-4](https://doi.org/10.1016/0022-3956(94)90009-4)
175. Glantz, L. A., & Lewis, D. A. (2000). Decreased dendritic spine density on prefrontal cortical pyramidal neurons in schizophrenia. *Archives of General Psychiatry, 57*(1), 65–73. <https://doi.org/10.1001/archpsyc.57.1.65>
176. Datta, D., Arion, D., Corradi, J. P., & Lewis, D. A. (2015). Altered Expression of CDC42 Signaling Pathway Components in Cortical Layer 3 Pyramidal Cells in Schizophrenia. *Biological Psychiatry, 78*(11), 775–785. <https://doi.org/10.1016/j.biopsych.2015.03.030>
177. Choi, I., Zhang, Y., Seegobin, S. P., Pruvost, M., Wang, Q., Purtell, K., Zhang, B., & Yue, Z. (2020). Microglia clear neuron-released  $\alpha$ -synuclein via selective autophagy and prevent neurodegeneration. *Nature Communications, 11*(1). <https://doi.org/10.1038/s41467-020-15119-w>
178. Huang, Y., Happonen, K. E., Burrola, P. G., O'Connor, C., Hah, N., Huang, L., Nimmerjahn, A., & Lemke, G. (2021). Microglia use TAM receptors to detect and engulf amyloid  $\beta$  plaques. *Nature Immunology, 22*(5), 586–594. <https://doi.org/10.1038/s41590-021-00913-5>
179. Podleśny-Drabiniok, A., Marcora, E., & Goate, A. M. (2020). Microglial Phagocytosis: A Disease-Associated Process Emerging from Alzheimer's Disease Genetics. *Trends in Neurosciences, 43*(12), 965–979.

<https://doi.org/10.1016/j.tins.2020.10.002>

180. Paloneva, J., Manninen, T., Christman, G., Hovanes, K., Mandelin, J., Adolfsson, R., Bianchin, M., Bird, T., Miranda, R., Salmaggi, A., Tranebjærg, L., Konttinen, Y., & Peltonen, L. (2002). Mutations in two genes encoding different subunits of a receptor signaling complex result in an identical disease phenotype. *American Journal of Human Genetics*, *71*(3), 656–662. <https://doi.org/10.1086/342259>
181. Satoh, J. I., Tabunoki, H., Ishida, T., Yagishita, S., Jinnai, K., Futamura, N., Kobayashi, M., Toyoshima, I., Yoshioka, T., Enomoto, K., Arai, N., Saito, Y., & Arima, K. (2012). Phosphorylated Syk expression is enhanced in Nasu-Hakola disease brains. *Neuropathology*, *32*(2), 149–157. <https://doi.org/10.1111/j.1440-1789.2011.01256.x>
182. Konishi, H., & Kiyama, H. (2018). Microglial TREM2/DAP12 signaling: A double-edged sword in neural diseases. *Frontiers in Cellular Neuroscience*, *12*(August), 1–14. <https://doi.org/10.3389/fncel.2018.00206>
183. Lampron, A., Larochelle, A., Laflamme, N., Préfontaine, P., Plante, M. M., Sánchez, M. G., Wee Yong, V., Stys, P. K., Tremblay, M.-È., & Rivest, S. (2015). Inefficient clearance of myelin debris by microglia impairs remyelinating processes. *Journal of Experimental Medicine*, *212*(4), 481–495. <https://doi.org/10.1084/jem.20141656>
184. McMahan, E. J., Bailey, S. L., Castenada, C. V., Waldner, H., & Miller, S. D. (2005). Epitope spreading initiates in the CNS in two mouse models of multiple sclerosis. *Nature Medicine*, *11*(3), 335–339. <https://doi.org/10.1038/nm1202>
185. Nikić, I., Merkler, D., Sorbara, C., Brinkoetter, M., Kreutzfeldt, M., Bareyre, F. M., Brück, W., Bishop, D., Misgeld, T., & Kerschensteiner, M. (2011). A reversible form of axon damage in experimental autoimmune encephalomyelitis and multiple sclerosis. *Nature Medicine*, *17*(4), 495–499. <https://doi.org/10.1038/nm.2324>
186. Healy, L. M., Perron, G., Won, S.-Y., Michell-Robinson, M. A., Rezk, A., Ludwin, S. K., Moore, C. S., Hall, J. A., Bar-Or, A., & Antel, J. P. (2016). MerTK Is a Functional Regulator of Myelin Phagocytosis by Human Myeloid Cells. *Journal of Immunology*, *196*(8), 3375–3384. <https://doi.org/10.4049/jimmunol.1502562>
187. Anderson, S. R., Roberts, J. M., Zhang, J., Steele, M. R., Romero, C. O., Bosco, A., & Vetter, M. L. (2019). Developmental Apoptosis Promotes a Disease-Related Gene Signature and Independence from CSF1R Signaling in Retinal Microglia. *Cell Reports*, *27*(7), 2002-2013.e5. <https://doi.org/10.1016/j.celrep.2019.04.062>
188. Dorman, L. C., Nguyen, P. T., Escoubas, C. C., Vainchtein, I. D., Xiao, Y., Lidsky, P. V., Wang, E. Y., Taloma, S. E., Nakao-Inoue, H., Rivera, B. M., Condello, C., Andino, R., Nowakowski, T. J., & Molofsky, A. V. (2021). A type I interferon response defines a conserved microglial state required for effective phagocytosis. *BioRxiv*, 2021.04.29.441889. <https://doi.org/10.1101/2021.04.29.441889>
189. Aspelund, A., Antila, S., Proulx, S. T., Karlsen, T. V., Karaman, S., Detmar, M., Wiig, H., & Alitalo, K. (2015). A dural lymphatic vascular system that drains brain interstitial fluid and macromolecules. *Journal of Experimental Medicine*, *212*(7), 991–999. <https://doi.org/10.1084/jem.20142290>
190. Louveau, A., Smirnov, I., Keyes, T. J., Eccles, J. D., Rouhani, S. J., Peske, J. D., Derecki, N. C., Castle,

- D., Mandell, J. W., Lee, K. S., Harris, T. H., & Kipnis, J. (2015). Structural and functional features of central nervous system lymphatic vessels. *Nature*, 523(7560), 337–341. <https://doi.org/10.1038/nature14432>
191. Brioschi, S., Wang, W.-L., Peng, V., Wang, M., Shchukina, I., Greenberg, Z. J., Bando, J. K., Jaeger, N., Czepielewski, R. S., Swain, A., Mogilenko, D. A., Beatty, W. L., Bayguinov, P., Fitzpatrick, J. A. J., Schuettpelz, L. G., Fronick, C. C., Smirnov, I., Kipnis, J., Shapiro, V. S., ... Colonna, M. (2021). Heterogeneity of meningeal B cells reveals a lymphopoietic niche at the CNS borders. *Science*, 373(6553), eabf9277. <https://doi.org/10.1126/science.abf9277>
192. Schafflick, D., Wolbert, J., Heming, M., Thomas, C., Hartlehnert, M., Börsch, A. L., Ricci, A., Martín-Salamanca, S., Li, X., Lu, I. N., Pawlak, M., Minnerup, J., Strecker, J. K., Seidenbecher, T., Meuth, S. G., Hidalgo, A., Liesz, A., Wiendl, H., & Meyer zu Horste, G. (2021). Single-cell profiling of CNS border compartment leukocytes reveals that B cells and their progenitors reside in non-diseased meninges. *Nature Neuroscience*. <https://doi.org/10.1038/s41593-021-00880-y>
193. Morioka, S., Perry, J. S. A., Raymond, M. H., Medina, C. B., Zhu, Y., Zhao, L., Serbulea, V., Onengut-Gumuscu, S., Leitinger, N., Kucenas, S., Rathmell, J. C., Makowski, L., & Ravichandran, K. S. (2018). Efferocytosis induces a novel SLC program to promote glucose uptake and lactate release. *Nature*, 563(7733), 714–718. <https://doi.org/10.1038/s41586-018-0735-5>
194. Mayer, C. T., Gazumyan, A., Kara, E. E., Gitlin, A. D., Golijanin, J., Viant, C., Pai, J., Oliveira, T. Y., Wang, Q., Escolano, A., Max, M.-R., Sanders, R. W., & Nussenzweig, M. C. (2017). The microanatomic segregation of selection by apoptosis in the germinal center. *Science*, 358(6360), eaao2602. <https://doi.org/10.1126/science.aao2602>
195. van Ham, T. J., Mapes, J., Kokel, D., & Peterson, R. T. (2010). Live imaging of apoptotic cells in zebrafish. *FASEB Journal*, 24(11), 4336–4342. <https://doi.org/10.1096/fj.10-161018>
196. Linsley, J. W., Shah, K., Castello, N., Chan, M., Haddad, D., Doric, Z., Wang, S., Leks, W., Mancini, J., Oza, V., Javaherian, A., Nakamura, K., Kokel, D., & Finkbeiner, S. (2021). Genetically encoded cell-death indicators (GEDI) to detect an early irreversible commitment to neurodegeneration. *Nature Communications*, 12(1), 1–14. <https://doi.org/10.1038/s41467-021-25549-9>
197. Shen, Y., Rosendale, M., Campbell, R. E., & Perrais, D. (2014). pHuji, a pH-sensitive red fluorescent protein for imaging of exo- and endocytosis. *Journal of Cell Biology*, 207(3), 419–432. <https://doi.org/10.1083/jcb.201404107>
198. Raymond, M. H., Davidson, A. J., Shen, Y., Tudor, D. R., Lucas, C. D., Morioka, S., Perry, J. S. A., Krapivkina, J., Perrais, D., Schumacher, L. J., Campbell, R. E., Wood, W., & Ravichandran, K. S. (2022). Live cell tracking of macrophage efferocytosis during Drosophila embryo development in vivo. *Science*, 375(6585), 1182–1187.
199. Tufan, T., Comertpay, G., Villani, A., Nelson, G. M., Terekhova, M., Kelley, S., Zakharov, P., Ellison, R. M., Shpynov, O., Raymond, M., Sun, J., Chen, Y., Bockelmann, E., Stremaska, M., Peterson, L. W., Boeckaerts, L., Goldman, S. R., Etchegaray, J. I., Artyomov, M. N., ... Ravichandran, K. S. (2024). Rapid unleashing of macrophage efferocytic capacity via transcriptional pause release. *Nature*, 628, 408–415.

<https://doi.org/10.1038/s41586-024-07172-y>

200. Morioka, S., Kajioaka, D., Yamaoka, Y., Ellison, R. M., Tufan, T., Werkman, I. L., Tanaka, S., Barron, B., Ito, S. T., Kucenas, S., Okusa, M. D., & Ravichandran, K. S. (2022). Chimeric efferocytic receptors improve apoptotic cell clearance and alleviate inflammation. *Cell*, *185*(26), 4887-4903.e17. <https://doi.org/10.1016/j.cell.2022.11.029>
201. Rossi, F., Casano, A. M., Henke, K., Richter, K., & Peri, F. (2015). The SLC7A7 Transporter Identifies Microglial Precursors prior to Entry into the Brain. *Cell Reports*, *11*(7), 1008–1017. <https://doi.org/10.1016/j.celrep.2015.04.028>
202. Spead, O., Verreet, T., Donelson, C. J., & Poulain, F. E. (2018). Characterization of the caspase family in zebrafish. *PLoS ONE*, *13*(5), e0197966. <https://doi.org/10.1371/journal.pone.0197966>
203. McDole, K., Guignard, L., Amat, F., Berger, A., Malandain, G., Royer, L. A., Turaga, S. C., Branson, K., & Keller, P. J. (2018). In Toto Imaging and Reconstruction of Post-Implantation Mouse Development at the Single-Cell Level. *Cell*, *175*(3), 859-876.e33. <https://doi.org/10.1016/j.cell.2018.09.031>
204. Huang, Q., Cohen, M. A., Alsina, F. C., Devlin, G., Garrett, A., McKey, J., Havlik, P., Rakhilin, N., Wang, E., Xiang, K., Mathews, P., Wang, L., Bock, C., Ruthig, V., Wang, Y., Negrete, M., Wong, C., Murthy, P. K. L., Zhang, S., ... Shen, X. (2020). Intravital imaging of mouse embryos. *Science*, *368*(6487), 181–186. <https://doi.org/10.1126/science.aba0210>
205. Filiano, A. J., Xu, Y., Tustison, N. J., Marsh, R. L., Baker, W., Smirnov, I., Overall, C. C., Gadani, S. P., Turner, S. D., Weng, Z., Peerzade, S., Chen, H., Lee, K. S., Scott, M. M., Beenhakker, M. P., Litvak, V., & Kipnis, J. (2016). Unexpected role of interferon- $\gamma$  in regulating neuronal connectivity and social behaviour. *Nature*, *535*(7612), 425–429. <https://doi.org/10.1038/nature18626>
206. Davie, K., Janssens, J., Koldere, D., De Waegeneer, M., Pech, U., Kreft, Ł., Albar, S., Makhzami, S., Christiaens, V., Bravo González-Blas, C., Poovathingal, S., Hulselmans, G., Spanier, K. I., Moerman, T., Vanspauwen, B., Geurs, S., Voet, T., Lammertyn, J., Thienpont, B., ... Aerts, S. (2018). A Single-Cell Transcriptome Atlas of the Aging Drosophila Brain. *Cell*, *174*(4), 982-998.e20. <https://doi.org/10.1016/j.cell.2018.05.057>
207. Zhang, Y., Chen, K., Sloan, S. A., Bennett, M. L., Scholze, A. R., O'Keefe, S., Phatnani, H. P., Guarnieri, P., Caneda, C., Ruderisch, N., Deng, S., Liddelow, S. A., Zhang, C., Daneman, R., Maniatis, T., Barres, B. A., & Wu, J. Q. (2014). An RNA-sequencing transcriptome and splicing database of glia, neurons, and vascular cells of the cerebral cortex. *Journal of Neuroscience*, *34*(36), 11929–11947. <https://doi.org/10.1523/JNEUROSCI.1860-14.2014>
208. Zhang, Y., Sloan, S. A., Clarke, L. E., Caneda, C., Plaza, C. A., Blumenthal, P. D., Vogel, H., Steinberg, G. K., Edwards, M. S. B., Li, G., Duncan, J. A., Cheshier, S. H., Shuer, L. M., Chang, E. F., Grant, G. A., Gephart, M. G. H., & Barres, B. A. (2016). Purification and Characterization of Progenitor and Mature Human Astrocytes Reveals Transcriptional and Functional Differences with Mouse. *Neuron*, *89*(1), 37–53. <https://doi.org/10.1016/j.neuron.2015.11.013>
209. Kimmel, C. B., Ballard, W. W., Kimmel, S. R., Ullmann, B., & Schilling, T. F. (1995). Stages of embryonic

- development of the zebrafish. *Developmental Dynamics*, 203(3), 253–310. <https://doi.org/10.1002/aja.1002030302>
210. Takahashi, H. (1977). Juvenile Hermaphroditism in the Zebrafish, *Brachydanio rerio*. *Bulletin of Fisheries Sciences, Hokkaido University*, 28(2), 57–65.
211. Kwan, K. M., Fujimoto, E., Grabher, C., Mangum, B. D., Hardy, M. E., Campbell, D. S., Parant, J. M., Yost, H. J., Kanki, J. P., & Chien, C.-B. (2007). The Tol2kit: A Multisite Gateway-Based Construction Kit for Tol2 Transposon Transgenesis Constructs. *Developmental Dynamics*, 236(11), 3088–3099. <https://doi.org/10.1002/dvdy.21343>
212. Kawakami, K. (2004). Transgenesis and gene trap methods in zebrafish by using the Tol2 transposable element. *Methods in Cell Biology*, 2004(77), 201–222. [https://doi.org/10.1016/s0091-679x\(04\)77011-9](https://doi.org/10.1016/s0091-679x(04)77011-9)
213. Ellett, F., Pase, L., Hayman, J. W., Andrianopoulos, A., & Lieschke, G. J. (2011). Mpeg1 Promoter Transgenes Direct Macrophage-Lineage Expression in Zebrafish. *Blood*, 117(4), 49–56. <https://doi.org/10.1182/blood-2010-10-314120>
214. Don, E. K., Formella, I., Badrock, A. P., Hall, T. E., Morsch, M., Hortle, E., Hogan, A., Chow, S., Gwee, S. S. L., Stoddart, J. J., Nicholson, G., Chung, R., & Cole, N. J. (2017). A Tol2 Gateway-Compatible Toolbox for the Study of the Nervous System and Neurodegenerative Disease. *Zebrafish*, 14(1), 69–72. <https://doi.org/10.1089/zeb.2016.1321>
215. Auer, T. O., Xiao, T., Bercier, V., Gebhardt, C., Duroure, K., Concordet, J.-P., Wyart, C., Suster, M., Kawakami, K., Wittbrodt, J., Baier, H., & Bene, F. Del. (2015). Deletion of a kinesin I motor unmasks a mechanism of homeostatic branching control by neurotrophin-3. *ELife*, 4(e05061), 1–26. <https://doi.org/10.7554/eLife.05061>
216. Meeker, N. D., Hutchinson, S. A., Ho, L., & Trede, N. S. (2018). Method for Isolation of PCR-Ready Genomic DNA from Zebrafish Tissues Method for isolation of PCR-ready genomic DNA from zebrafish tissues. *Biotechniques*, 43(5), 610–614. <https://doi.org/10.2144/000112619>
217. Parichy, D. M., Ransom, D. G., Paw, B., Zon, L. I., & Johnson, S. L. (2000). An orthologue of the kit-related gene *fms* is required for development of neural crest-derived xanthophores and a subpopulation of adult melanocytes in the zebrafish, *Danio rerio*. *Development*, 127(14), 3031–3044. <https://doi.org/10.1242/dev.127.14.3031>
218. Chang, C. T., Amack, J. D., & Whipps, C. M. (2016). Zebrafish Embryo Disinfection with Povidone-Iodine: Evaluating an Alternative to Chlorine Bleach. *Zebrafish*, 13, S96–S101. <https://doi.org/10.1089/zeb.2015.1229>
219. Preibisch, S., Saalfeld, S., & Tomancak, P. (2009). Globally optimal stitching of tiled 3D microscopic image acquisitions. *Bioinformatics*, 25(11), 1463–1465. <https://doi.org/10.1093/bioinformatics/btp184>
220. Lyons, D. A., Pogoda, H. M., Voas, M. G., Woods, I. G., Diamond, B., Nix, R., Arana, N., Jacobs, J., & Talbot, W. S. (2005). *erbb3* and *erbb2* are essential for Schwann cell migration and myelination in zebrafish. *Current Biology*, 15(6), 513–524. <https://doi.org/10.1016/j.cub.2005.02.030>
221. Ribera, A. B., & Nüsslein-Volhard, C. (1998). Zebrafish touch-insensitive mutants reveal an essential role

- for the developmental regulation of sodium current. *Journal of Neuroscience*, 18(22), 9181–9191. <https://doi.org/10.1523/jneurosci.18-22-09181.1998>
222. Williams, K., & Ribera, A. B. (2020). Long-lived zebrafish Rohon-Beard cells. *Developmental Biology*, 464(1), 45–52. <https://doi.org/10.1016/j.ydbio.2020.05.003>
223. Bernhardt, R. R., Chitnis, A. B., Lindamer, L., & Kuwada, J. Y. (1990). Identification of spinal neurons in the embryonic and larval zebrafish. *Journal of Comparative Neurology*, 302(3), 603–616. <https://doi.org/10.1002/cne.903020315>
224. Brown, R. I., Barber, H. M., & Kucenas, S. (2024). Satellite glial cells inhibit sensory axon repair following central branch axotomy of developing dorsal root ganglia. *Glia*, 72(10), 1766–1784.
225. Blader, P., Plessy, C., & Strähle, U. (2003). Multiple regulatory elements with spatially and temporally distinct activities control neurogenin1 expression in primary neurons of the zebrafish embryo. *Mechanisms of Development*, 120(2), 211–218. [https://doi.org/10.1016/S0925-4773\(02\)00413-6](https://doi.org/10.1016/S0925-4773(02)00413-6)
226. Moreno, R. L., & Ribera, A. B. (2014). Spinal neurons require Islet1 for subtype-specific differentiation of electrical excitability. *Neural Development*, 9(1), 1–18. <https://doi.org/10.1186/1749-8104-9-19>
227. Beckman, S. (2018). *Using Acridine Orange to Measure Cell Death in Ethanol-Treated Zebrafish Embryos*.
228. Lubin, A., Otterstrom, J., Hoade, Y., Bjedov, I., Stead, E., Whelan, M., Gestri, G., Paran, Y., & Payne, E. (2021). A versatile, automated and high-throughput drug screening platform for zebrafish embryos. *Biology Open*, 10(9), 1–11. <https://doi.org/10.1242/bio.058513>
229. Blume, Z. I., Lambert, J. M., Lovel, A. G., & Mitchell, D. M. (2020). Microglia in the developing retina couple phagocytosis with the progression of apoptosis via P2RY12 signaling. *Developmental Dynamics, February*, 7–9. <https://doi.org/10.1002/dvdy.163>
230. Burek, M. J., & Oppenheim, R. W. (1996). Programmed cell death in the developing nervous system. *Brain Pathology*, 6, 427–446.
231. Neniskyte, U., & Gross, C. T. (2017). Errant gardeners: Glial-cell-dependent synaptic pruning and neurodevelopmental disorders. *Nature Reviews Neuroscience*, 18(11), 658–670. <https://doi.org/10.1038/nrn.2017.110>
232. Kollros, J. J., & Thiesse, M. L. (1985). Growth and death of cells of the mesencephalic fifth nucleus in *Xenopus laevis* larvae. *Journal of Comparative Neurology*, 233(4), 481–489. <https://doi.org/10.1002/cne.902330407>
233. O'Connor, T. P., & Van Der Kooy, D. (1986). Cell death organizes the postnatal development of the trigeminal innervation of the cerebral vasculature. *Developmental Brain Research*, 27(1), 223–233. [https://doi.org/10.1016/0165-3806\(86\)90248-8](https://doi.org/10.1016/0165-3806(86)90248-8)
234. Novak, K. D., Prevet, D., Wang, S., Gould, T. W., & Oppenheim, R. W. (2000). Hepatocyte growth factor/scatter factor is a neurotrophic survival factor for lumbar but not for other somatic motoneurons in the chick embryo. *Journal of Neuroscience*, 20(1), 326–337. <https://doi.org/10.1523/jneurosci.20-01-00326.2000>
235. Braekevelt, C. R., Beazley, L. D., Dunlop, S. A., & Darby, J. E. (1986). Numbers of axons in the optic nerve

- and of retinal ganglion cells during development in the marsupial *Setonix brachyurus*. *Developmental Brain Research*, 25(1), 117–125. [https://doi.org/10.1016/0165-3806\(86\)90158-6](https://doi.org/10.1016/0165-3806(86)90158-6)
236. Gaze, R. M., & Grant, P. (1992). Spatio-temporal patterns of retinal ganglion cell death during *Xenopus* development. *Journal of Comparative Neurology*, 315(3), 264–274. <https://doi.org/10.1002/cne.903150303>
237. Georges, P., Madigan, M. C., & Provis, J. M. (1999). Apoptosis during development of the human retina: Relationship to foveal development and retinal synaptogenesis. *Journal of Comparative Neurology*, 413(2), 198–208. [https://doi.org/10.1002/\(SICI\)1096-9861\(19991018\)413:2<198::AID-CNE2>3.0.CO;2-J](https://doi.org/10.1002/(SICI)1096-9861(19991018)413:2<198::AID-CNE2>3.0.CO;2-J)
238. Francisco-Morcillo, J., Hidalgo-Sánchez, M., & Martín-Partido, G. (2004). Spatial and temporal patterns of apoptosis during differentiation of the retina in the turtle. *Anatomy and Embryology*, 208(4), 289–299. <https://doi.org/10.1007/s00429-004-0398-x>
239. Farah, M. H., & Easter, S. S. (2005). Cell birth and death in the mouse retinal ganglion cell layer. *Journal of Comparative Neurology*, 489(1), 120–134. <https://doi.org/10.1002/cne.20615>
240. Lance-Jones, C. (1982). Motoneuron cell death in the developing lumbar spinal cord of the mouse. *Developmental Brain Research*, 4(4), 473–479. [https://doi.org/10.1016/0165-3806\(82\)90192-4](https://doi.org/10.1016/0165-3806(82)90192-4)
241. Forger, N. G., & Breedlove, S. M. (1987). Motoneuronal death during human fetal development. *Journal of Comparative Neurology*, 264(1), 118–122. <https://doi.org/10.1002/cne.902640109>
242. Comans, P. E., McLennan, I. S., Mark, R. F., & Hendry, I. A. (1988). Mammalian motoneuron development: Effect of peripheral deprivation on motoneuron numbers in a marsupial. *Journal of Comparative Neurology*, 270(1), 111–120. <https://doi.org/10.1002/cne.902700109>
243. Rohon, J. V. (1884). Zur histogenese des Rückenmarkes der Forelle. *Sitzungsber Der Math-Phys.*
244. Beard, J. (1889). On the Early Development of *Lepidosteus osseus*. *Proceedings of the Royal Society of London*, 46(280–285), 108–118.
245. Coghill, G. E. (1914). Correlated Anatomical and Physiological Studies of the Growth of the Nervous System of Amphibia. *Journal of Comparative Neurology*, 24(2).
246. Hughes, A. (1957). The development of the primary sensory system in *Xenopus laevis*. *Journal of Anatomy*, 91(3), 323–338. [https://doi.org/10.1007/978-3-319-62419-8\\_300069](https://doi.org/10.1007/978-3-319-62419-8_300069)
247. Lamborghini, J. E. (1987). Disappearance of Rohon-Beard neurons from the spinal cord of larval *Xenopus laevis*. *Journal of Comparative Neurology*, 264(1), 47–55. <https://doi.org/10.1002/cne.902640105>
248. Nieuwenhuys, R. (1964). Comparative Anatomy of the Spinal Cord. *Progress in Brain Research*, 11(C), 1–57. [https://doi.org/10.1016/S0079-6123\(08\)64043-1](https://doi.org/10.1016/S0079-6123(08)64043-1)
249. Nakao, T., & Ishizawa, A. (1987). Development of the spinal nerves in the lamprey: I. Rohon-beard cells and interneurons. *Journal of Comparative Neurology*, 256(3), 342–355. <https://doi.org/10.1002/cne.902560304>
250. Fritsch, B., & Northcutt, R. G. (1993). Cranial and Spinal Nerve Organization in *Amphioxus* and Lampreys: Evidence for an Ancestral Craniate Pattern. *Acta Anatomica (Basel)*, 148(2–3), 96–109. <https://doi.org/10.1159/000147529>
251. Wicht, H., & Lacalli, T. C. (2005). The nervous system of *amphioxus*: Structure, development, and

- evolutionary significance. *Canadian Journal of Zoology*, 83(1), 122–150. <https://doi.org/10.1139/z04-163>
252. Waki, K., Imai, K. S., & Satou, Y. (2015). Genetic pathways for differentiation of the peripheral nervous system in ascidians. *Nature Communications*, 6. <https://doi.org/10.1038/ncomms9719>
253. Humphrey, T. (1944). Primitive neurons in the embryonic human central nervous system. *Journal of Comparative Neurology*, 81(1), 1–45. <https://doi.org/10.1002/cne.900810102>
254. Youngstrom, K. A. (1944). Intramedullary sensory type ganglion cells in the spinal cord of human embryos. *Journal of Comparative Neurology*, 81(1), 47–53. <https://doi.org/10.1002/cne.900810103>
255. Humphrey, T. (1950). Intramedullary sensory ganglion cells in the roof plate area of the embryonic human spinal cord. *Journal of Comparative Neurology*, 92(3), 333–399.
256. Yajima, H., Suzuki, M., Ochi, H., Ikeda, K., Sato, S., Yamamura, K. ichi, Ogino, H., Ueno, N., & Kawakami, K. (2014). Six1 is a key regulator of the developmental and evolutionary architecture of sensory neurons in craniates. *BMC Biology*, 12, 1–18. <https://doi.org/10.1186/1741-7007-12-40>
257. Roberts, A., & Smyth, D. (1974). The development of a dual touch sensory system in embryos of the amphibian *Xenopus laevis*. *Journal of Comparative Physiology*, 88(1), 31–42. <https://doi.org/10.1007/BF00695921>
258. Pietri, T., Manalo, E., Ryan, J., Saint-Amant, L., & Washbourne, P. (2009). Glutamate drives the touch response through a rostral loop in the spinal cord of zebrafish embryos. *Developmental Neurobiology*, 69(12), 780–795. <https://doi.org/10.1002/dneu.20741>
259. Roberts, A., & Hayes, B. P. (1977). The anatomy and function of “free” nerve endings in an amphibian skin sensory system. *Proceedings of the Royal Society of London - Biological Sciences*, 196(1125), 415–429. <https://doi.org/10.1098/rspb.1977.0048>
260. Eichler, V. B., & Porter, R. A. (1981). Rohon-Beard cells in frog development: A study of temporal and spatial changes in a transient cell population. *Journal of Comparative Neurology*, 203(1), 121–130. <https://doi.org/10.1002/cne.902030110>
261. Reyes, R., Haendel, M., Grant, D., Melancon, E., & Eisen, J. S. (2004). Slow Degeneration of Zebrafish Rohon-Beard Neurons during Programmed Cell Death. *Developmental Dynamics*, 229(1), 30–41. <https://doi.org/10.1002/dvdy.10488>
262. Palanca, A. M. S., Lee, S. L., Yee, L. E., Joe-Wong, C., Trinh, L. A., Hiroyasu, E., Husain, M., Fraser, S. E., Pellegrini, M., & Sagasti, A. (2013). New transgenic reporters identify somatosensory neuron subtypes in larval zebrafish. *Developmental Neurobiology*, 73(2), 152–167. <https://doi.org/10.1002/dneu.22049>
263. Saint-Amant, L., & Drapeau, P. (1998). Time course of the development of motor behaviors in the zebrafish embryo. *Journal of Neurobiology*, 37(4), 622–632. [https://doi.org/10.1002/\(SICI\)1097-4695\(199812\)37:4<622::AID-NEU10>3.0.CO;2-S](https://doi.org/10.1002/(SICI)1097-4695(199812)37:4<622::AID-NEU10>3.0.CO;2-S)
264. Saint-Amant, L., & Drapeau, P. (2000). Motoneuron activity patterns related to the earliest behavior of the zebrafish embryo. *Journal of Neuroscience*, 20(11), 3964–3972. <https://doi.org/10.1523/jneurosci.20-11-03964.2000>
265. Gleason, M. R., Higashijima, S.-I., Dallman, J., Liu, K., Mandell, G., & Fetcho, J. R. (2003). Translocation

- of CaM kinase II to synaptic sites in vivo. *Nature Neuroscience*, 6(3), 217–218. <https://doi.org/10.1038/nn1011>
266. McLean, D. L., & Fetcho, J. R. (2008). Using Imaging and Genetics in Zebrafish to Study Developing Spinal Circuits In Vivo. *Developmental Neurobiology*, 68(6), 817–834. <https://doi.org/doi:10.1002/dneu.20617>
267. Williams, J. A., Barrios, A., Gatchalian, C., Rubin, L., Wilson, S. W., & Holder, N. (2000). Programmed cell death in zebrafish Rohon Beard neurons is influenced by TrkC1/NT-3 signaling. *Developmental Biology*, 226(2), 220–230. <https://doi.org/10.1006/dbio.2000.9860>
268. Svoboda, K. R., Linares, A. E., & Ribera, A. B. (2001). Activity regulates programmed cell death of zebrafish Rohon-Beard neurons. *Development*, 128(18), 3511–3520.
269. Cornell, R. A., & Eisen, J. S. (2002). Delta/Notch signaling promotes formation of zebrafish neural crest by repressing neurogenin 1 function. *Development*, 129(11), 2639–2648. <https://doi.org/10.1242/dev.129.11.2639>
270. Rossi, C. C., Kaji, T., & Artinger, K. B. (2009). Transcriptional control of rohon-beard sensory neuron development at the neural plate border. *Developmental Dynamics*, 238(4), 931–943. <https://doi.org/10.1002/dvdy.21915>
271. Korzh, V., Sleptsova, I., Liao, J., He, J., & Gong, Z. (1998). Expression of zebrafish bHLH genes *ngn1* and *nrd* defines distinct stages of neural differentiation. *Developmental Dynamics*, 213(1), 92–104. [https://doi.org/10.1002/\(SICI\)1097-0177\(199809\)213:1<92::AID-AJA9>3.0.CO;2-T](https://doi.org/10.1002/(SICI)1097-0177(199809)213:1<92::AID-AJA9>3.0.CO;2-T)
272. Lo, A. C., Houenou, L. J., & Oppenheim, R. W. (1995). Apoptosis in the nervous system: Morphological features, methods, pathology, and prevention. *Archives of Histology and Cytology*, 58(2), 139–149. <https://doi.org/10.1679/aohc.58.139>
273. Gavrieli, Y., Sherman, Y., & Ben-Sasson, S. A. (1992). Identification of programmed cell death in situ via specific labeling of nuclear DNA fragmentation. *Journal of Cell Biology*, 119(3), 493–501. <https://doi.org/10.1083/jcb.119.3.493>
274. Hilinski, W. C., Bostrom, J. R., England, S. J., Juárez-Morales, J. L., de Jager, S., Armant, O., Legradi, J., Strähle, U., Link, B. A., & Lewis, K. E. (2016). *Lmx1b* is required for the glutamatergic fates of a subset of spinal cord neurons. *Neural Development*, 11(1), 1–21. <https://doi.org/10.1186/s13064-016-0070-1>
275. Attili, S., & Hughes, S. M. (2014). Anaesthetic Tricaine Acts Preferentially on Neural Voltage-Gated Sodium Channels and Fails to Block Directly Evoked Muscle Contraction. *PLoS ONE*, 9(8). <https://doi.org/10.1371/journal.pone.0103751>
276. Niell, C. M., & Smith, S. J. (2005). Functional imaging reveals rapid development of visual response properties in the zebrafish tectum. *Neuron*, 45(6), 941–951. <https://doi.org/10.1016/j.neuron.2005.01.047>
277. Muto, A., Ohkura, M., Kotani, T., Higashijima, S., Nakai, J., & Kawakami, K. (2011). Genetic visualization with an improved GCaMP calcium indicator reveals spatiotemporal activation of the spinal motor neurons in zebrafish. *Proceedings of the National Academy of Sciences*, 108(13), 5425–5430. <https://doi.org/10.1073/pnas.1000887108>
278. Szobota, S., Gorostiza, P., Bene, F. Del, Wyart, C., Fortin, D. L., Kolstad, K. D., Tulyathan, O., Volgraf, M.,

- Numano, R., Aaron, H. L., Scott, E. K., Kramer, R. H., Flannery, J., Baier, H., Trauner, D., & Isacoff, E. Y. (2007). Neurotechnique Remote Control of Neuronal Activity with a Light-Gated Glutamate Receptor. *Neuron*, *54*(4), 535–545. <https://doi.org/10.1016/j.neuron.2007.05.010>
279. Martin, S. J., Reutelingsperger, C. P. M., McGahon, A. J., Rader, J. A., van Schie, R. C. A. A., LaFace, D. M., & Green, D. R. (1995). Early Redistribution of Plasma Membrane Phosphatidylserine Is a General Feature of Apoptosis Regardless of the Initiating Stimulus: Inhibition by Overexpression of Bcl-2 and Abl. *Journal of Experimental Medicine*, *182*(5), 1545–1556. <https://doi.org/10.1084/jem.182.5.1545>
280. Schoonheim, P. J., Arrenberg, A. B., Bene, F. Del, & Baier, H. (2010). Optogenetic Localization and Genetic Perturbation of Saccade-Generating Neurons in Zebrafish. *Journal of Neuroscience*, *30*(20), 7111–7120. <https://doi.org/10.1523/JNEUROSCI.5193-09.2010>
281. Metcalfe, W. K., Myers, P. Z., Trevarrow, B., Bass, M. B., & Kimmel, C. B. (1990). Primary neurons that express the L2/HNK-1 carbohydrate during early development in the zebrafish. *Development*, *110*(2), 491–504. <https://doi.org/10.1242/dev.110.2.491>
282. Blader, P., Fischer, N., Gradwohl, G., Guillemot, F., & Strähle, U. (1997). The activity of Neurogenin1 is controlled by local cues in the zebrafish embryo. *Development*, *124*(22), 4557–4569. <https://doi.org/10.1242/dev.124.22.4557>
283. Tsuchida, T., Ensini, M., Morton, S. B., Baldassare, M., Edlund, T., Jessell, T. M., & Pfaff, S. L. (1994). Topographic organization of embryonic motor neurons defined by expression of LIM homeobox genes. *Cell*, *79*(6), 957–970. [https://doi.org/10.1016/0092-8674\(94\)90027-2](https://doi.org/10.1016/0092-8674(94)90027-2)
284. Appel, B., & Eisen, J. S. (1998). Regulation of neuronal specification in the zebrafish spinal cord by Delta function. *Development*, *125*(3), 371–380. <https://doi.org/10.1242/dev.125.3.371>
285. Segawa, H., Miyashita, T., Hirate, Y., Higashijima, S.-I., Chino, N., Uyemura, K., Kikuchi, Y., & Okamoto, H. (2001). Functional repression of Islet-2 by disruption of complex with Ldb impairs peripheral axonal outgrowth in embryonic zebrafish. *Neuron*, *30*(2), 423–436. [https://doi.org/10.1016/S0896-6273\(01\)00283-5](https://doi.org/10.1016/S0896-6273(01)00283-5)
286. Navajas Acedo, J. (2023). Persistence of the primary somatosensory system in zebrafish. *BioRxiv*.
287. Higashijima, S.-I., Hotta, Y., & Okamoto, H. (2000). Visualization of cranial motor neurons in live transgenic zebrafish expressing green fluorescent protein under the control of the Islet-1 promoter/enhancer. *Journal of Neuroscience*, *20*(1), 206–218. <https://doi.org/10.1523/jneurosci.20-01-00206.2000>
288. Pittman, A. J., Law, M.-Y., & Chien, C.-B. (2008). Pathfinding in a large vertebrate axon tract: Isotypic interactions guide retinotectal axons at multiple choice points. *Development*, *135*(17), 2865–2871. <https://doi.org/10.1242/dev.025049>
289. Won, Y.-J., Ono, F., & Ikeda, S. R. (2011). Identification and modulation of voltage-gated Ca<sup>2+</sup> currents in zebrafish Rohon-Beard neurons. *Journal of Neurophysiology*, *105*(1), 442–453. <https://doi.org/10.1152/jn.00625.2010>
290. Tuttle, A. M., Miller, L. N., Royer, L. J., Wen, H., Kelly, J. K., Calistri, N. L., Heiser, L. M., & Nechiporuk, A. V. (2024). Single-cell analysis of Rohon-Beard neurons implicates Fgf signaling in axon maintenance and

- cell survival. *Journal of Neuroscience*, 44(16), 1–16.
291. Kanungo, J., Li, B., Zheng, Y., & Pant, H. C. (2006). Cyclin-dependent kinase 5 influences Rohon-Beard neuron survival in zebrafish. *Journal of Neurochemistry*, 99(1), 251–259. <https://doi.org/10.1111/j.1471-4159.2006.04114.x>
292. Dehkordi, M. H., Munn, R. G. K., & Fearnhead, H. O. (2022). Non-Canonical Roles of Apoptotic Caspases in the Nervous System. *Frontiers in Cell and Developmental Biology*, 10(February), 1–12. <https://doi.org/10.3389/fcell.2022.840023>
293. Woo, M., Hakem, R., Soengas, M. S., Duncan, G. S., Shahinian, A., Kägi, D., Hakem, A., McCurrach, M., Khoo, W., Kaufman, S. A., Senaldi, G., Howard, T., Lowe, S. W., & Mak, T. W. (1998). Essential contribution of caspase 3/CPP32 to apoptosis and its associated nuclear changes. *Genes and Development*, 12(6), 806–819.
294. Porter, A. G., & Ja, R. U. (1999). Emerging roles of caspase-3 in apoptosis. *Cell Death and Differentiation*, 6(2), 99–104.
295. Kari, S., Subramanian, K., Agata, I., Akshaya, A., & Harja, O. Y. (2022). Programmed cell death detection methods: a systematic review and a categorical comparison. *Apoptosis*, 27(7), 482–508. <https://doi.org/10.1007/s10495-022-01735-y>
296. Kuo, C. T., Zhu, S., Younger, S., Jan, L. Y., & Jan, Y. N. (2006). Identification of E2/E3 Ubiquitinating Report Enzymes and Caspase Activity Regulating Drosophila Sensory Neuron Dendrite Pruning. *Neuron*, 51(3), 283–290. <https://doi.org/10.1016/j.neuron.2006.07.014>
297. Williams, D. W., Kondo, S., Krzyzanowska, A., Hiromi, Y., & Truman, J. W. (2006). Local caspase activity directs engulfment of dendrites during pruning. *Nature Neuroscience*, 9(10), 1234–1236. <https://doi.org/10.1038/nn1774>
298. Schoenmann, Z., Assa-Kunik, E., Tiomny, S., Minis, A., Haklai-Topper, L., Arama, E., & Yaron, A. (2010). Axonal Degeneration Is Regulated by the Apoptotic Machinery or a NAD<sup>+</sup>-Sensitive Pathway in Insects and Mammals. *Journal of Neuroscience*, 30(18), 6375–6386. <https://doi.org/10.1523/JNEUROSCI.0922-10.2010>
299. Meng, L., Mulcahy, B., Cook, S. J., Neubauer, M., Wan, A., Jin, Y., & Yan, D. (2015). The Cell Death Pathway Regulates Synapse Elimination through Cleavage of Gelsolin in *Caenorhabditis elegans* Neurons. *Cell Reports*, 11(11), 1737–1748. <https://doi.org/10.1016/j.celrep.2015.05.031>
300. Huesmann, G. R., & Clayton, D. F. (2006). Dynamic Role of Postsynaptic Caspase-3 and BIRC4 in Zebra Finch Song-Response Habituation. *Neuron*, 52(6), 1061–1072. <https://doi.org/10.1016/j.neuron.2006.10.033>
301. Campbell, D. S., & Okamoto, H. (2013). Local caspase activation interacts with Slit-Robo signaling to restrict axonal arborization. *Journal of Cell Biology*, 203(4), 657–672. <https://doi.org/10.1083/jcb.201303072>
302. Li, Z., Jo, J., Jia, J.-M., Lo, S.-C., Whitcomb, D. J., Jiao, S., Cho, K., & Sheng, M. (2010). Caspase-3 Activation via Mitochondria Is Required for Long-Term Depression and AMPA Receptor Internalization. *Cell*, 141(5), 859–871. <https://doi.org/10.1016/j.cell.2010.03.053>

303. Ertürk, A., Wang, Y., & Sheng, M. (2014). Local Pruning of Dendrites and Spines by Caspase-3- Dependent and Proteasome-Limited Mechanisms. *Journal of Neuroscience*, 34(5), 1672–1688. <https://doi.org/10.1523/JNEUROSCI.3121-13.2014>
304. Wang, J.-Y., Chen, F., Fu, X.-Q., Ding, C.-S., Zhou, L., Zhang, X.-H., & Luo, Z.-G. (2014). Caspase-3 Cleavage of Dishevelled Induces Elimination of Postsynaptic Structures. *Developmental Cell*, 28(6), 670–684. <https://doi.org/10.1016/j.devcel.2014.02.009>
305. Weghorst, F., Mirzakhanyan, Y., Samimi, K., Dhillon, M., Barzik, M., Cunningham, L. L., Gershon, P. D., & Cramer, K. S. (2020). Caspase-3 Cleaves Extracellular Vesicle Proteins During Auditory Brainstem Development. *Frontiers in Cellular Neuroscience*, 14(November), 1–21. <https://doi.org/10.3389/fncel.2020.573345>
306. Fernando, P., Kelly, J. F., Balazsi, K., Slack, R. S., & Megeney, L. A. (2002). Caspase 3 activity is required for skeletal muscle differentiation. *Proceedings of the National Academy of Sciences*, 99(17), 11025–11030. <https://doi.org/10.1073/pnas.162172899>
307. Rebellato, P., Kaczynska, D., Kanatani, S., Rayyes, I. Al, Zhang, S., Villaescusa, C., Falk, A., Arenas, E., Hermanson, O., Louhivuori, L., & Uhlén, P. (2019). The T-type Ca<sup>2+</sup> Channel Cav3.2 Regulates Differentiation of Neural Progenitor Cells during Cortical Development via Caspase-3. *Neuroscience*, 402, 78–89. <https://doi.org/10.1016/j.neuroscience.2019.01.015>
308. Nguyen, T. T. M., Gadet, R., Lanfranchi, M., Lahaye, R. A., Yandiev, S., Lohez, O., Mikaelian, I., Jabbour, L., Rimokh, R., Courchet, J., Saudou, F., Popgeorgiev, N., & Gillet, G. (2023). Mitochondrial Bcl-xL promotes brain synaptogenesis by controlling non-lethal caspase activation. *iScience*, 26(5), 106674. <https://doi.org/10.1016/j.isci.2023.106674>
309. Keary III, K. M., Gu, Q.-H., Chen, J., & Li, Z. (2023). Dendritic distribution of autophagosomes underlies pathway-selective induction of LTD. *Cell Reports*, 42(8), 112898. <https://doi.org/10.1016/j.celrep.2023.112898>
310. Grasl-Kraupp, B., Ruttkay-Nedecky, B., Koudelka, H., Bukowska, K., Bursch, W., & Schulte-Hermann, R. (1995). In Situ Detection of Fragmented DNA (TUNEL Assay) Fails to Discriminate Among Apoptosis, Necrosis, and Autolytic Cell Death: A Cautionary Note. *Hepatology*, 21(5), 1465–1468.
311. Yu, P., Zhang, X., Liu, N., Tang, L., Peng, C., & Chen, X. (2021). Pyroptosis: mechanisms and diseases. *Signal Transduction and Targeted Therapy*, 6(128). <https://doi.org/10.1038/s41392-021-00507-5>
312. Scully, R., Panday, A., Elango, R., & Willis, N. A. (2019). DNA double-strand break pathway choice in somatic mammalian cells. *Nature Reviews Molecular Cell Biology*, 20(11), 698–714. <https://doi.org/10.1038/s41580-019-0152-0>
313. Kockx, M. M., Muhring, J., & de Meyer, G. R. Y. (1998). RNA Synthesis and Splicing Interferes with DNA in Situ End Labeling Techniques Used to Detect Apoptosis. *American Journal of Pathology*, 152(4), 885–888.
314. Ju, B.-G., Lunyak, V. V., Perissi, V., Garcia-Bassets, I., Rose, D. W., Glass, C. K., & Rosenfeld, M. G. (2006). A Topoisomerase IIb-Mediated dsDNA Break Required for Regulated Transcription. *Science*,

- 312(5781), 1798–1803.
315. Suberbielle, E., Sanchez, P. E., Kravitz, A. V., Wang, X., Ho, K., Eilertson, K., Devidze, N., Kreitzer, A. C., & Mucke, L. (2013). Physiologic brain activity causes DNA double-strand breaks in neurons, with exacerbation by amyloid- $\beta$ . *Nature Neuroscience*, *16*(5), 613–621. <https://doi.org/10.1038/nn.3356>
316. Madabhushi, R., Gao, F., Pfenning, A. R., Pan, L., Yamakawa, S., Seo, J., Rueda, R., Phan, T. X., Yamakawa, H., Pao, P.-C., Stott, R. T., Gjoneska, E., Nott, A., Cho, S., Kellis, M., & Tsai, L.-H. (2015). Activity-Induced DNA Breaks Govern the Expression of Neuronal Early-Response Genes Article Activity-Induced DNA Breaks Govern the Expression of Neuronal Early-Response Genes. *Cell*, *161*(7), 1592–1605. <https://doi.org/10.1016/j.cell.2015.05.032>
317. Gao, Y., Sun, Y., Frank, K. M., Dikkes, P., Fujiwara, Y., Seidl, K. J., Sekiguchi, J. M., Rathbun, G. A., Swat, W., Wang, J., Bronson, R. T., Malynn, B. A., Bryans, M., Zhu, C., Chaudhuri, J., Davidson, L., Ferrini, R., Stamato, T., Orkin, S. H., ... Alt, F. W. (1998). A Critical Role for DNA End-Joining Proteins in Both Lymphogenesis and Neurogenesis. *Cell*, *95*(7), 891–902.
318. Baleriola, J., Suárez, T., & de la Rosa, E. J. (2010). DNA-PK promotes the survival of young neurons in the embryonic mouse retina. *Cell Death and Differentiation*, *17*(11), 1697–1706. <https://doi.org/10.1038/cdd.2010.46>
319. Wei, P.-C., Chang, A. N., Kao, J., Du, Z., Meyers, R. M., Alt, F. W., & Schwer, B. (2016). Long Neural Genes Harbor Recurrent DNA Break Clusters in Neural Stem/Progenitor Cells. *Cell*, *164*(4), 644–655. <https://doi.org/10.1016/j.cell.2015.12.039>
320. Kanoh, M., Takemura, G., Misao, J., Hayakawa, Y., Aoyama, T., Nishigaki, K., Noda, T., Fujiwara, T., Fukuda, K., Minatoguchi, S., & Fujiwara, H. (1999). Significance of Myocytes With Positive DNA In Situ Nick End-Labeling (TUNEL) in Hearts With Dilated Cardiomyopathy: not apoptosis but DNA repair. *Circulation*, *99*(21), 2757–2764. <https://doi.org/10.1161/01.CIR.99.21.2757>
321. Makarevich, A. V., & Markkula, M. (2002). Apoptosis and Cell Proliferation Potential of Bovine Embryos Stimulated with Insulin-Like Growth Factor I During In Vitro Maturation and Culture. *Biology of Reproduction*, *66*(2), 386–392.
322. Geske, F. J., Nelson, A. C., Lieberman, R., Strange, R., Sun, T., & Gerschenson, L. E. (2000). DNA repair is activated in early stages of p53-induced apoptosis. *Cell Death and Differentiation*, *7*(4), 393–402.
323. Geske, F. J., Lieberman, R., Strange, R., & Gerschenson, L. E. (2001). Early stages of p53-induced apoptosis are reversible. *Cell Death and Differentiation*, *8*(2), 182–191.
324. Tang, H. L., Yuen, K. L., Tang, H. M., & Fung, M. C. (2009). Reversibility of apoptosis in cancer cells. *British Journal of Cancer*, *100*(1), 118–122. <https://doi.org/10.1038/sj.bjc.6604802>
325. Tang, H. L., Tang, H. M., Mak, K. H., Hu, S., Wang, S. S., Wong, K. M., Wong, C. S. T., Wu, H. Y., Law, H. T., Liu, K., Talbot Jr., C. C., Lau, W. K., Montell, D. J., & Fung, M. C. (2012). Cell survival, DNA damage, and oncogenic transformation after a transient and reversible apoptotic response. *Molecular Biology of the Cell*, *23*(12), 2240–2252. <https://doi.org/10.1091/mbc.E11-11-0926>
326. Nano, M., & Montell, D. J. (2024). Apoptotic signaling: Beyond cell death. *Seminars in Cell and*

- Developmental Biology*, 156, 22–34. <https://doi.org/10.1016/j.semcdb.2023.11.002>
327. Galluzzi, L., Aaronson, S. A., Abrams, J., Alnemri, E. S., Andrews, D. W., Baehrecke, E. H., Bazan, N. G., Blagosklonny, M. V., Blomgren, K., Borner, C., Bredesen, D. E., Brenner, C., Castedo, M., Cidlowski, J. A., Ciechanover, A., Cohen, G. M., de Laurenzi, V., de Maria, R., Deshmukh, M., ... Kroemer, G. (2009). Guidelines for the use and interpretation of assays for monitoring cell death in higher eukaryotes. *Cell Death and Differentiation*, 16(8), 1093–1107. <https://doi.org/10.1038/cdd.2009.44>
328. Navajas Acedo, J. (2024). Complete persistence of the primary somatosensory system in zebrafish. *Developmental Biology*, 515(February), 178–185. <https://doi.org/10.1016/j.ydbio.2024.05.004>
329. Liu, K. E., & Kucenas, S. (2024). Rohon-beard neurons do not succumb to programmed cell death during zebrafish development. *Developmental Biology*, 515(February), 186–198. <https://doi.org/10.1016/j.ydbio.2024.06.020>
330. Parichy, D. M., Elizondo, M. R., Mills, M. G., Gordon, T. N., & Engeszer, R. E. (2009). Normal Table of Postembryonic Zebrafish Development: Staging by Externally Visible Anatomy of the Living Fish. *Developmental Dynamics*, 238(12), 2975–3015. <https://doi.org/10.1002/dvdy.22113>
331. Rasmussen, J. P., Vo, N. T., & Sagasti, A. (2018). Fish Scales Dictate the Pattern of Adult Skin Innervation and Vascularization. *Developmental Cell*, 46(3), 344–359.e4. <https://doi.org/10.1016/j.devcel.2018.06.019>
332. Sire, J.-Y., Allizard, F., Babiari, O., Bourguignon, J., & Quilhac, A. (1997). Scale development in zebrafish (*Danio rerio*). *Journal of Anatomy*, 190(4), 545–561.
333. Kim, C.-H., Ueshima, E., Muraoka, O., Tanaka, H., Yeo, S.-Y., Huh, T.-L., & Miki, N. (1996). Zebrafish elav/HuC homologue as a very early neuronal marker. *Neuroscience Letters*, 216(2), 109–112.
334. Park, H.-C., Kim, C.-H., Bae, Y.-K., Yeo, S.-Y., Kim, S.-H., Hong, S.-K., Shin, J., Yoo, K.-W., Hibi, M., Hirano, T., Miki, N., Chitnis, A. B., & Huh, T.-L. (2000). Analysis of upstream elements in the HuC promoter leads to the establishment of transgenic Zebrafish with fluorescent neurons. *Developmental Biology*, 227(2), 279–293. <https://doi.org/10.1006/dbio.2000.9898>
335. Hans, S., Kaslin, J., Freudenreich, D., & Brand, M. (2009). Temporally-Controlled Site-Specific Recombination in Zebrafish. *PLoS ONE*, 4(2). <https://doi.org/10.1371/journal.pone.0004640>
336. Bakūnaitė, E., Gečaitė, E., Lazutka, J., & Balciunas, D. (2024). Highly efficient tamoxifen-inducible Cre recombination in embryonic, larval and adult zebrafish. *BioRxiv*.
337. Hans, S., Freudenreich, D., Geffarth, M., Kaslin, J., Machate, A., & Brand, M. (2011). Generation of a Non-Leaky Heat Shock – Inducible Cre Line for Conditional Cre/Lox Strategies in Zebrafish. *Developmental Dynamics*, 240(1), 108–115. <https://doi.org/10.1002/dvdy.22497>
338. He, S., Tian, Y., Feng, S., Wu, Y., Shen, X., Chen, K., He, Y., Sun, Q., Li, X., Xu, J., Wen, Z., & Qu, J. Y. (2020). In vivo single-cell lineage tracing in zebrafish using high-resolution infrared laser-mediated gene induction microscopy. *ELife*, 9, 1–30.
339. Elsaid, R., Mikdache, A., Diabanguaya, P., Gros, G., & Hernández, P. P. (2024). A noninvasive photoactivatable split-Cre recombinase system for genome engineering in zebrafish. *ELife*, 27(8). <https://doi.org/10.1016/j.isci.2024.110476>

340. Mosimann, C., Kaufman, C. K., Li, P., Pugach, E. K., Tamplin, O. J., & Zon, L. I. (2011). Ubiquitous transgene expression and Cre-based recombination driven by the ubiquitin promoter in zebrafish. *Development*, *138*(1), 169–177. <https://doi.org/10.1242/dev.059345>
341. Le, X., Langenau, D. M., Keefe, M. D., Kutok, J. L., Neubergh, D. S., & Zon, L. I. (2007). Heat shock-inducible Cre/Lox approaches to induce diverse types of tumors and hyperplasia in transgenic zebrafish. *Proceedings of the National Academy of Sciences*, *104*(22), 9410–9415. <https://doi.org/10.1073/pnas.0611302104>
342. Carney, T. J., & Mosimann, C. (2018). Switch and Trace: Recombinase Genetics in Zebrafish. *Trends in Genetics*, *34*(5), 362–378. <https://doi.org/10.1016/j.tig.2018.01.004>
343. Knogler, L. D., & Drapeau, P. (2014). Sensory gating of an embryonic zebrafish interneuron during spontaneous motor behaviors. *Frontiers in Neural Circuits*, *8*(SEP), 1–16. <https://doi.org/10.3389/fncir.2014.00121>
344. Knafo, S., Fidelin, K., Prendergast, A., Tseng, P. E. B., Parrin, A., Dickey, C., Böhm, U. L., Figueiredo, S. N., Thouvenin, O., Pascal-Moussellard, H., & Wyart, C. (2017). Mechanosensory neurons control the timing of spinal microcircuit selection during locomotion. *eLife*, *6*. <https://doi.org/10.7554/eLife.25260>
345. Bhatt, D. H., McLean, D. L., Hale, M. E., & Fetcho, J. R. (2007). Grading Movement Strength by Changes in Firing Intensity versus Recruitment of Spinal Interneurons. *Neuron*, *53*(1), 91–102. <https://doi.org/10.1016/j.neuron.2006.11.011>
346. McLean, D. L., Fan, J., Higashijima, S.-I., Hale, M. E., & Fetcho, J. R. (2007). A topographic map of recruitment in spinal cord. *Nature*, *446*(7131), 71–75. <https://doi.org/10.1038/nature05588>
347. Won, Y.-J., Ono, F., & Ikeda, S. R. (2012). Characterization of Na<sup>+</sup> and Ca<sup>2+</sup> Channels in Zebrafish Dorsal Root Ganglion Neurons. *PLoS ONE*, *7*(8), 1–15. <https://doi.org/10.1371/journal.pone.0042602>
348. Liu, Y.-C., & Hale, M. E. (2017). Local Spinal Cord Circuits and Bilateral Mauthner Cell Activity Function Together to Drive Alternative Startle Behaviors. *Current Biology*, *27*(5), 697–704. <https://doi.org/10.1016/j.cub.2017.01.019>
349. McGraw, H. F., Snelson, C. D., Prendergast, A., Suli, A., & Raible, D. W. (2012). Postembryonic neuronal addition in Zebrafish dorsal root ganglia is regulated by Notch signaling. *Neural Development*, *7*(23), 1–13.
350. Kague, E., Gallagher, M., Burke, S., Parsons, M., Franz-Odenaal, T., & Fisher, S. (2012). Skeletogenic Fate of Zebrafish Cranial and Trunk Neural Crest. *PLoS One*, *7*(11), 1–13. <https://doi.org/10.1371/journal.pone.0047394>
351. O'Brien, G. S., Rieger, S., Wang, F., Smolen, G. A., Gonzalez, R. E., Buchanan, J., & Sagasti, A. (2012). Coordinate development of skin cells and cutaneous sensory axons in zebrafish. *Journal of Comparative Neurology*, *520*(4), 816–831. <https://doi.org/10.1002/cne.22791>
352. Henderson, K. W., Roche, A., Menelaou, E., & Hale, M. E. (2020). Hindbrain and Spinal Cord Contributions to the Cutaneous Sensory Innervation of the Larval Zebrafish Pectoral Fin. *Frontiers in Neuroanatomy*, *14*(October), 1–15. <https://doi.org/10.3389/fnana.2020.581821>
353. An, M., Luo, R., & Henion, P. D. (2002). Differentiation and Maturation of Zebrafish Dorsal Root and Sympathetic Ganglion Neurons. *Journal of Comparative Neurology*, *446*(3), 267–275.

<https://doi.org/10.1002/cne.10214>

354. Umeda, K., Ishizuka, T., Yawo, H., & Shoji, W. (2016). Position- and quantity-dependent responses in zebrafish turning behavior. *Scientific Reports*, 6(February), 1–11. <https://doi.org/10.1038/srep27888>
355. Pineda, R. H., Svoboda, K. R., Wright, M. A., Taylor, A. D., Novak, A. E., Gamse, J. T., Eisen, J. S., & Ribera, A. B. (2006). Knockdown of Nav1.6a Na<sup>+</sup> channels affects zebrafish motoneuron development. *Development*, 133(19), 3827–3836. <https://doi.org/10.1242/dev.02559>
356. Katz, H. R., Menelaou, E., & Hale, M. E. (2021). Morphological and physiological properties of Rohon-Beard neurons along the zebrafish spinal cord. *Journal of Comparative Neurology*, 529(7), 1499–1515. <https://doi.org/10.1002/cne.25033>
357. Pan, Y. A., Freundlich, T., Weissman, T. A., Schoppik, D., Wang, X. C., Ciruna, B., Sanes, J. R., Lichtman, J. W., & Schier, A. F. (2013). Zebrafish: multispectral cell labeling for cell tracing and lineage analysis in zebrafish. *Development*, 140(13), 2835–2846. <https://doi.org/10.1242/dev.094631>
358. Easley-Neal, C., Fierro, J., Buchanan, J., & Washbourne, P. (2013). Late Recruitment of Synapsin to Nascent Synapses Is Regulated by Cdk5. *Cell Reports*, 3(4), 1199–1212. <https://doi.org/10.1016/j.celrep.2013.03.031>
359. Wells, S., Nornes, S., & Lardelli, M. (2011). Transgenic zebrafish recapitulating tbx16 gene early developmental expression. *PLoS ONE*, 6(6). <https://doi.org/10.1371/journal.pone.0021559>
360. Du, X. fei, Xu, B., Zhang, Y., Chen, M. jia, & Du, J. lin. (2018). A transgenic zebrafish model for in vivo long-term imaging of retinotectal synaptogenesis. *Scientific Reports*, 8(1), 1–11. <https://doi.org/10.1038/s41598-018-32409-y>
361. Gross, G. G., Junge, J. A., Mora, R. J., Kwon, H.-B., Olson, C. A., Takahashi, T. T., Liman, E. R., Ellis-davies, G. C. R., McGee, A. W., Sabatini, B. L., Roberts, R. W., & Arnold, D. B. (2013). Recombinant Probes for Visualizing Endogenous Synaptic Proteins in Living Neurons. *Neuron*, 78(6), 971–985. <https://doi.org/10.1016/j.neuron.2013.04.017>
362. Suppermpool, A., Lyons, D. G., Broom, E., & Rihel, J. (2024). Sleep pressure modulates single-neuron synapse number in zebrafish. *Nature*, 629(November 2022). <https://doi.org/10.1038/s41586-024-07367-3>
363. Kimura, Y., Okamura, Y., & Higashijima, S.-I. (2006). alx, a Zebrafish Homolog of Chx10, Marks Ipsilateral Descending Excitatory Interneurons That Participate in the Regulation of Spinal Locomotor Circuits. *Journal of Neuroscience*, 26(21), 5684–5697. <https://doi.org/10.1523/JNEUROSCI.4993-05.2006>
364. Satou, C., Kimura, Y., Kohashi, T., Horikawa, K., Takeda, H., Oda, Y., & Higashijima, S.-I. (2009). Functional Role of a Specialized Class of Spinal Commissural Inhibitory Neurons during Fast Escapes in Zebrafish. *Journal of Neuroscience*, 29(21), 6780–6793. <https://doi.org/10.1523/JNEUROSCI.0801-09.2009>
365. Meyer, M. P., Trimmer, J. S., Gilthorpe, J. D., & Smith, S. J. (2005). Characterization of Zebrafish PSD-95 Gene Family Members. *Journal of Neurobiology*, 63(2), 91–105. <https://doi.org/10.1002/neu.20118>
366. Chen, T.-W., Wardill, T. J., Sun, Y., Pulver, S. R., Renninger, S. L., Baohan, A., Schreiter, E. R., Kerr, R. A., Orger, M. B., Jayaraman, V., Looger, L. L., Svoboda, K., & Kim, D. S. (2013). Ultrasensitive fluorescent proteins for imaging neuronal activity. *Nature*, 499(7458), 295–300. <https://doi.org/10.1038/nature12354>

367. Chen, J., Xia, L., Bruchas, M. R., & Solnica-Krezel, L. (2017). Imaging early embryonic calcium activity with GCaMP6s transgenic zebrafish. *Developmental Biology*, 430(2), 385–396. <https://doi.org/10.1016/j.ydbio.2017.03.010>
368. Marvin, J. S., Scholl, B., Wilson, D. E., Podgorski, K., Kazemipour, A., Müller, J. A., Schoch, S., Quiroz, F. J. U., Rebola, N., Bao, H., Little, J. P., Tkachuk, A. N., Cai, E., Hantman, A. W., Wang, S. S., Depiero, V. J., Borghuis, B. G., Chapman, E. R., Dietrich, D., ... Looger, L. L. (2018). Stability, affinity, and chromatic variants of the glutamate sensor iGluSnFR. *Nature Methods*, 15(11), 936–939. <https://doi.org/10.1038/s41592-018-0171-3>
369. Pichler, P., & Lagnado, L. (2020). Motor Behavior Selectively Inhibits Hair Cells Activated by Forward Motion in the Lateral Line of Zebrafish. *Current Biology*, 30(1), 150-157.e3. <https://doi.org/10.1016/j.cub.2019.11.020>
370. Wagner, D. E., Weinreb, C., Collins, Z. M., Briggs, J. A., Megason, S. G., & Klein, A. M. (2018). Single-cell mapping of gene expression landscapes and lineage in the zebrafish embryo. *Science*, 360(6392), 1–7.
371. Lencer, E., Prekeris, R., & Artinger, K. B. (2021). Single-cell rna analysis identifies pre-migratory neural crest cells expressing markers of differentiated derivatives. *ELife*, 10, 1–20. <https://doi.org/10.7554/eLife.66078>
372. Kelly, J. J., Wen, H., & Brehm, P. (2023). Single cell RNA-seq analysis of spinal locomotor circuitry in larval zebrafish. *ELife*, 12, 1–36.
373. Saunders, L. M., Srivatsan, S. R., Duran, M., Dorrity, M. W., Ewing, B., Linbo, T. H., Shendure, J., Raible, D. W., Moens, C. B., Kimelman, D., & Trapnell, C. (2023). Embryo-scale reverse genetics at single-cell resolution. *Nature*, 623(7988), 782–791.
374. Inoue, A., Takahashi, M., Hatta, K., Hotta, Y., & Okamoto, H. (1994). Developmental Regulation of Islet-1 mRNA Expression During Neuronal Differentiation in Embryonic Zebrafish. *Developmental Dynamics*, 199(1), 1–11.
375. Beattie, C. E., Hatta, K., Halpern, M. E., Liu, H., Eisen, J. S., & Kimmel, C. B. (1997). Temporal Separation in the Specification of Primary and Secondary Motoneurons in Zebrafish. *Developmental Biology*, 187(2), 171–182.
376. Cretokos, C. J., & Grunwald, D. J. (1999). alyron, an Insertional Mutation Affecting Early Neural Crest Development in Zebrafish. *Developmental Biology*, 210(2), 322–338.
377. Lewis, K. E., & Eisen, J. S. (2001). Hedgehog signaling is required for primary motoneuron induction in zebrafish. *Development*, 128(18), 3485–3495.
378. Liu, C., Ma, W., Su, W., & Zhang, J. (2012). Prdm14 acts upstream of islet2 transcription to regulate axon growth of primary motoneurons in zebrafish. *Development*, 139(24), 4591–4600. <https://doi.org/10.1242/dev.083055>
379. Dyer, C., Linker, C., Graham, A., & Knight, R. (2014). Specification of Sensory Neurons Occurs Through Diverse Developmental Programs Functioning in the Brain and Spinal Cord. *Developmental Dynamics*, 243(11), 1429–1439. <https://doi.org/10.1002/DVDY.24184>

380. Kucenas, S., Soto, F., Cox, J. A., & Voigt, M. M. (2006). Selective labeling of central and peripheral sensory neurons in the developing zebrafish using p2x3 receptor subunit transgenes. *Neuroscience*, *138*(2), 641–652. <https://doi.org/10.1016/j.neuroscience.2005.11.058>
381. Rodríguez-Aznar, E., Barrallo-Gimeno, A., & Nieto, M. A. (2013). Scratch2 Prevents Cell Cycle Re-Entry by Repressing miR-25 in Postmitotic Primary Neurons. *Journal of Neuroscience*, *33*(12), 5095–5105. <https://doi.org/10.1523/JNEUROSCI.4459-12.2013>
382. Story, G. M., Peier, A. M., Reeve, A. J., Eid, S. R., Mosbacher, J., Hricik, T. R., Earley, T. J., Hergarden, A. C., Andersson, D. A., Hwang, S. W., McIntyre, P., Jegla, T., Bevan, S., & Patapoutian, A. (2003). ANKTM1, a TRP-like Channel Expressed in Nociceptive Neurons, Is Activated by Cold Temperatures. *Cell*, *112*(6), 819–829.
383. Bandell, M., Story, G. M., Hwang, S. W., Viswanath, V., Eid, S. R., Petrus, M. J., Earley, T. J., & Patapoutian, A. (2004). Noxious Cold Ion Channel TRPA1 Is Activated by Pungent Compounds and Bradykinin. *Neuron*, *41*(6), 849–857.
384. Jordt, S.-E., Bautista, D. M., Chuang, H., McKemy, D. D., Zygmunt, P. M., Högestätt, E. D., Meng, I. D., & Julius, D. (2004). Mustard oils and cannabinoids excite sensory nerve fibres through the TRP channel ANKTM1. *Nature*, *427*(6971), 260–265. <https://doi.org/10.1038/nature02237.1>
385. Esancy, K., Condon, L., Feng, J., Kimball, C., Curtright, A., & Dhaka, A. (2018). A zebrafish and mouse model for selective pruritus via direct activation of TRPA1. *ELife*, *7*, 1–24.
386. Schlüter, G. (1973). Ultrastructural observations on cell necrosis during formation of the neural tube in mouse embryos. *Zeitschrift Für Anatomie Und Entwicklungsgeschichte*, *141*(3), 251–264. <https://doi.org/10.1007/BF00519046>
387. Savill, J., Dransfield, I., Gregory, C., & Haslett, C. (2002). A blast from the past: Clearance of apoptotic cells regulates immune responses. *Nature Reviews Immunology*, *2*(12), 965–975. <https://doi.org/10.1038/nri957>
388. Paolicelli, R. C., Bolasco, G., Pagani, F., Maggi, L., Scianni, M., Panzanelli, P., Giustetto, M., Ferreira, T. A., Guiducci, E., Dumas, L., Ragozzino, D., & Gross, C. T. (2011). Synaptic pruning by microglia is necessary for normal brain development. *Science*, *333*(6048), 1456–1458. <https://doi.org/10.1126/science.1202529>
389. Arcuri, C., Mecca, C., Bianchi, R., Giambanco, I., & Donato, R. (2017). The pathophysiological role of microglia in dynamic surveillance, phagocytosis and structural remodeling of the developing CNS. *Frontiers in Molecular Neuroscience*, *10*(June), 1–22. <https://doi.org/10.3389/fnmol.2017.00191>
390. Lecours, C., Bordeleau, M., Cantin, L., Parent, M., Di Paolo, T., & Tremblay, M.-È. (2018). Microglial implication in Parkinson's disease: Loss of beneficial physiological roles or gain of inflammatory functions? *Frontiers in Cellular Neuroscience*, *12*(August), 1–8. <https://doi.org/10.3389/fncel.2018.00282>
391. Wang, J., Wang, J., Wang, J., Yang, B., Weng, Q., & He, Q. (2019). Targeting microglia and macrophages: A potential treatment strategy for multiple sclerosis. *Frontiers in Pharmacology*, *10*(March), 1–13. <https://doi.org/10.3389/fphar.2019.00286>
392. Comer, A. L., Carrier, M., Tremblay, M.-È., & Cruz-Martín, A. (2020). The Inflamed Brain in Schizophrenia:

- The Convergence of Genetic and Environmental Risk Factors That Lead to Uncontrolled Neuroinflammation. *Frontiers in Cellular Neuroscience*, 14(274). <https://doi.org/10.3389/fncel.2020.00274>
393. Catts, V. S., Fung, S. J., Long, L. E., Joshi, D., Vercammen, A., Allen, K. M., Fillman, S. G., Rothmond, D. A., Sinclair, D., Tiwari, Y., Tsai, S. Y., Weickert, T. W., & Weickert, C. S. (2013). Rethinking schizophrenia in the context of normal neurodevelopment. *Frontiers in Cellular Neuroscience*, 7(MAY), 1–27. <https://doi.org/10.3389/fncel.2013.00060>
394. Bianchin, M. M., Martin, K. C., De Souza, A. C., De Oliveira, M. A., & De Mello Rieder, C. R. (2010). Nasu-Hakola disease and primary microglial dysfunction. *Nature Reviews Neurology*, 6(9), 1–2. <https://doi.org/10.1038/nrneurol.2010.17-c1>
395. Perry, V. H., Nicoll, J. A. R., & Holmes, C. (2010). Microglia in neurodegenerative disease. *Nature Reviews Neurology*, 6(4), 193–201. <https://doi.org/10.1038/nrneurol.2010.17>
396. Tremblay, M.-È., Cookson, M. R., & Civiero, L. (2019). Glial phagocytic clearance in Parkinson's disease. *Molecular Neurodegeneration*, 14(1), 1–14. <https://doi.org/10.1186/s13024-019-0314-8>
397. Kalia, L. V., Kalia, S. K., & Lang, A. E. (2015). Disease-modifying strategies for Parkinson's disease. *Movement Disorders*, 30(11), 1442–1450. <https://doi.org/10.1002/mds.26354>
398. Cork, S. M., & Van Meir, E. G. (2011). Emerging roles for the BAI1 protein family in the regulation of phagocytosis, synaptogenesis, neurovasculature, and tumor development. *Journal of Molecular Medicine*, 89(8), 743–752. <https://doi.org/10.1007/s00109-011-0759-x>
399. Fond, A. M., & Ravichandran, K. S. (2016). Clearance of dying cells by phagocytes: mechanisms and implications for disease pathogenesis. *Advances in Experimental Medicine and Biology*, 930, 25–49. <https://doi.org/10.1007/978-3-319-39406-0>
400. Levin, R., Grinstein, S., & Canton, J. (2016). The life cycle of phagosomes: formation, maturation, and resolution. *Immunological Reviews*, 273(1), 156–179. <https://doi.org/10.1111/imr.12439>
401. Madej, M. P., Töpfer, E., Boraschi, D., & Italiani, P. (2017). Different regulation of interleukin-1 production and activity in monocytes and macrophages: Innate memory as an endogenous mechanism of IL-1 inhibition. *Frontiers in Pharmacology*, 8(JUN), 1–12. <https://doi.org/10.3389/fphar.2017.00335>
402. Xu, J., Wang, T., Wu, Y., Jin, W., & Wen, Z. (2016). Microglia Colonization of Developing Zebrafish Midbrain Is Promoted by Apoptotic Neuron and Lysophosphatidylcholine. *Developmental Cell*, 38(2), 214–222. <https://doi.org/10.1016/j.devcel.2016.06.018>
403. Wu, S., Xue, R., Hassan, S., Nguyen, T. M. L., Wang, T., Pan, H., Xu, J., Liu, Q., Zhang, W., & Wen, Z. (2018). Il34-Csf1r Pathway Regulates the Migration and Colonization of Microglial Precursors. *Developmental Cell*, 46(5), 552-563.e4. <https://doi.org/10.1016/j.devcel.2018.08.005>
404. Langenberg, T., Kahana, A., Wszalek, J. A., & Halloran, M. C. (2008). The Eye Organizes Neural Crest Cell Migration. *Developmental Dynamics*, 237(6), 1645–1652. <https://doi.org/10.1002/dvdy.21577>
405. Whitlock, K. E., Smith, K. M., Kim, H., & Harden, M. V. (2005). A role for foxd3 and sox10 in the differentiation of gonadotropin-releasing hormone (GnRH) cells in the zebrafish *Danio rerio*. *Development*, 132(24), 5491–5502. <https://doi.org/10.1242/dev.02158>

406. Park, H.-C., Mehta, A., Richardson, J. S., & Appel, B. (2002). *olig2* Is Required for Zebrafish Primary Motor Neuron and Oligodendrocyte Development. *Developmental Biology*, 368, 356–368. <https://doi.org/10.1006/dbio.2002.0738>
407. Takada, N., Kucenas, S., & Appel, B. (2010). Sox10 Is Necessary for Oligodendrocyte Survival Following Axon Wrapping. *Glia*, 58(8), 996–1006. <https://doi.org/10.1002/glia.20981>
408. Dutton, J. R., Antonellis, A., Carney, T. J., Rodrigues, F. S. L. M., Pavan, W. J., Ward, A., & Kelsh, R. N. (2008). An evolutionarily conserved intronic region controls the spatiotemporal expression of the transcription factor Sox10. *BMC Developmental Biology*, 8(105), 1–20. <https://doi.org/10.1186/1471-213X-8-105>
409. Santos-Ledo, A., Garcia-Macia, M., Campbell, P. D., Gronska, M., & Marlow, F. L. (2017). Kinesin-1 promotes chondrocyte maintenance during skeletal morphogenesis. *PLoS Genetics*, 13(7).
410. Eason, J., Williams, A. L., Chawla, B., Apsey, C., & Bohnsack, B. L. (2017). Differences in Neural Crest Sensitivity to Ethanol Account for the Infrequency of Anterior Segment Defects in the Eye Compared with Craniofacial Anomalies in a Zebrafish Model of Fetal Alcohol Syndrome. *Birth Defects Research*, 109(15), 1212–1227. <https://doi.org/10.1002/bdr2.1069>
411. Knight, R. D., & Schilling, T. F. (2006). Cranial Neural Crest and Development of the Head Skeleton. In J.-P. Saint-Jeannet (Ed.), *Neural Crest Induction and Differentiation* (pp. 120–133). Springer, Boston, MA. [https://doi.org/10.1007/978-0-387-46954-6\\_7](https://doi.org/10.1007/978-0-387-46954-6_7)
412. Britsch, S., Goerich, D. E., Riethmacher, D., Peirano, R. I., Rossner, M., Nave, K. A., Birchmeier, C., & Wegner, M. (2001). The transcription factor Sox10 is a key regulator of peripheral glial development. *Genes and Development*, 15(1), 66–78. <https://doi.org/10.1101/gad.186601>
413. Brown, R. I., Kawakami, K., & Kucenas, S. (2022). A novel gene trap line for visualization and manipulation of *erbb3b+* neural crest and glial cells in zebrafish. *Developmental Biology*, 482(November 2021), 114–123. <https://doi.org/10.1016/j.ydbio.2021.12.007>
414. Schmucker, J., Ader, M., Brockschneider, D., Brodarac, A., Bartsch, U., & Riethmacher, D. (2003). *erbB3* Is Dispensable for Oligodendrocyte Development In Vitro and In Vivo. *Glia*, 75(April), 67–75. <https://doi.org/10.1002/glia.10275>
415. Scott, K., Rourke, R. O., Winkler, C. C., Kearns, C. A., & Appel, B. (2021). Temporal single-cell transcriptomes of zebrafish spinal cord pMN progenitors reveal distinct neuronal and glial progenitor populations. *Developmental Biology*, 479, 37–50. <https://doi.org/10.1016/j.ydbio.2021.07.010>
416. Shin, J., Park, H.-C., Topczewska, J. M., Mawdsley, D. J., & Appel, B. (2003). Neural cell fate analysis in zebrafish using *olig2* BAC transgenics. *Methods in Cell Science*, 25(1–2), 7–14.
417. Marisca, R., Hoche, T., Agirre, E., Hoodless, L. J., Barkey, W., Auer, F., Castelo-Branco, G., & Czopka, T. (2020). Functionally Distinct Subgroups of Oligodendrocyte Precursor Cells Integrate Neural Activity and Execute Myelin Formation. *Nature Neuroscience*. <https://doi.org/10.1101/689505>
418. Zhou, T., Li, Y., Li, X., Zeng, F., Rao, Y., He, Y., Wang, Y., Liu, M., Li, D., Xu, Z., Zhou, X., Du, S., Niu, F., Peng, J., Mei, X., Ji, S., Shu, Y., & Lu, W. (2022). Microglial debris is cleared by astrocytes via C4b-

- facilitated phagocytosis and degraded via RUBICON-dependent noncanonical autophagy in mice. *Nature Communications*, 13(6233), 1–22. <https://doi.org/10.1038/s41467-022-33932-3>
419. Han, C. Z., Juncadella, I. J., Kinchen, J. M., Buckley, M. W., Klibanov, A. L., Dryden, K., Onengut-Gumuscu, S., Erdbrügger, U., Turner, S. D., Shim, Y. M., Tung, K. S., & Ravichandran, K. S. (2016). Macrophages redirect phagocytosis by non-professional phagocytes and influence inflammation. *Nature*, 539(7630), 570–574. <https://doi.org/10.1038/nature20141>
420. Colucci-Guyon, E., Tinevez, J. Y., Renshaw, S. A., & Herbomel, P. (2011). Strategies of professional phagocytes in vivo: Unlike macrophages, neutrophils engulf only surface-associated microbes. *Journal of Cell Science*, 124(18), 3053–3059. <https://doi.org/10.1242/jcs.082792>
421. Morales, M., Findley, A. P., & Mitchell, D. M. (2024). Intercellular contact and cargo transfer between Müller glia and to microglia precede apoptotic cell clearance in the developing retina. *Development*, 151(1), 1–14. <https://doi.org/10.1242/dev.202407>
422. Galloway, D. A., Phillips, A. E. M., Owen, D. R. J., & Moore, C. S. (2019). Phagocytosis in the brain: Homeostasis and disease. *Frontiers in Immunology*, 10(MAR), 1–15. <https://doi.org/10.3389/fimmu.2019.00790>
423. Nazareth, L., St John, J., Murtaza, M., & Ekberg, J. (2021). Phagocytosis by Peripheral Glia: Importance for Nervous System Functions and Implications in Injury and Disease. *Frontiers in Cell and Developmental Biology*, 9(April). <https://doi.org/10.3389/fcell.2021.660259>
424. Raiders, S., Han, T., Scott-Hewitt, N., Kucenas, S., Lew, D., Logan, M. A., & Singhvi, A. (2021). Engulfed by Glia: Glial Pruning in Development, Function, and Injury across Species. *Journal of Neuroscience*, 41(5), 823–833. <https://doi.org/10.1523/jneurosci.1660-20.2020>
425. Elmore, M. R. P., Najafi, A. R., Koike, M. A., Dagher, N. N., Spangenberg, E. E., Rice, R. A., Kitazawa, M., Matusow, B., Nguyen, H., West, B. L., & Green, K. N. (2014). Colony-stimulating factor 1 receptor signaling is necessary for microglia viability, unmasking a microglia progenitor cell in the adult brain. *Neuron*, 82(2), 380–397. <https://doi.org/10.1016/j.neuron.2014.02.040>
426. Oosterhof, N., Kuil, L. E., van der Linde, H. C., Burm, S. M., Berdowski, W., van Ijcken, W. F. J., van Swieten, J. C., Hol, E. M., Verheijen, M. H. G., & van Ham, T. J. (2018). Colony-Stimulating Factor 1 Receptor (CSF1R) Regulates Microglia Density and Distribution, but Not Microglia Differentiation In Vivo. *Cell Reports*, 24(5), 1203-1217.e6. <https://doi.org/10.1016/j.celrep.2018.06.113>
427. Blevins, G., & Fedoroff, S. (1995). Microglia in Colony-Stimulating Factor 1-Deficient op/op Mice. *Journal of Neuroscience Research*, 40(4), 545–544.
428. Węgiel, J., Wiśniewski, H. M., Dziewiątkowski, J., Tarnawski, M., Kozielski, R., Trenkner, E., & Wiktor-Jędrzejczak, W. (1998). Reduced number and altered morphology of microglial cells in colony stimulating factor-1-deficient osteopetrotic op/op mice. *Brain Research*, 804(1), 135–139.
429. Lin, H., Lee, E., Hestir, K., Leo, C., Huang, M., Bosch, E., Halenbeck, R., Wu, G., Zhou, A., Behrens, D., Hollenbaugh, D., Linnemann, T., Qin, M., Wong, J., Chu, K., Doberstein, S. K., & Williams, L. T. (2008). Discovery of a Cytokine and Its Receptor by Functional Screening of the Extracellular Proteome. *Science*,

320(5877), 807–811.

430. Erlich, B., Zhu, L., Etgen, A. M., Dobrenis, K., & Pollard, J. W. (2011). Absence of colony stimulation factor-1 receptor results in loss of microglia, disrupted brain development and olfactory deficits. *PLoS ONE*, *6*(10). <https://doi.org/10.1371/journal.pone.0026317>
431. Greter, M., Lelios, I., Pelczar, P., Hoeffel, G., Price, J., Leboeuf, M., Kündig, T. M., Frei, K., Ginhoux, F., Merad, M., & Becher, B. (2012). Stroma-derived interleukin-34 controls the development and maintenance of langerhans cells and the maintenance of microglia. *Immunity*, *37*(6), 1050–1060. <https://doi.org/10.1016/j.immuni.2012.11.001>
432. Wang, Y., Szretter, K. J., Vermi, W., Gilfillan, S., Rossini, C., Cella, M., Barrow, A. D., Diamond, M. S., & Colonna, M. (2012). IL-34 is a tissue-restricted ligand of CSF1R required for the development of Langerhans cells and microglia. *Nature Immunology*, *13*(8), 753–760. <https://doi.org/10.1038/ni.2360>
433. Caetano-Lopes, J., Henke, K., Urso, K., Duryea, J., Charles, J. F., Warman, M. L., & Harris, M. P. (2020). Unique and non-redundant function of csf1r paralogues in regulation and evolution of post-embryonic development of the zebrafish. *Development*, *147*(2), 1–11. <https://doi.org/10.1242/dev.181834>
434. Ferrero, G., Miserocchi, M., Di Ruggiero, E., & Wittamer, V. (2021). A csf1rb mutation uncouples two waves of microglia development in zebrafish. *Development (Cambridge)*, *148*(1). <https://doi.org/10.1242/dev.194241>
435. Jin, H., Li, L., Xu, J., Zhen, F., Zhu, L., Liu, P. P., Zhang, M., Zhang, W., & Wen, Z. (2012). Runx1 regulates embryonic myeloid fate choice in zebrafish through a negative feedback loop inhibiting Pu.1 expression. *Blood*, *119*(22), 5239–5249. <https://doi.org/10.1182/blood-2011-12-398362>
436. Li, L., Jin, H., Xu, J., Shi, Y., & Wen, Z. (2011). Irf8 regulates macrophage versus neutrophil fate during zebrafish primitive myelopoiesis. *Blood*, *117*(4), 1359–1369. <https://doi.org/10.1182/blood-2010-06-290700>.The
437. Berdowski, W. M., van der Linde, H. C., Breur, M., Oosterhof, N., Beerepoot, S., Sanderson, L., Wijnands, L. I., de Jong, P., Tsai-Meu-Chong, E., de Valk, W., de Witte, M., van IJcken, W. F. J., Demmers, J., van der Knaap, M. S., Bugiani, M., Wolf, N. I., & van Ham, T. J. (2022). Dominant-acting CSF1R variants cause microglial depletion and altered astrocytic phenotype in zebrafish and adult-onset leukodystrophy. *Acta Neuropathologica*, *144*(2), 211–239. <https://doi.org/10.1007/s00401-022-02440-5>
438. Monier, A., Adle-Biassette, H., Delezoide, A. L., Evrard, P., Gressens, P., & Verney, C. (2007). Entry and distribution of microglial cells in human embryonic and fetal cerebral cortex. *Journal of Neuropathology and Experimental Neurology*, *66*(5), 372–382. <https://doi.org/10.1097/nen.0b013e3180517b46>
439. Morsch, M., Radford, R., Lee, A., Don, E. K., Badrock, A. P., Hall, T. E., Cole, N. J., & Chung, R. (2015). In vivo characterization of microglial engulfment of dying neurons in the zebrafish spinal cord. *Frontiers in Cellular Neuroscience*, *9*(August), 1–11. <https://doi.org/10.3389/fncel.2015.00321>
440. Wu, S., Nguyen, L. T. M., Pan, H., Hassan, S., Dai, Y., Xu, J., & Wen, Z. (2020). Two phenotypically and functionally distinct microglial populations in adult zebrafish. *Science Advances*, *6*(November), 21–25.
441. Kondo, Y., & Duncan, I. D. (2015). Selective Reduction in Microglia Density and Function in the White

- Matter of Colony-stimulating factor-1 – Deficient Mice. *Journal of Neuroscience Research*, 87(12), 2686–2695. <https://doi.org/10.1002/jnr.22096>
442. Matcovitch-Natan, O., Winter, D. R., Giladi, A., Aguilar, S. V., Spinrad, A., Sarrazin, S., Ben-Yehuda, H., David, E., González, F. Z., Perrin, P., Keren-Shaul, H., Gury, M., Lara-Astaiso, D., Thaiss, C. A., Cohen, M., Halpern, K. B., Baruch, K., Deczkowska, A., Lorenzo-Vivas, E., ... Amit, I. (2016). Microglia development follows a stepwise program to regulate brain homeostasis. *Science*, 353(6301). <https://doi.org/10.1126/science.aad8670>
443. Easley-Neal, C., Foreman, O., Sharma, N., Zarrin, A. A., & Weimer, R. M. (2019). CSF1R Ligands IL-34 and CSF1 Are Differentially Required for Microglia Development and Maintenance in White and Gray Matter Brain Regions. *Frontiers in Immunology*, 10(September). <https://doi.org/10.3389/fimmu.2019.02199>
444. Kana, V., Desland, F. A., Casanova-Acebes, M., Ayata, P., Badimon, A., Nabel, E., Yamamuro, K., Sneeboer, M., Tan, I.-L., Flanigan, M. E., Rose, S. A., Chang, C., Leader, A., Le Bourhis, H., Sweet, E. S., Tung, N., Wroblewska, A., Lavin, Y., See, P., ... Merad, M. (2019). CSF-1 controls cerebellar microglia and is required for motor function and social interaction. *Journal of Experimental Medicine*, 216(10), 2265–2281.
445. Xu, J., Du, L., & Wen, Z. (2012). Myelopoiesis During Zebrafish Early Development. *Journal of Genetics and Genomics*, 39(9), 435–442. <https://doi.org/10.1016/j.jgg.2012.06.005>
446. Gore, A. V., Pillay, L. M., Venero, M., & Brant, G. (2018). The zebrafish: A fantastic model for hematopoietic development and disease. *WIREs Developmental Biology*, 7(3), 1–17. <https://doi.org/10.1002/wdev.312>
447. Rasmussen, J. P., Sack, G. S., Martin, S. M., & Sagasti, A. (2015). Vertebrate epidermal cells are broad-specificity phagocytes that clear sensory axon debris. *Journal of Neuroscience*, 35(2), 559–570. <https://doi.org/10.1523/JNEUROSCI.3613-14.2015>
448. Morales, R. A., & Allende, M. L. (2019). Peripheral Macrophages Promote Tissue Regeneration in Zebrafish by Fine-Tuning the Inflammatory Response. *Frontiers in Immunology*, 10(February), 1–14. <https://doi.org/10.3389/fimmu.2019.00253>
449. Shiau, C. E., Kaufman, Z., Meireles, A. M., & Talbot, W. S. (2015). Differential requirement for irf8 in formation of embryonic and adult macrophages in zebrafish. *PLoS ONE*, 10(1), 1–15. <https://doi.org/10.1371/journal.pone.0117513>
450. Ong, S. L. M., de Vos, I. J. H. M., Meroshini, M., Poobalan, Y., & Dunn, N. R. (2020). Microfibril-associated glycoprotein 4 (Mfap4) regulates haematopoiesis in zebrafish. *Scientific Reports*, 4, 1–12. <https://doi.org/10.1038/s41598-020-68792-8>
451. Myllymäki, H., Yu, P. P., & Feng, Y. (2022). Opportunities presented by zebrafish larval models to study neutrophil function in tissues. *International Journal of Biochemistry and Cell Biology*, 148(February), 1–8. <https://doi.org/10.1016/j.biocel.2022.106234>
452. Tsarouchas, T. M., Wehner, D., Cavone, L., Munir, T., Keatinge, M., Lambertus, M., Underhill, A., Barrett, T., Kassapis, E., Ogryzko, N., Feng, Y., van Ham, T. J., Becker, T., & Becker, C. G. (2018). Dynamic control of proinflammatory cytokines Il-1 $\beta$  and Tnf- $\alpha$  by macrophages in zebrafish spinal cord regeneration. *Nature Communications*, 9(4670). <https://doi.org/10.1038/s41467-018-07036-w>

453. Kuil, L. E., Oosterhof, N., Ferrero, G., Mikulášová, T., Hason, M., Dekker, J., Rovira, M., van der Linde, H. C., van Strien, P. M. H., de Pater, E., Schaaf, G., Bindels, E. M. J., Wittamer, V., & van Ham, T. J. (2020). Zebrafish macrophage developmental arrest underlies depletion of microglia and reveals Csf1r-independent metaphocytes. *ELife*, *9*(2015), 1–27. <https://doi.org/10.7554/eLife.53403>
454. Sharrock, A. V., Mulligan, T. S., Hall, K. R., Williams, E. M., White, D. T., Zhang, L., Emmerich, K., Matthews, F., Nimmagadda, S., Washington, S., Le, K. D., Meir-Levi, D., Cox, O. L., Saxena, M. T., Calof, A. L., Lopez-Burks, M. E., Lander, A. D., Ding, D., Ji, H., ... Mumm, J. S. (2022). NTR 2.0: a rationally engineered prodrug-converting enzyme with substantially enhanced efficacy for targeted cell ablation. *Nature Methods*, *19*(2), 205–215. <https://doi.org/10.1038/s41592-021-01364-4>
455. Bagnara, J. T., & Matsumoto, J. (2006). Comparative Anatomy and Physiology of Pigment Cells in Nonmammalian Tissues. In J. J. Nordlund, R. E. Boissy, V. J. Hearing, R. A. King, W. S. Oetting, & J.-P. Ortonne (Eds.), *The Pigmentary System: Physiology and Pathophysiology* (2nd ed., pp. 11–59). Blackwell Publishing Ltd.
456. Parichy, D. M., & Turner, J. M. (2003). Temporal and cellular requirements for Fms signaling during zebrafish adult pigment pattern development. *Development*, *130*(5), 817–833. <https://doi.org/10.1242/dev.00307>
457. Zhu, Y. (2019). *Novel Roles of Glial Precursors in Early Neurogenesis* (Vol. 2). University of Virginia.
458. Schafer, D. P., Heller, C. T., Gunner, G., Heller, M., Gordon, C., Hammond, T., Wolf, Y., Jung, S., & Stevens, B. (2016). Microglia contribute to circuit defects in *Mecp2* null mice independent of microglia-specific loss of *Mecp2* expression. *ELife*, *5*(2016JULY), 1–19. <https://doi.org/10.7554/eLife.15224>
459. Wu, T., Dejanovic, B., Gandham, V. D., Gogineni, A., Edmonds, R., Schauer, S., Srinivasan, K., Huntley, M. A., Wang, Y., Wang, T. M., Hedehus, M., Barck, K. H., Stark, M., Ngu, H., Foreman, O., Meilandt, W. J., Elstrott, J., Chang, M. C., Hansen, D. V., ... Hanson, J. E. (2019). Complement C3 Is Activated in Human AD Brain and Is Required for Neurodegeneration in Mouse Models of Amyloidosis and Tauopathy. *Cell Reports*, *28*(8), 2111–2123.e6. <https://doi.org/10.1016/j.celrep.2019.07.060>
460. Rajendran, L., & Paolicelli, R. C. (2018). Microglia-Mediated Synapse Loss in Alzheimer's Disease. *Journal of Neuroscience*. <https://doi.org/10.1523/JNEUROSCI.1136-17.2017>
461. Hong, S., Beja-Glasser, V. F., Nfonoyim, B. M., Frouin, A., Li, S., Rmakrishnan, S., Merry, K. M., Shi, Q., Rosenthal, A., Barres, B. A., Lemere, C. A., Selkoe, D. J., & Stevens, B. (2016). Complement and microglia mediate early synapse loss in Alzheimer mouse models. *Science*, *352*(6286).
462. Huang, X., Fowler, C., Li, Y., Li, Q.-X., Sun, J., Pan, Y., Jin, L., Perez, K. A., Dubois, C., Lim, Y. Y., Drysdale, C., Rumble, R. L., Chinnery, H. R., Rowe, C. C., Martins, R. N., Maruff, P., Doecke, J. D., Lin, Y., Belaidi, A. A., ... Gu, B. J. (2024). Clearance and transport of amyloid  $\beta$  by peripheral monocytes correlate with Alzheimer's disease progression. *Nature Communications*, *15*(7998), 1–17. <https://doi.org/10.1038/s41467-024-52396-1>
463. Feinberg, I. (1982). Schizophrenia: Caused by a fault in programmed synaptic elimination during adolescence? *Journal of Psychiatric Research*, *17*(4), 319–334. [149](https://doi.org/10.1016/0022-</a></p>
</div>
<div data-bbox=)

464. Weinberger, D. R. (1987). Implications of Normal Brain Development for the Pathogenesis of Schizophrenia. *Archives of General Psychiatry*, 45(11), 1055. <https://doi.org/10.1001/archpsyc.1988.01800350089019>
465. Hill, J. J., Hashimoto, T., & Lewis, D. A. (2006). Molecular mechanisms contributing to dendritic spine alterations in the prefrontal cortex of subjects with schizophrenia. *Molecular Psychiatry*, 11(6), 557–566. <https://doi.org/10.1038/sj.mp.4001792>
466. Sellgren, C. M., Gracias, J., Watmuff, B., Biag, J. D., Thanos, J. M., Whittredge, P. B., Fu, T., Worringer, K., Brown, H. E., Wang, J., Kaykas, A., Karmacharya, R., Goold, C. P., Sheridan, S. D., & Perlis, R. H. (2019). Increased synapse elimination by microglia in schizophrenia patient-derived models of synaptic pruning. *Nature Neuroscience*, 22(3), 374–385. <https://doi.org/10.1038/s41593-018-0334-7>
467. Zikopoulos, B., & Barbas, H. (2010). Changes in prefrontal axons may disrupt the network in autism. *Journal of Neuroscience*, 30(44), 14595–14609. <https://doi.org/10.1523/JNEUROSCI.2257-10.2010>
468. Suzuki, K., Sugihara, G., Ouchi, Y., Nakamura, K., Futatsubashi, M., Takebayashi, K., Yoshihara, Y., Omata, K., Matsumoto, K., Tsuchiya, K. J., Iwata, Y., Tsujii, M., Sugiyama, T., & Mori, N. (2013). Microglial activation in young adults with autism spectrum disorder. *Archives of General Psychiatry*, 70(1), 49–58. <https://doi.org/10.1001/jamapsychiatry.2013.272>
469. Squarzoni, P., Oller, G., Hoeffel, G., Pont-Lezica, L., Rostaing, P., Low, D., Bessis, A., Ginhoux, F., & Garel, S. (2014). Microglia Modulate Wiring of the Embryonic Forebrain. *Cell Reports*, 8(5), 1271–1279. <https://doi.org/10.1016/j.celrep.2014.07.042>
470. Chen, S.-Y., Pan, C.-J., Nandigama, K., Mansfield, B. C., Ambudkar, S. V., & Chou, J. Y. (2008). The glucose-6-phosphate transporter is a phosphate-linked antiporter deficient in glycogen storage disease type Ib and Ic. *FASEB Journal*, 22(7), 2206–2213. <https://doi.org/10.1096/fj.07-104851>
471. Pan, C.-J., Chen, S.-Y., Jun, H. S., Lin, S. R., Mansfield, B. C., & Chou, J. Y. (2011). SLC37A1 and SLC37A2 Are Phosphate-Linked, Glucose-6-Phosphate Antiporters. *PLoS One*, 6(9), 1–8. <https://doi.org/10.1371/journal.pone.0023157>
472. Kim, J. Y., Tillison, K., Zhou, S., Wu, Y., & Smas, C. M. (2007). The major facilitator superfamily member Slc37a2 is a novel macrophage-specific gene selectively expressed in obese white adipose tissue. *American Journal of Physiology, Endocrinology and Metabolism*, 293(1), 110–120. <https://doi.org/10.1152/ajpendo.00404.2006>
473. Wang, Z., Zhao, Q., Nie, Y., Yu, Y., Misra, B. B., Zabalawi, M., Chou, J. W., Key, C.-C. C., Molina, A. J., Quinn, M. A., Fessler, M. B., Parks, J. S., McCall, C. E., & Zhu, X. (2020). Solute Carrier Family 37 Member 2 (SLC37A2) Negatively Regulates Murine Macrophage Inflammation by Controlling Glycolysis. *IScience*, 2. <https://doi.org/10.1016/j.isci.2020.101125>
474. Hammond, T. R., Dufort, C., Dissing-Olesen, L., Giera, S., Young, A., Wysoker, A., Walker, A. J., Gergits, F., Segel, M., Nemes, J., Marsh, S. E., Saunders, A., Macosko, E., Ginhoux, F., Chen, J., Franklin, R. J. M., Piao, X., McCarroll, S. A., & Stevens, B. (2019). Single-Cell RNA Sequencing of Microglia throughout

- the Mouse Lifespan and in the Injured Brain Reveals Complex Cell-State Changes. *Immunity*, 50(1), 253-271.e6. <https://doi.org/10.1016/j.immuni.2018.11.004>
475. Morrice, J. R., Gregory-Evans, C. Y., & Shaw, C. A. (2018). Modeling Environmentally-Induced Motor Neuron Degeneration in Zebrafish. *Scientific Reports, March*, 1–11. <https://doi.org/10.1038/s41598-018-23018-w>
476. von Tscharner, V., & Schwarz, G. (1979). Complex Formation of Acridine Orange with Single-Stranded Polyriboadenylic Acid and 5' -AMP : Cooperative Binding and Intercalation Between Bases. *Biophysics of Structure and Mechanism*, 5(1), 75–90.
477. Kapuscinski, J., & Darzynkiewicz, Z. (1987). Interactions of Acridine Orange with Double Stranded Nucleic Acids. Spectral and Affinity Studies. *Journal of Biomolecular Structure & Dynamics*, 5(1), 127–143.
478. Kusuzaki, K., Murata, H., Takeshita, H., Hashiguchi, S., Nozaki, T., Emoto, K., Ashihara, T., & Hirasawa, Y. (2000). Intracellular binding sites of acridine orange in living osteosarcoma cells. *Anticancer Research*, 20(2A), 971–975. <https://pubmed.ncbi.nlm.nih.gov/10810383/>
479. Nies, P. Van, Westerlaken, I., Blanken, D., Salas, M., Mencía, M., & Danelon, C. (2018). Self-replication of DNA by its encoded proteins in liposome-based synthetic cells. *Nature Communications*, 9(1), 1–12. <https://doi.org/10.1038/s41467-018-03926-1>
480. Delic, J., Coppey, J., Magdelenat, H., & Coppey-Moisan, M. (1991). Impossibility of Acridine Orange Intercalation in Nuclear DNA of the Living Cell. *Experimental Cell Research*, 194(1), 147–153.
481. Gillooly, D. J., Morrow, I. C., Lindsay, M., Gould, R., Bryant, N. J., Gaullier, J.-M., Parton, R. G., & Stenmark, H. (2000). Localization of phosphatidylinositol 3-phosphate in yeast and mammalian cells. *EMBO Journal*, 19(17), 4577–4588. <https://doi.org/10.1093/emboj/19.17.4577>
482. Farrell, J. A., Wang, Y., Riesenfeld, S. J., Shekhar, K., Regev, A., & Schier, A. F. (2018). Single-cell reconstruction of developmental trajectories during zebrafish embryogenesis. *Science*, 360(6392). <https://doi.org/10.1126/science.aar3131>
483. Sur, A., Wang, Y., Capar, P., Margolin, G., Prochaska, M. K., & Farrell, J. A. (2023). Single-cell analysis of shared signatures and transcriptional diversity during zebrafish development. *Developmental Cell*, 58(24), 3028-3047.e12. <https://doi.org/10.1016/j.devcel.2023.11.001>